Resistance to Flow Through Riparian Wetlands

C. Hodges, P. Diplas, and T. Younos

Final Report
May 1997

Submitted to: Virginia Water Resources Research Center
VWRRC Special Report No. SR1-1997

ABSTRACT

Increasing interest in the role of wetlands in pollutant removal, flood plain management, and sedimentation in recent years has prompted research into hydraulic processes inherent to these systems. The research described in this thesis focuses on flow processes within ecosystems known as riparian wetlands. An attempt has been made to summarize existing research in this field to ensure that a contribution will be made to the field of hydraulics. Included in this thesis are results from laboratory models investigating flow through vegetation in riparian wetlands. Particular emphasis in this research has been placed on velocity profile measurement of flow within vegetation. Measurements were taken within various density configuration of rigid simulated vegetation for emergent and submerged cases. In addition, many of the experiments tested the effect on the velocity profile when two distinct layers of vegetation are present. The results described herein should aid in visualization of flow processes within riparian wetlands.

ACKNOWLEDGMENTS

Funding for this study was partially provided by the Virginia Water Resources Research Center, Virginia Tech, Blacksburg, Virginia and partially provided by a grant from the National Science Foundation under project #CTS-9257335.

TABLE OF CONTENTS

Chapter **Page**

List of Tables vii

List of Figures x

List of Variables xiv

1 Introduction
- 1.1 General 1
- 1.2 Focus of Study 2
- 1.3 Objectives of Thesis 2
- 1.4 Layout of Thesis 3

2 State of the Art
- 2.1 General 4
- 2.2 Friction Relationships of Flow Through Channels 5
- 2.3 Studies in Grass-lined Channels 7
- 2.4 Studies in Wetlands 18
- 2.5 Recent Studies of Flow through Rigid Cylinders 22
- 2.6 Comparison of Studies 25
- 2.7 Summary 32

3 Objectives and Description of Research
- 3.1 General 33
- 3.2 Effect of Plant Density 33
- 3.3 Effect of Double-layered Vegetation 34
- 3.4 Resistance of Cylinders 34
- 3.5 Measurement of Velocity Profiles 35
- 3.6 Summary 35

4 Dimensional Analysis
- 4.1 General 37
- 4.2 Description of Variables 37
- 4.3 Analysis of Single-Layered Vegetation with Rigid Stems (Unsubmerged) 39
- 4.4 Analysis of Single-Layered Vegetation with Rigid Stems (Submerged) 41
- 4.5 Analysis of Double-Layered Vegetation 41
- 4.6 Summary 42

5 Experimental Apparatus and Procedure
5.1 General 43
5.2 Laboratory Equipment 43
5.3 Wetland Model Construction 46
5.4 Control Experiments 47
5.5 Experimental Procedure 48
5.5.1: Single Layered Vegetation 50
5.5.2: Double-layered Vegetation 54
5.6 Summary 59

6 Experimental Results
6.1 General 60
6.2 Data Collected From Laser Doppler Anemometer 60
6.3 Results from Single-Layered Vegetation Experiments 62
6.3.1: Measurements Immediately DS of the Dowel at 1-2 Dowel Diameters (6.35-12.70 mm) 62
6.3.2: Measurements In-line with Dowel (excluding those immediately downstream)6-14 Dowel Diameters DS from Vegetation 68
6.3.3:Measurements taken in the Unobstructed Flow region (not in-line with dowels) 75
6.4 Results from Double-Layered Vegetation Experiments 79
6.4.1: Measurements Immediately DS of the Dowel at 2 Dowel Diameters (12.70 mm) 81
6.4.2: Measurements In-line with Dowel (excluding those immediately downstream) 84
6.4.3:Measurements taken in the Unobstructed Flow region (not in-line with dowels) 89
6.5 Apparent Roughness Coefficients 91
6.6 Analysis of Experimental Data for Determination of Drag Force ... 92
6.7 Statistical Analysis of Experimental Data 96
6.8 Reynolds and Froude Numbers 102
6.9 Summary of Results 103

7 Conclusions 105

Literature Cited 108

Appendix 112

List of Tables **Page**

Table 2.1-Coefficients for Equations (2.4) and (2.5) 16

Table 2.2-Spacings Used for the Experiments by Hartley (1980) 23

Table 2.3-Froude Number Results as Shown by Hartley (1980) 24

Table 2.4-Summary of Experiments Using Cylindrical Non-Flexible Obstructions to Simulate Flow Through Vegetation 27

Table 2.5-Summary of Experiments Using Flexible Strips and/or Natural Vegetation 30

Table 4.1-Relevant Variables to be Used in Dimensional Analysis of Experiments 38

Table 5.1-Experiments for Unsubmerged, Single Layer Vegetation Case 52

Table 5.2-Experiments for Submerged, Single Layer Vegetation Case 52

Table 5.3-Experiments for Non-Uniform Height (Double-layered) Vegetation Case 57

Table 6.1-Analyzed Velocity Profile Data from Experiment 13 at Measurement Point 1 61

Table 6.2-Manning's Coefficients for Experiments 91

Table 6.3-Results from Equations Given in Blevens (1992) 94

Table 6.4-Calculation of Resistance Force in Channel 95

Table 6.5-Froude and Reynolds Numbers for Experimental Runs 104

Table A1-Experiment 4A, Measurement Point 1 115

Table A2-Experiment 4A, Measurement Point 2 115

Table A3-Experiment 4A, Measurement Point 3 119

Table A4-Experiment 4A, Measurement Point 4 119

Table A5-Experiment 4A, Measurement Point 5 120

List of Tables **Page**

Table A6-Experiment 4A, Measurement Point 6 120

Table A7-Experiment 4C, Measurement Point 1 122

Table A8-Experiment 4C, Measurement Point 2 123

Table A9-Experiment 4C, Measurement Point 3 128

Table A10-Experiment 4C, Measurement Point 4 129

Table A11-Experiment 5A, Measurement Point 1 131

Table A12-Experiment 5A, Measurement Point 2 131

Table A13-Experiment 5A, Measurement Point 3 132

Table A14-Experiment 5A, Measurement Point 4 132

Table A15-Experiment 5C, Measurement Point 1 134

Table A16-Experiment 5C, Measurement Point 2 135

Table A17-Experiment 6A, Measurement Point 1 138

Table A18-Experiment 6A, Measurement Point 2 138

Table A19-Experiment 6A, Measurement Point 3 139

Table A20-Experiment 6A, Measurement Point 4 139

Table A21-Experiment 6A, Measurement Point 5 140

Table A22-Experiment 6A, Measurement Point 6 140

Table A23-Experiment 6C, Measurement Point 1 142

Table A24-Experiment 6C, Measurement Point 2 146

Table A25-Experiment 6C, Measurement Point 3 147

Table A25(A)-Experiment 6C, Measurement Point 4 148

List of Tables **Page**

Table A26-Experiment 7, Measurement Point 1 150

Table A27-Experiment 7, Measurement Point 2 155

Table A28-Experiment 7, Measurement Point 3 156

Table A29-Experiment 7, Measurement Point 4 157

Table A30-Experiment 8, Measurement Point 1 159

Table A31-Experiment 8, Measurement Point 2 160

Table A32-Experiment 9, Measurement Point 1 162

Table A33-Experiment 9, Measurement Point 2 163

Table A34-Experiment 9, Measurement Point 3 164

Table A35-Experiment 10, Measurement Point 1 166

Table A36-Experiment 11, Measurement Point 1 168

Table A37-Experiment 11, Measurement Point 2 173

Table A38-Experiment 11, Measurement Point 3 174

Table A39-Experiment 12, Measurement Point 1 176

Table A40-Experiment 13, Measurement Point 1 178

Table A41-Experiment 13, Measurement Point 2 179

Table A42-Experiment 13, Measurement Point 3 180

Table A43-Experiment 13, Measurement Point 4 181

Table A44-Experiment 13, Measurement Point 5 182

Table A45-Experiment 14, Measurement Point 1 184

List of Figures **Page**

Figure 2.1-Plot of Manning's n as a Function of VR for Varying Grass Lengths 10

Figure 2.2-Velocity Profile over Vegetative Layer 11

Figure 2.3-Plot of Equation 2.15 for Wide Rectangular Channel 15

Figure 5.1-Photograph of Flume Used for Experiments 44

Figure 5.2-Mounting Apparatus Used to Hold the Laser Probe During Experiments 45

Figure 5.3-Photograph Showing the Placement of Stop Logs 48

Figure 5.4-Typical Logarithmic Velocity Profile Taken During a Control Run 49

Figure 5.5-Definition of Staggered and Linear Formations Used in Experiments 51

Figure 5.6-Profile Measurement Locations for Emergent Uniform 3.05 m Test Sections 55

Figure 5.7-Profile Measurement Locations for Submerged Uniform 3.05 m Test Sections 56

Figure 5.8-Profile Measurement Locations for Double Layered Uniform 3.05 m Test Sections 58

Figure 6.0-Schematic Diagram of Measurement Point Locations 62

Figure 6.1-Velocity Profile from Experiment 5A (Linear s/d=8) – Point 1 @ 2 Dowel Diameters DS (12.7 mm) 63

Figure 6.2-Surface Wave Formation Found in Staggered Array of Cylinders 65

Figure 6.3-Standing Wave Formation Looking Upstream in Flume 66

Figure 6.4-Progression of Velocity Profiles DS in Experiment 4A (Inline w/Dowels) 67

List of Figures **Page**

Figure 6.5-Progression of Velocity Profiles DS in Experiment 4C (Inline w/ Dowels) ... 67

Figure 6.6-Dimensionless Plots of Unsubmerged Experiments In-Line with Dowels (Profiles Immediately Downstream) ... 69

Figure 6.7-Dimensionless Plots of Submerged Experiment In-line with Dowels (Profiles Immediately Downstream) ... 70

Figure 6.8-Velocity Profile for Experiment 5A (linear s/d=8) – Point 3 @ 6 Dowel Diameters DS (38.1 mm) ... 73

Figure 6.9-Velocity Profile from Experiment 5C (Linear s/d=8) – Point 2 @ 4 Dowel Diameters DS (25.4 mm) ... 73

Figure 6.10-Dimensionless Plots of Unsubmerged Experiments Inline with Dowels (Profiles Immediately Downstream of Dowel are Excluded) ... 76

Figure 6.11-Dimensionless Plots of Submerged Experiments Inline with Dowels (Profiles Immediately Downstream of Dowel are Excluded) ... 77

Figure 6.12-Velocity Profile from Experiment 6A (Linear s/d=16) – Point 5 @ 4 Dowel Diameters DS (25.4 mm) & 8 Dowel Diameters Left of Center ... 78

Figure 6.13-Velocity Profile form Experiment 5A (Linear s/d=8) – Point 4 @ 4 Dowel Diameters DS (25.4 mm) & 4 Dowel Diameters Left of Center ... 79

Figure 6.14-Dimensionless Plots of Unsubmerged Experiments in Unobstructed Location ... 80

Figure 6.15-Velocity Profile from Experiment 9 [Linear s/d=8 (short), Linear s/d=16 (tall)] – Point 1 @ 4 Dowel Diameters (25.4 mm) DS from Tall Rod ... 82

Figure 6.16-Dimensionless Plots of Double Layer Experiments Inline with Dowels (Points Immediately Downstream of Dowels ... 83

Figure 6.17-Velocity Profile for Experiment 9 [Linear s/d=8 (short), Linear s/d=16 (tall)] – Point 2 @ 12 Dowel Diameters (76.2 mm) from Tall Rod ... 85

Figure 6.18-Progression of Velocity Profiles DS in Experiment 13 (Inline w/Dowels) ... 86

List of Figures Page

Figure 6.19-Dimensionless Plots of Double Layer Experiments Inline with Dowels (Profiles Immediately Downstream of Dowel are Excluded) 88

Figure 6.20-Velocity Profile from Experiment 9 [Linear s/d=8 (short), Linear s/d=16 (tall)] – Point 3 @ 4 Dowel Diameters (25.4 mm) DS, 4 Left of Centerline 89

Figure 6.21-Dimensionless Plots of Double Layer Experiments in Unobstructed Locations 90

Figure 6.22-Turbulence Intensities for the Profiles of Experiment 9 98

Figure 6.23- Turbulence Intensities for the Profiles of Experiments 7-13 (Double-Layered Vegetation Experiments @ 4 Dowel Diameters [25.4mm] DS)........... 99

Figure 6.24- Turbulence Intensities for the Profiles of Experiments 7-13 (Double-Layered Vegetation Experiments @ 12 Dowel Diameters [76.2mm] DS)......... 100

Figure 6.25- Experiment 6C, Profile 3, Measurement Point 3 (Bin Size = 0.03 m/s) 101

Figure 6.26- Experiment 11, Profile 2, Measurement Point 16 (Bin Size = 0.03 m/s) 101

Figure 6.27- Experiment 13, Profile 1, Measurement Point 11 (Bin Size = 0.03 m/s) 102

Figure A1-Velocity Profiles for Staggered Formation of 76.2 mm Rods with s/d=8 (Unsubmerged case) 114

Figure A2-Histograms for Experiment 4A (Staggered s/d=8), Profile 1 116

Figure A3-Velocity Profiles for Staggered Formation of 76.2 mm Rods with s/d=8 (Submerged case) 121

Figure A4-Histograms for Experiment 4C (Staggered s/d=8), Profile 2 124

Figure A5-Velocity Profiles for Linear Formation of 76.2 mm Rods with s/d=8 (Unsubmerged case) 130

Figure A6-Velocity Profiles for Linear Formation of 76.2 mm Rods with s/d=8 (Submerged case) 133

List of Figures | Page

Figure A7-Profiles for Single-layered Experiment 6A (Linear s/d=16) 136

Figure A8-Profiles for Single-layered Experiments 6C (Linear s/d=16 Submerged Case).. 141

Figure A9- Histograms for Experiment 6C (Linear s/d=16), Profile 1 143

Figure A10-Profiles for Double-layered Experiment 7 (Linear s/d=8 Short, Staggered s/d=16 Tall)... 149

Figure A11- Histograms for Experiment 7 (Linear s/d=8 Short, Staggered s/d=16 Tall), Profile 2 151

Figure A12-Profiles for Double-layered Experiment 8 (Linear s/d=8 Short, Staggered s/d=16 Tall)... 158

Figure A13-Profiles for Double-layered Experiment 9 (Linear s/d=8 Short, Staggered s/d=16 Tall)... 161

Figure A14-Profiles for Double-layered Experiment 10 (Linear s/d=8 Short, Staggered s/d=16 Tall)... 165

Figure A15-Profiles for Double-layered Experiment 11 (Staggered s/d=8 Short, Linear s/d=16 Tall) 167

Figure A16- Histograms for Experiment 11 (Staggered s/d=8 Short, Linear s/d=16 Tall), Profile 1 169

Figure A17-Profiles for Double-layered Experiment 12 (Staggered s/d=8 Short, Linear s/d=16 Tall) 175

Figure A18-Profiles for Double-layered Experiment 13 (Staggered s/d=8 Short, Staggered s/d=16 Tall).. 177

Figure A19-Profiles for Double-layered Experiment 14 (Staggered s/d=8 Short, Staggered s/d=16 Tall).. 183

Figure A20-User Dialog Box for Data Processing Software 185

LIST OF VARIABLES

a	Coefficient dependent upon channel shape
A	Wetted area perpendicular to flow
A_i	Projected area of the ith plant
A_p	Projected area normal to flow
A_v	Projected area covered by vegetation
b	A constant
c	Distance from the bed
C	A function designator
C_1	Vegetation density
C_2	Flexural characteristics of the vegetation
C_d	Coefficient of drag
d	Diameter of vegetation
ε_v	Skin Roughness
ε_c	Bed Roughness
f	Darcy's friction factor
F	Froude Number
F_d	Force of drag
g	Acceleration due to gravity
h	Vegetation height
h_c	Height of cavitation
H_v	Height of short vegetation
H_t	Height of tall vegetation
κ	von Karman's constant
k	Roughness height
K	Pre-multiplier
L	Length of vegetated section
m	Stem density (number/area)
MEI	flexural rigidity
n	Manning's coefficient
n_b	Boundary roughness caused by bed
n_s	Number of samples (measurements)
n_v	Number of vegetative stalks
q	Discharge per unit width
Q	Channel discharge
R	Hydraulic Radius
R_d	Reynold's number based on diameter of vegetation
R_e	Reynold's number based on flow depth
s	Spacing of short vegetation
s_t	Spacing of tall vegetation
S	Friction Slope

τ_o	Boundary shear stress
u	Velocity at distance from bed
U_*	Shear velocity
u_{*crit}	Critical shear velocity
U_s	Slip Velocity
u_{yv}	Velocity at top of vegetated layer
U	Cross-sectionally averaged velocity
U_m	Median Velocity in a set of measurements
W	Channel width
χ	A function designator
y'	Value of y at which velocity is zero
y	Distance measured from bed
y_n	Normal depth of flow
y_v	Distance to top of vegetation from bed
α	Constant exponent
β	Constant exponent
γ	Specific weight of fluid
μ	Viscosity
ρ	Fluid density
τ	Shear stress

Chapter 1
INTRODUCTION

1.1 General

Riparian wetlands are systems bordered on one or more sides by a stream of moving fresh water such as a river or creek. The characteristic feature of the ground saturation is that the water table is either at or above the ground surface for a substantial part of the water year. There is a great variety in the type and density of the vegetation in these ecosystems. Some areas may only be covered with a uniform layer of grass while others may have several layers such as grass, bushes, and trees. Though there are many biochemical and physical traits associated with each of these areas, there is one feature which is possessed by all. All wetlands act as an obstruction to the flow of water, resulting in additional resistance to flow.

Today, with growing interest on wetlands for their role in pollutant removal, flood plain management, and sediment deposition, greater focus needs to be turned to flow processes throughout these areas. Due to the density and height of the vegetation as well as the complicated flow patterns caused by its presence, traditional open channel formulations might not be suitable in describing flow in wetlands. Therefore, it is essential that fundamental research be done to quantify the effects which physical variables such as vegetation density, height, rigidity, and surface roughness have on flow through riparian wetlands.

1.2 Focus of Study

The purpose of this study is to examine the properties of flow through the vegetation typically found in riparian wetlands. Flow through riparian wetlands occurs during periods when excessive rainfall raises the water table above the ground level, or the stream actually exceeds its banks and inundates the surrounding terrain. Studies of riparian wetlands are needed to:

1. Formulate the variables characterizing the flow processes that occur in riparian wetlands.
2. Discover the shape and progression of velocity profiles as they interact with the vegetation found within the wetlands.
3. Discover the resistance caused by vegetation and determine how it will affect the sedimentation rate within the vegetated area.

1.3 Objectives of Thesis

The major objectives of this thesis are to:

1. Obtain velocity profiles for flow through simulated vegetation in order to visualize downstream profile progression.
2. Determine values for resistance caused by emergent, submerged, and double-layered vegetation for various flow and vegetation spacing conditions.
3. Examine the effects that scattered tall vegetation has on flow over and through submerged short vegetation.

1.4 Layout of Thesis

The first step in researching the resistance to flow through vegetation is to review the existing literature on the subject. Description of this previous research is described and summarized in Chapter 2. After the review of existing literature, the remaining chapters deal with procedures and results pertaining to the author's research. In Chapter 3 objectives and descriptions of this research are outlined. Chapter 4 focuses on the design of experiments through simple dimensional analysis. Experimental procedure and descriptions of equipment used during the experiments and analysis are described in Chapter 5. Results from measurements are discussed in Chapter 6. In Chapter 7, the conclusions from the research are summarized as well as a discussion of research efforts that need to be made in the future.

Chapter 2
STATE OF THE ART

2.1 General

Since the initial research of Chezy, Manning, Strickler, and countless other hydraulic engineers, much of the work done on the analysis of channel resistance relies upon the concept of a friction factor. This factor attempts to incorporate all of the channel bed and its side characteristics, which contribute to the loss of energy in flow, into a single number. Over the course of time, with the study of new aspects of flow phenomena and better understanding, many scientists attempted to move away from the use of a simplified roughness coefficient. Many researchers have performed experiments to determine empirical methods of obtaining estimates of bed shear and other characteristics from the roughness of the bed.

Sediment is not the only roughness element obstructing the flow and contributing to the loss of energy. The varieties of vegetative linings around the world cause greatly different flow patterns in otherwise hydraulically similar channels. This prompted scientists to study these patterns and resulted in large tables of Manning and Chezy coefficients related to various vegetation types. Eventually, this data was used in the formulations of n-UR diagrams such as those found in the research of Ree and Palmer (1949). A primary drawback in this system arose because density of vegetation (spacing of individual outcroppings), flexibility of vegetation, and the depth of submergence remained largely unconsidered. Some researchers have attempted to stay with the idea of a Manning coefficient and are working to correct the mentioned drawbacks of this system, while others are attempting to generalize the whole concept. The current focus in research concerning flow resistance due to vegetative flow attempts to determine resistance and shear based solely on the physical and geometrical characteristics of the vegetation.

2.2 Friction Relationships of Flow Through Channels

According to the Task Force Committee on Friction Factors (1963) , Antoine Chezy postulated in 1768 that the ratio of velocity squared to the product of the hydraulic radius and the channel slope would be constant for a given channel. The square root of this constant was later named the Chezy coefficient, and the idea of friction relationships in channels was born. It was over a hundred years later in 1889 when Manning (1889) first published the Manning's equation in the form it is used today (SI system):

$$U = \frac{R^{2/3} S^{1/2}}{n} \tag{2.1}$$

where U is the cross-sectionally averaged velocity, R is the hydraulic radius, S is the friction slope, and n is the Manning roughness coefficient. This was shown to be valid for fully rough flow conditions by Strickler in 1923 as stated in the summary by the Task Force (1963).

The first major research into the mechanics of boundary layer flows began in the early 1900's and culminated in the Karman-Prandtl relationships. The underlying concept of the formulation is that within the zone near the channel bed, velocity distributions depend only on the distance from the bed, roughness of the boundary, the kinematic viscosity of the fluid, and the flow shear velocity. The form of the derived formula used today for a rough boundary is shown in equation 2.2.

$$\frac{u}{u_*} = \frac{1}{\kappa} \ln \frac{y}{y'} \tag{2.2}$$

where u is the velocity at a distance y from the bed, u_* represents the shear velocity and is equivalent to $\sqrt{\tau_o / \rho}$, τ_o is the boundary shear stress, ρ is the fluid density, κ is von Karman's constant usually taken to be 0.4, and y' is the value of y at which velocity is zero. This result was shown by Rouse (1965) to be the underlying basis for many of the studies of velocity profiles which were to follow. From using the velocity distribution shown in equation (2.2), the discharge per unit width may be calculated through integration of the above equation and has the form:

$$q = \int_{y'}^{y_n} \frac{\sqrt{\tau_o}}{\kappa \sqrt{\rho}} \ln \frac{y}{y'} dy \tag{2.3}$$

where y_n is the depth of flow. If y' is sufficiently small, the second term after integration may be dropped, yielding the following result:

$$q = \frac{\sqrt{\tau_o}}{\kappa \cdot \sqrt{\rho}} \left(- y_n + y_n \cdot \ln\left(\frac{y_n}{y'} \right) \right) \tag{2.4}$$

The defining equation for the Darcy friction factor has the form:

$$f = 8 \frac{\tau_o / \rho}{U^2} \tag{2.5}$$

where f is the Darcy friction factor. Combination of equations (2.4) and (2.5) and simplification yields an expression for the friction coefficient of the form:

$$\frac{1}{\sqrt{f}} = a \log \frac{y_n}{y'} + b \tag{2.6}$$

where a and b are coefficients dependent upon the shape of the cross-section. Though this formula has proven to be useful in "clear" channel flow, it is no longer valid when vegetation partially blocks the channel. Adaptation of the formula to this condition is shown in detail further in the text.

2.3 Studies in Grass-lined Channels

The current research trend in the field of surface water modeling moves away from traditional empirical methods in an attempt to solve the equations of motion. In the area of wetland modeling, the trend is no different. Flow processes through wetlands exist as the culmination of many outside forces such as gravity, wind shear, bed shear, and vegetation drag. However, many researchers believe that these processes can all be accounted for by solving the equations of motion without using any empirical solutions. Though true, the amount of input data for each iteration in the solution would be enormous. Others believe that a more traditional approach is warranted and wish to modify existing methods of determining flow processes. In the following pages, discussion continues on the several methods of flow solutions as they have progressed from the early 1900's to the present in an attempt to weigh the advantages and disadvantages of each.

Since the beginning of the twentieth century, design of vegetatively lined channels has been performed through the use of curves relating the Manning coefficient (n) with the product of velocity and hydraulic radius of the channel (UxR). Examples of these curves are found in Morris and Wiggert (1963) for varying degrees of retardance. Figure 2.1 is a partial reproduction from Morris and Wiggert (1963) showing three curves A, B, and C which represent very high retardance (>30 inch grass height), high retardance (11-24 inches), and moderate retardance (6-10 inches), respectively. Morris and Wiggert (1963) state that "Although the grass length is perhaps of paramount importance in determining the degree of retardance, it should be understood that the type of grass and its stand also are significant." The stand mentioned in the previous quotation refers to the density of vegetation. One conclusion that can be drawn from Figure 2.1 is that n approaches a constant value for large values of UR.

The experiments by Ree and Palmer (1949), whose research is the basis of the above curves were limited in their scope. The preponderance of experiments conducted on various types of vegetation which lined both the banks and bed of the channel were performed in channels with slopes from 1-24% causing the vegetation to be prone from the flow of water. Very few experiments were conducted on channels with slopes less than 1 percent. Further research by Kouwen, Unny, and Hill (1969) has shown that when vegetation is prone and completely submerged by water, the values of n collapse onto a single curve. Figure 2.1 is an example of the type of curves that Ree and Palmer developed from their research. However, for flow conditions which are less than the height of the vegetation, flow resistance may increase, decrease, or remain steady with variation in water depth.

One major problem with the n vs. UR curves appears to be the effect of vegetative stiffness on the relationship. Though possible to develop curves for an individual type of vegetation in specific channels, the relationship does not necessarily hold when moved to another channel. Because different channels have different hydraulic and vegetative properties, it is reasonable to assume that flow properties in the second channel would not be the same as the first. For instance, if a plant has a higher stiffness, it has a higher resistance to bending. The effective result is a curve on an n-UR diagram higher than a curve from a corresponding channel lined with a plant having significantly lower flexural rigidity. Due to the problem with use of n vs. UR curves and experimental evidence that does not agree with the values given on the curves, many engineers have attempted to formulate a better method to model flow resistance through vegetation.

Experiments with fully submerged vegetation by Kouwen, Unny, and Hill (1969) indicate that estimation of n from the product of UR performs poorly when defining flow processes through a channel. The experiments of Kouwen et. al. elaborate upon a method proposed by Engelund (1964) who used slip velocity to maintain eddy viscosities during boundary calculations. A slip velocity refers to the formulation of a non-zero velocity condition at a boundary. If this velocity at the surface of the vegetation is subtracted from this point to the free surface, the profiles above the free surface is approximately logarithmic. Ultimately, Kouwen, et. al. (1969) developed an equation for the flow velocity in the channel which depends on two constants. These constants represent vegetative flexural characteristics and density of the vegetative mat. The major assumption made in

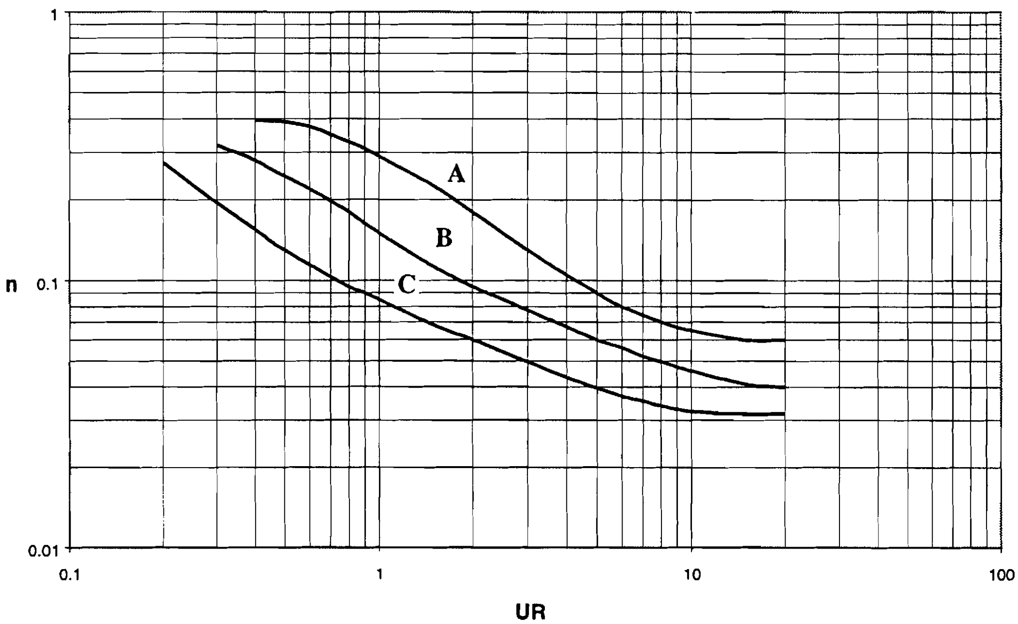

Figure 2.1: Plot of Manning's n as a function of UR for varying grass lengths.

Kouwen's work is that u_s, the slip velocity, is proportional to u_*. Kouwen, Unny, and Hill's (1969) theoretical work is summarized in the following paragraphs:

Assuming that the velocity has a magnitude of u_c at some distance c from the bed, equation (2.2) becomes:

$$\frac{u_c}{u_*} = \frac{1}{\kappa} \ln \frac{c}{y'} \tag{2.7}$$

where c is arbitrarily chosen as a distance from the bed and $u_* = \sqrt{gRS}$. If equation (2.7) is subtracted from equation (2.2) , c is set equal to y_v, and u_c is set equal to u_{yv}, where y_v is the deflected height of the vegetation (see Figure 2.2) and u_{yv} is the corresponding velocity at that height, the equation becomes:

$$\frac{u}{u_*} = \frac{u_{yv}}{u_*} + \frac{1}{\kappa} \ln\left(\frac{y}{y_v}\right) \tag{2.8}$$

which represents the velocity profile extending from the top of the vegetative layer. Figure 2.2 is a representation of a similar figure showing the velocity profile extending above the vegetative layer by Kouwen, Unny, and Hill (1969).

Integration in the same manner as equation (2.3) and simplification yields the following relationship:

$$\frac{U}{u_*} = C + \frac{1}{\kappa} \ln \frac{y_n}{\chi} \tag{2.9}$$

where y_n is the total flow depth,

$$C = \frac{1}{u_* y_n} \int_0^{y_v} u\, dy \tag{2.10}$$

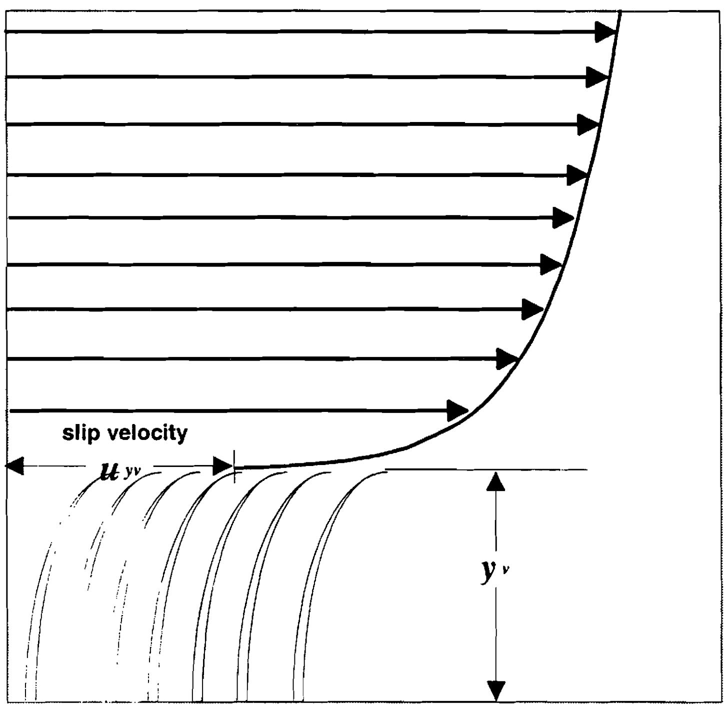

Figure 2.2: Velocity profile over vegetative layer.

and

$$\chi = y_v \exp\left(1 - \kappa \frac{u_{yv}}{u_*}\right)\left(1 - \frac{\kappa}{y_n}\right) \tag{2.11}$$

as adapted from Kouwen et al. (1969).

The final form of the equation derived by Kouwen et al. for flow retardance of vegetatively lined channels is:

$$\frac{\mathrm{U}}{\mathrm{u}_*} = \mathrm{C}_1 + \mathrm{C}_2 \ln\left(\frac{\mathrm{A}}{\mathrm{A_V}}\right) \tag{2.12}$$

where U is the cross-sectionally averaged flow velocity, u_* is the shear velocity, C_1 represents vegetation density, C_2 was determined experimentally and represents flexural characteristics of the vegetation , and A and A_V represent the total cross-sectional wetted area (ignoring vegetation) and the area overgrown by vegetation. Though this research alone was a major accomplishment in its departure from the use of the n vs. UR diagrams, Kouwen et al. believed it possible to eventually establish a correspondence between C_2 and the physical stiffness of the vegetation.

This work may be useful to determine the average velocity in a channel comprised of the types of vegetation tested in the experiments. However, it provides no insight at all into the velocity profile of flow through vegetation itself. As can be seen by equation (2.12), since the shape of the profile is unknown, this portion is set equal to the coefficient C_l which must be determined through experiments. Further experiments as reported by Kouwen et al. (1969) have shown the dependence of C_l upon the density of the vegetation.

Since the density varies greatly from site to site, this also places a strict limitation on the applicability of this research. This method also provides no way to determine the average velocity through partially submerged flow conditions which is the norm in a wetland environment. Through use of this original research, other researchers have concluded that use of the n-UR diagrams provides inaccurate results for determination of resistance in vegetatively lined channels.

A primary obstacle hindering new research is the inability to determine the flexural rigidity of plants in the field. In order to perform the necessary experiments to develop new relationships, materials must be used which accurately simulate natural vegetation. In experiments by Kouwen et. al, the vegetation was simulated using styrene strips glued to the bottom of the flume. There are many difficulties to overcome when attempting to define the flexural rigidity of plants. Though it is possible to measure the flexural rigidity of a plant, that rigidity can drastically change depending upon the cellular water content in the body of the plant. The only feasible way to simulate the behavior of such plants is to measure the rigidity at varying wetness conditions and average the result. From this, a material (probably some plastic variant) can be chosen which will adequately reproduce the estimated rigidity. The problem with using a representative material such as plastic is that it is unable to withstand or represent some of the physical processes which occur in plants when flow conditions exceed critical shear. When a critical shear exceedence develops, many plants are either broken or permanently bent. When this occurs to a majority of the plants in a given channel, the flow characteristics may be dramatically changed. Kouwen and Li (1980) discussed in some detail formulations concerning the flexural rigidity of vegetation. In their work, Kouwen and Li described separate experiments by Kouwen and Harrington (1974) and Eastgate (1966) that were performed to formulate empirical relationships between the critical shear velocity and the flexural rigidity of plants. Kouwen and Harrington (1974) based their experiments on simulated vegetation which behaved elastically throughout. The result is the following equation which predicts when the simulated vegetation will be prone.

$$u_* > u_{*crit} = 0.028 + 6.33(MEI)^2 \qquad (2.13)$$

where u_{*crit} is the critical shear velocity and MEI is the flexural rigidity in N-m^2 of a unit area which takes into account elasticity and density of the vegetation. A list of typical MEI values can be found in the article by Kouwen and Li (1980). For long and green Bermuda grass, Kouwen and Li report a range of 6.38 to 47.4 for the values of MEI. These values are dependent on stem length with longer stems having the greater MEI value.

Eastgate's experiments were performed on natural vegetation which was not completely elastic. The data from his experiments indicate that rigid vegetation will lie flat when

$$u_* > u_{*crit} = 0.23(MEI)^{0.106} \qquad (2.14)$$

Equations 2.13 and 2.14 yield very different results since equation 2.13 is for simulated vegetion behaving elastically throughout and equation 2.14 was derived from experiments on natural vegetation which was not completely elastic.

A new methodology developed by Kouwen and Li (1980) is to calculate u_{*crit} by using the smaller of the values obtained by equations (2.13) and (2.14) for estimation of the condition that will cause the vegetation to become prone. The importance of these equations relate to formulations created by Kouwen and Li describing the channel resistance relationship. The following equation was developed by Kouwen and Li to define a semilogarithmic relationship of the form:

$$\frac{1}{\sqrt{f}} = a + b\log\left(\frac{y_n}{k}\right) \tag{2.15}$$

where k is the roughness height of the vegetation which is determined from known drag and flexiblility properties of the vegetation. Kouwen and Li (1980) then developed Manning's coefficient as:

$$n = \frac{y_n^{1/6}}{\sqrt{8g}\left[a + b\log\left(\frac{y_n}{k}\right)\right]} \tag{2.16}$$

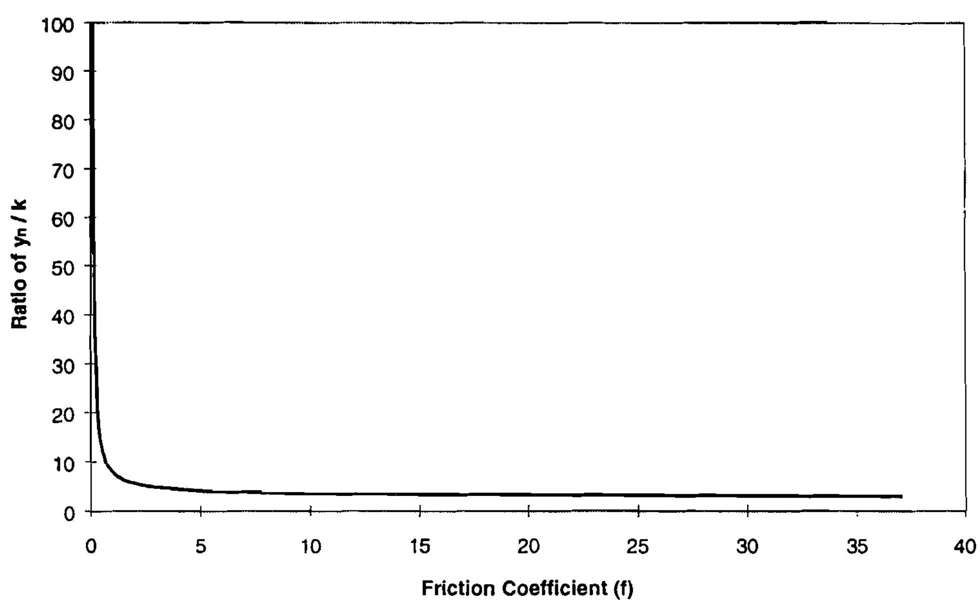

Figure 2.3. Plot of Equation 2.15 for Wide Rectangular Channel.

Kouwen and Li (1980) report that values of the coefficients obtained from values on plastic roughness are as observed in the following table:

Table 2.1: Coefficients for Equations (2.4) and (2.5)

a coefficient	*b* coefficient	Condition
0.15	1.85	$u_* / u_{*crit} \leq 1.0$
0.20	2.70	$1.0 < u_* / u_{*crit} \leq 1.5$
0.28	3.08	$1.5 < u_* / u_{*crit} \leq 2.5$
0.29	3.50	$u_* / u_{*crit} > 2.5$

Because equations 2.13 and 2.14 require the value of MEI, a method was developed for obtaining this parameter. Since it is extremely difficult to measure MEI for a given vegetation, Kouwen and Li developed a system of parameter optimization which yields an estimate of MEI. From an initial guess of MEI, *k* (the roughness height of the vegetation) may be calculated from

$$k = 0.14 y_v \left[\frac{\left(\frac{MEI}{\gamma y_n S} \right)^{0.25}}{y_v} \right]^{1.59} \tag{2.17}$$

where y_v = deflected vegetation height, $\gamma y_n S$ = the boundary shear stress, and MEI is as defined above. From this, flow rates can be calculated and compared to measured flows in an experiment. The errors between these two flows are minimized by optimizing the parameter MEI which in effect produces a better estimate of MEI for the given vegetation.

The method used by Kouwen and Li was to fit the n vs. UR curves presented earlier by optimizing MEI.

Petryk and Bosmajian (1975) attempted to construct a model of steady uniform flow assuming that gravity, drag forces on vegetation, and shear forces at the boundary are the only relevant flow forces. From these assumptions, the following equation for an estimate of the Manning n was developed (English units):

$$n = n_b \sqrt{1 + \frac{C_d \sum A_i}{2gAL} \left(\frac{1.49}{n_b} \right)^2 R^{4/3}} \qquad (2.18)$$

In the above equation, n_b represents the boundary roughness with no vegetation, R is the hydraulic radius, A_i is the projected area of the ith plant in the streamwise direction (perpendicular to the flow direction), and the term $C_d \sum A_i / AL$ represents the roughness element introduced by the presence of the vegetation . C_d is the drag coefficient for the entire canopy of vegetation, L is the channel length, and A is the cross-sectional area of flow. Petryk and Bosmajian suggest determination of the $C_d \sum A_i / AL$ term by using a known n and n_b for a known flow and backsolving equation 2.18 for $C_d \sum A_i / AL$. From this value, C_d can be assumed to remain constant for certain conditions which enables calculation of depth vs. Manning's n curves.

More recently, a study by Tsujimoto, Shimizu, and Nakagawa (1991) carried the experiments of Kouwen, Unny, and other researchers one step further by investigating the turbulence structure and velocity profiles of flow through vegetation. Although much work was done in their study in the investigations of these flow properties, a simplified model of rigid cylinders was used and it was left to future researchers to study the effect caused by the flexibility of plants.

Recent studies in Japan have applied the concept of "*honami*" to flow over vegetation. Although previously honami referred to an ordered fluctuation of grasses blown by wind in fields, the phenomena is also present in water flowing over vegetation. Though not much work has been done in applying this phenomenon to roughness parameters in rivers, Tsujimoto and Kitamura (1992) have done extensive research to determine the formation mechanism of the flow pattern.

2.4 Studies in Wetlands

Burke (1983) conducted a major field study in understanding the flow dynamics of salt water marshes. The major focus of the study was to examine the vertical flow patterns in Spartina alterniflora (a common marsh grass) under the forces of wind stress and the free surface pressure gradient. The modeling of the processes within the marsh was accomplished by collection of data relating to wind conditions, water surface slopes, water surface elevations, and velocity measurements. The method uses the $k-\varepsilon$ low Reynolds model to solve for flow conditions. Though the research does produce a model which gives good results, large numbers of finite element grid points are needed for solution and several other limitations apply as mentioned below.

In Burke's research, much emphasis was placed on the determination of an accurate method for characterizing the drag induced by vegetation. Burke(1983) states that in his research he has found that drag force is often described by the following formulation:

$$\textit{Drag per Unit Volume of Vegetated Flow} = \rho \frac{C_d a}{2} |u_i u_i| \tag{2.19}$$

where C_d is the drag coefficient and a is the density of vegetation described by the "projected area of obstruction, per unit volume at the level z, on a plane normal to the flow." This area is usually determined by field experiments through the use of grids.

Burke showed that the coefficient of drag may be represented by $C_d = b \cdot R_e^{c}$, where the Reynolds number is based on a length scale of leaves and c and b are constants. A major factor in resistance to flow through vegetation is also the angle of incidence of flow to the leaves on the vegetation. The angle of incidence is the angle measured between the plane of the leaf and the flow direction. As would be expected, as the angle of incidence increases, there is a corresponding increase in the drag by the vegetation.

Another major factor that contributes to the drag determination for a cluster of roughness elements is the sheltering effect. The sheltering effect refers to the difference in flow pattern caused by a cluster of vegetation compared with flow patterns around well-spaced vegetation. Burke described that the drag coefficient on an element in a group of elements is smaller than that for a single isolated element in steady uniform flow (this flow has same velocity as that measured between elements of clusters). Burke reported that the correlation usually found is that the coefficient of drag is approximately 3 times greater on a single element than on an element in cluster of elements. He states that although the exact cause is unknown, it is believed to be the effect of hydrodynamic interference of neighboring obstructions.

According to Burke (1983), there are several major areas which still need to be studied in order to gain a full understanding of flow processes through vegetative obstructions. He suggests more studies into the turbulent and physical nature of the obstructions such as the effect the plant geometry has on the drag values for flow. A second process to be investigated is the "sheltering" effect on C_d values. Sheltering as described above refers to the phenomenon that clustered groups of roughness elements have a lower C_d value than the sum of individual components in unobstructed flow. Finally, Burke suggests a study of the effect of skin friction on the drag coefficient. Skin friction refers to the surface roughness of the skin of the vegetation.

Another more recent study in the area of wetlands was performed by Roig (1994) at the University of California - Davis. Her study, as some previous channel models, hinged on the modeling of vegetation as non-flexible roughness elements. The primary focus of the study was to develop a flow model which adequately describes flow through a tidal wetland. Various configurations of the cylinders were tested in a laboratory flume from which measurements were taken. These results were used to create a flow model using an Army Corps of Engineers model called RMA. The RMA model was started in 1979 when the Waterways Experiment Station contracted with Resource Management Associates to create a three dimensional finite element model for sediment transport and flow. Roig used a modified version, the RMA-2V system (2-D), to model flow through the wetlands based on the data collected from flume experiments and site visits.

Kadlec (1990) points out several reasons why the resistance in wetlands should be calculated from drag on single roughness elements instead of channel bed equations. First, Kadlec (1990) points out , as stated earlier, that the Manning equation was developed for fully turbulent flow. However, conditions in wetlands do not allow the application of the Manning's formulation due to small slopes and shallow depths. Therefore instead of a constant coefficient, 'n' varies greatly depending on water depth and vegetative density. Secondly, Kadlec (1990) explores the use of the Darcy friction factor which has been used to describe flows in the transition and laminar regions. Though relationships can be derived by the friction factor approach, they are highly dependent upon water depth, bed slope, and vegetative type. In a discussion on problems with field measurements, Kadlec (1990) specifically discusses the difficulty in measuring velocity. Often the only recourse is through tracer dye studies which give a much higher velocity measurement than the actual flow through the system.

Kadlec (1990) points out that one of the most effective ways of describing flow through wetland systems is the combination of laminar and turbulent terms since both may be present. He gives the equation for drag on a single cylinder as:

$$F_d = C_d A_p \left(\frac{\rho u^2}{2} \right) \tag{2.20}$$

where F_d is the drag force, A_p describes the projected area of vegetation normal to flow, and u is the local velocity. Kadlec (1990) also points out the usefulness of the correlations between drag coefficients and the stem Reynolds number ($R_d = d\,\rho u / m$) where m is the stem density (number/area) and d is the diameter of the stem. Kadlec (1990) gives an equation for the estimation of the friction slope as:

$$S = \frac{5m\mu}{\rho g}u + \frac{md}{2g}u^2 \qquad (2.21)$$

where the first term is dominant when the Reynolds number goes below five and the second term becomes dominant once the Reynolds number reaches approximately 1000.

Kadlec simplified the relationship for a site with restricted depths and slopes to the form:

$$\frac{Q}{W} = K{y_n}^{\beta} S^{\alpha} = U_0 y_n \qquad (2.22)$$

where Q is the flow rate, K is a premultiplier, y_n is water depth, S is friction slope, U_o is the superficial velocity (velocity around y_n), and α and β are exponents. Kadlec showed that $\alpha = 1$ for laminar flow and 0.5 for turbulent flow.

2.5 Recent Studies of Flow through Rigid Cylinders

Tsujimoto, Shimizu, and Nakagawa (1991) conducted research in which velocity profiles were taken within an array of rigid cylinders. The velocity measurements were taken using a micro-propeller current meter. They used a $k-\varepsilon$ turbulence model to predict velocity profiles in the vegetated bed. Their results seem to indicate that the $k-\varepsilon$ model does a good job at predicting the shapes and magnitudes of the velocity profiles at various locations within the vegetated model for emergent vegetation. No attempt was made in the research to predict or measure profiles for a case with two distinct layers of vegetation. Hino (1981) also makes comparisons between experimental results and predictions based on a perturbation solution described in his work of velocity profiles for flow within vegetation. His results show that for a uniform density of leaves, predictions match experimental results very well. However, when a two-layered leaf distribution is used, the predicted results do not show the sharp inflections in the velocity profiles found during the actual experiments.

A piece of work which adds significantly to the area of flow through vegetation is the 1980 thesis of Hartley. Hartley's thesis focused on flow through vegetation in an unsubmerged flow condition. Experiments were carried out in a Plexiglas flume which was 6 inches wide and 8 feet long. Vegetation was simulated by .25 inch diameter Plexiglas cylinders which were 4 inches in height. Below is a table reproduced from his work showing the exact spacings that were used for the experiments.

Table 2.2: Spacings used for the experiments by Hartley (1980).

Pattern	Spacing (ft.)	Diameter (ft.)	Gap (ft.)	Density ($1/ft.^2$)
Staggered	.0781	.0208	.0573	164
Parallel	.0833	.0208	.0625	144
Random	.0833	.0208	.0625	144
Staggered	.0396	.0208	.0188	637
Parallel	.0435	.0208	.0227	528
Random	.0417	.0208	.0208	576

The primary experimental focus as dictated by dimensional analysis was to measure discharge for a constant set of depths over a range of slopes. These measurements were repeated for each of the six cylinder arrangements studied. Measured quantities included discharge, flow depth, and slope.

Regression analysis was performed on the data by first dividing it into laminar and turbulent categories using dye injection tests. Based on regression data, Hartley states that R_d, the stem based Reynold's number, appears to be a parameter significantly affecting f. Further, regression showed that the term (y_n/d) or depth of flow to vegetation diameter has a large effect on f. Further, the relationship between these two quantities appeared to be linear.

Hartley showed that Froude number based on the maximum velocity appears to have very little contribution to the overall resistance. However, when he analyzed a Froude number based on average velocity and vegetation diameter he discovered the observations shown in the Table 2.3:

Table 2.3: Froude number results as shown by Hartley (1980).

Condition	Froude Number $F = U/\sqrt{gd}$
Visible surface roughness	> .5
Surface waves on the order of cylinder diameter	> .7
Air bubble formation	>1.0
Complete aeration to channel bottom	>1.5

The effect of the bed slope on the resistance was analyzed and eventually deemed to be unimportant as an independent variable.

The purpose of the experiments by Zavistoski (1994) was to examine the local turbulence levels for flow through surface piercing vegetation. Tests included three different densities (randomly distributed) of dowels which were chosen by their wake interference patterns. The three densities were described by the percentage of the base area covered. These were 0.8, 1.4, and 6.5% of the base area respectively. All experiments were run at a cross-sectionally averaged velocity of 6 cm/s.

Zavistoski (1994) also performed experiments to characterize flow in the y (vertical) direction near the dowels. One primary focus was the study of the shift in the direction of the vertical velocity in the vicinity of the dowels. In the near bed region, turbulence intensities were the same for experiments run with and without dowels. Zavistoski (1994) confirmed that in the near-bed region, it is bed shear rather than wake interaction that dominates total shear. Further, Zavistoski states that the major effect of increasing dowel density was to increase turbulent levels so that a more uniform, bulk velocity profile was created.

2.6 Comparison of Studies

As can be seen from the preceding sections, many studies have examined the effects that vegetation has on the flow processes of fluid. In an attempt to present these studies in a form which enables more direct comparison, Tables 2.2 and 2.3 have been created and are shown on the following pages. Looking at these tables quickly reveals that many flow conditions for natural and simulated vegetation have been tested over the last few decades. Most of these studies attempt to describe flow through vegetation as a bulk flow process; however, studies such as Burke's and Roig's attempt to determine flow processes at finite grid spacings. The results obtained from the majority of studies deal with an average velocity instead of concentrating on the entire velocity profile within the vegetative layer. Equations listed in the tables appear as they do in their respective articles—no attempt has been made to convert to the system of variables used through this text. The author recommends that any interest in these equations be directed at the respective original article.

Spacings of obstructions in the studies which dealt with rigid obstructions vary from a s/d of around 4 up to a value around 30, where s is the horizontal distance between stems. Though this represents a fairly large range of spacings for the obstructions, no detailed analysis was attempted which would correlate spacing to changes in the shape of the velocity profile. Also, many of the studies assumed that the surface of the artificial vegetation was similar to that of natural vegetation. This may be valid for smoother vegetation, but is likely inaccurate in vegetation covered by rough bark. Roughness becomes a point of concern when examining the point of separation of flows around an obstruction. Movement of this point may dramatically affect the flow pattern and change the velocity profile as well as the drag coefficient. Another source of error which may creep into experiments comes from the resistance caused by the walls of flumes and channels. Even though the wall effect is a well known phenomenon which may dramatically affect flow in smaller flumes, none of the papers examined mentioned any correction techniques used. This could dramatically affect results from experiments in flumes which have a small width to depth ratio of flow.

Many of these studies yield results which are gleaned by making many assumptions as can be seen in Tables 2.2 and 2.3. Though these studies may be useful for the problem at hand to the research team, the restrictions may be too large to allow wide application to other sites. Due to this problem, research needs to be performed which will illustrate the fundamental effects that major variables, such as surface roughness and spacing, have on the velocity profiles and bulk resistance. The sensitivity of flow properties to these factors will enable researchers to determine applicability of previous results to other sites.

Table 2.4: Summary of Experiments using Cylindrical Non-Flexible Obstruction to Simulate Flow through Vegetation

Researcher	Date of Publication	Flume Width (feet)	Flume Length (feet)	Plant Submergence	Flow Regime	Hydraulic Data Collected
Hsieh	1964	2.5	30	Studied only partially submerged conditions.	Studies were performed in subcritical and supercritial ranges	A dynamometer was used to determine force on piers, discharge by manometer. and depth by point gage.
Li and Shen	1973	Plot width of 32.5 - 40 feet.	Plot length of 40 feet.	Method is only valid to calculate flow response due to cylindrical obstructions; only emergent (tall vegetation) conditions are important to analysis.	Steady, fully developed, uniform, subcritical flows (based on cylinder Reynold's #).	Average Bulk velocity, Avg. Boundary shear stress, and sediment transport rate.
Hartley, D.	1980	6 inches	8 feet	Tests were run for shallow flow (emergent vegetation)	Flow was maintained as uniform by using stop logs.	Discharge was measured over a constant set of depths for varying slopes and arrangements.
Tsujimoto, Shimizu, and Nakagawa	1991	1.64	39.4	All experiments were conducted under submerged flow conditions. However, the uniform velocity distribution was described for emergent conditions.	Turbulent flow, practically uniform due to weir downstream, velocity profile reached equilibrium at about 20 times	Use of micro-propeller currentmeter and hot-film anemometer enabled velocity and Reynold's stress measurements
Tsujimoto and Kitamura	1992	1.31	39.4	Limited to emergent conditions because flow over vegetation would cause the predominance of three - dimensionality.	All subcritical flows. More precise details were not given.	Use of micro-propeller currentmeter and capacity liminimeter to measure depth and velocity of flow.
Roig, Lisa	1994	1.5	>10	Emergent and submerged conditions were tested. Equations developed are valid for depth of flow less than 1.3 times the maximum height of vegetation	All flow was subcritical with depth Reynold's numbers in the range of 5440 to 58200.	Head loss distribution using five piezometer tubes.
Thornton, C.	1995	Simulated stream constructed in area 18 feet wide.	59	Emergent and submerged conditions were tested for various rigid and flexible natural vegetation lengths and types. (Corn, carex, sod, and field mix.)	Steady, subcritical flows were used in all tests. Three discharges used to model low, medium. and high flow.	Seven piezometers to calculate flow depth. Velocity and sediment yield were measured.

Table 2.4: Continued....

Researcher	Date of Publication	Equations	Major Assumptions and Restrictions	Model Description
Hsieh	1964	$C_R = \frac{F}{\frac{1}{2}\rho V^2 dD}$	Major restriction is that this study dealt specifically with bridge piers, which meant it ignored many of the factors which are found in vegetated areas.	Simulated cylindrical bridge piers were placed in flume at various spacing conditions.
Li and Shen	1973	Refer to paper. Used method developed by Petryk to calculate the drag coefficient. Main focus was to determine what plant configuration produced highest sediment yield.	Spacing of cylinders must be at least 3 diameters in transverse direction and 6 diameters in downstream direction.	No detailed description; however, cylindrical elements of .5 ft diameter were used.
Hartley, D.	1980	See text of thesis for major equations and review of previous literature.	Width of flume is small. Few arrangements of dowels were tested.	Vegetation was constructed using .25 inch Plexiglas cylinders, 4 inches high ground square and glued to the base.
Tsujimoto, Shimizu, and Nakagawa	1991	Refer to paper. Equations were developed using a k-E turbulence model in the 2-dimensional equations of turbulent flow.	Did not take into account fluctuations of vegetation due to flow which may have a significant impact upon flow structure over the bed.	Bottom of flume was acrylic plate with 3 meter smooth bed reach upstream of vegetative layer.
Tsujimoto and Kitamura	1992	Refer to paper for description of flow properties due to transverse flow. Primary focus was to develop trends and not empirical relations.	Did not test conditions for flow over vegetation because of the complexity of 3 dimensional flow.	Partial vegetation was situated along one side wall, with an acrylilc resin plate covering bed of other side.
Roig, Lisa	1994	$F = -0.0909\rho u^{2}(1-\eta)\Re'^{1/2}\left(\frac{h}{s}\right)^{1/2}$	Assumed roughness of dowels was similar to natural vegetation. Results are only valid for plants which have similar surface roughness as dowels. Never took into account wall shear.	Plywood base of 3/8 inch using 3/8 inch diameter wooden dowels with a test section of 8 foot length.
Thornton, C.	1995	See text of publication for major equations.	Assumed base weight of vegetative plug was constant for all samples. Did not take into account changes due to different bedload compositions.	Concrete capped channel with vegetative inserts in both meandering and straight sections of channel.

Table 2.4: Continued....

Researcher	Date of Publication	Spacing of Obstructions	Slope (ft/ft)	Contribution from Experiment
Hsieh	1964	Spacings of 5, 6, 7.5, 10, and 30 were simulated (in a single row).	Not Given	The major emphasis of this study is to desribe the effect that the Froude number has on drag for cylindrical pier spacings. Shows that for supercritical flow, the resistance coefficient is independent of spacing.
Li and Shen	1973	Square and triangular spacing at various row intervals.	0.002	Determination of configuration of vegetation which produces the highest sediment yield for a given flow condition.
Hartley, D.	1980	6 spacings were used: 2 staggered, 2 parallel, and 2 random	Varied	Major trends in surface conditions were noted and recorded. In addition, changes in dicharge were related to changes in configuration and slope for constant depths.
Tsujimoto, Shimizu, and Nakagawa	1991	Arranged in equi-spacing (1 cylinder in a square s x s). The two spacings used were 1 and 2 cm. Heights were 4.1 and 4.6 cm and diameters 0.1 and 0.15 cm.	Not Given Probably 0	Describes change in suspended sediment transport in a vegetated sand bed channel due to bed vegetation density.
Tsujimoto and Kitamura	1992	Placed in a square pattern at equal spacing (exact dimensions were unspecified), vertical cylinders with equal diameter and height used as model plants.	Not Given	Describes mixing and water surface fluctuations across transitional boundary in compound channe. Shows the presence of flow shearing between the two zones. A transverse velocity was observed which was largely dependent on water-surface fluctuation.
Roig, Lisa	1994	s/d= 4 s/d = 6 s/d = 8 s/d = 12 Uniform and non-uniform height.	0	The major contribution was the formulation of the given equation which estimated the bulk vegetative resistence force to emergent or shallowly submerged flow over stiff vegetation with a similar surface roughness to wooden dowels.
Thornton, C.	1995	Varied because of differing diameters of vegetation; however, lowest density was around 5000 stems/ sq. meter.	0.004	Determination of which natural vegetative types and lengths produced the highest sediment yield. Development of equations to estimate sediment yield and the amount of sediment entrained. Observed effects of oscillation of vegetation.

Table 2.5: Summary of Experiments using Flexible Strips and/or Natural Vegetation

Researcher	Date of Publication	Plant Submergence	Flow Regime	Equations
Kouwen, Unny, and Hill	1969	Submerged during all flow tests in this study.	Practically uniform. Slopes .0005 - .01. Depths 15 - 40 cm. Discharge .0027 - .1421 cms.	$\frac{U}{u_*} = C_1 + C_2 \ln\left(\frac{A}{A_v}\right)$
Petryk and Bosmajian	1975	For the theoretical work done here, flow depth is assumed to be less than or equal to the vegetation height.	Derivation of equations are for steady, uniform flow.	$n = n_b \sqrt{1 + \frac{C_d \sum A_i}{2gAL}\left(\frac{1.49}{n_b}\right)^2 \left(\frac{A}{P}\right)^{4/3}}$
Chen	1976	Used natural vegetation. Seems to have used results from both submerged and emergent vegetations.	Slopes 0.001-.555. Tests used laminar flow conditions. Used data from other regimes by other researchers.	$f = \frac{510{,}000 S_o^{0.662}}{R}$
Kouwen and Li	1980	Not stated. A large amount of previous data from natural vegetion experiments was used to give estimates of MEI.	Not stated. From data, probably for fully rough, turbulent case.	$k = 0.14h \left[\frac{\left(\frac{MEI}{\gamma y_n S}\right)^{0.25}}{h}\right]^{1.59}$
Burke	1982	All sorts of vegetation, natural and artifical were tested in this study. Rigid cylinders, flexible plastic strips, and natural vegetations were used.	Tidally steady, tidally unsteady, and wind driven flow. Solves the Navier-Stokes equations with various assumptions.	See paper for equations. There is a large quantity reported and explained in the work.
Hammer and Kadlec	1986	Not explicityly stated; however, uses same underlying equation as the Kadlec 1990 work and emergent condition is assumed to be prevalent	Not stated. However, uses same flow distribution equation as Kadlec 1990.	$w\Phi_c \frac{\partial s}{\partial t} = \frac{\partial}{\partial z}\left(\alpha d^{\beta+1} w \frac{\partial h}{\partial z}\right) + w(P - E + A - I)$
Kadlec	1990	Never explicitly states the submergence condition; however, analysis of resulting equation shows that an emergent condition is assumed to be prevalent.	According to paper, results are valid for turbulent, laminar, and transitional flow.	$\frac{Q}{W} = K d^{\beta} S^{\alpha} = V_0 \hat{d}$
Masterman and Thorne	1991	Not directly relevant to this study.	The equations in this study have been derived for a turbulent flow condition.	$y_l = y_r = \frac{dk}{3.5 D_{84}}$
Ikeda and Kanazawa	1996	Tested for submerged conditions.	Turbulent Flow	See article for equations relating to flow conditions.

Table 2.5: Continued.....

Researcher	Date of Publication	Major Assumptions and Restrictions	Analysis	Contribution from Research
Kouwen, Unny, and Hill	1969	The study doesn't attempt to study flow structure within vegetative layer. This causes a lump estimation of this flow into one of the coefficients in the equation.	The equation has constants which must be verified by tests in any new condition. C_1 is very channel dependent. More studies need to verify adaptibility to new channels.	Research yields a method for determining flow through vegetation once certain constants are identified for a particular channel.
Petryk and Bosmajian	1975	Velocity is assumed to be low to prevent plant bending. Assumed uniform distribution of vegetation in transverse direction. Large variations in velocity do not occur over flow depth. Approach velocity to each plant is the same.	From results shown in comparison to US Dept. of Agriculture Data, the estimation of vegetation density which comes from the equation seems to be an overprediction (although published results are within the same order of magnitude.)	The equations predect the variation of Manning n with depth. Provides a way to estimate vegetation density by a measured value of Manning's n or vice versa.
Chen	1976	Restricted to turf which has physical characteristics similar to Kentucky Blue grass and Bermuda grass.	The study seems to yield a good estimate of how laminar flow on the stated turf reacts to differing bed slope conditions.	Provides an estimate of f for a channel given a bed slope and Reynolds number.
Kouwen and Li	1980	Assume that channel can be divided into sections which have uniform flow properties.	Cannot really analyze this artical because no comparison to real situations was discussed. Some experiments for predicted results vs. actual need to be performed.	Provided a method by which to design a channel with a specific vegetative lining and cross-section.
Burke	1982	Assumes a hydraulically smooth boundary (bed). Does not take into account the effect of vegetative skin friction on flow.	The paper provides a model for flow through vegetation. It was applied to circular cylinders, flexible vegetation, and natural vegetation all with seemingly good results when compared to observed values.	Provides an excellent review of research done prior to this paper. Yields a flow model which the paper states does not need a lot of adjustment to contants when doing new studies.
Hammer and Kadlec	1986	To accurately use the model, a large variety of field parameters are needed. This causes the model to be very site specific.	Many more studies would have to be done to test the validity of the results to other sites. Also, at first glance, it can be seen that with the correct choice of variables for the Kadlec 1990 equation and manipulation, the Manning equation is revealed.	This research gives a one dimensional finite difference model for calculation of water surface conditions in wetlands. However, a large amount of calibration time and data would be needed to adequately describe actual conditions.
Kadlec	1990	Assumes that depth and slope is restricted in the wetland of choice. The results yielded in this investigation are extremely site specific.	Basically the results of this paper are to use a power law of a particular form in a curve fitting exercise to estimate discharge. Gives excellent discussion on previous work in the field and its implications.	Yields a method of estimating the volumetric flow rate through parameters identified in field visits.
Masterman and Thorne	1991	The study assumes that no trees or vegetation greater than water depth are present. Requires prediction of shear stress distribution. Requires bed to be non-vegetated (compound channel).	This method as presented appears to give a good idea of the effect vegetation has on channel capacity. It is based largely on the work of Kouwen and Li regarding use of effective roughness height.	Yields a method which may be used to give an idea of how changes in bank vegetation will effect the discharge capacity of a channel.
Ikeda and Kanazawa	1996	Restricted to flow above a flexible canopy.	Was focussed on the structure of turbulent flow and organized vortices.	Shows that the velocity profile has an inflection near the top of the plant layer, turbulent intensity and Reynolds stress become stronger near the top of vegetation.

2.7 Summary

An attempt has been made here to summarize the large amount of research that has been performed to characterize flow through vegetation. The research shows that although much has been done to characterize the resistance to flow through vegetation, there are areas where there has still been little or no research focus. One such area is the flow through double-layered vegetation. Double-layered as mentioned in this report will refer to a flow moving through an area covered with two major interdispersed clusters of vegetation--one shorter, and the other tall enough that it is not likely to be submerged. Although measurements of profiles in single-layered vegetation have been taken recently by several researches mentioned in the previous section, to the author's knowledge, none have been performed which will characterize changes in the profiles caused by the presence of two-layers of vegetation as commonly found in riparian wetlands. These measurements will be necessary for any future research which attempts to create a more general model for flow through any type of vegetation.

Chapter 3
OBJECTIVES AND DESCRIPTIONS OF RESEARCH EFFORTS

3.1 General

After conducting the literature review summarized in the previous chapter, several areas of research in flow processes through vegetation appear to be lacking, or nonexistent. As mentioned in the introduction, the efforts of this research will deal solely with rigid vegetation. Following is a list of the major objectives comprising the experimental portion of this research.

1. Study the effect that plant density has on flow through vegetation.
2. Study the effect that two representative heights of vegetation have when imposed on each other.
3. Study the resistance caused by various plant densities in emergent, submerged, and double layered cases.
4. Examine the statistical distribution of measurements taken for each condition.

These objectives have guided the formulation of experiments and analysis of results described in subsequent chapters.

3.2 Effect of Plant Density

A portion of this study deals with analyzing the effect that plant density variation has on flow characteristics. In order to accomplish this goal, several densities were tested while holding as many parameters constant as possible. In addition, Plexiglas was used to construct all of the models for the experiments in order to minimize the effects of skin roughness and focus on form roughness. Skin roughness refers to drag caused by the roughness on the surface an obstacle while form roughness refers to drag caused by the presence of an obstacle in flow. Li and Shen (1973) performed extensive testing of various configurations of cylinders. They showed that the mean drag coefficient for a system of staggered cylinders decreases with increasing dowel density, while in parallel (square) configurations the mean drag coefficient increases with density. The purpose of the present research is not to repeat the efforts of Li and Shen (1973); however, an attempt has been made to confirm their results while focussing on the goals and objectives of this thesis.

3.3 Effect of Double-layered Vegetation

As mentioned previously, a common characteristic of riparian wetlands is the presence of at least two major layers of vegetation. A lower layer consists of the tall grasses commonly identified with wetlands. The second layer is made up of tall vegetation including trees able to thrive in these saturated areas. Currently, little research has been conducted which focuses on flow through the two distinct layers of vegetation (double-layered flow phenomenon). The only source of research that the author has found into double-layered flow is a study by Petryk and Bosmajian (1975). That study was performed on shorter vegetation, such as cotton and wheat, and extrapolated to flow through a heavily wooded flood plain. The purpose of the research presented in this report will be to identify the effects that two distinct layers of vegetation have on flow characteristics.

3.4 Resistance of Cylinders

As one would expect, the presence of any obstruction to flow will act to retard flow and increase depth. There will be little emphasis on development of bulk resistance (total resistance throughout a channel section) formulations based on the resistance caused by the presence of the simulated vegetation in this report. Many other researchers have focused on the resistance caused by cylinders in their research (see Chapter 2). Therefore, extensive testing of resistance coefficients has not been performed in this study. However, an equivalent Manning's n was calculated for each experiment for comparison to the control runs.

3.5 Measurement of Velocity Profiles

The major focus of this report is to measure and characterize changes in velocity profiles resulting from variations in density and spacing of vegetation for emergent, submerged, and double-layered flow conditions. Velocity profiles taken for all of the experiments are shown in the Appendix of this report. To the author's knowledge, no other study has undertaken the task of measuring the progression of velocity profiles in flow through vegetation.

3.6 Summary

As outlined above, a basic understanding of the effects that the variables related to flow through vegetation have on flow conditions is needed. Previous research has concentrated on measurement of flow resistance through rigid and flexible vegetation. However, little research into the transformation of velocity profiles caused by the presence of these obstructions has been undertaken. Measurement of changes to velocity profiles will aid researchers in understanding the effects of variability in density, spacing, height, and form roughness of vegetation. The research contained within this thesis focuses on changes in density and height, leaving the other variables for future research. The focus of the following chapter is a dimensional analysis of important variables for this research effort.

Chapter 4
DIMENSIONAL ANALYSIS

4.1 General

Experiments have been carried out for several setups. Each of them tests the variation in flow parameters resulting from changes in the physical characteristics of the vegetation. Differences in the important variables for these experiments necessitate the need for the performance of several different dimensional analyses. The dimensional analysis below will begin in a general form and be carried on to the specific experimental setups based on stated assumptions.

The purpose of the following analysis is to identify the important variables describing flow for these experiments. Once important variables are listed, those that have little effect in these experiments are dropped. The final group of variables will guide design of the experiments. Examination of experimental results may yield understanding into the relationships between these variables. This final step will be carried out in chapters 5-7.

4.2 Description of Variables

Variables defining flow properties and channel geometry in a test section are shown in table 4.1 for the general flow case. From this, the case for unsubmerged flow, submerged flow, and flow in double-layered vegetation will be analyzed.

For the general case, the variables describing the various model parameters are as follows:

$$f_1(D, H_v, H_t, d, s, s_t, \varepsilon_v, \varepsilon_c, U, y_n, EI, S_f, g, \rho, \mu) = 0 \tag{4.1}$$

Table 4.1: Relevant variables to be used in dimensional analysis of experiments

Variable	Units	Description of Variable
F_d	F	Drag force on system
H_v	L	Height of vegetative layer 1
H_t	L	Height of vegetative layer 2
d	L	Diameter of vegetation
s	L	Spacing of vegetation (linear/staggered short vegetation)
s_t	L	Spacing of vegetation (linear/staggered tall vegetation)
ε_v	L	Skin roughness of vegetation
ε_c	L	Bed roughness of channel
U	L/T	Average velocity through channel
y_n	L	Depth of normal flow
EI	FL^2	Vegetative stiffness
S	-	Friction slope
G	L/T^2	Acceleration due to gravity
ρ	FT^2/L^4	Density of fluid
μ	FT/L^2	Dynamic viscosity of fluid

All fifteen variables are described by three basic dimensions: length, force, and time. From this information, the Buckingham Pi theorem states that the number of dimensionless parameters obtained is twelve for this experiment. The repeating variables chosen to perform the dimensional analysis are velocity (U), diameter of vegetation (d) which is assumed to be constant, and the density of fluid (ρ). Determination of the dimensionless parameters results in the following quantities.

$$f_2\left(\frac{F_d}{\rho U^2 d^2}, \frac{H_v}{d}, \frac{H_t}{d}, \frac{s}{d}, \frac{s_t}{d}, \frac{y_n}{d}, \frac{\varepsilon_c}{d}, \frac{\varepsilon_v}{d}, \frac{EI}{\rho U^2 d^4}, S, \frac{g\,d}{u^2}, \frac{\mu}{\rho U d}\right) = 0 \quad (4.2)$$

As stated previously, this contains the dimensionless parameters for the generalized case. The spacing terms (s and s_t) used in the above equation may be for either the linear or staggered arrangement of dowels. For a definition of this term, see Figure 5.5. Equation 4.2 will be simplified and further analyzed for each of the specific cases evaluated in the experiments. The first analysis will be performed for the emergent vegetation case.

4.3 Analysis of Single-Layered Vegetation with Rigid Stems (Unsubmerged)

For the emergent vegetation case and with the use of rigid dowels to simulate the plants several of the parameters can be dropped initially. These parameters are the quantities describing the height of the vegetation, the height and spacing of the tall vegetation, and the flexural rigidity of the vegetation. The vegetative heights, H_v and H_t, may be dropped because the vegetation is emergent, extending throughout the depth of flow. Flexural rigidity is considered to be infinite for these experiments because the force created by the flow is unable to bend the rigid dowels. This means that the rods remain vertical (e.g. EI=constant) throughout the experiments and this term can be dropped. The spacing term s_t is dropped because tall vegetation is not used in these experiments. The spacing parameter, s, (see Figure 5.5) describes both the staggered and linear arrangement and may be inserted for the linear parameter at any time without bias. Once these parameters are removed, equation 4.2 becomes:

$$f_3\left(\frac{F_d}{\rho U^2 d^2}, \frac{s}{d}, \frac{y_n}{d}, \frac{\varepsilon_c}{d}, \frac{\varepsilon_v}{d}, S, \frac{g\,d}{U^2}, \frac{\mu}{\rho U d}\right)=0 \tag{4.3}$$

Examination of the last two terms of equation 4.3 reveals the Froude number and the Reynolds number. Both of these parameters may play an important role in the analysis of the unsubmerged flow case and will remain in the analysis at this point. It is impossible to maintain both Reynolds and Froude similitude when moving from a model to a prototype. This is because maintaining Reynolds similarity requires that the product LU (length x velocity) be maintained, while Froude similarity requires that the quotient U^2/L be maintained. Clearly, these two parameters cannot be maintained simultaneously. Froude number must be considered since the plants pierce the free surface and cause wave formation. Reynolds number must be studied since flow rates are high enough that the viscous and inertia terms should be important in describing the flow characteristics.

For the condition of a smooth surface (approximately no skin roughness) obtained through the use of Plexiglas dowels for all of the surfaces in the experiments, the two roughness terms may be removed from the analysis due to their relatively small contribution to the overall drag (flow resistance). The equation is further reduced to:

$$f_3\left(\frac{F_d}{\rho U^2 d^2}, \frac{s}{d}, \frac{y_n}{d}, S \quad, F, R_e\right) = 0 \tag{4.4}$$

This is the furthest simplification of parameters that can be made before analysis of experimental data is performed. The outcome of such analysis may reveal relationships between variables which will further simplify the relationship for the unsubmerged flow case.

4.4 Analysis of Single-Layered Vegetation with Rigid Stems (Submerged)

The analysis for the submerged flow case is virtually identical to that for the emergent case. One exception is that the height of the vegetation becomes important in describing the flow through and over the vegetation. Another major difference is that the surface piercing effects of the vegetation are eliminated since the dowels are completely immersed in flow. However, shallow submergence still causes the formation of surface deformations due to the presence of the vegetation. Therefore, Froude number is still considered at this point to play a considerable role in describing the flow properties. The following dimensionless parameters describe the flow through submerged vegetation:

$$f_4\left(\frac{F_d}{\rho U^2 d^2}, \frac{s}{d}, \frac{H_v}{d}, \frac{y_n}{d}, S, F, R_e\right) = 0 \qquad (4.5)$$

4.5 Analysis of Double-Layered Vegetation

The depth of flow for the double-layered flow case is above the level of the shorter vegetation and below that of the taller vegetation. The two additional parameters that become important for these experiments are the height and the spacing of the taller vegetation. Following are the dimensionless parameters which describe flow through the double-layered vegetation.

$$f_5\left(\frac{F_d}{\rho U^2 d^2}, \frac{s}{d}, \frac{s_t}{d}, \frac{H_v}{d}, \frac{H_t}{d}, \frac{y_n}{d}, S, F, R_e\right) = 0 \qquad (4.6)$$

Since this research effort is dealing with simulation of flow in riparian wetlands, it is assumed that the taller vegetation is never submerged by flow. This will allow the elimination of H_t as a parameter in the above equation. The elimination of the term results in the following list of variables.

$$f_5\left(\frac{F_d}{\rho U^2 d^2}, \frac{s}{d}, \frac{s_t}{d}, \frac{H_v}{d}, \frac{y_n}{d}, S \ , F, R_e\right) = 0 \tag{4.7}$$

4.6 Summary

The first step of the above analysis was listing all variables that are important in determining flow through vegetation. This list was simplified by removing insignificant variables for each flow case. The goal was to provide a simplified list of dimensionless variables around which to base the experimental design of this research. Although many of the variables have been eliminated, there are still many left in each flow case. It is uncertain at this point if the first term which corresponds to drag may be eliminated. This may be done if it can be shown that S, the friction slope, adequately describes resistance in each case.

The remaining parameters will be used in formulation of an experimental design. For the purpose of the experiments, many of the variables will be held constant in order to begin the formulation of relationships between variables. The major variables studied during these experiments are the spacing parameters for both short and tall vegetation. Friction slope, channel bed slope, and dowel heights were held constant throughout these experiments. Experimental conditions and methods are described in detail in the following chapter.

Chapter 5
EXPERIMENTAL APPARATUS AND PROCEDURE

5.1 General

The objective of this chapter is to describe the equipment and laboratory methods used for the experiments described within this report. Experiments have been designed to make maximum use of the equipment available while minimizing problems such as channel wall effects. All relevant material relating to the methods of operation of this equipment will also be introduced in this chapter.

5.2 Laboratory Equipment

All experiments were performed in a tilting recirculating laboratory flume located in the Hydraulics Laboratory of the Civil Engineering Department at Virginia Polytechnic Institute and State University. The channel of the flume is constructed from Plexiglas and has approximate dimensions of 4.86 meters (16 ft.) in length, 0.305 meters (1 ft.) in width, and 0.610 meters (2 ft.) in height. The flume is equipped with two pumps delivering inflow from two large orifices 3 inches in diameter. Manometers are attached to the flume that allow measurement of discharge through the orifices. The maximum flow through each orifice is approximately 0.0057 m^3/s. The flume was equipped with a tailgate which was used to decrease the effect of the M2 drawdown curve, a problem that is typically encountered in relatively short flumes. The M2 drawdown curve causes the water surface to slope down towards the end of the flume at the outlet; thus becoming non-uniform. In an attempt to diffuse the inflow, a screen is located at the upstream end of the flume for use as an energy dissipation mechanism. In Figure 5.1 a photograph depicts the flume which was used for the experiments.

Flow rates in the flume were calculated by using the flow curves and equations provided by the flume manufacturer. These equations use energy information to calculate flow rates from reading two differential manometers attached to the flume. Prior to the experiments flow equations were validated through measurement of velocity profiles and the use of integration to calculate the flow rate. Flows calculated by the flow equations and velocity profile integration were not significantly different; therefore, the manometers were used to monitor flow conditions for the remainder of the experiments.

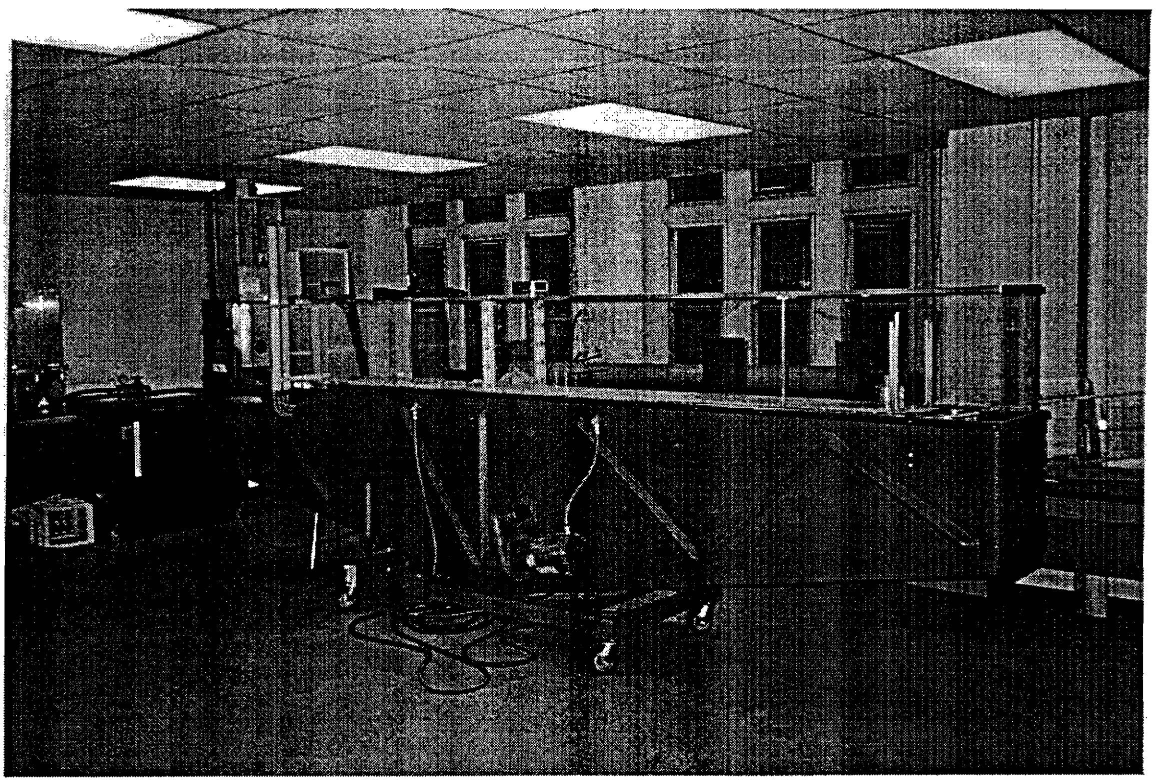

Figure 5.1 Photograph of flume used for experiments.

Measurement of the bed slope of the flume was performed using a WILD N3 optical micrometer. A slight bow in the bottom of the flume causes the tail end to have a negative slope. Due to this, the flume was tilted in order to ensure that the slope was always positive. The average slope on the flume measured by the micrometer was 0.0030 m/m. Experiments and control runs performed were at this slope.

Velocity measurements taken during the course of the experiments were measured by Dantec's 1-D laser doppler velocimeter. The instrument is a helium-neon class IIIb laser with a maximum data rate of approximately 800 Hz. Maximum measurement detection range for the instrument is between -40 m/s and 200 m/s, which enables measurement of flow in the negative (upstream) direction. The velocity probe is cylindrical in shape with dimensions of 275 mm in length and 60 mm in diameter. The probe was mounted on the device shown in Figure 5.2 and took measurements by emitting the laser beam through the Plexiglas side of the flume. The back scatter (reflection) from the beam is collected from the front probe lens and sent through a fiber optic cable to the processor unit. The processor unit converts the reflected beam into a velocity measurement and stores it on a personal computer for later analysis.

The mounting device for the laser was built from wood and supported a large threaded rod. A track located on the front of the mount guided the laser probe in the positive or negative vertical direction. Vertical increments were measured to confirm that one revolution of the threaded rod corresponds to a change of 2.31 mm in elevation of the probe. These results were tested to ensure their accuracy over the entire range of elevations used for the experiments.

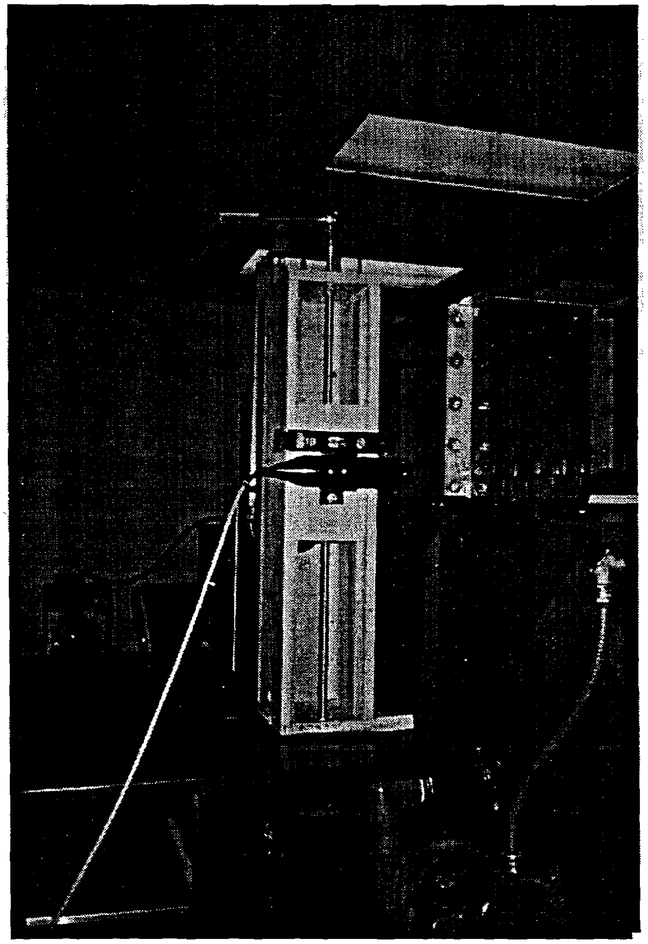

Figure 5.2 Mounting apparatus used to hold the laser probe during experiments.

5.3 Wetland Model Construction

The base of the wetland model used during the experiments were constructed of 0.953 cm (3/8 inch) thick Plexiglas. Plexiglas was used due to its low coefficient of roughness and because it will not warp with time like wooden bases. The base for the model was made of three Plexiglas rectangular sections which each measured 0.305 meters (1 ft.) in width and 1.22 meters (4 ft.) in length. These sections were placed in series in the bottom of the flume to give a total model section base length of 3.66 meters (12 ft.). Twelve mounting screws attached the base to the channel bed. To ensure a proper seal around the base, waterproof weather stripping was used between adjacent sections and between each section and the walls of the flume.

Plexiglas rods of 0.635 cm (¼ inch) in diameter were used to simulate rigid vegetation. Again, the choice of Plexiglas was primarily to eliminate the presence of skin roughness in the experiments. The rods were attached to the Plexiglas base by drilling 0.635 cm (¼ inch) diameter holes in the base and hammering in the rods until they were flush with the bottom surface. The holes were drilled using a drill press to ensure that all rods were exactly perpendicular to the base of the model. The test section with holes covered approximately 3.05 meters (10 ft.) of the Plexiglas base.

5.4 Control Experiments

To be able to analyze experimental data, there must be control runs with which to make a comparison. The control experiment for this set of measurements consisted of depth measurements and velocity profiles for the bare flume case. Bare flume refers to the condition where there are no dowels attached to the base. Because there is a large M2 draw-down curve at the lower end of the flume, stop logs were used to maintain uniform flow as closely as possible. The "stop logs" consist of 0.635 cm (¼ inch) diameter dowels which have been cut to stretch across the width of the flume. A picture of stop logs in place can be seen in Figure 5.3. This method was also used to maintain uniform flow in experimental runs.

Several velocity profiles were taken to ensure that the flow had developed into the common logarithmic velocity profile. One of the profiles from a control run can be seen in Figure 5.4. As mentioned above, these profiles were integrated to obtain discharge, ensuring that the manometers were giving accurate discharge readings. These runs were also used to measure the normal flow depth for each of the experimental flows. The normal depth was used to calculate the Manning roughness coefficient for the Plexiglas bottom of the empty channel, which is 0.007 for both flow rates. Flow rates used during each experiment are described in detail in the following section.

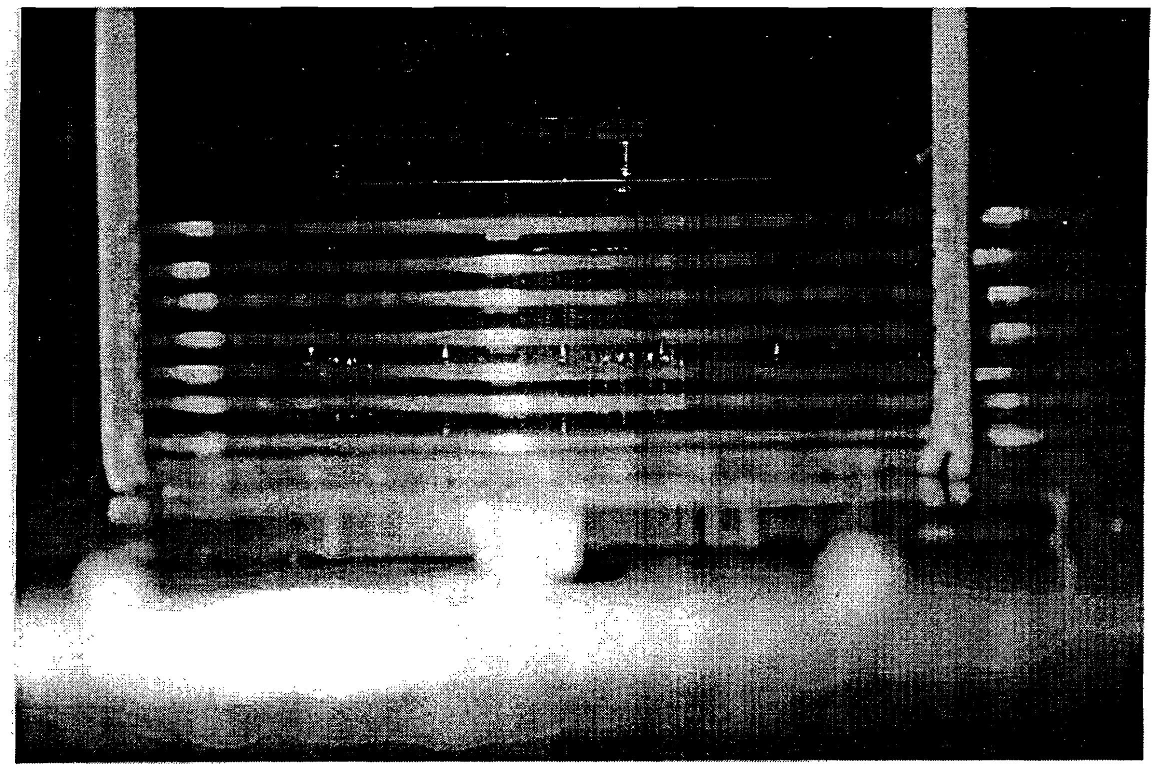

Figure 5.3 Photograph showing the placement of stop logs.

5.5 Experimental Procedure

The experiments consisted of several distinct runs, each attempting to isolate the effect that density and flow rate have on the overall flow pattern. Tables 5.1, 5.2, and 5.3 in the following sections show the sequence of experiments as performed. This includes experiments for the single layered emergent, single layered submerged, and double layered conditions. These tables also include the flow rates used for each experiment and the locations of profile measurements.

The attempt was made to take several thousand measurements at each location over the span of 20-30 seconds. A primary reason for this was to ensure that measurements were

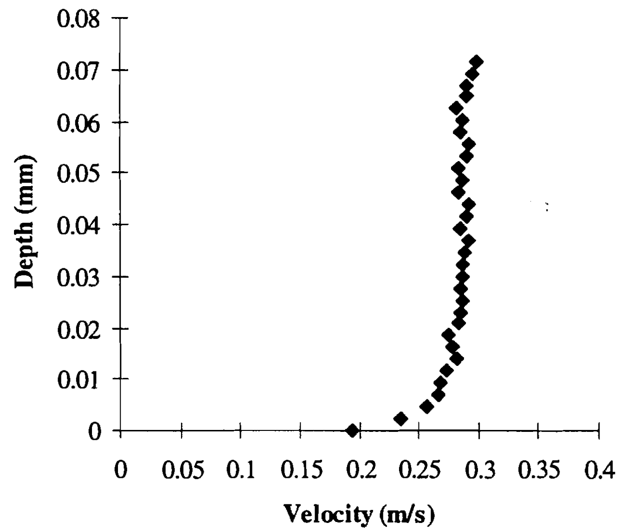

Figure 5.4. Typical logarithmic velocity profile taken during a control run

taken over a period long enough that all data was not captured inside an individual turbulent fluctuation. Second, there was a desire to statistically analyze the data. In order to achieve this goal, a relatively large sample was needed to achieve good results during statistical analysis.

At optimal operating conditions, the laser doppler unit was found to be able to take approximately 800 measurements per second. This sampling rate was too high to produce the desired number of samples over the measurement period. Therefore, artifical dead time was introduced to enable the measurement of approximately 5000 points over the 20-30 second period that was chosen as the optimal duration. The effect of the dead time was forcing the instrument to wait a user defined number of microseconds between measurements.

5.5.1 Single Layered Vegetation

In the context of this report, "single layered vegetation" refers to a situation in which water is flowing through vegetation which is all one representative height. Experiments in this series were performed to determine the effect that the presence of rigid vegetation of different densities has on the flow. Tables 5.1 and 5.2 outline the flows, densities, and profile measurement locations used for each of these experiments. As seen in the tables, the experiments consisted of several different formations of dowels both staggered and linear.

Figure 5.5 shows what is meant by the expressions "staggered" and "linear". The staggered formations of this experiment consist of 3 different spacings of formations. In an attempt to uniquely characterize each spacing by one measured parameter, a s/d or spacing/dowel diameter parameter will be used throughout the rest of this discussion. For the staggered formation the "s" parameter was measured as the distance between a central rod and a side of the square that would be created by connecting the surrounding rods. The visualization for this spacing parameter is also shown in Figure 5.5.

One staggered and two linear formations were used for experiments. The staggered formation consisted of $s/d = 8$ and corresponds to experiment 4A and 4C. Linear formations consisted of $s/d = 8$ and $s/d = 16$. Density was not increased beyond this point due to inability for the laser beam to cut through the narrow openings left by smaller configurations without rotation of the beam.

Vegetative height was maintained at a constant 7.62 cm (3 in.) for the single layered experiments. Several factors limit the choice of the height for the simulated vegetation. One factor was the restriction in the flow capacity of the flume. Because velocity profiles were being measured, it was necessary to make flow as deep as possible without creating wall effects. For the case in which the vegetation emerges through the surface of the water,

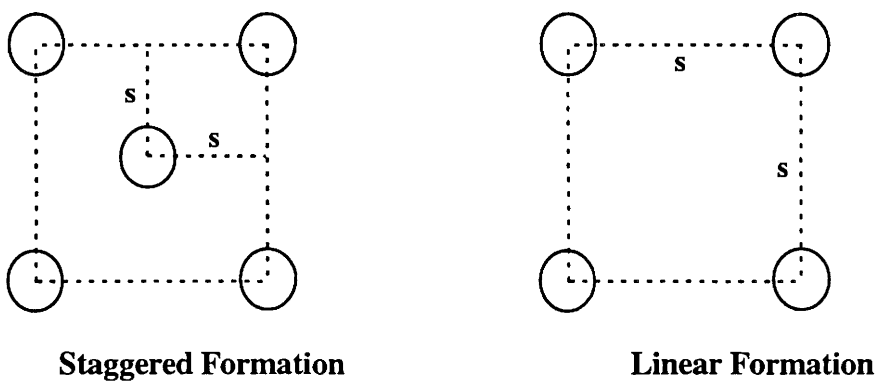

Figure 5.5: Definition of staggered and linear formations used in experiments.

it was decided that a flow of .0057 m^3/s would be used (half the total flow capacity of the flume). In testing the submerged case, a flow of 0.0113 m^3/s would be used. After some initial tests it was determined that a dowel height of 7.62 cm (3 in.) would remain unsubmerged in a flow of 0.0057 m^3/s and submerged by a flow of 0.0113 m^3/s.

Each configuration of dowels was tested during submerged and emergent conditions. The flow rate used during emergent tests was 0.0057 m^3/s. Normal depth was recorded using a point gauge with a vernier and velocity profiles were taken both along the centerline of the channel and to the left side of the centerline. Two sets of measurements were taken in an attempt to determine the differences in flow profiles when flow is in line

Table 5.1: Experiments for Unsubmerged, Single Layer Vegetation Case

Experiment	Profile	Location	Q (CMS)	Configuration
4A	1	12.7 mm downstream from rod	0.00569	Staggered s/d = 8
	2	38.1 mm downstream from rod	0.00569	
	3	63.5 mm downstream from rod	0.00569	
	4	88.9 mm downstream from rod	0.00569	
	5	25.4 mm downstream, 25.4 mm left	0.00569	
	6	76.2 mm downstream, 25.4 mm left	0.00569	
5A	1	12.7 mm downstream from rod	0.00569	Linear s/d = 8
	2	25.4 mm downstream from rod	0.00569	
	3	38.1 mm downstream from rod	0.00569	
	4	25.4 mm downstream, 25.4 mm left	0.00569	
6A	1	12.7 mm downstream from rod	0.00569	Linear s/d = 16
	2	38.1 mm downstream from rod	0.00569	
	3	63.5 mm downstream from rod	0.00569	
	4	88.9 mm downstream from rod	0.00569	
	5	25.4 mm downstream, 50.8 mm left	0.00569	
	6	76.2 mm downstream, 50.8 mm left	0.00569	

Table 5.2: Experiments for Submerged, Single Layer Vegetation Case

Experiment	Profile	Location	Q (CMS)	Configuration
4C	1	12.7 mm downstream from rod	0.01138	Staggered s/d = 8
	2	38.1 mm downstream from rod	0.01138	
	3	63.5 mm downstream from rod	0.01138	
	4	88.9 mm downstream from rod	0.01138	
5C	1	12.7 mm downstream from rod	0.01138	Linear s/d = 8
	2	25.4 mm downstream from rod	0.01138	
6C	1	12.7 mm downstream from rod	0.01138	Linear s/d = 16
	2	38.1 mm downstream from rod	0.01138	
	3	63.5 mm downstream from rod	0.01138	
	4	88.9 mm downstream from rod	0.01138	

with the dowels and when flow is in an unobstructed portion of the flow field. The locations of the measurement points within the dowels are shown in Figure 5.6. The number of profiles taken was chosen to show how the profile progressed when moving downstream. Naturally as the vegetative density increases, there is less space for the profile to transform before the next element is encountered. This explains the decrease in the number of measurements taken as the density increased.

In order to produce continuous velocity profiles, the experiments were designed to take more vertical measurement points in locations where inflections were expected. For these experiments, an inflection was expected near the bed. Therefore, more measurements were taken near the bed. As distance from the bed increased, fewer points were taken in the vertical portion of the velocity profile. In the case of experiments for emergent vegetation, 14-18 points were taken vertically. This increased to 20-23 points for the experiments dealing with submerged vegetation. Detailed vertical measurement locations can be found for each experiment in the Appendix.

Once tests for emergent conditions were concluded, the same configurations were tested when the simulated vegetation was totally submerged. For this case discharge was increased to 0.0113 m^3/s. As in the emergent vegetation experiments, the length of dowels used was 7.62 cm (3 inches) and the diameter 0.635 cm (¼ inch). Figure 5.7 depicts the configurations and measurement points for the submerged experiments. All profiles taken during submerged vegetation experiments were inline with the dowels.

5.5.2 Double-Layered Vegetation

For the purpose of these experiments, the term "double-layered" will be used to describe the case where there are two representative layers of vegetation. Such a case often appears in riparian wetlands where there is a representative grass layer (lower) and a canopy layer (upper). This experiment addresses the problem of modeling flow through double layered vegetation found in riparian wetlands. For these experiments certain rods are replaced with rods longer in length, i.e. 12.7 cm (5 in.). For these experiments, two different flows were introduced into each configuration of dowels. Each flow condition submerged the shorter rods but did not submerge the longer rods tested. For the first flow condition, the discharge was maintained at the maximum capacity of the flume--0.0113 m^3/s. During the second condition, experiments were performed with a flow of 0. 0.0106 m^3/s. For a complete list of flow rates and configurations used in these experiments, refer to Table 5.3.

The tall rod configurations used during these tests were staggered $s_t/d = 16$ and linear $s/d = 16$. The spacing of the shorter level of vegetation was kept at linear $s_t/d = 8$ or staggered $s/d = 8$. Pictures of these setups along with velocity measurement point locations are shown in Figure 5.8. Since the maximum flow produced by the flume was unable to totally submerge the tall vegetative layer, test were not performed with both layers completely submerged. In addition, the tall layer of vegetation would almost never be submerged in a riparian wetland. As in the first experiment, the water depth was kept as low as possible in order to minimize the effects from the flume side walls. Measurement points for double-layered experiments coincide as closely as possible with those points used

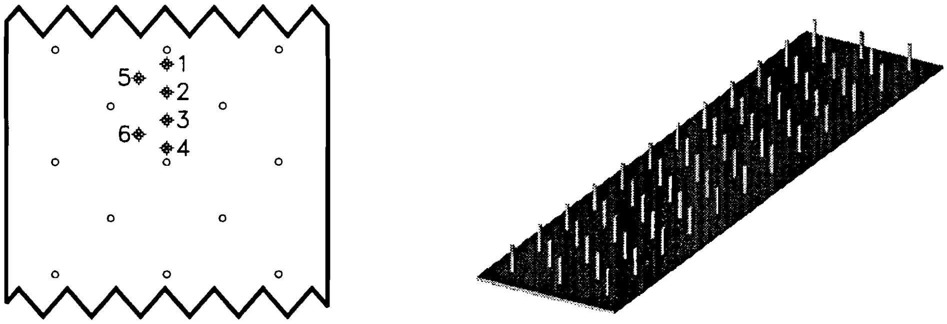

Measurement locations of Experiment 4a for staggered s/d = 8

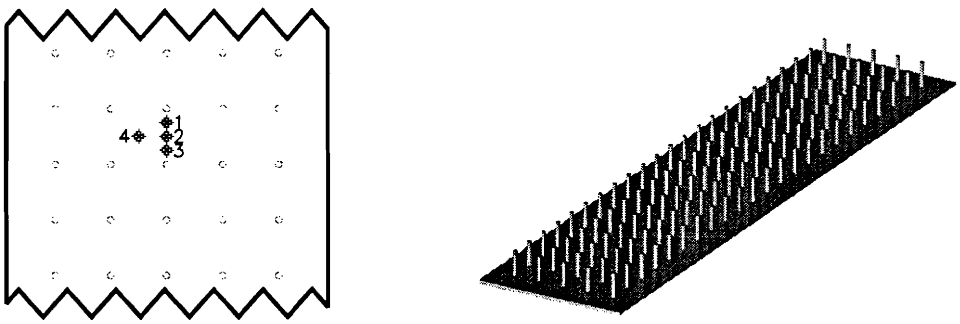

Measurement locations of Experiment 5a for linear s/d = 8

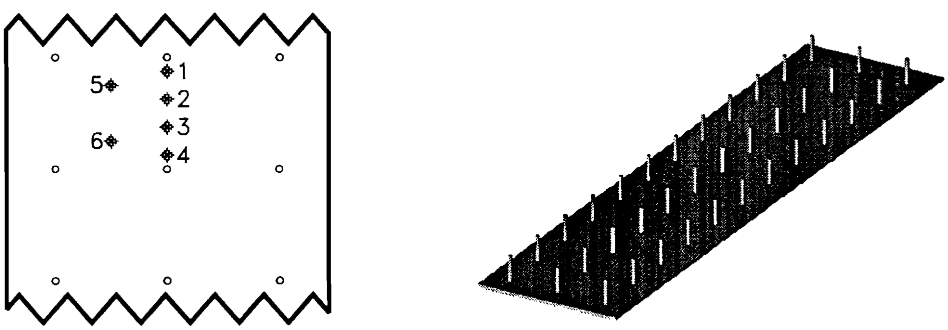

Measurement locations of Experiment 6a for linear s/d = 16

Figure 5.6 Profile measurement locations for emergent uniform 3.05 m test sections.

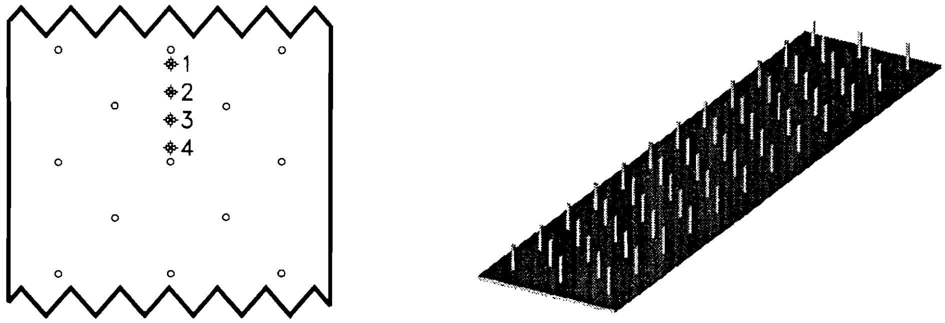

Measurement locations of Experiment 4c for staggered s/d = 8

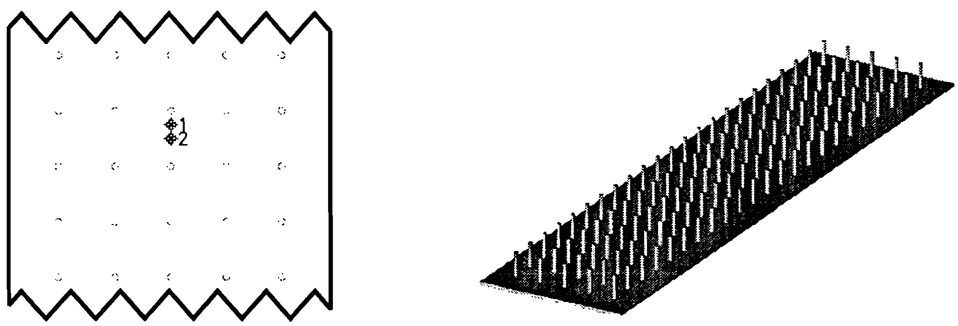

Measurement locations of Experiment 5c for linear s/d = 8

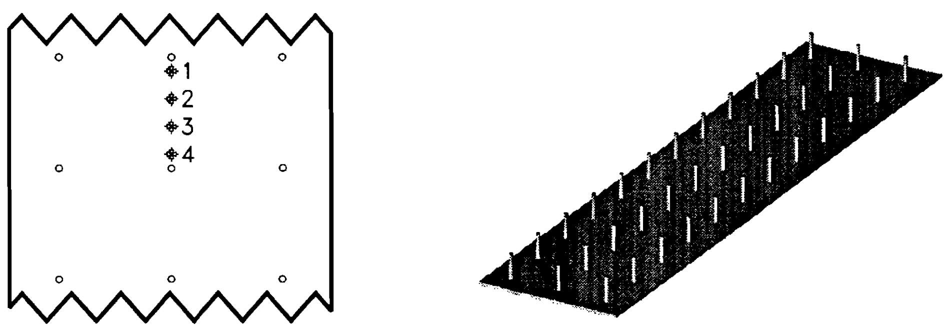

Measurement locations of Experiment 6c for linear s/d = 16

Figure 5.7 Profile measurement locations for submerged uniform 3.05 m test sections.

for studies on the single vegetative layer. For experiments involving double-layered vegetation, 19-25 vertical measurements were used to create velocity profiles. Because several inflection points were noted for some instances in the double-layered vegetationexperiments, vertical measurement spacing was altered to take more measurements around points of inflection (See Appendix).

Table 5.3: Experiments for Non-Uniform Height (Double-layered) Vegetation Case

Experiment	Profile	Location	Q (CMS)	Configuration
7	1	25.4 mm downstream from tall rod	0.01138	Linear s/d = 8 (short)
	2	76.2 mm downstream from tall rod	0.01138	Staggered s_t/d =16 (tall)
	3	127.0 mm downstream from tall rod	0.01138	
	4	177.8 mm downstream from tall rod	0.01138	
8	1	25.4 mm downstream from tall rod	0.01061	
	2	127.0 mm downstream from tall rod	0.01061	
9	1	25.4 mm downstream from tall rod	0.01138	Linear s/d = 8 (short)
	2	76.2 mm downstream from tall rod	0.01138	Linear s_t/d =16 (tall)
	3	25.4 mm downstream, 25.4 mm left	0.01138	
10	1	25.4 mm downstream from tall rod	0.01061	
11	1	25.4 mm downstream from tall rod	0.01138	Staggered s/d = 8 (short)
	2	76.2 mm downstream from tall rod	0.01138	Linear s_t/d =16 (tall)
	3	25.4 mm downstream, 25.4 mm left	0.01138	
12	1	25.4 mm downstream from tall rod	0.00991	
13	1	25.4 mm downstream from tall rod	0.01138	Staggered s/d=8(short)
	2	76.2 mm downstream from tall rod	0.01138	Staggered s_t/d=16(tall)
	3	127.0 mm downstream from tall rod	0.01138	
	4	177.8 mm downstream from tall rod	0.01138	
	5	25.4 mm downstream, 25.4 mm left	0.01138	
14	1	76.2 mm downstream from tall rod	0.01061	

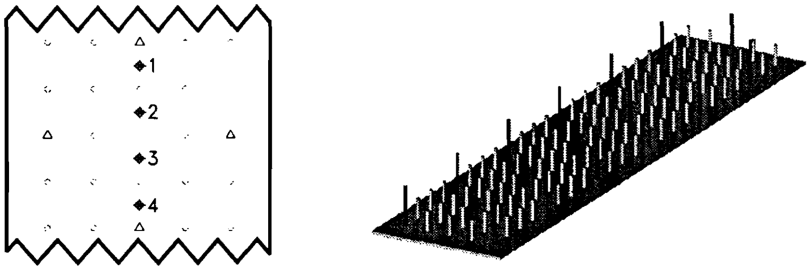

Measurement locations of Experiment 7 for short linear s/d = 8, tall staggered $s_t/d = 16$

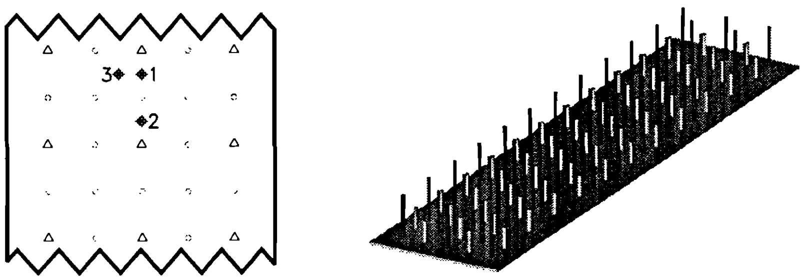

Measurement locations of Experiment 9 for short linear s/d = 8, tall linear $s_t/d = 16$

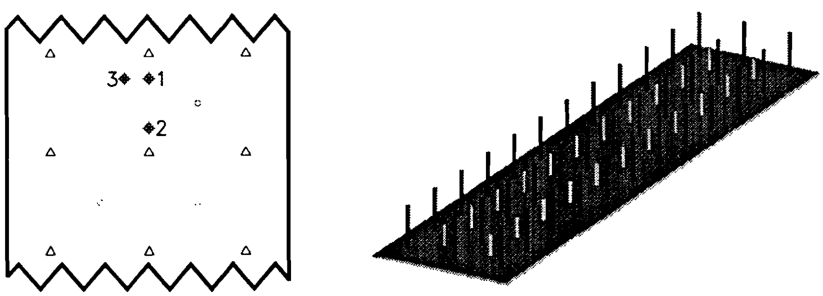

Measurement locations of Experiment 11 for short staggered s/d = 8, tall linear $s_t/d = 16$

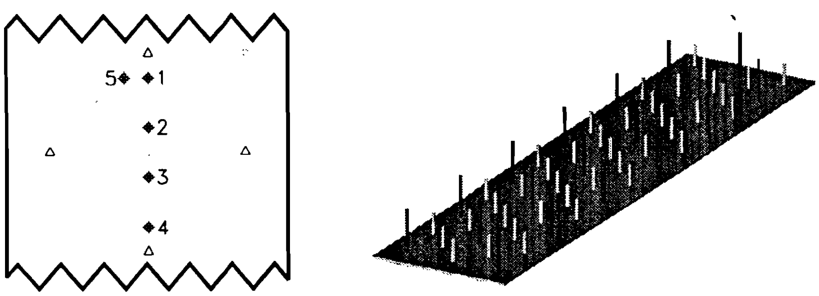

Measurement locations of Experiment 13 for short staggered s/d = 8, tall staggered $s_t/d = 16$

Figure 5.8 Profile measurement locations for double-layered uniform 3.05 m test sections.

5.6 Summary

The previous pages have described the rational behind the experimental procedure and outlined the procedure used during the course of this research. These included tests for both the single-layered emergent and submerged conditions. In addition, the double-layered vegetation case that occurs in many riparian wetlands was tested. Further details and results from these experiments will be discussed in subsequent chapters.

Chapter 6
EXPERIMENTAL RESULTS

6.1 General

Results from experiments described in previous sections are shown in the following pages. Much of this data is introduced in the form of normal and dimensionless velocity profiles created from the measurements. The reduction of data to non-dimensional parameters was incorporated to more effectively describe characteristic trends under various flow conditions and locations. Next the data is analyzed for determination of apparent roughness coefficients caused by the presence of the various configurations of dowels. In addition, this data has been subjected to several statistical tests for interpretation of the data.

6.2 Data Collected From Laser Doppler Anemometer

Data was processed and transferred to disk using software operating in conjunction with the Dantec Laser Doppler Anemometry system. This data was analyzed using software written by the author of this report. The software took raw velocity data and performed statistical analysis to obtain the mean, mode, median, range of measurements, skew, sampling frequency, number of samples, and RMS at each measurement location. Results of this analysis were converted to a tabular format. An example of one of these tables can be found in Table 6.1. In addition to tabulated values, the program also enables the user to view and print histograms of measurements at each point. In the interest of space in this report, complete tables and histograms for all experiments have not been included. A complete copy of all tables and histograms may be requested through Dr. Panos Diplas at Virginia Tech.

Table 6.1: Analyzed velocity profile data from Experiment 13 at measurement point 1.

Average Velocity (m/s)	Depth (m)	Maximum Velocity (m/s)	Minimum Velocity (m/s)	Standard Deviation (m/s)	Number of Samples	Sampling Frequency (Hz)	3rd Moment Skew	Kurtosis
0.2524	0.0000	0.4835	0.0198	0.0735	549	27.431	-0.078	3.027
0.2750	0.0046	0.5872	0.0066	0.0769	4596	229.777	-0.164	3.169
0.2600	0.0092	0.5420	-0.0160	0.0775	5042	252.063	-0.166	2.865
0.2616	0.0139	0.5420	-0.0405	0.0799	5261	263.031	-0.110	3.024
0.2668	0.0185	0.5175	-0.0160	0.0779	5337	266.820	-0.248	3.086
0.2638	0.0231	0.5061	-0.0160	0.0780	5235	261.725	-0.205	2.964
0.2710	0.0277	0.5061	0.0066	0.0744	5523	276.128	-0.295	3.027
0.2818	0.0323	0.5533	0.0066	0.0744	5596	279.780	-0.321	3.162
0.2832	0.0370	0.5175	-0.0047	0.0754	5542	277.070	-0.319	3.141
0.2877	0.0416	0.5420	-0.0537	0.0759	5442	272.075	-0.290	3.156
0.2902	0.0462	0.5175	0.0198	0.0720	5374	268.691	-0.379	2.997
0.3064	0.0508	0.5872	-0.1009	0.0737	4760	237.983	-0.379	3.475
0.3160	0.0554	0.6098	-0.0650	0.0776	5400	269.997	-0.324	3.530
0.3343	0.0601	0.6343	-0.0047	0.0846	5495	274.748	-0.448	3.394
0.3535	0.0647	0.6230	0.0198	0.0919	5631	281.498	-0.642	3.227
0.3861	0.0693	0.6796	-0.0650	0.1018	5266	263.277	-0.722	3.358
0.4102	0.0716	0.7154	-0.0292	0.0969	5712	285.567	-0.928	3.989
0.4478	0.0739	0.6796	0.0556	0.0834	5728	286.380	-1.199	5.212
0.4859	0.0762	0.7474	0.0198	0.0759	5689	284.411	-1.658	7.671
0.5408	0.0785	0.7361	0.1649	0.0519	6017	300.831	-1.228	8.005
0.5641	0.0808	1.2847	0.1291	0.0552	5209	260.420	0.357	13.978
0.5356	0.0854	1.1282	-0.1254	0.1260	145	6.886	-0.598	10.696

6.3 Results From Single-layered Vegetation Experiments

Several trends were noticed when the experiments were subdivided into three distinctively different classes (shown schematically in Figure 6.0):

1. Measurements taken immediately downstream of a dowel (See Figure 6.1).

2. Measurements taken in-line, but not immediately downstream of a dowel.
3. Measurements taken in the unobstructed flow region (at half the distance between two consecutive longitudinal series of dowels).

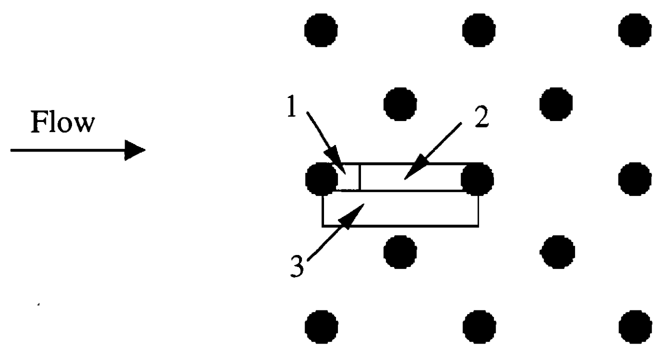

Figure 6.0: Schematic Diagram of Measurement Point Locations

Dimensionless plots for these classes will be shown in the following paragraphs with discussion of general flow trends observed for both the submerged and non-submerged flow cases.

6.3.1. Measurements Immediately DS of the Dowel at 2 Dowel Diameters (12.70 mm)

Several general trends were noticed in the profiles taken immediately downstream of the dowels. One major characteristic found in all of the measurements taken at this location was the identification of flow in the upstream (negative) direction for almost every measurement point taken directly behind a dowel. Although this occurred for instantaneous velocity measurements, none of the average velocities for a location were negative. A graph showing a typical velocity profile located downstream of a dowel is shown in Figure 6.1. The distance downstream from a dowel in Figure 6.1 is given by the dowel diameters in the downstream direction.

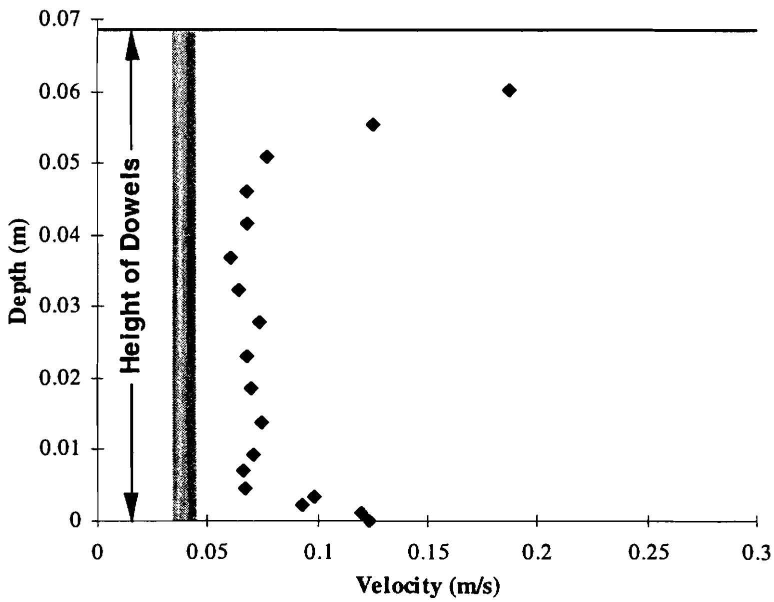

Figure 6.1: Velocity Profile from Experiment 5A (Linear s/d=8) — Profile 1 @ 2 Dowel Diameters DS (12.7 mm)

A second characteristic of profiles taken directly downstream of the dowel is the presence of a spike in the velocity near the bed. One possible explanation of this occurrence is the presence of a junction vortex which is interacting with the dowel. The vortex may form where the dowels and the bed connect and cause increased velocities directly behind the dowel and near the bed. This may produce a scouring action in the presence of sediment. However, no additional experiments were performed to validate this hypothesis. About 3 mm above the bed the velocity decreases. From here to near the surface of the water the velocity is nearly constant. As the water surface is approached, the velocity profile begins increasing at around 60% of the total flow depth as shown in Figure 6.1. In the case of emergent experiments, this inflection may be caused by the surface wave formation at the dowel. The water "piles up" to a crest just upstream of a dowel and forms a trough just downstream. An effect of this may be localized increases in velocity at the free surface. Momentum exchange between water particles near the surface and those below the surface would be expected to cause a velocity increase for some distance underneath the free surface. The effect of this would be an inflection point on the velocity profile within the vegetation.

The placement of the inflection point seems to be very dependent upon the location of the profiles in the downstream direction. Figures 6.4 and 6.5 show series of velocity profiles as they progress downstream from a dowel. As shown in Figure 6.4, with the exception of the profiles immediately downstream (2 diameters), the inflection point of each profile is not very distinct for Experiment 4A (Staggered s/d = 8). In fact, the emergent vegetation experiments show an inflection point near the free surface that is not very pronounced except for those measurements taken immediately downstream of a dowel. The only visually distinct inflections that occurred in all of these experiments were those found during the transition from zero velocity at the bed to the velocity within the vegetation.

One very visible formation during these experiments were the wake interference patterns between dowels. Each dowel produces a wake which extend downstream and interact with those from other dowels. These patterns set up interesting standing wavelike formations on the water surface as shown in the schematic diagram below, Figure 6.2. A picture of the surface waves looking up the flume is shown in Figure 6.3.

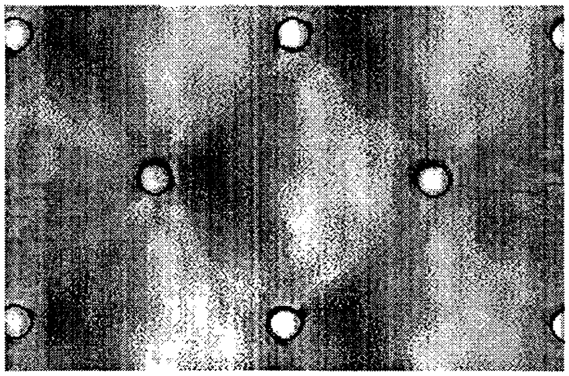

Figure 6.2: Surface wave formation found in staggered array of cylinders

The inflection points were much more pronounced for experiments in which the vegetation was totally submerged. Figure 6.5 shows the progression of velocity profiles downstream for the staggered arrangement of s/d=8. As can be seen in the figure, a very distinct inflection occurs near the free surface in all of the profiles. However in some experiments, the inflection point is not as sharp as the profiles progress downstream. In addition, the point of inflection moves further from the free surface as the profiles progress downstream. This seems to indicate that momentum exchange is more efficient as distance downstream from a dowel increases. Ikeda and Kanazawa (1996) mentioned the existence of an inflection point near the surface of flexible vegetation during their experiments. However, their experiments with submerged flexible vegetation do not seem to have the same sharp inflection as shown in Figure 6.5. In addition, the author has not found any literature elsewhere that notes the vertical change in inflection moving downstream from a dowel.

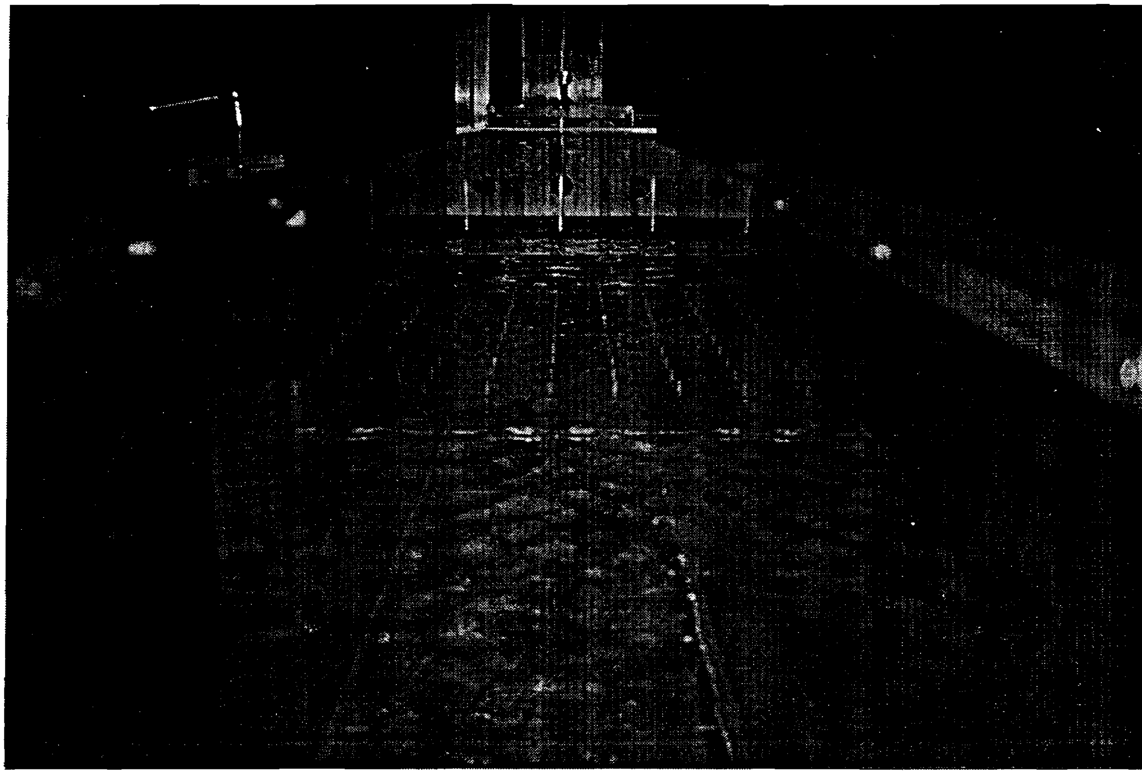

Figure 6.3: Surface wave formation looking upstream in flume.

In order to determine if the shape of the velocity profile was independent of the flow conditions, the velocity profiles were reduced to a non-dimensional form. A dimensionless velocity reading was created through division of mean velocity by the shear velocity:

$$\frac{U}{U*} = \frac{U}{\sqrt{gy_n S}} \tag{6.1}$$

where U is time-averaged velocity at a point distance y from the channel bottom, g is acceleration due to gravity, y_n is flow depth and S is the energy slope. The dimensionless term y*=y / y_n, where y_n is the total depth of flow.

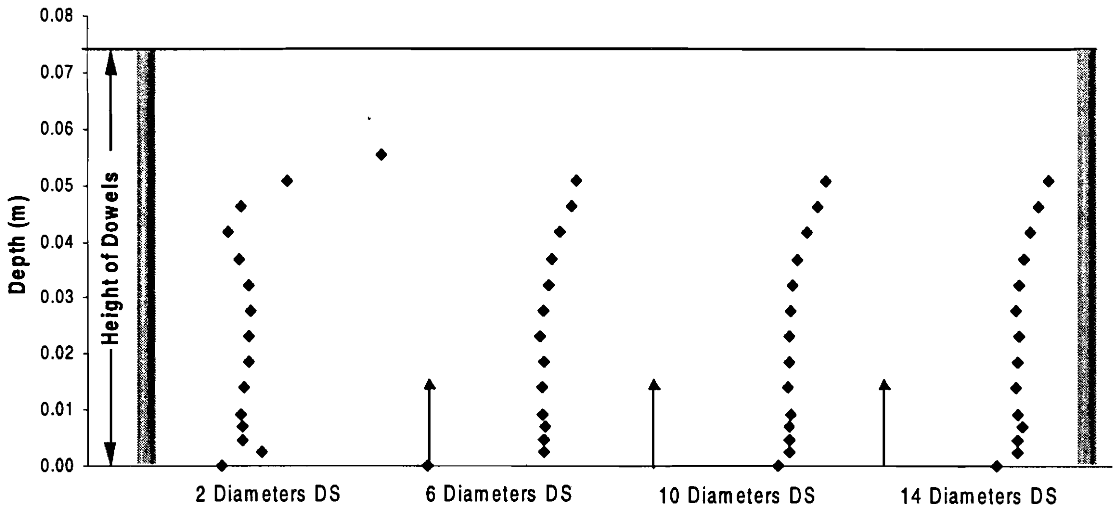

Figure 6.4: Progression of Velocity Profiles DS in Experiment 4A (Inline w/dowels) Staggered s/d=8

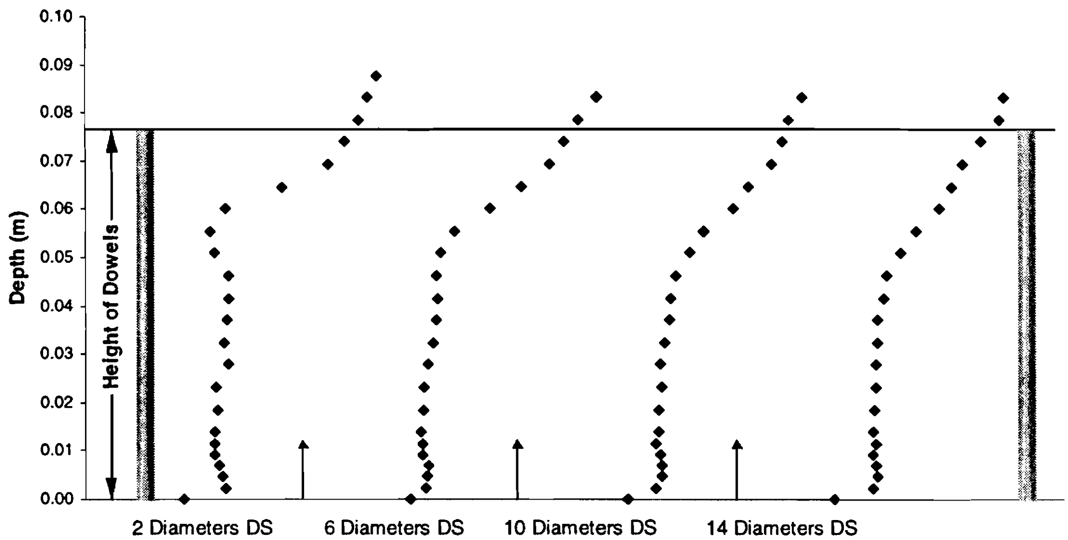

Figure 6.5: Progression of Velocity Profiles DS in Experiment 4C (Inline w/dowels) Staggered s/d=8

As can be seen from Figures 6.6 and 6.7, the semi-logarithmic dimensionless profiles follow similar trends for the submerged and unsubmerged flow cases. A line through the points may be used to estimate the velocity at any point along most of the profile. Once the surface is approached, the dimensionless velocity does not appear to fall on the same line (see Figure 6.7). This trend is much more pronounced in the experiments where the dowels were completely submerged. An apparent cause for the difference is due to the dramatic increase in velocity during the transition of flow from within the formation of dowels to flow above the formation. In fact, the profile above the dowels seems to approach the logarithmic profile of an unvegetated channel if a slip velocity is assumed to occur near the surface of the vegetation. This result seems to concur with the observations of Kouwen, Unny, and Hill (1969).

6.3.2. Measurements In-line with Dowel (excluding those immediately downstream) 6 - 14 Dowel Diameters DS from Vegetation

The second group of measurements were those taken in-line, but not immediately downstream of the dowel (See Tables 5.1 and 5.2 for exact locations of individual profiles). Unlike measurements taken directly behind the dowel, as described in the section above, no negative velocity readings occurred at these measurement locations. In addition, the spike in the velocity profile near the bed as described in the previous section was much smaller. As distance downstream of the dowel increased, this spike in the velocity profile was not perceptible. An example of a profile taken in this group is shown in Figure 6.8.

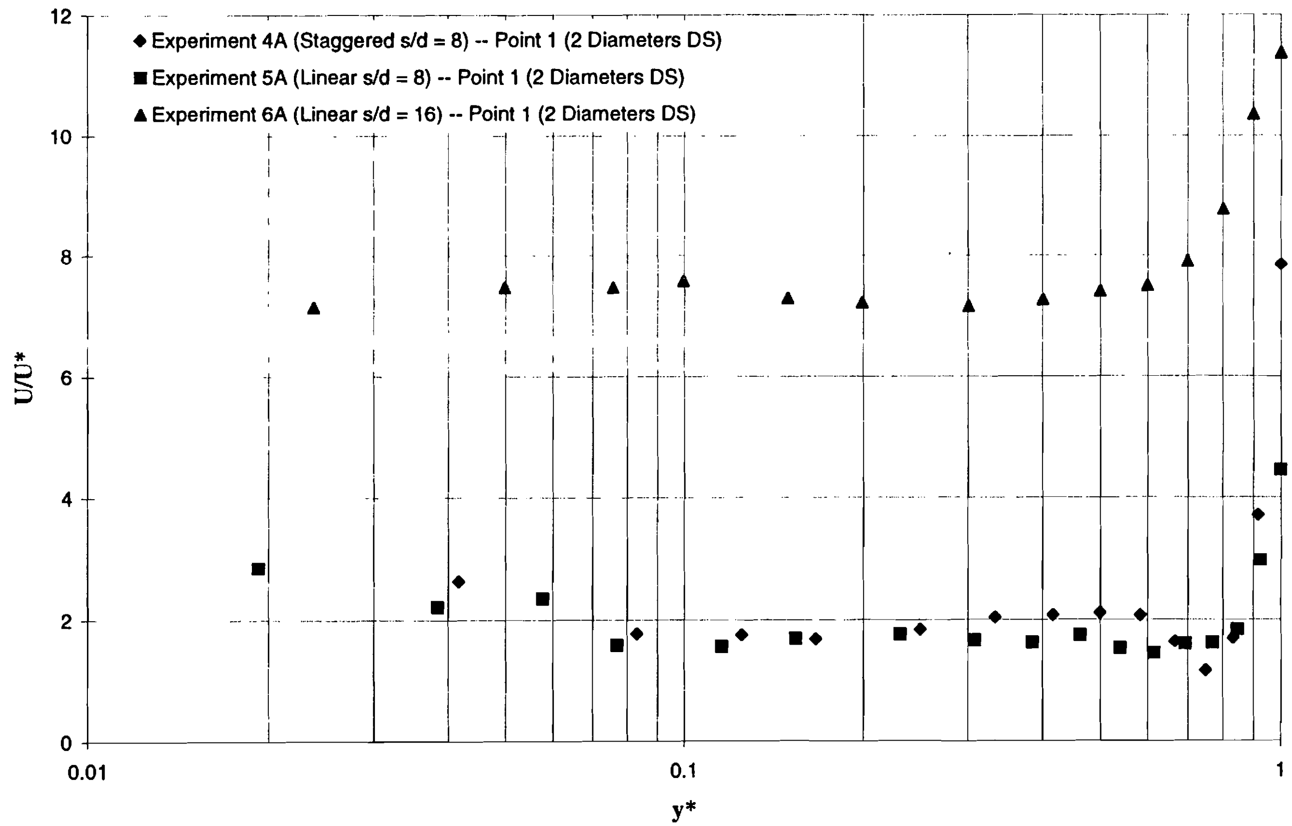

Figure 6.6: Dimensionless Plots of Unsubmerged Experiments In-Line with Dowels (Profiles immediately downstream).

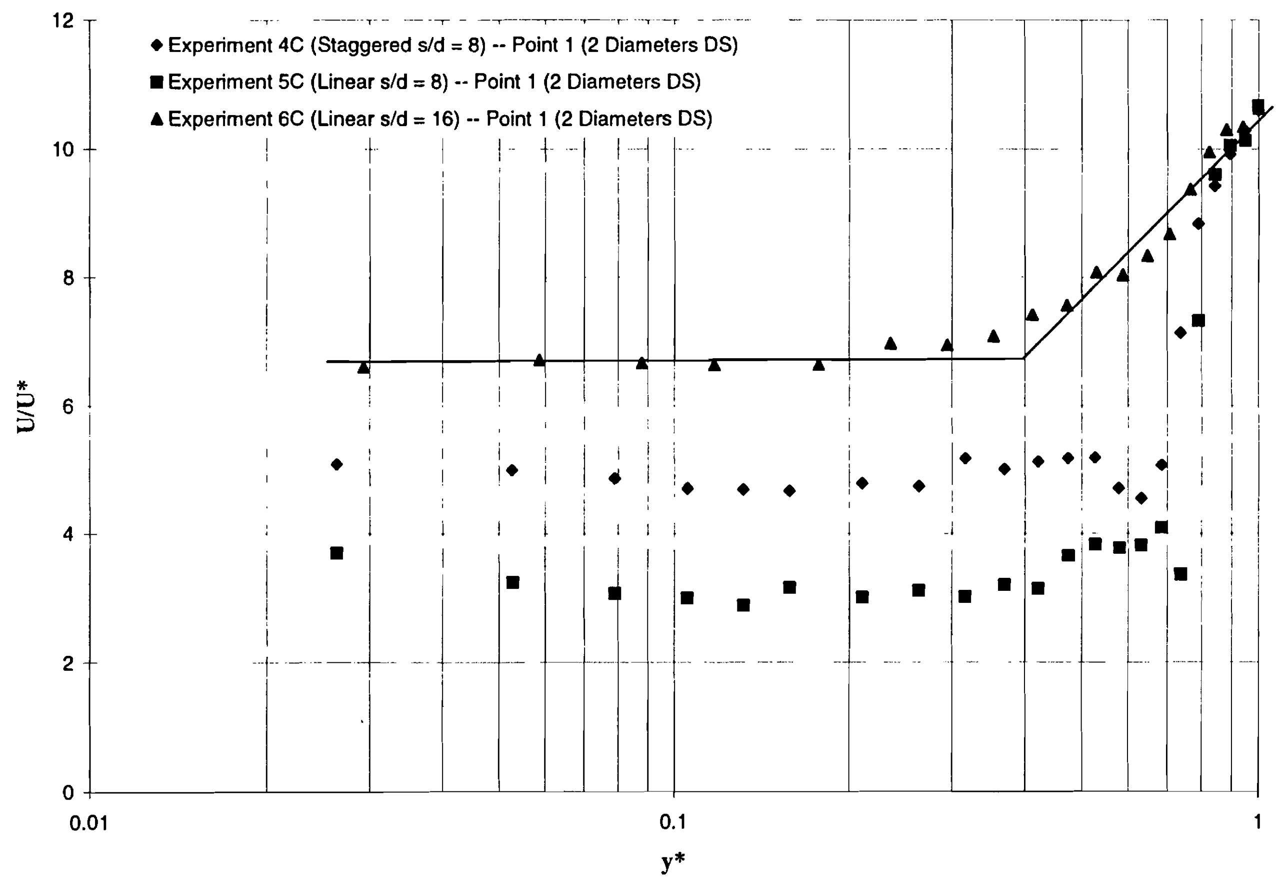

Figure 6.7: Dimensionless Plots of Submerged Experiments In-line with Dowels (Profiles immediately downstream)

For the unsubmerged flow case, the profiles taken in this cluster of experiments seem to be nearly vertical. Figure 6.8 shows that a vertical line placed through the data points would match the profile very closely. As dowel density is increased, this vertical line describing the velocity shifts to the left toward the y-axis while maintaining nearly the same shape. Although very distinct inflection points are not evident for the dimensional plots of these emergent vegetation experiments, Figure 6.10 shows that an inflection does occur when the data is converted to a dimensionless form. This effect can be seen more clearly in the complete set of normal velocity profiles found in the Appendix.

Profiles taken when the dowels were completely submerged have some interesting differences from those described in Figure 6.8. An example of a profile for the submerged flow case is shown in Figure 6.9. The profiles in Figures 6.8 and 6.9 were taken in the same density and arrangement of dowels.

As can be seen from these figures, the shape of the submerged velocity profile looks very similar to that of the unsubmerged profile to a point. At approximately 6 cm from the bed (78% height of dowels), there is an inflection in the velocity profile. From this point and higher, the velocity profile resembles a typical logarithmic profile. Although previous researchers, such as Kouwen, et al (1969), have suggested that an inflection occurs at the top of the vegetation, the configurations tested in this research show that the inflection occurs well below the surface of the vegetation. This concurs with more current research such as that of Tsujimoto, Shimizu, and Nakagawa (1991) which shows the inflection point to occur below the top of the vegetative layer. Ikeda and

Kanazawa (1996) mention the existence of the inflection point near the surface but do not mention the exact location or variation between experiments.

It appears that the effect of the shear force exerted on the flow within the vegetation, by the faster moving flow above the vegetation, extends down into the vegetative column. As mentioned previously, this effect varies with distance downstream from the dowel. This variation causes the vertical position of the inflection on the profile to increasingly move closer to the bed when moving in the downstream direction (See Figure 6.5). A possible explanation for this is that as flow gets further from an upstream dowel, shear stress from the flow above the vegetation can exert more influence on flow within the vegetation. This momentum exchange is taking place between the faster moving flow above the vegetation and the slower moving flow through the vegetation. One interesting point to notice however is that the average velocity within the vegetation is nearly the same for a submerged experiment as an unsubmerged experiment with the same configuration; although the flow being used for these experiments was twice as great as that in the unsubmerged experiments.

Composite non-dimensional profiles of all experiments taken in this classification are shown in Figures 6.10 and 6.11. Parameters were converted to non-dimensional form by the process described in the previous section. These figures show that the shape of the profiles is similar between all experiments. As shown in Figure 6.10, dimensionless velocity profiles for each experiment tend to form clusters with velocity profiles from

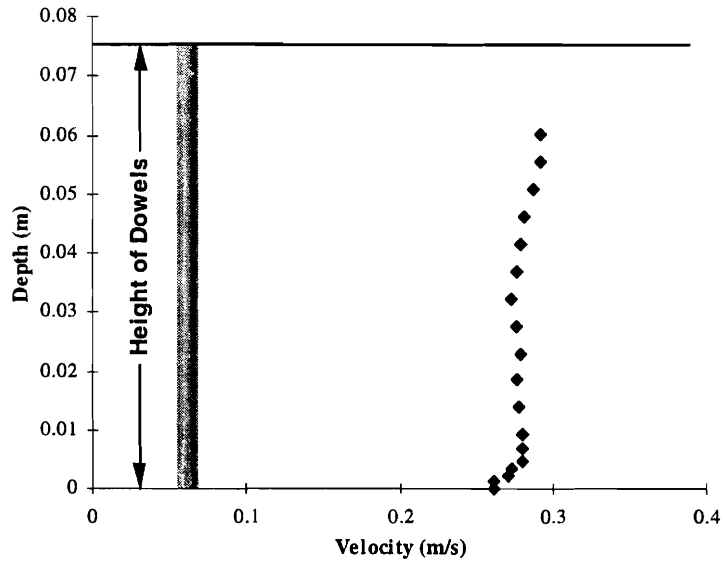

Figure 6.8: Velocity Profile from Experiment 5A (Linear s/d=8)—Point 3 @ 6 Dowel Diameters DS (38.1 mm)

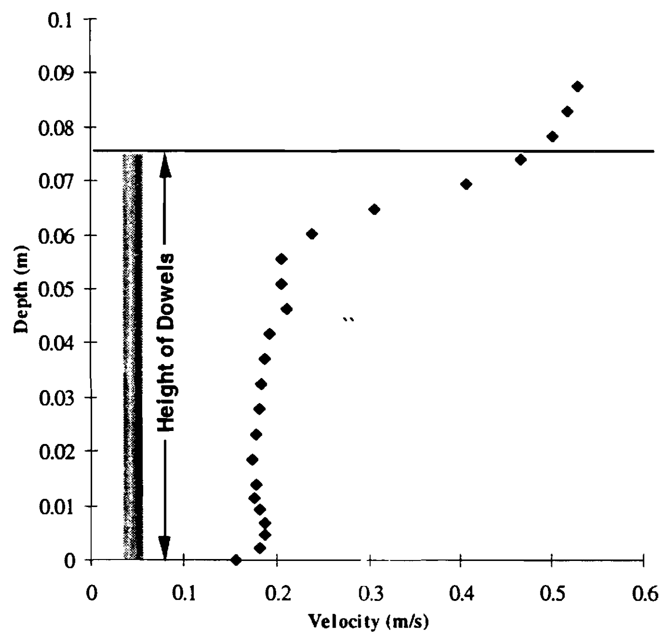

Figure 6.9: Velocity Profile from Experiment 5C (Linear s/d=8) — Point 2 @ 4 Dowel Diameters DS (25.4 mm)

other locations within the same experiment. In all cases, the velocity profiles are nearly vertical (horizontal on dimensionless plots) until just before reaching the free surface. At that point an inflection occurs and the dimenionless velocity increases until the free surface is reached. Like the normal velocity profiles, a variation in the location of the inflection point can be seen in the dimensionless graphs although it is not nearly as noticeable as those shown in the normally plotted velocity profiles.

As the density of dowels increased with a constant discharge in the channel, dimensionless velocity profiles plotted higher on the velocity axis as shown in Figures 6.10 and 6.11. Although both staggered and linear configurations of dowels were used, no noticeable differences in the general shape of the profiles were noted. Comparison of Figures 6.10 and 6.11 will show that the average dimensionless velocity within the vegetation is lower for the same configuration of submerged vegetation experiments than that for emergent vegetation experiments, even though the discharge rate was doubled. This was not the case for the dimensional velocity profiles. This is expected to be caused by the chosen method of non-dimensionalizing the data. The velocity is divided by the shear velocity to create the dimensionless velocity. The shear velocity is much higher for the submerged vegetation experiments (due to increased flow depth) while the average velocity within the vegetation changes little. Therefore, the non-dimensional velocity for the submerged vegetation case will be lower than that for the emergent vegetation case for a significant portion of the profile. However, once the profiles reached the inflection point near the height of the vegetation, the dimensionless velocities for the submerged vegetation experiments plot higher than those for the emergent vegetation experiments. This is expected since the velocity within this portion of the profiles is much greater than any velocities seen in the emergent vegetation experiments.

6.3.3. Measurements taken in the unobstructed flow region (not in-line with dowels).

In addition to measurements taken in-line with the dowels, profiles were also taken for the unsubmerged case to the left of the channel centerline where the flow was unobstructed by dowels (exactly between series of dowels). Results from these experiments show that with a sparse vegetative configuration (s/d=16), the profiles more closely resemble a typical logarithmic profile. However, as density increases the profiles go through a metamorphosis to more closely resembling those taken in-line with the dowels. Figure 6.12 shows an example of a profile taken in an unobstructed portion of the channel for the least dense (s/d=16, linear) configuration of dowels. Figure 6.13 portrays the velocity profile for the densest (s/d=8, linear) configuration of dowels.

As mentioned above, the velocity profiles taken at an unobstructed location in the dowel arrangement approach the shape of those in-line with the dowels as vegetative density increases. In addition, the location in the dowel array with the highest average velocity seems to shift from an unobstructed portion of the channel to a location just upstream of a dowel. Comparing measurements from experiments 6A (s/d=16, linear) and 5A (s/d=8, linear) shows this phenomenon. Examination of measurement point 3 (just upstream of the dowel) for experiment 5A (the densest configuration of dowels) shows a depth-averaged velocity of approximately 0.28 m/s. Measurement point 4 in the same experiment (unobstructed location) yields an average velocity of approximately 0.17 m/s. This trend is reversed in experiment 6A (the least dense configuration of dowels). Measurement point 4 (just upstream of dowel) of experiment 6A has an depth-averaged

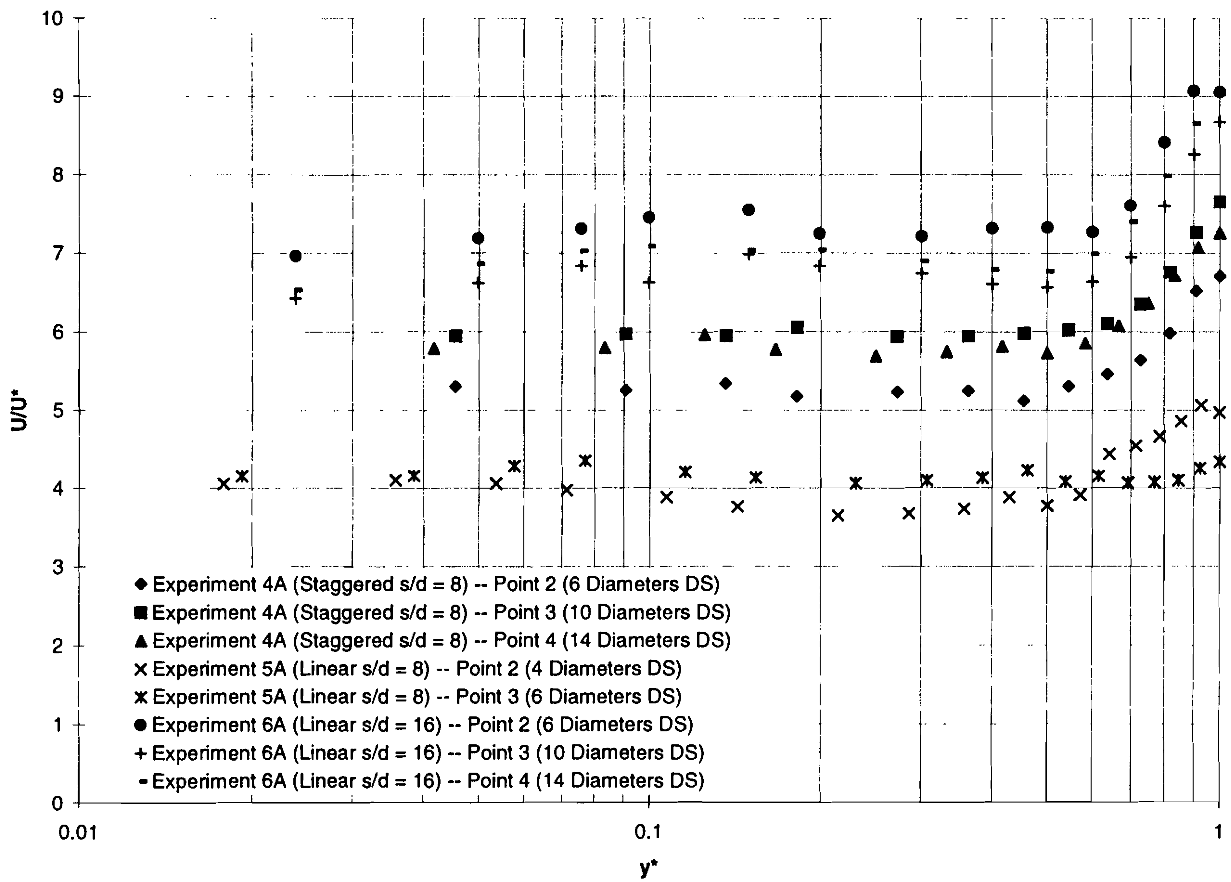

Figure 6.10: Dimensionless Plots of Unsubmerged Experiments Inline with Dowels (Profiles immediately downstream of dowel are excluded).

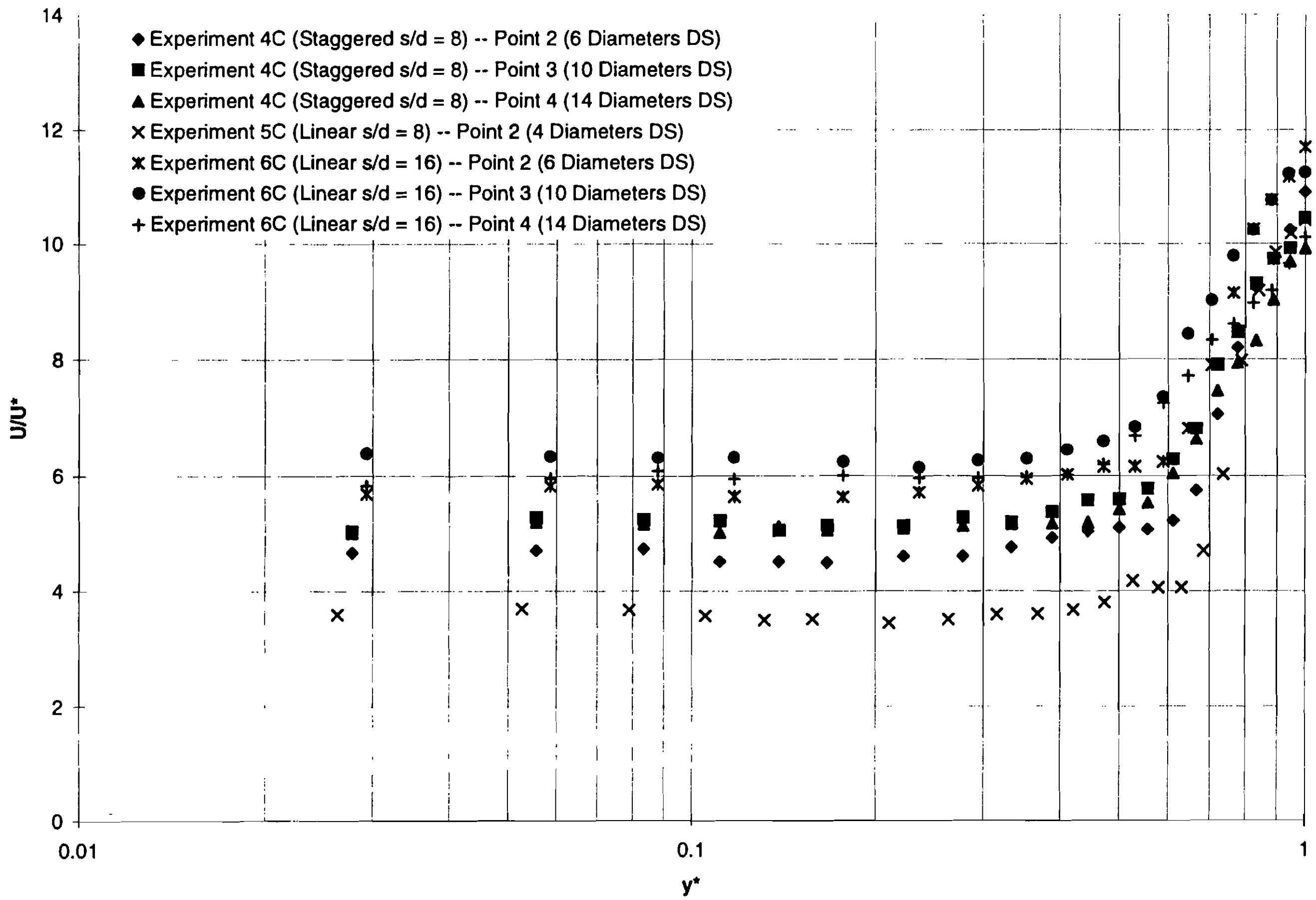

Figure 6.11: Dimensionless Plots of Submerged Experiments Inline with Dowels (Profiles immediately downstream of dowel are excluded)

velocity of approximately 0.27 m/s. However, both profiles taken in unobstructed locations for the same configuration (s/d=16, linear) yield depth-averaged velocities of approximately 0.38 m/s In addition, Figure 6.14 shows the dimensionless plot of profiles taken in the unobstructed portion of the dowel arrangement. This plot shows that profiles taken in unobstructed locations for sparsely vegetated configurations do not significantly change shape with progression downstream for the vegetation densities examined here. This trend may end once a critical density is reached; however, tests were not performed during this research to verify this speculation.

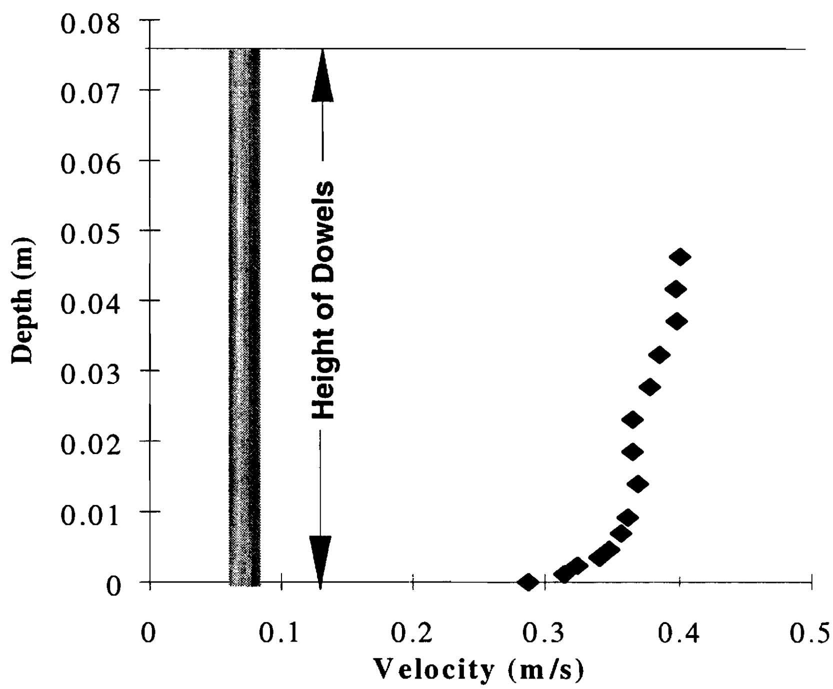

Figure 6.12: Velocity Profile from Experiment 6A (Linear s/d=16) — Point 5 @ 4 Dowel Diameters DS (25.4 mm) & 8 Dowel Diameters Left of Center

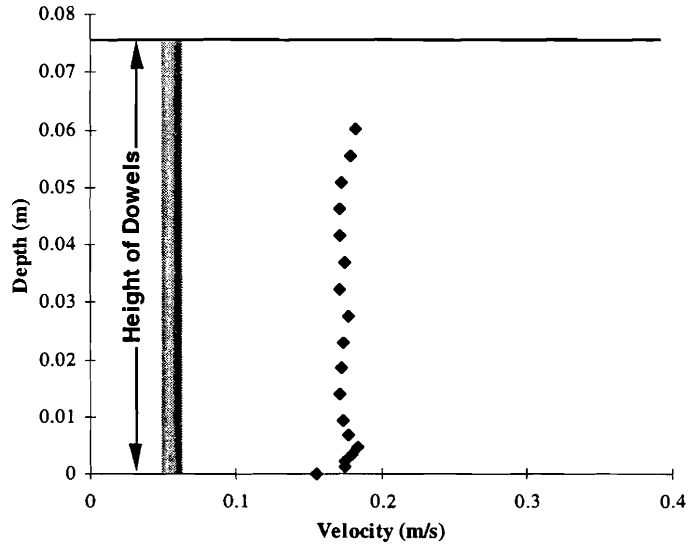

Figure 6.13: Velocity Profile from Experiment 5A (Linear s/d=8) — Point 4 @ 4 Dowel Diameters DS (25.4 mm) & 4 Dowel Diameters Left of Center

6.4 Results From Double-layered Vegetation Experiments

As in the previous section, the results from the double-layered vegetation experiments will be divided into three (3) categories:

1. Measurements taken immediately downstream of a dowel.
2. Measurements taken in-line, but not immediately downstream of a tall dowel.
3. Measurements taken in the unobstructed flow region (not in-line).

Due to the pump capacity of the flume used for experiments, flow could not submerge the taller vegetation during any of the experiments. All measurements were taken during a flow that submerges the shorter vegetation, but does not submerge the taller vegetation (see Chapter 5).

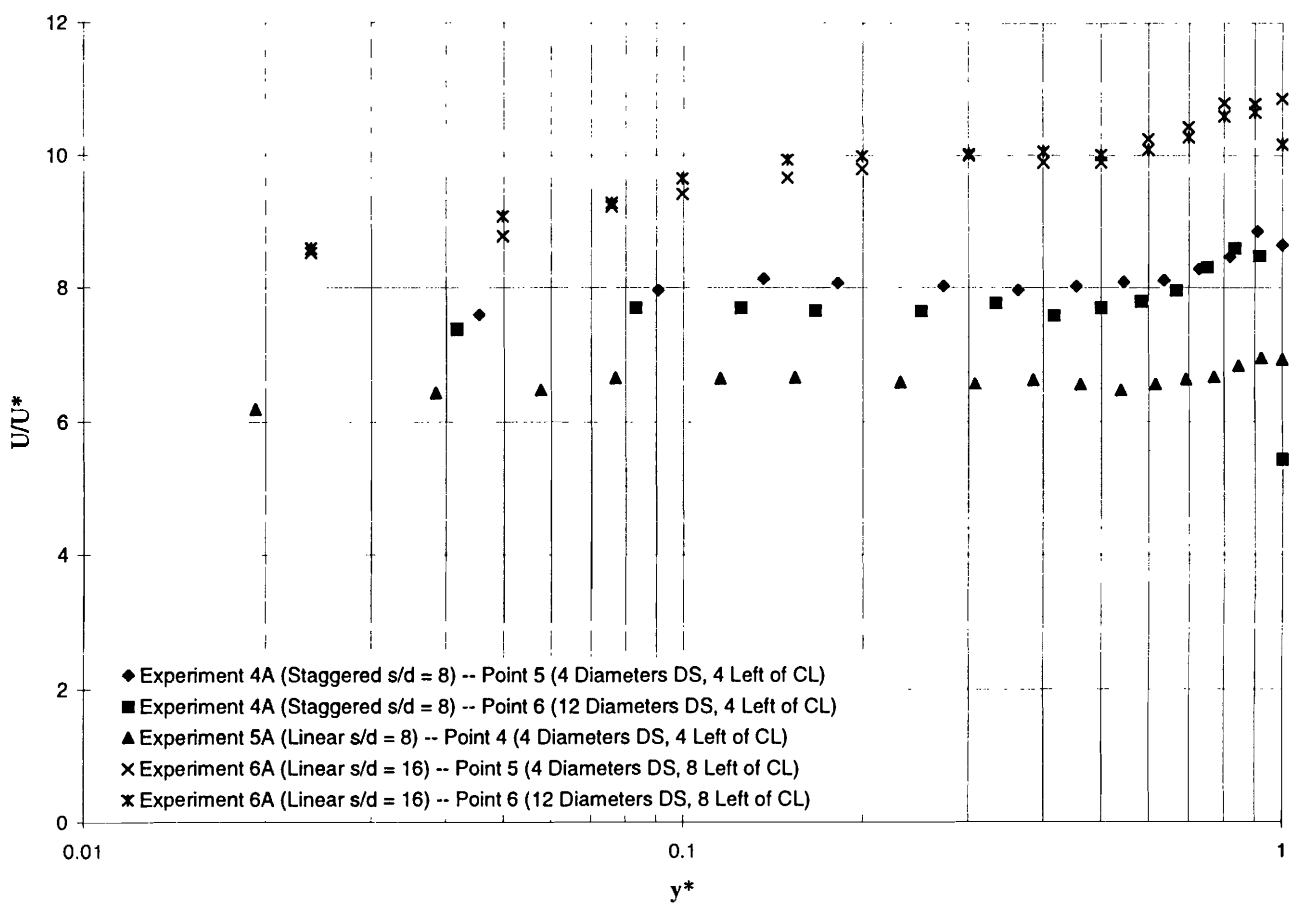

Figure 6.14: Dimensionless Plots of Unsubmerged Experiments in Unobstructed Location

6.4.1. Measurements Immediately Downstream of the Dowel (4 Dowel Diameters; 25.40 mm)

As in experiments for the single-layer vegetative case, the most unusual looking velocity profiles occurred directly downstream of the dowels. In addition to the spike in the velocity profile near the bed, there were several inflection points in the profile near the top of the shorter vegetation. A typical velocity profile taken directly behind a dowel for this formation is shown in Figure 6.15. The profiles described in this section are those taken immediately downstream of a tall dowel. Profiles taken immediately downstream of short dowels are grouped together with measurements discussed in section 6.4.2.

This velocity profile looks very similar to that described for in the submerged condition of the single-layered vegetation case. However, just under the top of the shorter vegetation there is an inflection that causes the velocity to decrease until the top of the shorter vegetation is reached. At this point, another inflection occurs and the velocity seems to increase in a linear fashion (see Figure 6.15). All of the profiles taken directly downstream of dowels can be found in the Appendix. Dimensionless profiles are shown in Figure 6.16.

Of the double-layered vegetation experiments, the measurements directly downstream of dowels were the only measurements in which there was a profound double inflection near the surface. The following section describes the general single inflection point that occurs for most profiles taken in the double-layered case. Notice that in all cases, the first inflection generally occurs at a point approximately 80% of the height of the shorter vegetation.

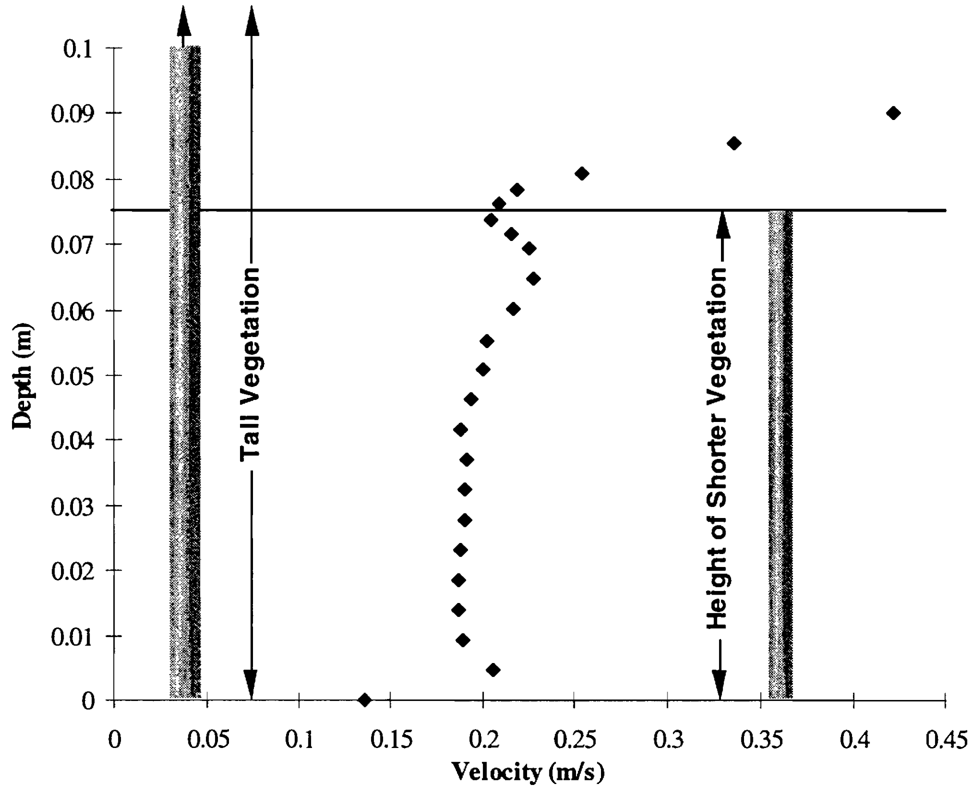

Figure 6.15: Velocity Profile from Experiment 9 [Linear s/d=8 (short), Linear s/d=16 (tall)] — Point 1 @ 4 Dowel Diameters (25.4 mm) DS from Tall Rod

Figure 6.16 shows that for all experiments except experiment 13, a very sharp inflection occurs at a short distance below the free surface (at approximately y*=0.8). As with the single layered vegetation experiments, the dimensionless velocity within the shorter vegetation is nearly vertical. Most of dimensionless profiles like the profiles plotted normally show two distinct inflection points. The one exception to this was experiment 13 which overall represents the least dense configuration of the double layered vegetation experiments.

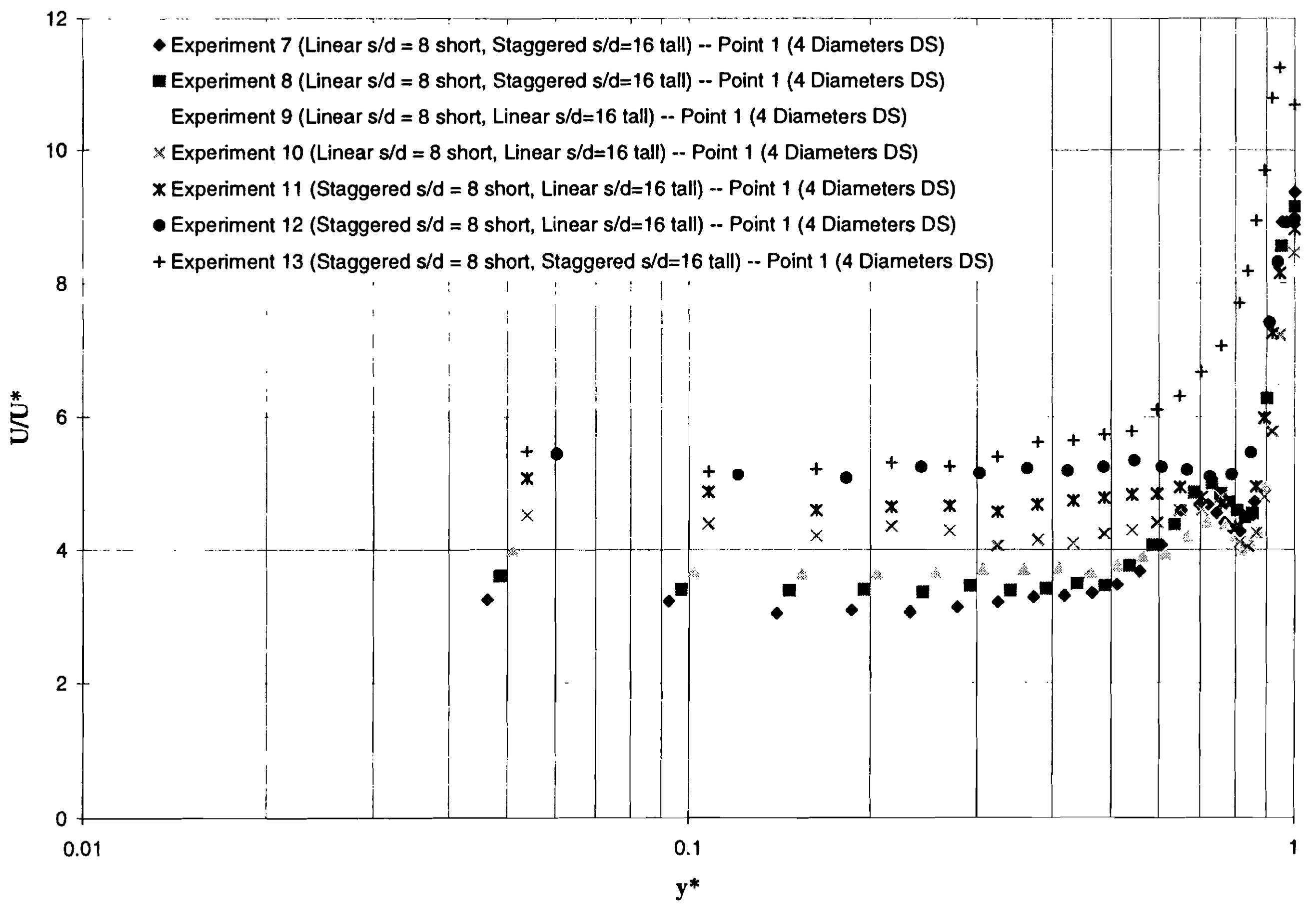

Figure 6.16: Dimensionless Plots of Double Layer Experiments Inline with Dowels (Points immediately downstream of dowels)

As can be seen when comparing Figures 6.11 and 6.16, there are many comparisons between dimensionless plots of the submerged vegetation case and the double-layered vegetation case. Within the short vegetation, the profiles plot is the same vertical region of the graph. This supports the finding the placement of tall dowels within the array causes the average velocity within the short dowels to drop only a small amount. In addition, the maximum dimensionless velocities seen in both Figures 6.11 and 6.16 are very comparable (approximately 11.7 in both cases). The major difference found between these two plots is the presence of a negative inflection in the dimensionless velocities of the double-layered vegetation case. This inflection has been discussed in detail in the previous paragraph.

6.4.2. Measurements In-line with Dowel (excluding those directly downstream)

As briefly mentioned above, all of the profiles taken in-line with the dowels, but not immediately downstream have a single inflection point. The profiles themselves look like nothing more than the intersection of two lines. An example of a profile of this type can be seen in Figure 6.17. Plots of all profiles taken in this classification can be found in the Appendix.

As seen in Figure 6.17, from the bed to a depth approximately 80% of the height of the shorter vegetation, velocity appears nearly constant. There are two major factors which seem to contribute to this characteristic. One is the shear force interaction between flow above and that within the shorter vegetation. Because the density of vegetation is much lower above the level of the shorter vegetation, the water there is moving at a higher velocity. This difference in velocity creates a shear force that seems to affect velocity well down into the shorter vegetation. An example of the progression of a velocity profile downstream of a tall dowel is shown in Figure 6.18. This figure demonstrates the vertical nature of the profiles between the dowels, and the changes in the shape and vertical location of the inflection points.

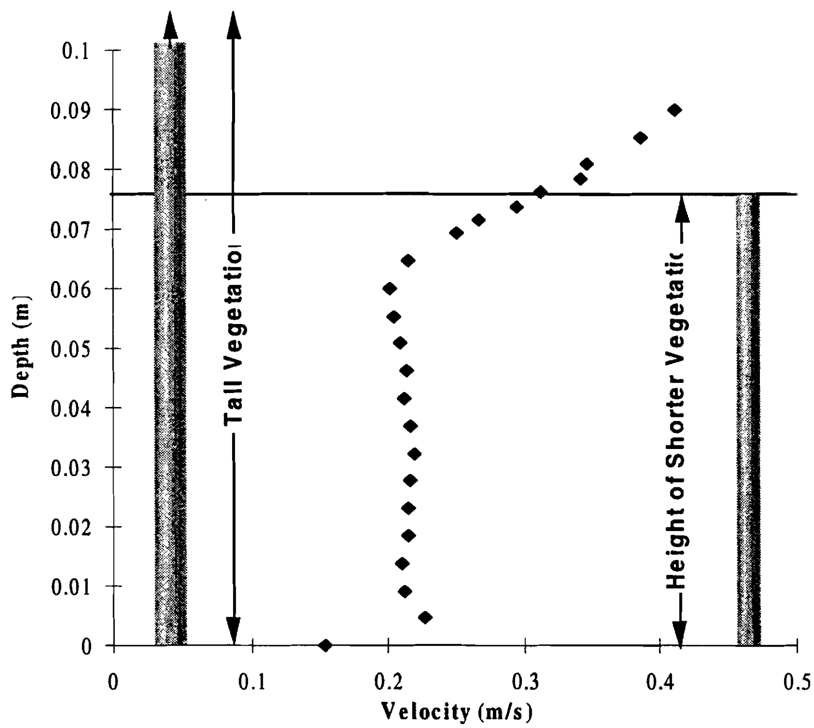

Figure 6.17: Velocity Profile from Experiment 9 [Linear s/d=8 (short), Linear s/d=16 (tall)] —Measurement Point 2 @ 12 Dowel Diameters (76.2 mm) from Tall Rod

A second factor that seems to play a role in the shape of the profile is the combined wake interference pattern caused by the interaction between those of the taller and shorter vegetation. From the surface, the standing wave formation looks similar to that shown in Figure 6.2. However, these surface waves seem to result mostly from the presence of the tall vegetation. Although the extent of the interaction between these two patterns is not fully understood at this time, one characteristic seems to stand out in all of

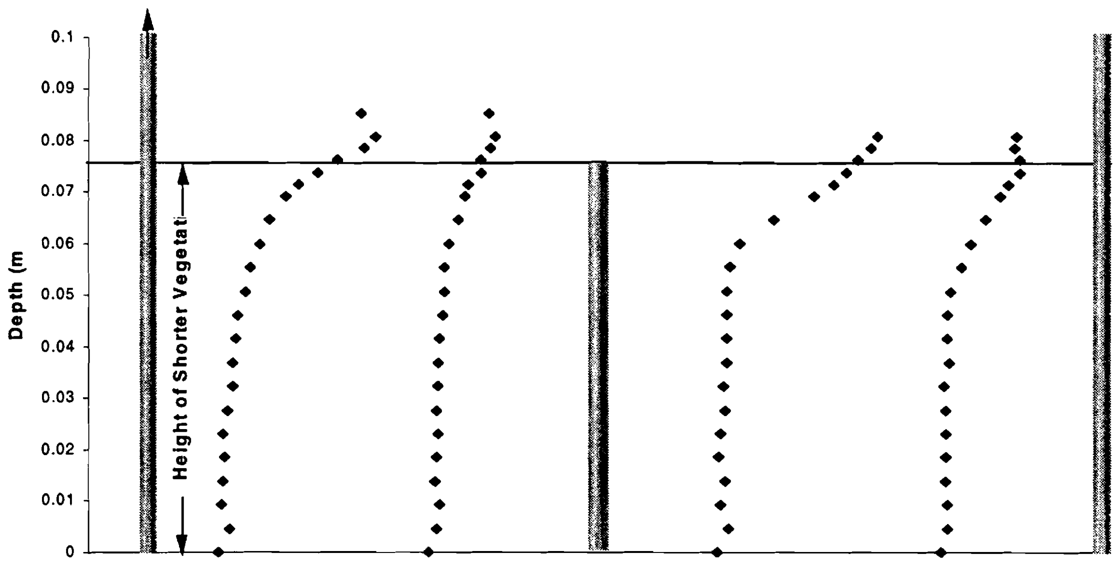

Figure 6.18: Progression of Velocity Profiles DS in Experiment 13 (Inline w/dowels)

the double-layer vegetation experiments. As shown in Figure 6.17, the inflection point in the profile is very well formed. The formation of the inflection point always appears to be more pronounced for measurements taken behind a short dowel than at other places in the flow field. It is found at the other measurement locations, but the inflection is more gradual than in a profile taken immediately downstream of a short dowel.

Unlike results from the single-layered vegetation experiments, the profile above the top of the short vegetation did not resemble a logarithmic profile offset by a slip velocity. This was expected because the tall vegetation is emergent even though the shorter vegetation is submerged. Although it was expected that the introduction of tall vegetation would cause the velocity to significantly decrease within the shorter vegetation, this was not clearly evident. Examination of the data shows that the average velocity within the short vegetation remains nearly the same for the submerged single-layered vegetation case and the double-layered vegetation case with the same short vegetation configuration. For example, comparison of experiment 5C Point 2 (25.4 mm DS) and experiment 9 Point 1 (25.4 mm DS) shows that the average velocity decreases from 0.22 m/s to 0.20 m/s when going from single-layered vegetation case to the double-layered case. Instead of a large decrease in the velocity in the short vegetation, the effect of the introduction of tall vegetation is to increase the depth of flow above the short vegetation. However, only slight increases in the normal depth for double-layered vegetation experiments were noticed. For instance, in experiment 5C Point 2 mentioned above, the normal depth measured upstream in the dowel array was 0.1031 meters. However, for experiment 9, the normal depth measured at the same location increased to 0.1050 m.

Figure 6.18 demonstrates the variable characteristics of the inflection point found near the top of the vegetation. Although the inflection point occurs at approximately the 80% height range for several of the profiles described herein, it should be mentioned that the height of the inflection varies depending on distance downstream from a dowel. The profile measured immediately downstream of a dowel has the highest inflection point. Points taken further downstream from the tall dowels tend to have lower inflection points. In addition, the inflection points seem to be most pronounced in profiles immediately dowstream of a short dowel. No other research dealing with flow through two layers of vegetation was found which could confirm this observation.

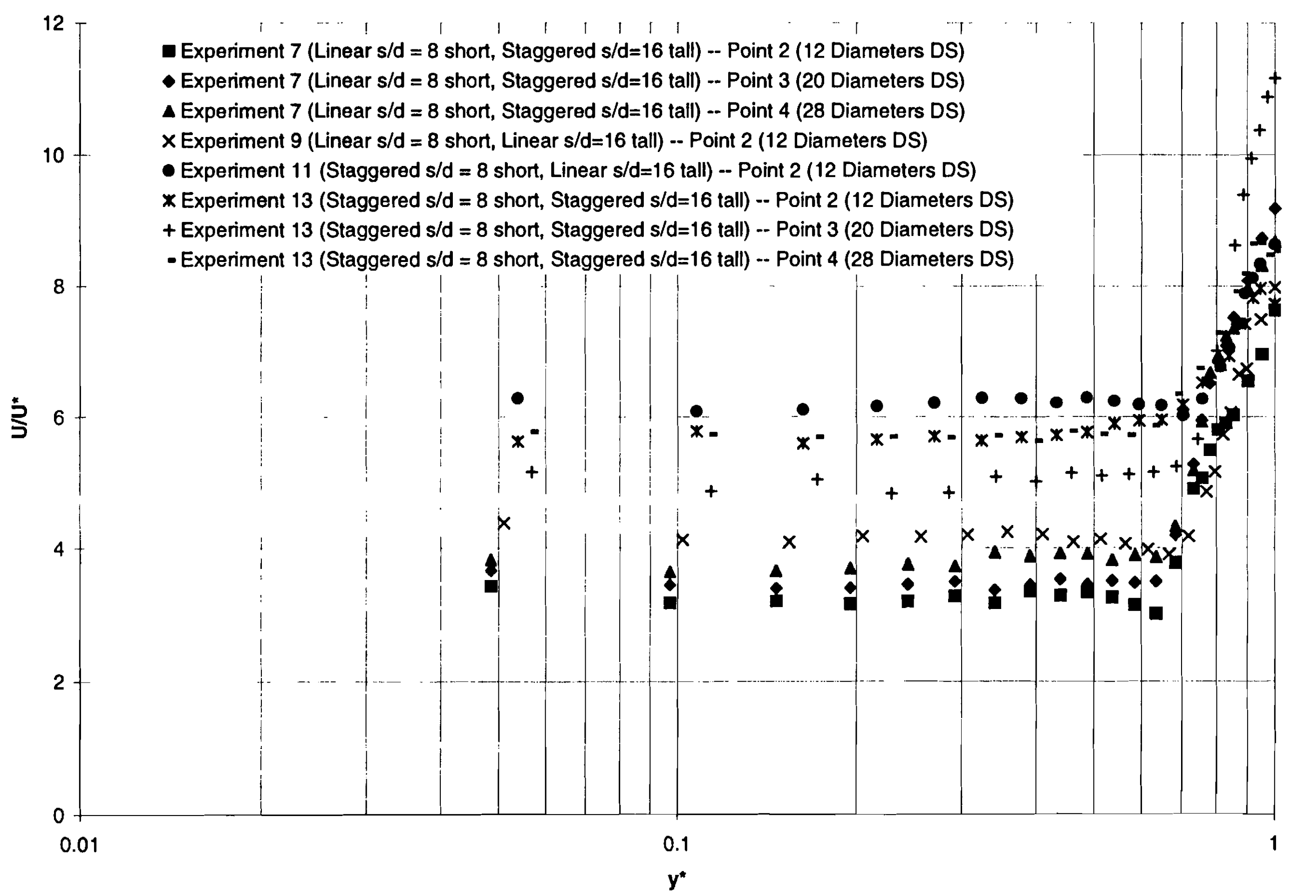

Figure 6.19: Dimensionless Plots of Double Layer Experiments Inline with Dowels (Profiles immediately downstream of dowel are excluded)

6.4.3. Measurements taken in the unobstructed flow region (not in-line with dowels)

The major trend noted in profiles taken in an unobstructed portion of the dowel array is that they follow a continuous curve and do not exhibit a sharp inflection point for sparse configurations of dowels. This distinction can be noticed upon comparison of Figure 6.17 and Figure 6.20. A dimensionless plot portraying profiles taken in this portion of the dowel arrays can be found in Figure 6.21. A second trend is that the magnitude of the velocity within the short vegetation is much higher in an unobstructed location than for measurement points inline with the dowels. Comparison between Figure 6.20 and the last profile in Figure 6.5 shows that measurements taken in unobstructed portions of the channel for the double-layered vegetation case closely resemble some profiles from the single-layered vegetation submerged flow case.

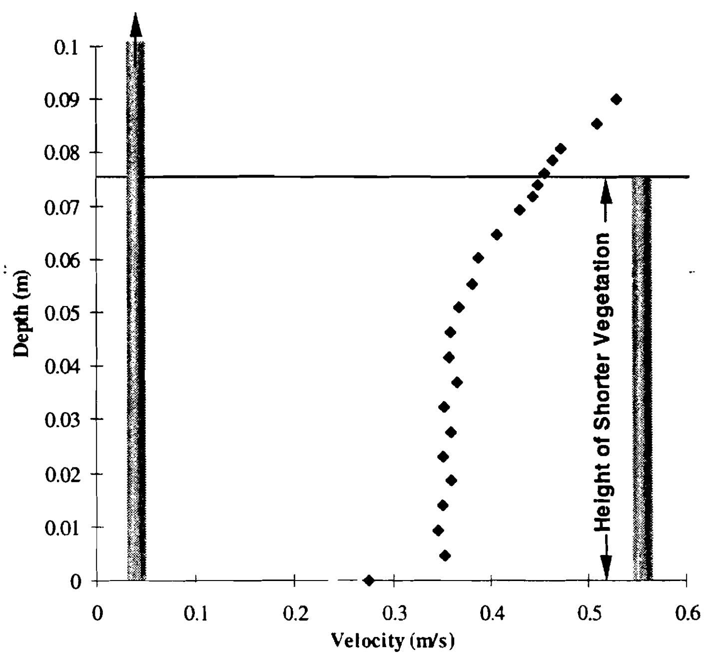

Figure 6.20: Velocity Profile from Experiment 9 [Linear s/d=8 (short), Linear s/d=16 (tall)] — Point 3 @ 4 Dowel Diameters (25.4 mm) DS, 4 Left of Centerline

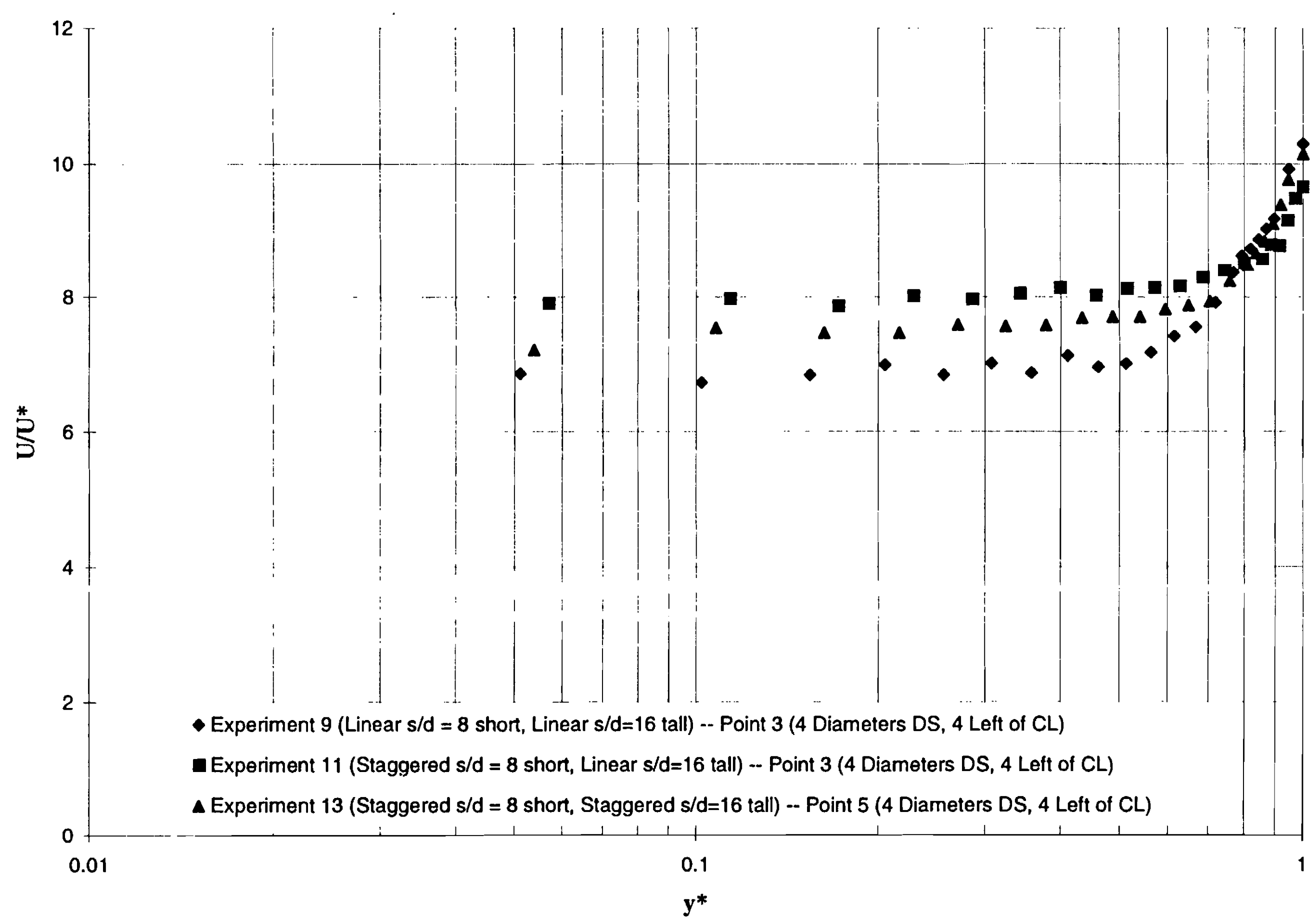

Figure 6.21: Dimensionless Plots of Double Layer Experiments in Unobstructed Locations

6.5 Apparent Roughness Coefficients

One method of characterizing the resistance to flow caused by the presence of vegetation is through the development of a roughness coefficient. The Manning formula has been used for the empirical solution of an estimated roughness coefficient for each dowel formation. In this manner, an estimate of the net increase in roughness caused by the various configurations of dowels can be formulated. Below, Table 6.2 shows the Manning n for each configuration of dowels as well as the calculated n coefficients for each of the control runs. These values were computed by solution of the Manning equation found in Chapter 2 in equation 2.1.

Table 6.2: Manning's coefficients for experiments

Experiment	Single/Double Layered	Configuration	Manning's n
Control 1	No Dowels	No Dowels	0.0071
Control 2	No Dowels	No Dowels	0.0071
4A	S	Staggered s/d = 8	0.0229
5A	S	Linear s/d = 8	0.0279
6A	S	Linear s/d = 16	0.0199
4C	S	Staggered s/d = 8 (Submerged)	0.0222
5C	S	Linear s/d = 8 (Submerged)	0.0236
6C	S	Linear s/d = 16 (Submerged)	0.0188
7	D	Linear s/d = 8 (short), staggered s/d = 16 (tall)	0.0247
8	D	Linear s/d = 8 (short), staggered s/d = 16 (tall)	0.0246
9	D	Linear s/d = 8 (short), linear s/d = 16 (tall)	0.0267
10	D	Linear s/d = 8 (short), linear s/d = 16 (tall)	0.0260
11	D	Staggered s/d = 8 (short), linear s/d = 16 (tall)	0.0210
12	D	Staggered s/d = 8 (short), linear s/d = 16 (tall)	00214
13	D	Staggered s/d = 8 (short), staggered s/d = 16 (tall)	0.0218
14	D	Staggered s/d = 8 (short), staggered s/d = 16 (tall)	0.0220

Table 6.2 shows a range of calculated Manning n values for the experiments to be between approximately .019 to .027. The average Manning value for all experiments is 0.023. Although there does not appear to be a significant variation in the Manning values tested in these experiments, use of the average value for normal depth prediction would

give an inaccurate estimate of depth for individual experiments. In addition, use of the average Manning n would ignore differences in density, configuration, and number of layers of vegetation in the model.

As expected, the least dense configuration of dowels produced the lowest Manning n value, while the densest configuration produced the largest n value. As shown above, all n values calculated for the experiments with dowels in the channel are significantly higher than the values of the control runs. Control runs were taken at two flow magnitudes corresponding to those used in the experiments and explained in Chapter 5. Manning n values calculated from both of these flow cases were approximately 0.007 which is within the expected range of values for a Plexiglas flume.

For the single-layered vegetation case, the Manning n values were always higher for the emergent condition. This is expected since some flow during the submerged vegetation case is above the dowels and encounters less resistance than flow within the vegetation. The effect of this is reduction of the average Manning value throughout the section. Roughness values calculated during these experiments should be associated with form drag created by the presence of the dowels. Because the material used for the dowels is Plexiglas, there should be very little skin drag associated with the dowels.

6.6 Analysis of Experimental Data for Determination of Drag Force

The attempt has been made to determine the drag force created by the existence of the dowel array in the open channel by two methods. First, equations described by Blevins (1992) were used to calculate the drag force on single dowels. This result was then multiplied by the number of dowels in the entire system in an attempt to create a total drag force on the system. Second, a shear force was calculated from the friction factor, f , in the channel. This shear force was used to calculate a resistance force in the channel which was then used for comparison to the method from Blevins (1992).

The method introduced by Blevins (1992) consists of calculation of three components of drag created by a cylinder piercing the free surface: spray and wave drag, ventilation drag, and hydrodynamic drag. Spray and wave drag refers to drag caused by the formation of a wave just upstream of the dowel. Ventilation drag refers to drag within the height of the depression formed just downstream of a dowel. Hydrodynamic drag refers to drag below the level of the depression. Spray and wave drag is given by the equation:

$$F_{d_1} = \tfrac{1}{2}\rho U^2\left(0.24d^2\right) \tag{6.2}$$

wheres F_d is the force of drag. The second component, ventilation drag is given by the following equation:

$$F_{d_2} = \tfrac{1}{2}\rho U^2 d\left(1+\frac{gh_c}{U^2}\right)h_c C_d \tag{6.3}$$

where $h_c = U^2|c_p| / 2g$ (c_p=-0.62 for a cylinder) and C_d = 0.5 from a table in Blevins (1992). The final component, hydrodynamic drag is given by the following equation:

$$F_{d_3} = \tfrac{1}{2}\rho U^2 d\left(y_n - h\right)C_d \tag{6.4}$$

where C_d = 1.1 from a table in Blevins.

Calculation of the individual components of the drag force were performed for emergen experiments, 4A (staggered s/d=8, 5A (linear s/d=8), and 6A (linear s/d=16) by using the above equations and is summarized in Table 6.3. The total force given in the last column of Table 6.3 represents the drag on all dowels in the 3.05 meter (10 ft.) test section.

Table 6.3: Results from Equations Given in Blevins(1992)

Experiment	Spray Drag (N)	Ventilation Drag (N)	Hydrodynamic Drag (N)	Total Drag On All Dowels (N)
4A	0.0328	0.0024	0.113	2.866
5A	0.0004	0.0005	0.0187	4.983
6A	0.0005	0.0008	0.0202	1.931

The second method used to calculate the total drag force in the channel employed the use of a Darcy friction factor, f. Equations given in Henderson (1966) were used to correlate the calculated Manning n in the previous section to the drag force in the channel. Equation 6.5 shows the formula used to correlate the Manning n with the Darcy f.

$$f = \frac{8n^2 g}{R^{1/3}} \tag{6.5}$$

This equation was used to calculate the friction factor for all emergent single-layered vegetation experiments. These are shown in Table 6.4.

A second formulation shown in Equation 6.6 was then used to calculate the boundary shear stress.

$$\tau_o = \frac{\rho f U^2}{8} \tag{6.6}$$

This boundary shear was multiplied by the wetted perimeter and the distance moved downstream in order to calculate a resistance force. This consisted of calculations in two areas within the dowel array: a cross-section taken through the dowels (resistance in dowels from Table 6.4) and a cross-section between dowels (resistance not in dowels from Table 6.4). The summation of the shear force in both areas and extended through the entire 3.05 meter (10 foot) test section are shown in Table 6.4.

Table 6.4: Calculation of Resistance Force in Channel

Experiment	**f**	**Shear** (kg / ms^2)	**Resistance (in Dowels)** N	**Resistance (not in Dowels)** N	**Total Resistance** N
4A	0.116	1.307	0.327	1.681	2.008
5A	0.168	1.437	0.635	1.927	2.563
6A	0.090	1.223	0.177	1.507	1.683

Comparison of Table 6.4 to Table 6.3 shows that resistance forces calculated from projection drag on a single cylinder throughout the array yields a higher total drag force than calculation of a bulk resistance force based on shear in the channel. This would seem to indicate that it is not valid to assume that drag on a single cylinder in an array of cylinders may be multiplied by the total number of cylinders to produce the total drag force. Results from these experiments seem to indicate that the resistance force caused by a single cylinder in an array of cylinders is less than that of a single cylinder alone.

A third method that was attempted for calculation of drag force was one given by Li and Shen (1973) shown in equation 6.5.

$$\left(Wly_n - \tfrac{1}{4}n_v y_n \pi d^2\right)\gamma S = \left(Wl - \tfrac{1}{4}n_v \pi d^2\right)\tau_o + \tfrac{1}{2}\rho U^2 y_n d \sum \overline{C_d} \qquad (6.5)$$

where W is the width of the test section, l is the length of the test section, n_v is the total number of vegetative stalks, $\tau_o = \rho\, g y_n S$, and $\sum \overline{C_d}$ is the sum of the mean drag coefficient. Li and Shen (1973) noted that this method is valid for "...vegetations, whose heights are of the same order of magnitude as flow depth...the spacing between the cylinders is at least 6 diameters in the downstream direction and 3 diameters in the transverse dierection." Although the models used in these experiments met the criteria for use of this model, calculated values of $\sum \overline{C_d}$ for both experiments 4A and 5A yielded negative results; therefore, this method could not be used in comparison with the drag force calculated by the equations from Blevins (1992).

6.7 Statistical Analysis of Experimental Data

Several statistical parameters have been computed to analyze the data points of the velocity profiles measured in these experiments. The first of these, the mean, was used to create the velocity profiles seen in the previous section. No data points were excluded when calculating the mean velocity at any given location—including the negative velocity readings found directly downstream of a dowel.

In addition to mean velocity, a RMS value was calculated for each set of velocity measurements. The RMS, or standard deviation, value was calculated by the following equation:

$$RMS = \sqrt{\frac{\sum (U_i - \overline{U})^2}{(n_s - 1)}} \qquad (6.6)$$

where U_i represents an individual velocity measurement, $\overline{U}$ represents the mean velocity of individual measurements (U_i) in the group, and n is the total number of measurements taken at that particular location.

As can be seen in Figure 6.22, several general trends relating to standard deviation in velocity measurements may be noted. In order to produce a plot that can be prepared to similar plots, the standard deviation is non-dimensionalized by dividing the standard deviation by the average of all of the velocity measurements in the same data set. This value is know as the coefficient of variation in statistics, and the turbelence intensity when related to velocity. The first noticeable trend is that the standard deviation in velocity measurements for any given profile is highest near the bed. From this point, the deviation generally decreases until the water surface is reached. Secondly, deviation for a group of experiments is highest in those profiles taken immediately downstream of a dowel. In addition, the profiles taken in an unobstructed portion of the dowel array tend to have the lowest average RMS values. The values for the control run were included in Figure 6.22 to show a typical RMS distribution for a logarithmic profile.

Figures 6.23 and 6.24 show turbulence intensities for double-layered vegetation experiments. Figure 6.23 shows curves for all double-layered vegetation experiments that have measurement taken immediately downstream of a tall dowel (4 dowel diameters). The figure shows that there is a definite trend in the relative deviation for all of these experiments. Standard deviation appears to be nearly constant throughout the short vegetation. Near the surface the deviation for all of these experiments increases briefly, but then decreases when measurements move closer to the free surface. Note that

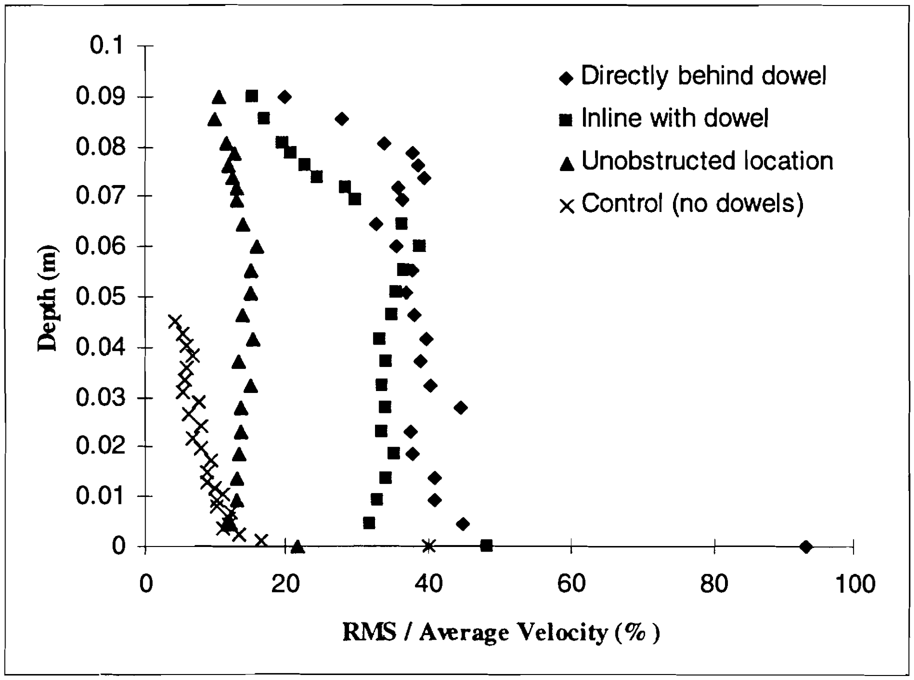

Figure 6.22: Turbulence Intensities for the Profiles of Experiment 9

all of these experiments are taken immediately downstream of a tall dowel. Although this is the case, the range of constant standard deviation is from the bed to a height of approximately 7.6 cm (the height of the shorter vegetation) above the bed.

Figure 6.24 contains plots of measurement taken at 12 dowel diameters downstream of a tall dowel. This figure shows that as distance increases downstream from a tall dowel, the standard deviation in measurements varies with density of the configuration. The standard deviation of Experiments 11 and 13 are lower than those of the other experiments. This seems to stem from the difference in density in the short vegetation for each experiment. Experiments 11 and 13 were performed with a staggered arrangement of dowels (s/d=8) unlike the remaining experiments shown on the plot which were constructed using a linear arrangement (s/d=8).

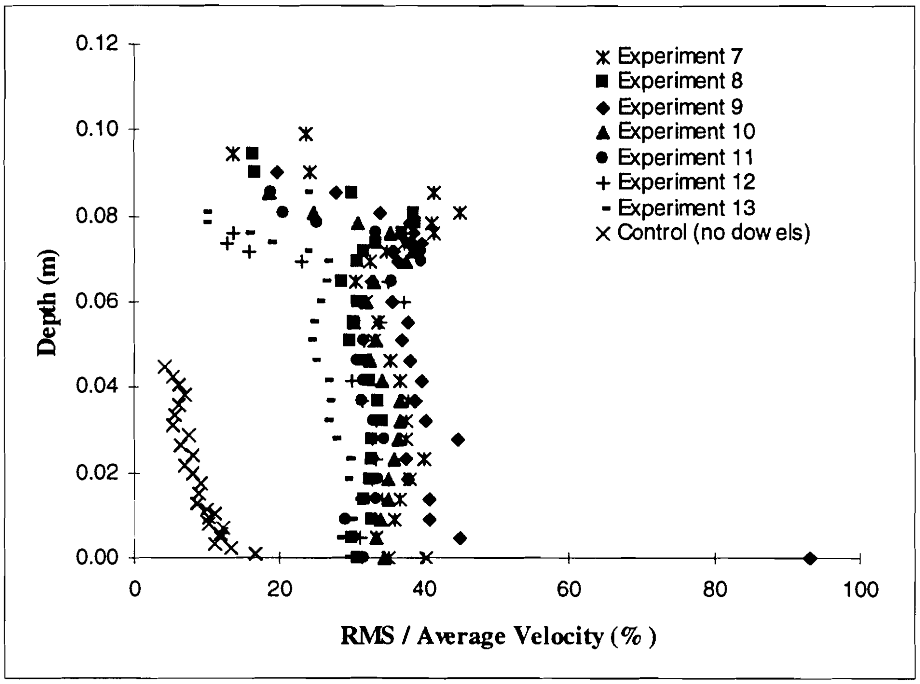

Figure 6.23: Turbelence Intensities for the Profiles of Experiments 7-13 (Double-Layered Vegetation Experiments @ 4 Dowel Diameters [25.4mm] DS)

In order to determine if the velocity data was normally distributed, the skew coefficient was calculated at each measurement location. The skew measures a data set to determine if it is symmetrically distributed. Skew is calculated by the following equation found in Wine (1964):

$$Skew = \frac{n_s}{(n_s - 1)(n_s - 2)} \sum \frac{(Ui - \overline{U})}{RMS^3} \qquad (6.7)$$

where n_s is the number of samples, Ui is an individual measurement, and the RMS is the standard deviation. A skew of exactly zero indicates that the distribution is normally distributed. A negative value indicates that the distribution is skewed left and a positive value indicates that the distribution is skewed right.

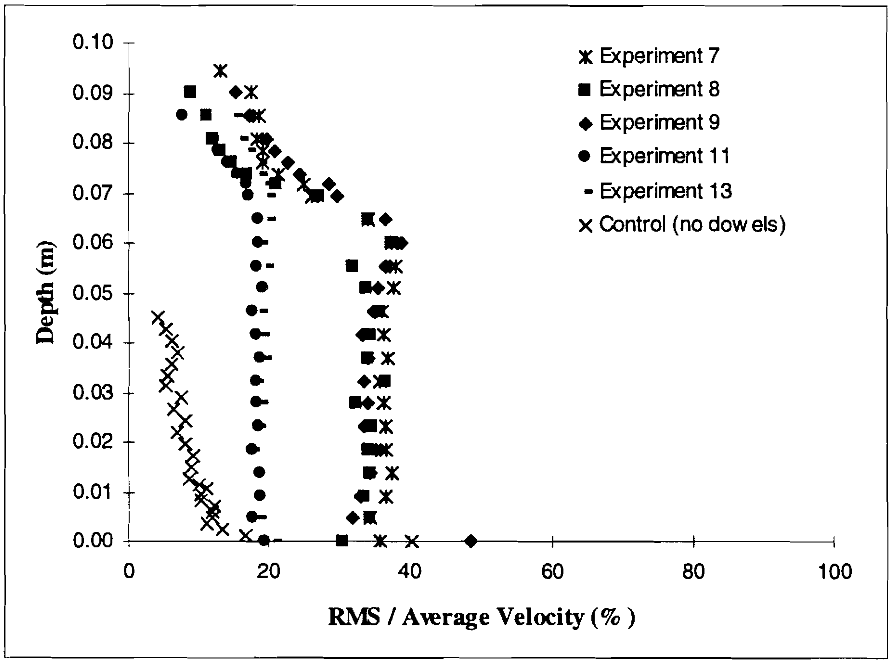

Figure 6.24 Turbulence Intensities for the Profiles of Experiments 7-13 (Double-Layered Vegetation Experiments @ 12 Dowel Diameters[76.2mm] DS)

Although this gives some indication of measurement points relative to the mean, this test alone is not adequate to determine the normality of a data set. Therefore, a goodness of fit test called the Chi squared test was used to test for normality. The method for this test will not be discussed here, but the author recommends the statistical manual by Wine (1964) for the theory and methodology behind this test. Using the Chi squared test for the 90% and 95% confidence intervals, data for almost all measurements were found not to be normally distributed. Approximately 10 data sets passed the Chi squared test; however, these results were not valid due to the low number of samples at these locations. The Chi squared analysis required a relatively large number of samples in order to yield accurate results. Figures 6.25, 6.26, and 6.27 show theoretical normal distributions plotted on top of actual histograms. These figures visually show that data taken during experiments is not normally distributed.

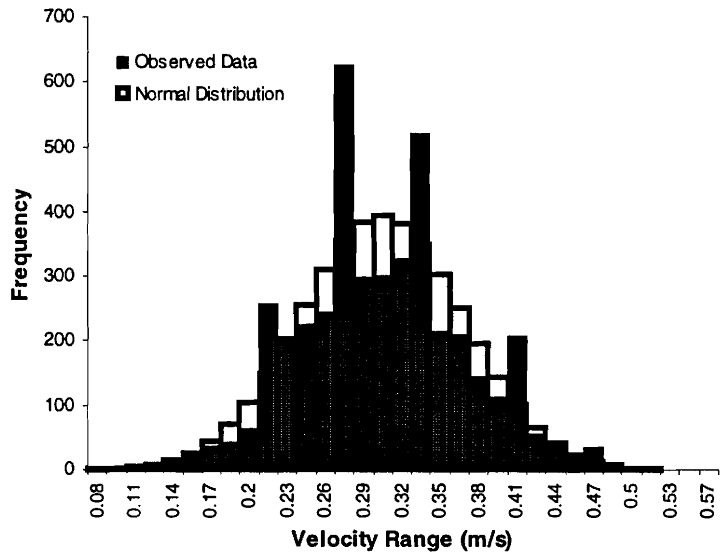

Figure 6.25: Experiment 6C Profile 3 Measurement Point 5

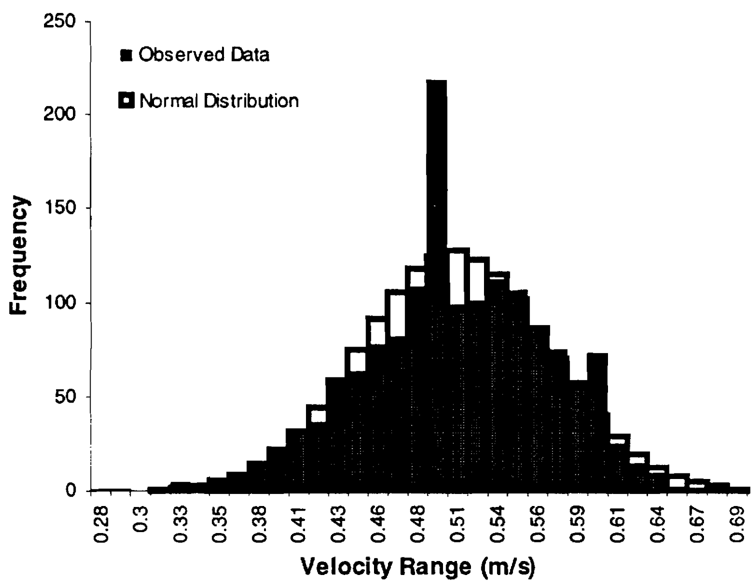

Figure 6.26: Experiment 11 Profile 2 Measurement Point 16

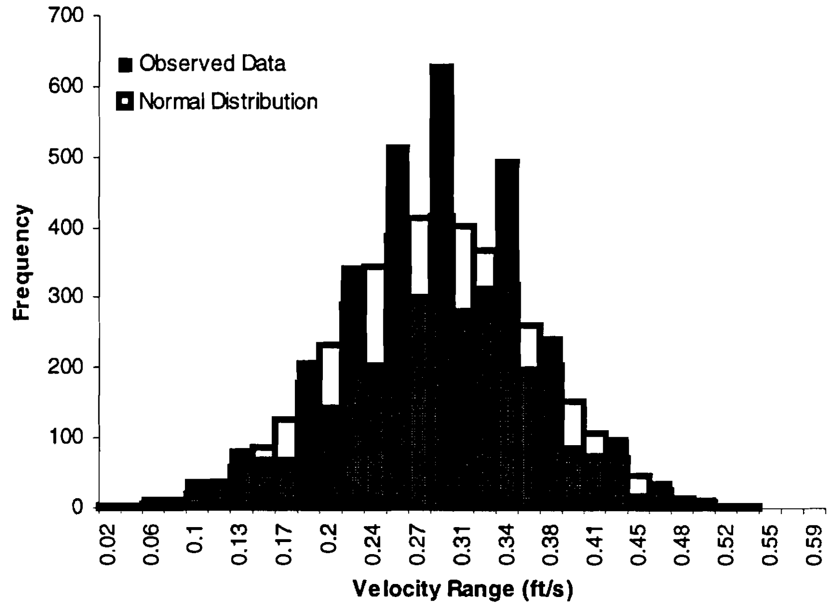

Figure 6.27: Experiment 13 Profile 1 Measurement Point 1

6.8 Reynolds and Froude Numbers

As mentioned previously in Chapter 4, it is believed that in studies involving emergent vegetation, both Reynolds and Froude numbers are important for any modeling attempt. Through the use of average flow velocities as well as normal depths caused by the various configurations of dowels, Froude and Reynolds numbers (depth and diameter based) have been calculated in Table 6.5. As seen in the table, as the density of vegetation increases for a constant Q, the normal depth increases. All Froude numbers calculated for these experiments show flow to be well within the subcritical range. Depth based Reynolds numbers ranged between approximately 20000 and 40000 for all experiments. These values indicate that experiments were conducted under turbulent flow conditions.

6.9 Summary of Results

The main purpose of these experiments was to study the effect vegetation has on flow. There are several generalizations that have appeared over the course of these experiments.

1. As density of vegetation increases for a constant Q, the normal depth increases.
2. The inflection point of the velocity profile is higher as the density of vegetation increases.
3. For high vegetative densities, the shape of the velocity profile within the shorter vegetation is nearly vertical.
4. For the submerged case, the inflection point of the profile is well below the top of the vegetation
5. As density increases, measurements of the velocity profiles in-line with dowels become almost identical to profiles taken at an unobstructed position.
6. Negative (upstream) flows exist directly downstream of dowels.
7. In measurements taken immediately downstream of a dowel, the combination of wake and shear forces creates a spike in the velocity profile near the bed.

Results of the experiments have been used to calculate and compare Manning's roughness coefficients for the various configurations of dowels. In addition, some statistical analysis has been performed to determine the standard deviation of the data, and to show that the data is not normally distributed based on a Chi squared test. Finally, although staggered and linear configurations of dowels were used in the experiments, the general trends mentioned above were found in both arrangements. This can be seen most clearly in the dimensionless plots of the profiles included in the previous pages.

Table 6.5: Froude and Reynolds Numbers for Experimental Runs

Single-layered vegetation

Experiment	Description	Upstream (m)	Up Datum (m)	Downstream (m)	Down Datum (m)	Q (m^3/s)	U (avg) (m/s)	F	Rd (diameter)	Re (depth)
EXP 6A	Linear s/d = 16	0.2376	0.1809	0.2342	0.1818	0.0057	0.356	0.477	2434	20090
EXP 6C	Linear s/d = 16	0.2687	0.1809	0.2665	0.1818	0.0114	0.441	0.475	3012	40180
EXP 4A	Staggered s/d = 8	0.2438	0.1816	0.2399	0.1812	0.0057	0.318	0.407	2173	20090
EXP 4C	Staggered s/d = 8	0.2801	0.1816	0.2768	0.1812	0.0114	0.390	0.397	2669	40180
EXP 5A	Linear s/d = 8	0.2531	0.1818	0.2519	0.1810	0.0057	0.263	0.315	1799	20090
EXP 5C	Linear s/d = 8	0.2849	0.1818	0.2796	0.1810	0.0114	0.379	0.376	2588	40180

Double-layered vegetation

Experiment	Description	Upstream (m)	Up Datum (m)	Downstream (m)	Down Datum (m)	Q (m^3/s)	U (avg) (m/s)	F	Rd (diameter)	Re (depth)
EXP 7	Linear s/d=8 short, Staggered s/d = 16 (tall)	0.2868	0.1805	0.2805	0.1815	0.0114	0.377	0.382	2577	40180
EXP 8		0.2814	0.1805	0.2685	0.1815	0.0106	0.400	0.433	2736	37490
EXP 9	Linear s/d=8 short, Linear s/d = 16 (tall)	0.2930	0.1805	0.2782	0.1815	0.0114	0.386	0.396	2638	40180
EXP 10		0.2855	0.1805	0.2711	0.1815	0.0106	0.389	0.414	2657	37490
EXP 11	Staggered s/d=8 short, Linear s/d = 16 (tall)	0.2762	0.1813	0.2709	0.1815	0.0114	0.418	0.446	2854	40180
EXP 12		0.2683	0.1813	0.2625	0.1815	0.0099	0.401	0.450	2743	34990
EXP 13	Staggered s/d=8 short, Stag. s/d = 16 (tall)	0.2791	0.1819	0.2727	0.1813	0.0114	0.408	0.431	2791	40180
EXP 14		0.2737	0.1804	0.2693	0.1813	0.0106	0.396	0.426	2705	37490

Chapter 7
CONCLUSIONS

This research was performed for a simple case using materials that decrease surface roughness and holding constant many variables such as slope, flow, and vegetative flexibility. The major variable tested was density of vegetation. In order to gain a better understanding of flow processes within riparian wetlands, the variables held constant in these experiments should be studied further.

Several major trends were discovered during the course of experiments performed for this research. These are discussed in detail in Chapter 6, but will also be mentioned briefly in the following sentences. As vegetative density increases, the shape of the velocity profile within the shorter vegetation becomes nearly vertical. This trend was noticed to occur for nearly the entire height of the vegetation for the submerged vegetation condition and for the double-layered vegetation tests as well as for higher densities of the non-submerged tests.

For the submerged vegetation case, the inflection point of the profile is below the top of the vegetation. The exact location of this inflection varied with distance from an upstream dowel, flow rate, and density of vegetation. The trend identified is that as a velocity profile progresses in the downstream direction, the inflection point seems to move closer to the bed.

Finally, a study of standard deviation in the velocity measurements show trends in the deviation encountered across experimental configurations. The results from these experiments shows that the highest deviation occurs in measurement taken immediately downstream of a dowel. The smaller standard deviations occur in experiments conducted with lower vegetative densities or profiles measured in an unobstructed portion of the channel (between dowels).

During creation of histograms, some distributions appear to be skewed, although most experiments taken at all locations within the vegetation appear to be nearly normally distributed. When a chi squared analysis of the experiments was run, this apparent normality appeared unfounded. None of the distributions passed the chi square test for normality. Histograms included in the Appendix show this aspect for several experiments. Although two peaks occur on a few of the histograms, it should be noticed that the shape is highly dependent upon the bin size used to create the histograms. This should give insight on the expected deviation in measurements at various vertical locations for similar experiments.

Although an attempt was made to study and analyze important variables, it was impossible to examine all relevant variables during this research. Several key areas need to be examined in order to gain a better understanding of flow through riparian wetlands. First, the effect of flexibility in vegetation needs to be understood. Many researchers have undertaken a study of this variable with some of the research summarized in Chapter 2. Second, a study examining the effects of skin drag needs to be undertaken. The experiments described in this text studied only form drag and did not examine the effect of skin drag. It would be useful to examine the effects that increased skin roughness has on the shape and magnitude of velocity profiles.

One of the major goals of an understanding of the processes in riparian wetlands is to come up with a model that adequately predicts the sediment yield due to the presence of the vegetation. Therefore, research using sediment needs to be performed which characterizes the areas within vegetation corresponding to the highest sedimentation and scour rates. In addition, research needs to be performed which characterizes the effect that branches have on velocity profiles and sedimentation rate.

Study of flow through riparian wetlands is a fascinating, but extremely complex undertaking. Only by the contributions of many researchers who explore different aspects of flow variables will hydraulic researhers begin to understand in detail the processes governing these areas. Through this undertaking, models may be developed which will predict flow responses due to the presence of riparian vegetation.

Literature Cited

Blevins, Robert. Applied Fluid Dynamics Handbook. Krieger Publishing Company, Malabar,Florida, 1992, p.365.

Burke, Roger W. "Free Surface Flow Through Salt Marsh Grass", PhD Dissertation, Mass. Institute of Technology.

Ceinzelmann, CH. and Wallisch, S. "Benthic settlement and bed erosion. A review" J. of Hydraulic Research, 29(3), 355-371, (1991).

Chen, Cheng-lung. "Flow Resistance in Broad Shallow Grassed Channels". J. Hydraulics Division, ASCE, 102(3), 307-322, (1976).

Chow, Ven Te. Open Channel Hydraulics. McGraw-Hill Book Company., Inc., New York, 1959.

Eastgate, W.I., "Vegetated Stabilization of Grassed Waterways and Dam Bywashes," thesis presented to the University of Queensland, at St. Lucia, Queensland, Australia, in 1966, in partial fulfillment of the requirements for the degree of Masters of Engineering Science.

Engelund, F., "A Practical Approach to Self-Preserving Turbulent Flows," ACTA Polytechnica Scandivavia, Civil Engineering and Building Construction Series No. 27, Copenhagen, 1964, 23 pp.

Hartley, David M. "Resistance to Shallow Flow Through Vegetation", M.S. thesis, Colorado State University, 1980.

Henderson, F.M. Open Channel Flow. Macmillan Publishing Co., New York, 1966.

Hino, Mikio. "Ecohydrodynamics", Advances in Hydroscience, Vol.12, , 143-151, (1981).

Hsieh, T., "Resistance of cylinder Piers in Open-Channel Flow," Journal of the Hydraulics Division, ASCE, Vol.90, No. HY1, Proc. Paper 3770, Jan., 1964, pp. 161-173.

Ikeda, S. and Izumi, N. "Width and Depth of Self-Formed Straight Gravel Rivers with Bank Vegetation" Water Resources, 26(10), 2353-2364, (1990).

Ikeda, S. And Kanazawa, M. "Three-Dimensional Organized Vortices above Flexible Water Plants", J. of Hydraulic Engineering, Vol 122(11), 634-640,(1996) Kadlec, R.H. "Overland Flow in Wetlands: Vegetation Resistance." Journal of Hydraulic Engineering, v.116 n5, May 1990, p. 691-706

King, MacArthur, Dexter, Smith. "Two-Dimensional Finite Element Simulation of the Flooding Characteristics in Kawainui Marsh, Hawaii." Proceedings of 1990 National Conference in Hydraulic Engineering, ASCE 1990, p.664-669.

King, I and Roig, L. "Finite Element Modeling of Flow in Wetlands." Proceedings - National Conference on Hydraulic Engineering, ASCE: New York, NY p.286-291, 1991.

Kouwen, N., and Harrington, R.A., "A Criterion for Vegetation Stiffness," *Agricultural and Urban Considerations in Irrigation and Drainage,* ASCE, 1974, pp. 273-284.

Kouwen, N., Unny, T.E. , and Hill. "Flow retardance in vegetated channels." J. Irrigation and Drainage, ASCE, 95(2), 329, (1969).

Kouwen, N., and Unny, T.E., "Flexible Roughness in Open Channels," Journal of Hydraulics Division, ASCE, Vol. 99, No. HY5, Proc. Paper 9723, May, 1973 pp. 713-728.

Kouwen, N. and R.M. Li. "Biomechanics of vegetated channel linings" J. Hydraulic Division, ASCE, 106(6) 1085-1103, (1980).

Fathi-Maghadam M. and Kouwen N. "Nonrigid, Nonsubmerged, Vegetative Roughness on Floodplains", J. of Hydraulic Engineering, Vol 123(1), 51 - 57,(1997)

Li and Shen. "Effect of Tall Vegetation on Flow and Sediment" Journal of the Hydraulic Division, ASCE 99(5), 793-814. (1994)

Manning, R. "On the Flow of Water in Open Channels and Pipes." Trans., Inst. Of Civil Engrs. Of Ireland, Dublin, Iredland, 20, 161-166, (1889).

Masterman, R. "Vegetation effects on riverbank stability." PhD Dissertation, Univ. of Nottingham.

Masterman, R. and Thorne, C.R. "Predicting influence of bank vegetation on channel capacity " JHE, ASCE, 118(7), 1052-1058, (1992).

Mitsch, William and Gosselink, James. "Wetlands" Van Nostrand Reinhold: New York, (1993).

Morris, H.M. and Wiggert, J.M. Applied Hydraulics in Engineering. John Wiley & Sons: New York, 1963, p. 489.

Palmer, V.J., "A Method for Designing Vegetated Waterways," Agricultural Engineering, Vol.26, No. 12, Dec., 1945, pp. 516-520.

Petryk, s. and Bosmajian, G. "Analysis of Flow Through Vegetation" J. Hydraulics Division, ASCE, 101(7), 871-884, (1975).

Ree, W.O., and Palmer, V.J., "Flow of Water in Channels Protected by Vegetative Linings." U.S. Dept. of Agriculture, Feb. 1949, 115 pp.

Ree, W.O., "Retardation Coefficients for Row Crops in Diversion Terraces, "Transactions of the American Society of Agricultural Engineers, Vol. 1, 1958, pp. 78-80.

Robert, A. "Boundary roughness in coarse-grained channels" Progress in Physical Geography, 14, 42-70 (1990).

Roig, Lisa. "Hydrodynamic Modeling of Flows in Tidal Wetlands." UC-Davis. 1994, PhD Dissertation.

Roig, Lisa. "Mathematical Theory and Numerical Methods for the Modelling of Wetland Hydraulics." International Water Resources Engineering Conference - Proceedings, ASCE: New York, v1, 1995, p. 249-253.

Rouse, H. "Critical Analysis of Open Channel Resistance," Journal of the Hydraulics Division, ASCE, Vol. 91, No. HY4, Proc. Paper 4387, July, 1965, pp. 1-25.

Shrestha, P. "Multiphase Distribution of Cohesive Sediments and Associated Toxic Heavy Metals in Surface Water Systems." PhD. Dissertation, University of California Davis, 1991.

Streeter, V.L., Fluid Mechanics , 5th ed., McGraw-Hill Book Co., Inc., New York, NY, 1971.

Task Force on Friction Factors in Open Channels of the Committee on Hydromechanics of the Hydraulics Division. "Friction Factors in Open Channels," Journal of the Hydraulics Division, ASCE, Vol. 89, No. HY2, March, 1963, pp. 97-143.

Thompson, G.T. and Roberson, J.A. "A theory of flow resistance for vegetated channels". Transaction of the American Society of Agricultural Engin., 19(2), 341-354 (1979).

Thornton, C. "Sediment Deposition and Entrapment in Submerged Stream Vegetation". Thesis in Department of Civil Engineering, Colorado State University, 1995.

Tsujimoto, T., Shimizu, Y., and Nakagawa, H. "Turbulent Flow and Suspended Sediment Transport in Vegetated Sand Bed Channel." XXIV IAHR Congress, Madrid: 1991.

Tsujimoto, Tetsuro. "Unstable Phenomena Appearing in Open-Channel Flows with Vegetation". Advances in Hydro-Science and Engineering, Volume 1, 1390-1397.

Tsujimoto, Tetsuro. "Spectral Analysis of Velocity and Water-Surface Fluctuations Appearing in an Open Channel With Vegetated and Non-Vegetated Regions in a Cross-Section." Proceedings of 6th International Symposium on Stochastic Hydraulics, Taipei, 361-367, (1992).

Tsujimoto, Tetsuro. "Progressive Research Report of KHL". Hydraulics Laboratory Department of Civil Engineering at Kanazawa University,1-107 ,(1992).

Vreugdenhil, C.B. "Numerical Methods for Shallow-Water Flow". Kluwer Academic Publishers: Boston, 1994.

Wine, Lowell. Statistics for Scientists and Engineers. Prentice-Hall Inc., Englewood Cliffs, N.J., 1964.

Zavistoski, Rebecca. "Hydrodynamic effects of Surface Piercing Plants", thesis, Mass. Institute of Technology, 1994.

APPENDIX

This appendix contains all of the summarized data and velocity profiles for experiments described in previous chapters. In the following pages, tables are introduced which summarize the following data for each experiment:

1. Average Velocity—the average velocity for all measurements at that location.
2. Depth—distance from the bed
3. Maximum Velocity—the maximum velocity measured at that location
4. Minimum Velocity—the minimum velocity measured at that location
5. Standard Deviation(RMS)—as defined in Chapter 6
6. Number of Samples—the number of measurements taken at that location
7. Sampling Frequency—average sampling rate for the measurement location
8. Coefficient of Skewness—as defined in Chapter 6
9. Kurtosis—defined below

Kurtosis gives an estimation of the peakedness of data and is calculated by the following equation:

$$Kurtosis = \frac{1}{n_s}\frac{\sum\left(u_i - \bar{u}\right)}{RMS^4} \tag{A.1}$$

A calculation of kurtosis on a normal distribution will yield a value of exactly 3. Data included in the tables was processed from raw data collected from the laser doppler velocimeter. In addition to tables of data, velocity profiles have been normally plotted and included in the Appendix for every experiment. Histograms for representative profiles from each group of experiments have also been included in the Appendix.

Velocity ranges for calculation of frequency for these histograms is variable. The bin sizes (velocity ranges) were varied in each location to give exactly 20 bins over the velocity measurement range.

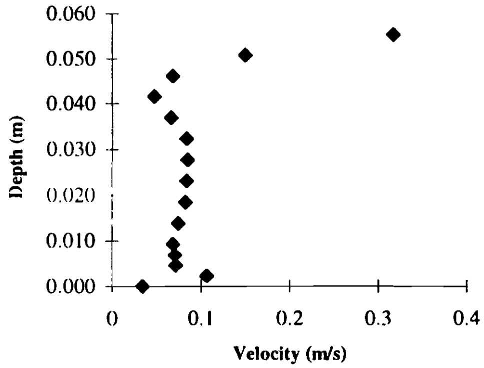

12.7 mm downstream from rod

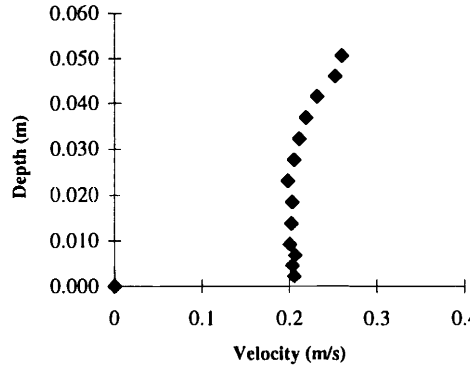

38.1 mm downstream from rod

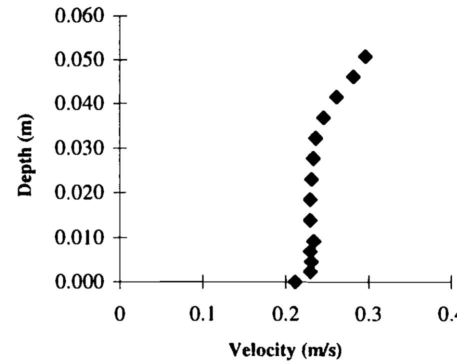

63.5 mm downstream from rod

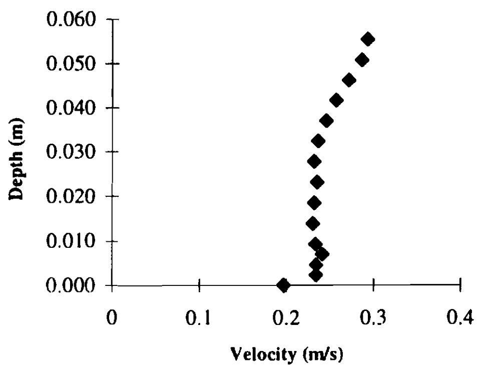

88.9 mm downstream from rod

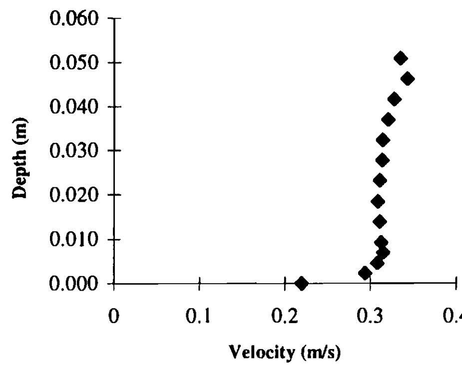

25.4 mm downstream from rod
25.4 mm left of centerline

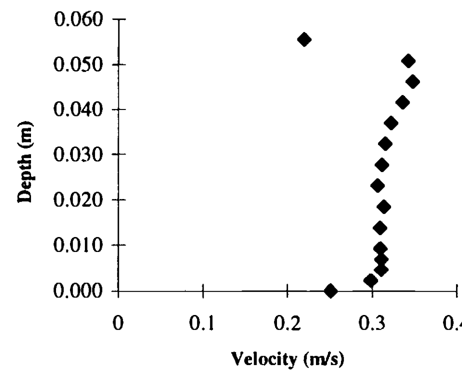

76.2 mm downstream from rod
25.4 mm left of centerline

Figure A1: Velocity Profiles for Staggered Formation of 76.2 mm Rods with s/d = 8 (Unsubmerged case)

Table A1: Experiment 4A, Measurement Point 1

Average Velocity (m/s)	Depth (m)	Maximum Velocity (m/s)	Minimum Velocity (m/s)	Standard Deviation (m/s)	Number of Samples	Sampling Frequency (Hz)	3rd Moment Skew	Kurtosis
0.034	0.0000	0.2149	-0.2412	0.1415	16	0.154	-0.2204	1.5999
0.106	0.0023	0.3369	-0.1830	0.0865	256	1.869	-0.1889	3.3982
0.072	0.0046	0.3257	-0.1943	0.0917	463	3.136	-0.1367	2.8544
0.071	0.0069	0.3745	-0.1605	0.0807	511	3.470	0.1269	3.0071
0.068	0.0092	0.3125	-0.1718	0.0867	656	4.413	0.0205	2.6401
0.074	0.0139	0.3613	-0.2412	0.0856	767	5.119	-0.189	3.3224
0.082	0.0185	0.3125	-0.2187	0.0858	1000	7.046	-0.1866	2.8874
0.084	0.0231	0.3745	-0.2055	0.0905	1000	8.032	-0.2362	2.9625
0.085	0.0277	0.3613	-0.3201	0.0894	1000	8.477	-0.3215	3.3165
0.084	0.0323	0.3857	-0.1718	0.0863	1000	10.216	-0.1049	2.9036
0.066	0.0370	0.3501	-0.1943	0.0891	1000	10.234	-0.0681	2.8235
0.047	0.0416	0.3501	-0.1718	0.0831	1000	10.173	0.2379	2.9642
0.069	0.0462	0.3989	-0.1830	0.0879	1000	9.681	0.1961	2.9248
0.150	0.0508	0.3989	-0.1136	0.0874	1000	7.656	0.0093	2.8163
0.317	0.0554	0.5303	-0.0291	0.0765	288	1.972	-0.6714	4.039

Table A2: Experiment 4A, Measurement Point 2

Average Velocity (m/s)	Depth (m)	Maximum Velocity (m/s)	Minimum Velocity (m/s)	Standard Deviation (m/s)	Number of Samples	Sampling Frequency (Hz)	3rd Moment Skew	Kurtosis
0.208	0.0023	0.3497	0.0556	0.0525	159	1.079	0.0088	3.251
0.208	0.0023	0.3497	0.0556	0.0525	159	1.079	0.0088	3.251
0.205	0.0046	0.3497	0.0556	0.0518	416	2.781	0.077	2.7789
0.203	0.0069	0.3742	0.0669	0.0541	590	3.983	0.1109	2.7896
0.207	0.0092	0.3987	0.0443	0.0536	622	4.216	0.0995	3.1411
0.200	0.0139	0.3987	0.0556	0.0539	847	5.680	0.199	2.9817
0.202	0.0185	0.3874	0.0443	0.0530	960	6.508	0.1758	2.8998
0.203	0.0231	0.3629	0.0443	0.0523	1000	8.154	-0.0668	3.0485
0.198	0.0277	0.3629	0.0311	0.0545	1000	9.114	0.1071	2.92
0.205	0.0323	0.3987	0.0669	0.0537	1000	7.910	-0.0261	2.8834
0.211	0.0370	0.3497	0.0556	0.0512	1000	7.001	-0.1254	2.8798
0.218	0.0416	0.3742	0.0311	0.0519	912	6.163	-0.2099	3.1302
0.231	0.0462	0.4364	0.0669	0.0529	1000	6.892	0.0451	3.13
0.252	0.0508	0.4119	0.0914	0.0475	1000	8.786	-0.1152	2.9334

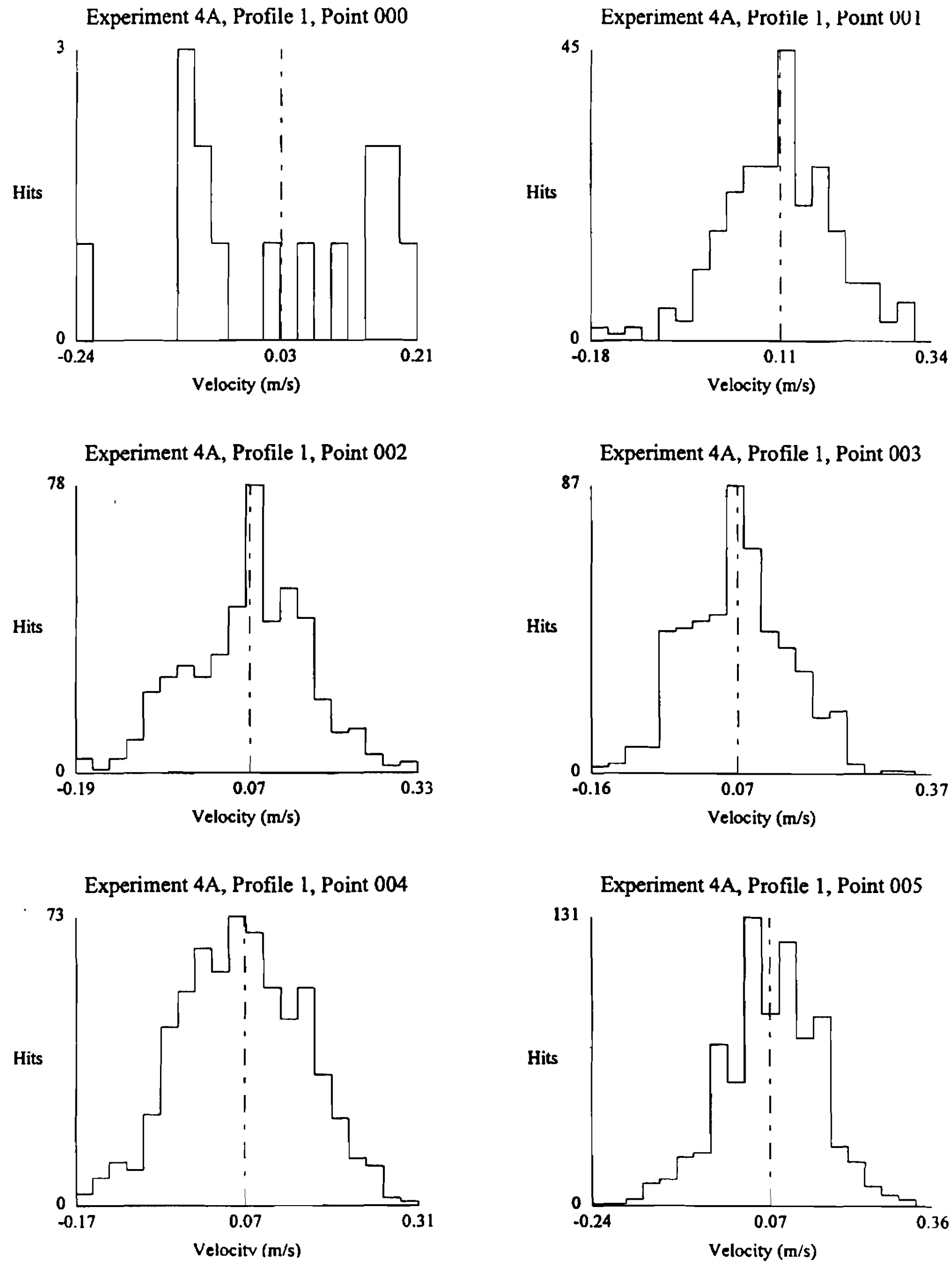

Figure A2: Histograms for Experiment 4A (Staggered s/d=8), Profile 1

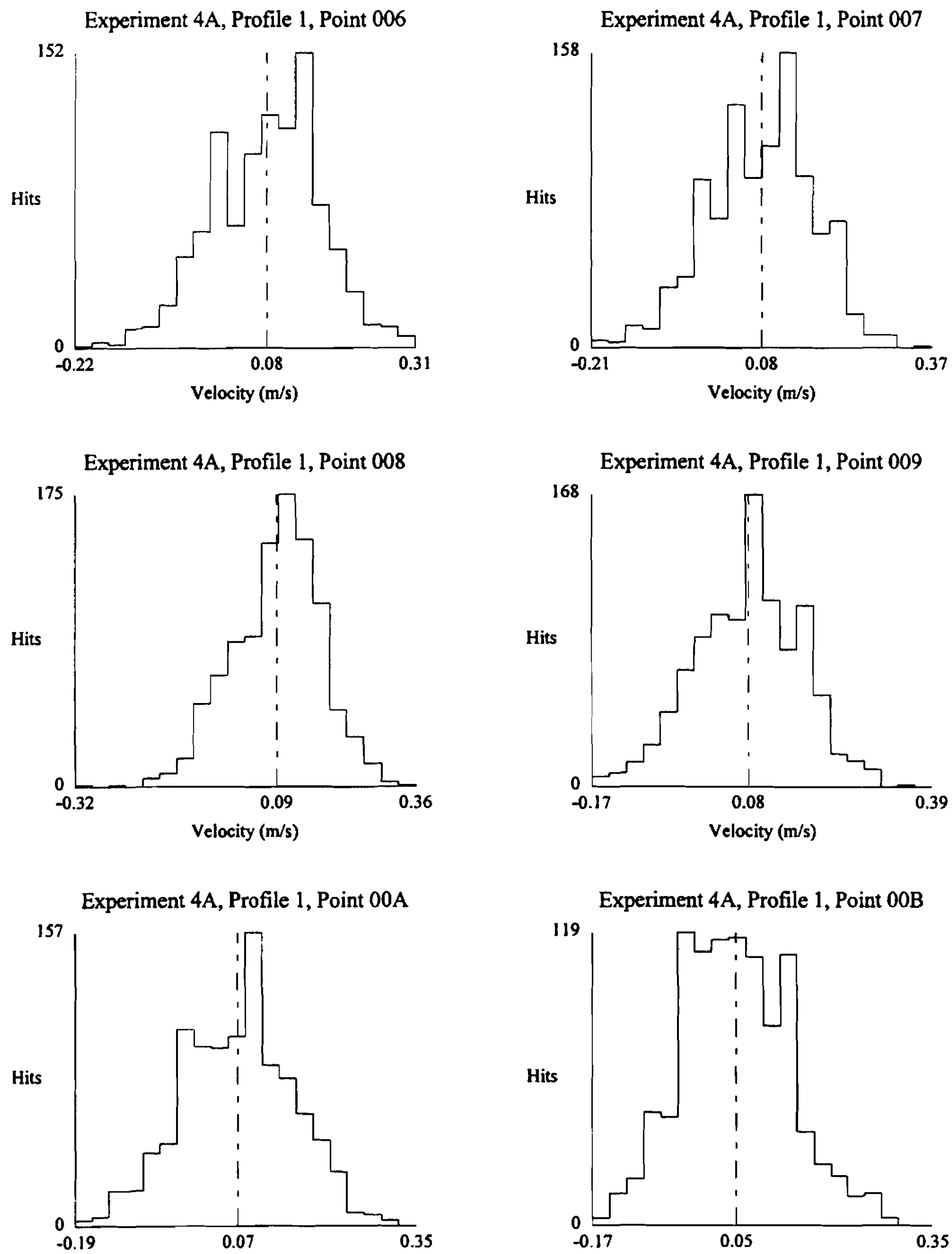

Figure A2 continued....

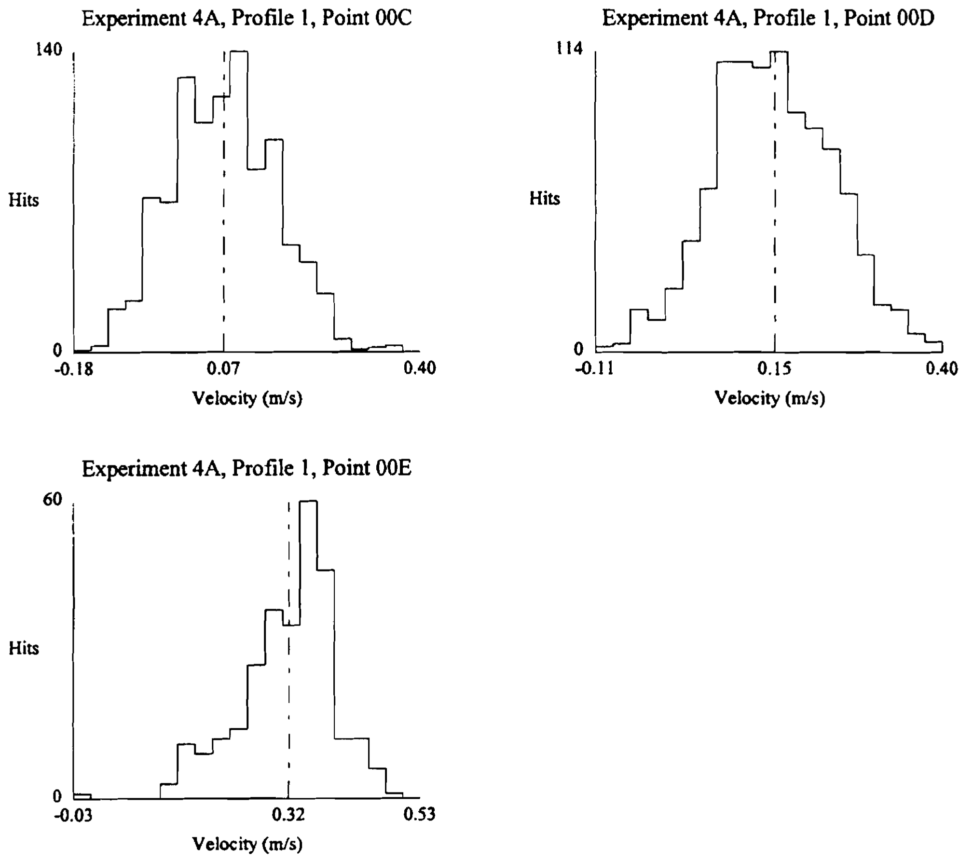

Figure A2 continued....

Table A3: Experiment 4A, Measurement Point 3

Average Velocity (m/s)	Depth (m)	Maximum Velocity (m/s)	Minimum Velocity (m/s)	Standard Deviation (m/s)	Number of Samples	Sampling Frequency (Hz)	3rd Moment Skew	Kurtosis
0.2113	0.0000	0.3742	0.1159	0.0447	144	1.024	0.492	3.315
0.2298	0.0023	0.3629	0.0801	0.0436	511	3.475	-0.022	2.892
0.2308	0.0046	0.3742	0.0914	0.0442	1000	8.651	0.077	2.817
0.2300	0.0069	0.3742	0.1046	0.0439	1000	10.686	0.118	2.916
0.2339	0.0092	0.3629	0.1046	0.0453	1000	7.741	0.023	2.824
0.2295	0.0139	0.3365	0.1159	0.0418	1000	12.499	-0.001	2.538
0.2298	0.0185	0.3742	0.1046	0.0439	1000	10.466	0.118	2.906
0.2311	0.0231	0.3987	0.1159	0.0434	1000	8.840	0.062	2.820
0.2329	0.0277	0.3742	0.1046	0.0435	1000	9.103	0.033	2.697
0.2360	0.0323	0.3497	0.1046	0.0432	1000	9.523	0.064	2.606
0.2456	0.0370	0.3874	0.1159	0.0427	975	6.616	-0.125	3.043
0.2614	0.0416	0.3742	0.1046	0.0419	1000	9.226	-0.072	2.933
0.2811	0.0462	0.3987	0.1404	0.0399	1000	10.527	-0.249	3.068
0.2960	0.0508	0.3987	0.1649	0.0372	1000	10.656	-0.216	3.037

Table A4: Experiment 4A, Measurement Point 4

Average Velocity (m/s)	Depth (m)	Maximum Velocity (m/s)	Minimum Velocity (m/s)	Standard Deviation (m/s)	Number of Samples	Sampling Frequency (Hz)	3rd Moment Skew	Kurtosis
0.1964	0.0000	0.3120	0.0914	0.0451	144	1.285	0.048	2.507
0.2336	0.0023	0.3742	0.1046	0.0398	880	6.157	0.044	2.780
0.2340	0.0046	0.3497	0.0914	0.0411	1000	26.621	0.009	2.573
0.2408	0.0069	0.3742	0.1159	0.0419	1000	31.726	0.077	2.784
0.2330	0.0092	0.3497	0.1159	0.0414	1000	38.427	0.034	2.619
0.2296	0.0139	0.3365	0.1291	0.0391	1000	36.684	0.070	2.717
0.2319	0.0185	0.3497	0.1159	0.0397	1000	34.346	0.091	2.742
0.2348	0.0231	0.3742	0.1159	0.0385	1000	37.643	0.162	3.040
0.2313	0.0277	0.3497	0.1159	0.0406	1000	27.095	0.157	2.655
0.2363	0.0323	0.3742	0.1159	0.0394	1000	26.246	0.192	3.097
0.2453	0.0370	0.3629	0.1291	0.0401	1000	35.304	-0.017	2.783
0.2569	0.0416	0.3629	0.1291	0.0392	1000	26.430	-0.258	2.862
0.2712	0.0462	0.4232	0.1536	0.0372	1000	22.636	-0.070	3.073
0.2856	0.0508	0.4232	0.1781	0.0339	1000	24.036	-0.132	2.917
0.2931	0.0554	0.3742	0.1895	0.0300	1000	8.073	-0.228	3.113

Table A5: Experiment 4A, Measurement Point 5

Average Velocity (m/s)	Depth (m)	Maximum Velocity (m/s)	Minimum Velocity (m/s)	Standard Deviation (m/s)	Number of Samples	Sampling Frequency (Hz)	3rd Moment Skew	Kurtosis
0.2194	0.0000	0.3007	0.1046	0.0480	32	0.310	-0.781	3.097
0.2937	0.0023	0.3742	0.1781	0.0343	1500	12.311	-0.368	2.838
0.3079	0.0046	0.3874	0.2026	0.0295	1500	19.896	-0.318	3.069
0.3146	0.0069	0.3987	0.2026	0.0287	1500	19.144	-0.347	3.278
0.3123	0.0092	0.3987	0.1895	0.0307	1500	32.006	-0.316	3.223
0.3102	0.0139	0.3874	0.1781	0.0310	1500	29.454	-0.457	3.381
0.3080	0.0185	0.3987	0.1895	0.0319	1500	38.010	-0.399	3.155
0.3102	0.0231	0.3987	0.2026	0.0310	1500	48.455	-0.289	3.086
0.3128	0.0277	0.4119	0.2026	0.0307	1500	42.532	-0.264	3.229
0.3138	0.0323	0.3987	0.2026	0.0299	1500	52.575	-0.365	3.276
0.3202	0.0370	0.4119	0.1781	0.0309	1500	58.144	-0.328	3.500
0.3275	0.0416	0.4119	0.1895	0.0302	1500	61.823	-0.282	3.485
0.3424	0.0462	0.4232	0.2385	0.0256	1500	59.231	-0.329	3.594
0.3344	0.0508	0.4232	0.2272	0.0302	1500	52.893	-0.265	3.279

Table A6: Experiment 4A, Measurement Point 6

Average Velocity (m/s)	Depth (m)	Maximum Velocity (m/s)	Minimum Velocity (m/s)	Standard Deviation (m/s)	Number of Samples	Sampling Frequency (Hz)	3rd Moment Skew	Kurtosis
0.2509	0.0000	0.3629	0.1159	0.0459	112	1.053	-0.434	3.413
0.2983	0.0023	0.3874	0.1781	0.0347	832	12.275	-0.267	3.111
0.3109	0.0046	0.3874	0.1895	0.0305	1500	28.424	-0.273	2.987
0.3109	0.0069	0.3987	0.2026	0.0300	1500	45.604	-0.374	3.109
0.3095	0.0092	0.3987	0.2140	0.0309	1500	54.584	-0.196	2.797
0.3087	0.0139	0.3987	0.2026	0.0300	1500	54.486	-0.222	3.081
0.3136	0.0185	0.3987	0.2140	0.0303	1500	40.784	-0.182	2.832
0.3062	0.0231	0.4119	0.2026	0.0334	1500	46.767	-0.272	2.977
0.3110	0.0277	0.3987	0.1781	0.0332	1500	34.933	-0.479	3.402
0.3148	0.0323	0.4364	0.1895	0.0329	1500	36.140	-0.257	3.126
0.3217	0.0370	0.4119	0.2140	0.0315	1500	44.230	-0.215	2.969
0.3356	0.0416	0.4232	0.2385	0.0300	1500	30.077	-0.308	3.128
0.3473	0.0462	0.4232	0.2385	0.0278	1500	20.560	-0.346	3.285
0.3426	0.0508	0.4477	0.2517	0.0307	1500	32.828	-0.125	2.936
0.2194	0.0554	0.9963	-0.7003	0.1703	463	3.135	-0.739	7.155

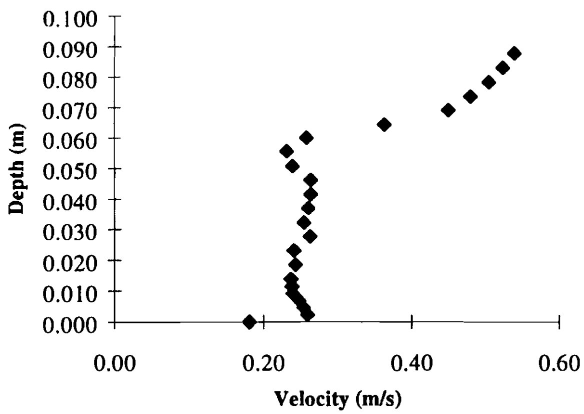

Located 12.7 mm downstream of dowel

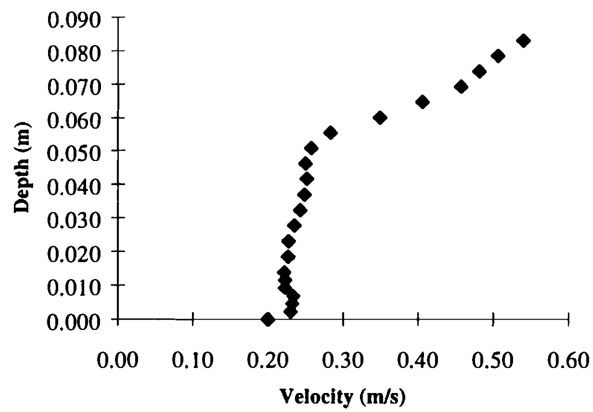

Located 38.1 mm downstream of dowel

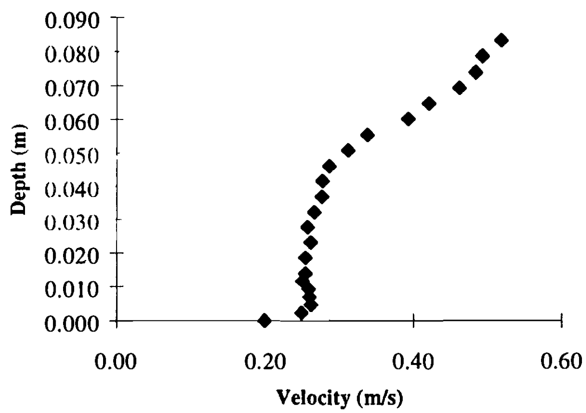

Located 63.5 mm downstream of dowel

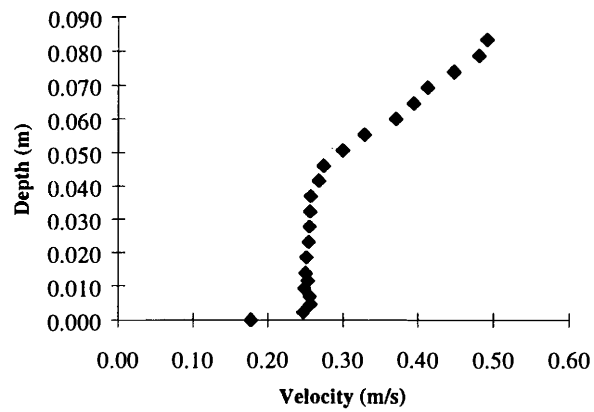

Located 88.9 mm downstream of dowel

Figure A3: Velocity Profiles for Staggered Formation of 76.2 mm Rods with s/d = 8 (Submerged case)

Table A7: Experiment 4C, Measurement Point 1

Average Velocity (m/s)	Depth (m)	Maximum Velocity (m/s)	Minimum Velocity (m/s)	Standard Deviation (m/s)	Number of Samples	Sampling Frequency (Hz)	3rd Moment Skew	Kurtosis
0.1807	0.0000	0.4722	0.0198	0.0891	64	0.484	0.300	3.233
0.2587	0.0023	0.4609	-0.0895	0.0889	560	3.779	-0.424	3.254
0.2535	0.0046	0.5759	-0.0763	0.0980	1033	7.711	-0.559	3.405
0.2470	0.0069	0.4948	-0.1367	0.1016	907	9.710	-0.552	3.123
0.2388	0.0092	0.5175	-0.1254	0.1007	1133	11.643	-0.483	3.181
0.2380	0.0139	0.4835	-0.1725	0.0964	1500	14.471	-0.568	3.737
0.2368	0.0185	0.4835	-0.0895	0.0967	1500	20.517	-0.445	3.135
0.2427	0.0231	0.5307	-0.1725	0.0974	1500	24.008	-0.410	3.367
0.2405	0.0277	0.5420	-0.0763	0.0966	1500	22.543	-0.475	3.237
0.2624	0.0323	0.5307	-0.1725	0.0958	1039	28.072	-0.664	3.784
0.2541	0.0370	0.5985	-0.1367	0.1016	1500	29.638	-0.623	3.629
0.2599	0.0416	0.5646	-0.1951	0.0937	1500	28.667	-0.416	3.653
0.2631	0.0462	0.6456	-0.0763	0.1039	1500	25.479	-0.378	3.308
0.2632	0.0508	0.5985	-0.1951	0.1127	1500	27.316	-0.393	3.206
0.2390	0.0554	0.6230	-0.3101	0.1276	1500	29.004	-0.317	3.086
0.2307	0.0601	0.6230	-0.2630	0.1419	1500	23.224	-0.286	2.639
0.2573	0.0647	0.5759	-0.1612	0.1383	1327	23.790	-0.369	2.649
0.3626	0.0693	0.6343	-0.1254	0.1152	1375	27.173	-0.851	3.768
0.4490	0.0739	0.6343	0.1291	0.0597	1326	26.624	-0.509	4.128
0.4787	0.0785	0.6343	0.3007	0.0528	1500	32.088	-0.066	2.760
0.5038	0.0832	0.6343	0.3120	0.0487	1500	36.002	-0.046	2.850
0.5225	0.0878	0.6570	0.3987	0.0420	1344	25.712	-0.153	3.007
0.5387	0.0924	0.6343	0.4364	0.0476	48	0.659	-0.124	2.068

Table A8: Experiment 4C, Measurement Point 2

Average Velocity (m/s)	Depth (m)	Maximum Velocity (m/s)	Minimum Velocity (m/s)	Standard Deviation (m/s)	Number of Samples	Sampling Frequency (Hz)	3rd Moment Skew	Kurtosis
0.2002	0.0000	0.4477	0.0554	0.0585	237	1.641	0.446	3.898
0.2304	0.0023	0.4364	0.0798	0.0530	844	5.718	0.065	3.120
0.2326	0.0046	0.5209	0.0310	0.0553	1500	14.765	0.033	3.516
0.2338	0.0069	0.4721	0.0197	0.0577	1500	20.904	0.100	3.675
0.2228	0.0092	0.4721	0.0441	0.0587	1500	23.680	0.241	3.222
0.2230	0.0139	0.4965	0.0066	0.0582	1500	23.687	0.251	3.653
0.2218	0.0185	0.4139	0.0441	0.0574	1500	41.735	0.095	2.891
0.2274	0.0231	0.4477	0.0441	0.0573	1500	50.512	0.072	3.220
0.2277	0.0277	0.4852	0.0685	0.0585	1500	53.450	0.059	2.928
0.2351	0.0323	0.4721	0.0685	0.0600	1500	51.758	-0.065	3.123
0.2433	0.0370	0.4364	0.0685	0.0585	1500	41.856	0.046	2.971
0.2489	0.0416	0.4608	0.0441	0.0614	1500	38.588	0.056	3.256
0.2522	0.0462	0.4721	0.0554	0.0668	1500	49.901	0.102	3.040
0.2503	0.0508	0.4852	0.0798	0.0650	1500	50.739	0.204	3.155
0.2579	0.0554	0.5096	0.0554	0.0667	1500	62.975	0.268	3.299
0.2839	0.0601	0.5697	0.0685	0.0673	1500	62.239	0.029	3.134
0.3490	0.0647	0.6298	0.0197	0.0770	1500	65.889	-0.144	3.137
0.4061	0.0693	0.6298	0.1642	0.0686	1500	71.551	-0.386	3.234
0.4569	0.0739	0.6298	0.1999	0.0600	1500	87.080	-0.270	3.157
0.4811	0.0785	0.6410	0.2938	0.0531	1500	96.329	-0.068	2.923
0.5066	0.0832	0.6654	0.3182	0.0519	1500	88.897	-0.106	2.954
0.5397	0.0878	0.7368	0.3538	0.0568	1500	66.184	0.019	2.992

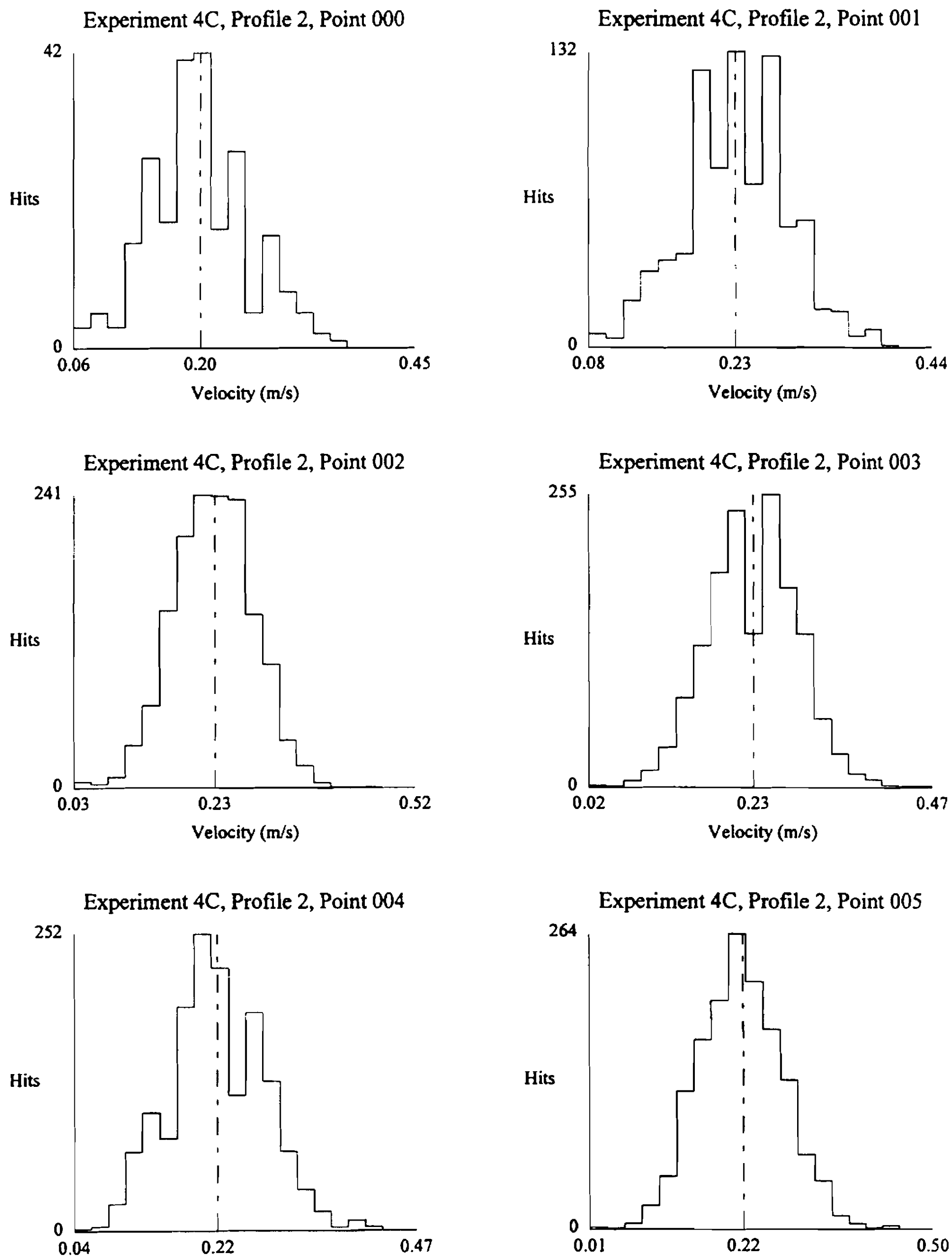

Figure A4: Histograms for Experiment 4C (Staggered s/d=8), Profile 2

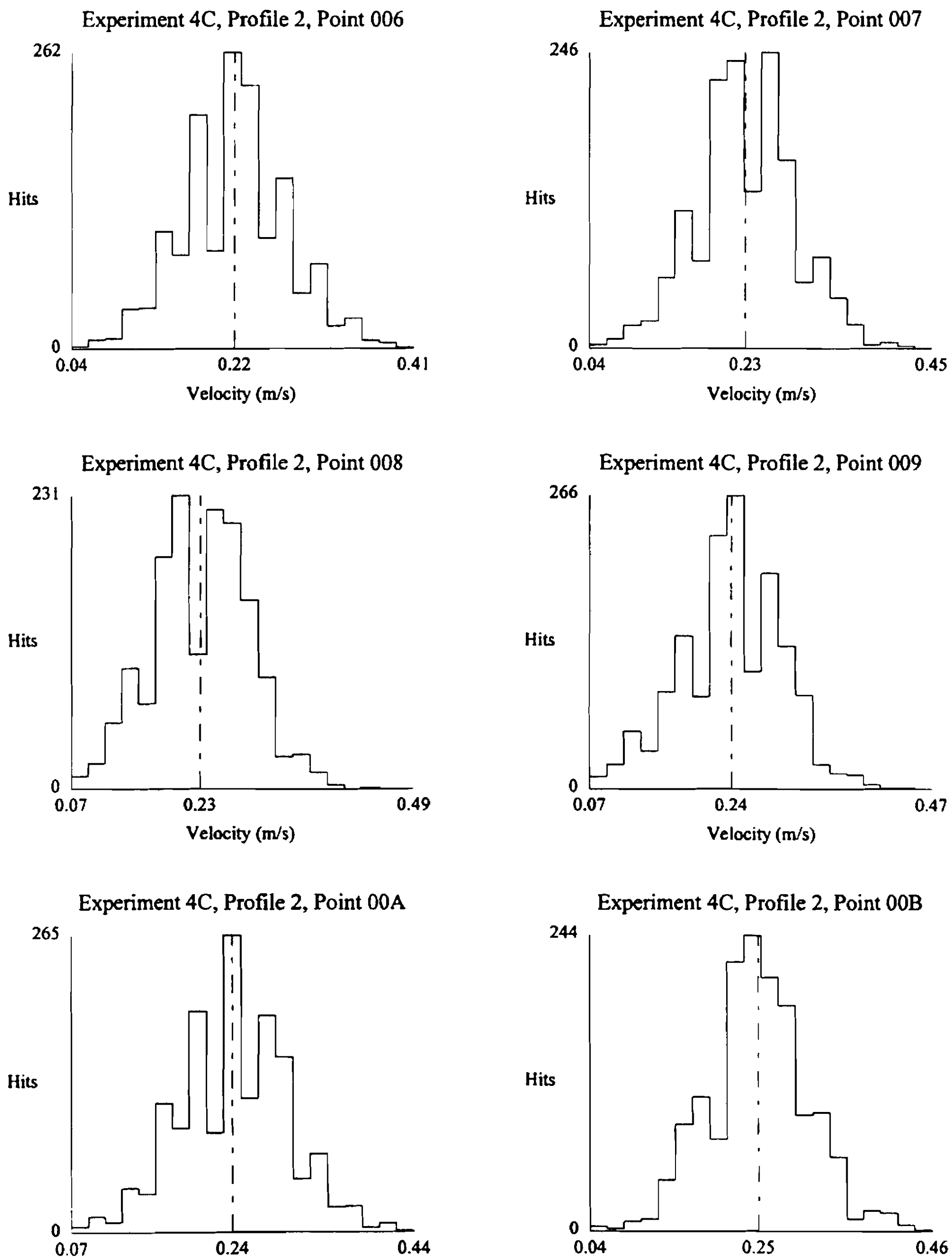

Figure A4 continued....

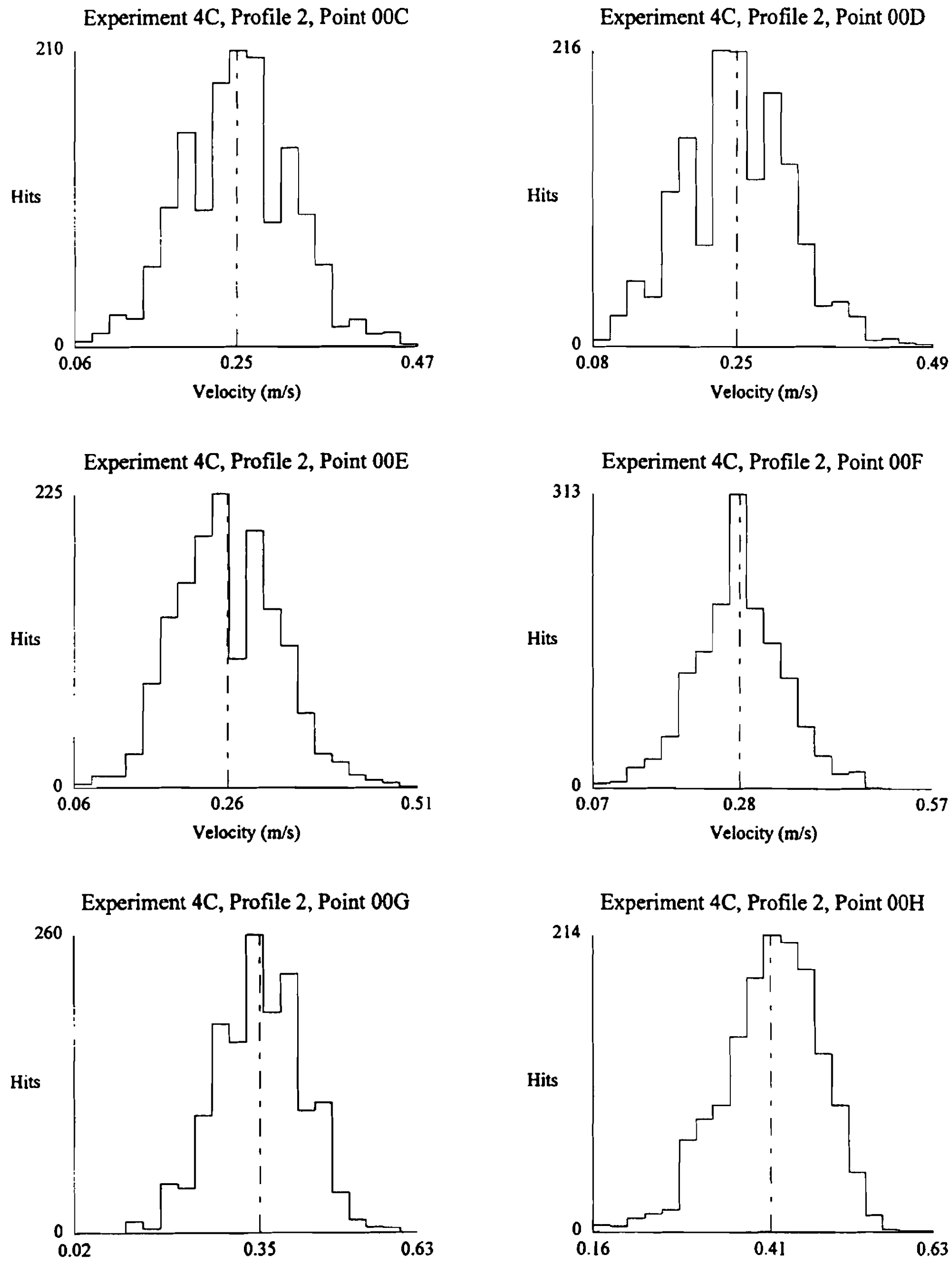

Figure A4 continued....

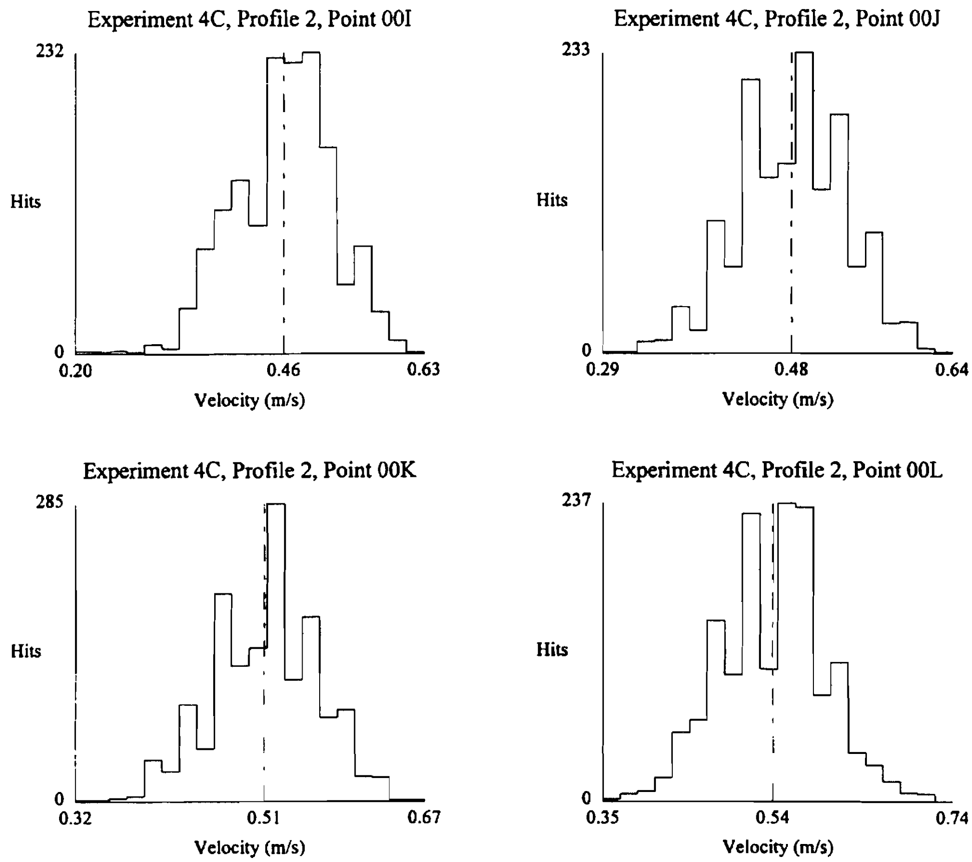

Figure A4 continued....

Table A9: Experiment 4C, Measurement Point 3

Average Velocity (m/s)	Depth (m)	Maximum Velocity (m/s)	Minimum Velocity (m/s)	Standard Deviation (m/s)	Number of Samples	Sampling Frequency (Hz)	3rd Moment Skew	Kurtosis
0.1991	0.0000	0.3613	0.0685	0.0546	128	0.881	0.253	3.087
0.2487	0.0023	0.4608	0.1154	0.0488	1500	10.394	0.083	3.088
0.2610	0.0046	0.4233	0.1286	0.0509	1500	28.735	0.113	2.872
0.2591	0.0069	0.4233	0.0798	0.0507	1500	43.458	0.060	2.911
0.2581	0.0092	0.4477	0.1154	0.0508	1500	48.721	0.104	3.037
0.2499	0.0139	0.4364	0.1286	0.0492	1500	51.105	0.247	2.977
0.2536	0.0185	0.4233	0.0798	0.0500	1500	40.265	0.117	2.928
0.2537	0.0231	0.4477	0.1042	0.0497	1500	46.206	0.173	3.015
0.2609	0.0277	0.4608	0.1286	0.0521	1500	35.565	0.230	3.155
0.2569	0.0323	0.4608	0.0310	0.0516	1500	33.785	0.096	3.377
0.2655	0.0370	0.4477	0.1042	0.0558	1500	43.576	0.161	3.003
0.2755	0.0416	0.4834	0.1286	0.0557	1500	36.549	0.131	2.822
0.2768	0.0462	0.4834	0.0798	0.0556	1500	24.271	0.017	2.783
0.2856	0.0508	0.5641	0.1286	0.0592	1500	39.375	0.234	3.116
0.3110	0.0554	0.4946	0.1042	0.0632	1500	48.264	0.011	2.820
0.3369	0.0601	0.5190	0.1286	0.0653	1500	49.013	0.059	2.634
0.3915	0.0647	0.6110	0.1774	0.0721	1500	48.121	0.013	2.805
0.4192	0.0693	0.5997	0.1774	0.0673	1500	67.002	-0.348	2.984
0.4603	0.0739	0.6223	0.2750	0.0574	1500	54.919	-0.250	2.933
0.4821	0.0785	0.6335	0.3257	0.0535	1500	50.395	-0.220	2.667
0.4912	0.0832	0.6692	0.3125	0.0563	1500	76.414	0.021	2.743
0.5169	0.0878	0.8926	0.3125	0.0565	1500	33.066	0.364	4.641

Table A10: Experiment 4C, Measurement Point 4

Average Velocity (m/s)	Depth (m)	Maximum Velocity (m/s)	Minimum Velocity (m/s)	Standard Deviation (m/s)	Number of Samples	Sampling Frequency (Hz)	3rd Moment Skew	Kurtosis
0.1774	0.0000	0.3007	0.0556	0.0553	144	0.974	0.111	2.658
0.2472	0.0023	0.4119	0.1159	0.0440	799	11.450	0.239	2.937
0.2568	0.0046	0.4232	0.1159	0.0442	1500	35.217	0.088	2.989
0.2554	0.0069	0.4232	0.1046	0.0469	1500	63.557	0.124	3.060
0.2481	0.0092	0.3742	0.0914	0.0445	1500	81.666	0.077	2.750
0.2529	0.0139	0.4119	0.1159	0.0475	1500	67.880	0.159	2.878
0.2497	0.0185	0.3987	0.1159	0.0450	1500	81.416	0.069	2.816
0.2511	0.0231	0.3874	0.1159	0.0477	1500	67.319	0.025	2.678
0.2540	0.0277	0.3987	0.1046	0.0474	1500	46.488	-0.063	2.923
0.2553	0.0323	0.4364	0.1291	0.0494	1500	40.766	0.214	2.940
0.2558	0.0370	0.4232	0.1159	0.0475	1500	54.587	0.059	3.057
0.2565	0.0416	0.4722	0.0914	0.0478	1500	41.731	0.141	3.229
0.2679	0.0462	0.4364	0.1046	0.0508	1500	26.555	0.184	3.149
0.2735	0.0508	0.4948	0.0669	0.0550	1500	35.871	0.380	3.482
0.2987	0.0554	0.4835	0.1404	0.0570	1500	47.470	0.180	2.911
0.3279	0.0601	0.5646	0.1404	0.0671	1500	40.385	0.147	2.653
0.3694	0.0647	0.5533	0.1649	0.0649	1500	42.743	-0.182	2.662
0.3930	0.0693	0.5759	0.1895	0.0665	1500	39.229	-0.307	2.709
0.4119	0.0739	0.5759	0.1536	0.0580	1500	32.723	-0.302	2.988
0.4463	0.0785	0.5985	0.2272	0.0550	1500	29.818	-0.377	3.338
0.4796	0.0832	0.6230	0.2875	0.0543	1500	37.272	-0.402	3.046
0.4906	0.0878	0.6683	0.3007	0.0497	1021	13.095	0.008	3.210

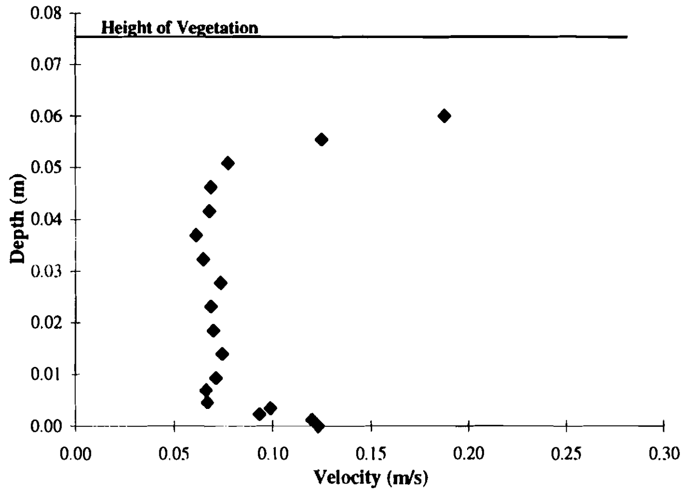

Located 12.7 mm downstream of rod

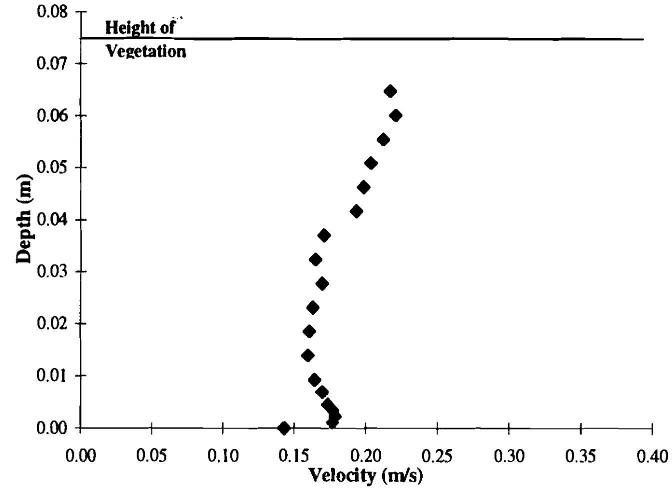

Located 25.4 mm downstream of rod

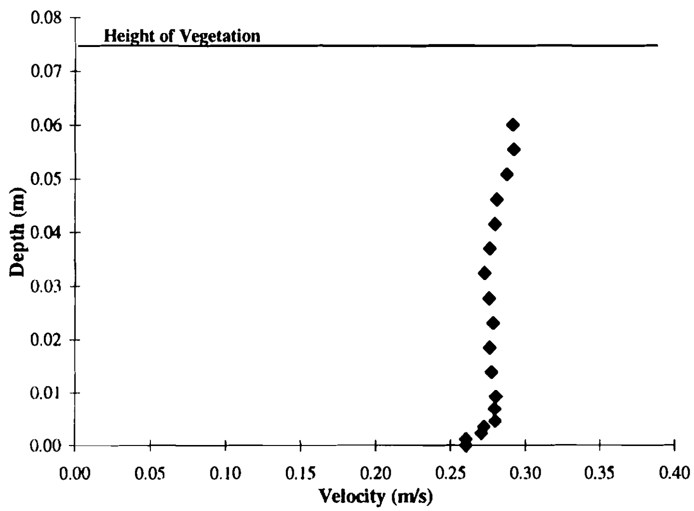

Located 38.1 mm downstream of rod

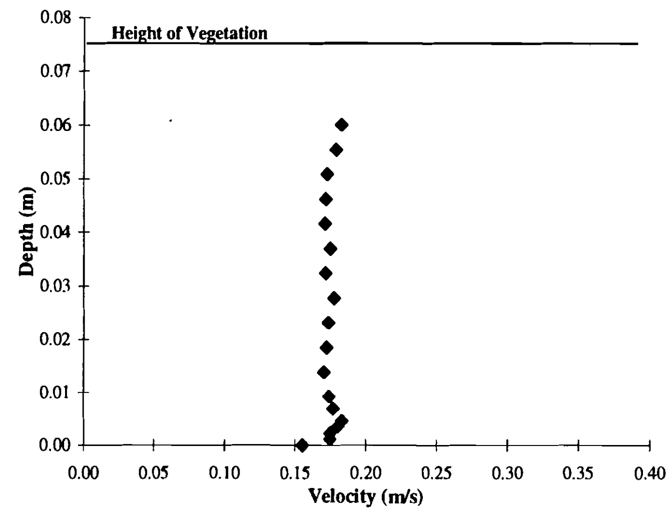

Located 25.4 mm downstream, 25.4 mm left of rod

Figure A5: Velocity Profiles for Linear Formation of 76.2 mm Rods with s/d = 8 (Unsubmerged case)

Table A11: Experiment 5A Measurement Point 1

Average Velocity (m/s)	Depth (m)	Maximum Velocity (m/s)	Minimum Velocity (m/s)	Standard Deviation (m/s)	Number of Samples	Sampling Frequency (Hz)	3rd Moment Skew	Kurtosis
0.123	0.0000	0.3572	-0.1687	0.0691	1500	11.408	0.1027	3.095
0.120	0.0011	0.3930	-0.1329	0.0691	1500	22.843	0.0611	3.1244
0.093	0.0023	0.3195	-0.1442	0.0775	1500	48.768	0.0655	2.7709
0.099	0.0035	0.3685	-0.1216	0.0690	1500	78.006	0.0453	2.9403
0.067	0.0046	0.3195	-0.1687	0.0812	1500	79.025	0.0697	2.7547
0.066	0.0069	0.3082	-0.1687	0.0795	1500	107.234	0.0956	2.7182
0.071	0.0092	0.3440	-0.2517	0.0854	1500	91.527	-0.0682	3.0596
0.074	0.0139	0.3440	-0.1800	0.0797	1500	88.477	0.0078	2.8977
0.070	0.0185	0.3195	-0.1442	0.0787	1500	98.085	0.1746	2.7698
0.069	0.0231	0.3082	-0.1687	0.0757	1500	96.261	0.0424	2.7427
0.074	0.0277	0.3685	-0.1442	0.0770	1500	60.808	0.1174	2.7659
0.065	0.0323	0.3195	-0.1442	0.0746	1500	75.201	0.1115	2.9676
0.061	0.0370	0.3440	-0.1800	0.0824	1500	67.075	0.1582	2.7436
0.068	0.0416	0.3817	-0.1687	0.0762	1500	79.038	0.0904	2.7814
0.068	0.0462	0.2950	-0.1442	0.0744	1500	80.644	0.0323	2.9789
0.077	0.0508	0.3082	-0.1555	0.0719	1500	69.425	0.0603	2.7094
0.125	0.0554	0.3572	-0.0745	0.0710	1500	101.344	0.1314	2.8798
0.187	0.0601	0.3930	-0.0632	0.0725	1200	8.014	-0.1721	2.6875

Table A12: Experiment 5A Measurement Point 2

Average Velocity (m/s)	Depth (m)	Maximum Velocity (m/s)	Minimum Velocity (m/s)	Standard Deviation (m/s)	Number of Samples	Sampling Frequency (Hz)	3rd Moment Skew	Kurtosis
0.1428	0.0000	0.2750	0.0310	0.0483	48	0.371	0.109	2.840
0.1770	0.0011	0.3501	0.0197	0.0572	560	3.773	0.220	3.163
0.1790	0.0023	0.3613	-0.0047	0.0612	752	5.119	0.097	2.869
0.1771	0.0035	0.3501	-0.0291	0.0598	1500	10.542	-0.043	2.894
0.1735	0.0046	0.3745	0.0197	0.0582	1500	15.785	0.042	2.866
0.1696	0.0069	0.3745	-0.0047	0.0607	1500	24.666	0.137	2.669
0.1642	0.0092	0.3613	-0.0160	0.0617	1500	28.220	0.091	2.899
0.1594	0.0139	0.4233	-0.0160	0.0609	1500	19.869	0.286	3.262
0.1604	0.0185	0.3745	-0.0535	0.0631	1500	22.728	0.144	2.689
0.1629	0.0231	0.3857	-0.0291	0.0636	1500	21.598	0.207	2.859
0.1695	0.0277	0.3745	-0.0291	0.0588	1500	17.777	0.098	2.909
0.1648	0.0323	0.3745	-0.0291	0.0620	1500	17.528	0.111	2.841
0.1707	0.0370	0.3613	0.0066	0.0602	1500	25.592	0.127	2.694
0.1936	0.0416	0.3613	0.0197	0.0601	1500	22.238	0.076	2.519
0.1985	0.0462	0.3745	0.0197	0.0560	1500	14.956	0.001	2.775
0.2037	0.0508	0.3745	0.0310	0.0569	1500	16.799	-0.129	2.820
0.2121	0.0554	0.4120	-0.0160	0.0580	1500	16.946	-0.156	2.886
0.2208	0.0601	0.3989	-0.0160	0.0559	1500	16.610	-0.201	2.850
0.2170	0.0647	0.3257	0.0910	0.0530	112	0.796	-0.136	2.488

Table A13: Experiment 5A Measurement Point 3

Average Velocity (m/s)	Depth (m)	Maximum Velocity (m/s)	Minimum Velocity (m/s)	Standard Deviation (m/s)	Number of Samples	Sampling Frequency (Hz)	3rd Moment Skew	Kurtosis
0.1552	0.0000	0.3120	0.0556	0.0566	64	0.450	0.482	3.176
0.1748	0.0011	0.3497	0.0311	0.0558	160	1.157	0.256	3.230
0.1750	0.0023	0.3252	0.0198	0.0512	320	2.142	0.197	3.203
0.1802	0.0035	0.3365	0.0066	0.0530	831	5.559	-0.072	3.065
0.1830	0.0046	0.3742	0.0556	0.0517	1055	7.077	0.143	2.631
0.1768	0.0069	0.3874	0.0066	0.0514	1500	10.750	0.172	3.096
0.1739	0.0092	0.3497	0.0198	0.0526	1500	10.190	0.296	2.948
0.1707	0.0139	0.3742	0.0311	0.0508	1500	10.826	0.184	2.934
0.1722	0.0185	0.3874	0.0066	0.0519	1296	8.650	0.178	3.119
0.1737	0.0231	0.3629	-0.0292	0.0550	1424	9.652	0.119	3.037
0.1776	0.0277	0.3365	0.0198	0.0519	975	6.578	0.108	2.742
0.1717	0.0323	0.3629	0.0066	0.0522	1022	6.890	0.149	3.069
0.1746	0.0370	0.3629	0.0311	0.0516	991	6.638	0.274	3.064
0.1708	0.0416	0.3497	0.0066	0.0525	1056	7.112	0.102	2.829
0.1714	0.0462	0.3365	0.0066	0.0503	1168	7.861	0.101	2.773
0.1724	0.0508	0.3252	-0.0160	0.0502	1054	7.049	-0.034	2.792
0.1788	0.0554	0.3365	-0.0047	0.0500	1199	8.044	0.104	2.936
0.1825	0.0601	0.3120	0.0311	0.0481	528	3.525	-0.005	3.039

Table A14: Experiment 5A Measurement Point 4

Average Velocity (m/s)	Depth (m)	Maximum Velocity (m/s)	Minimum Velocity (m/s)	Standard Deviation (m/s)	Number of Samples	Sampling Frequency (Hz)	3rd Moment Skew	Kurtosis
0.2602	0.0011	0.3629	0.1159	0.0429	319	2.206	-0.136	3.129
0.2602	0.0011	0.3629	0.1159	0.0429	319	2.206	-0.136	3.129
0.2706	0.0023	0.3874	0.1159	0.0399	672	4.557	-0.240	3.175
0.2722	0.0035	0.3874	0.1649	0.0360	1500	13.025	-0.065	2.782
0.2797	0.0046	0.3874	0.1291	0.0354	1500	11.712	-0.264	3.256
0.2793	0.0069	0.3987	0.1536	0.0337	1500	26.357	-0.190	3.271
0.2802	0.0092	0.3874	0.1536	0.0348	1500	30.333	-0.245	3.093
0.2770	0.0139	0.4119	0.1404	0.0384	1500	33.206	-0.376	3.257
0.2759	0.0185	0.3742	0.1046	0.0373	1500	28.902	-0.408	3.312
0.2784	0.0231	0.4232	0.1046	0.0364	1500	22.821	-0.288	3.423
0.2756	0.0277	0.3742	0.1291	0.0396	1500	23.515	-0.404	3.135
0.2722	0.0323	0.4119	0.0914	0.0382	1500	20.330	-0.487	3.865
0.2757	0.0370	0.3742	0.1404	0.0391	1500	33.500	-0.177	2.947
0.2791	0.0416	0.3874	0.0066	0.0375	1500	27.178	-0.523	4.858
0.2805	0.0462	0.3987	0.1536	0.0389	1500	20.499	-0.226	3.033
0.2872	0.0508	0.3742	0.1159	0.0381	1500	22.017	-0.350	3.168
0.2921	0.0554	0.3987	0.1649	0.0370	1500	25.810	-0.195	2.819
0.2912	0.0601	0.4232	0.1404	0.0406	1500	27.365	-0.202	3.106

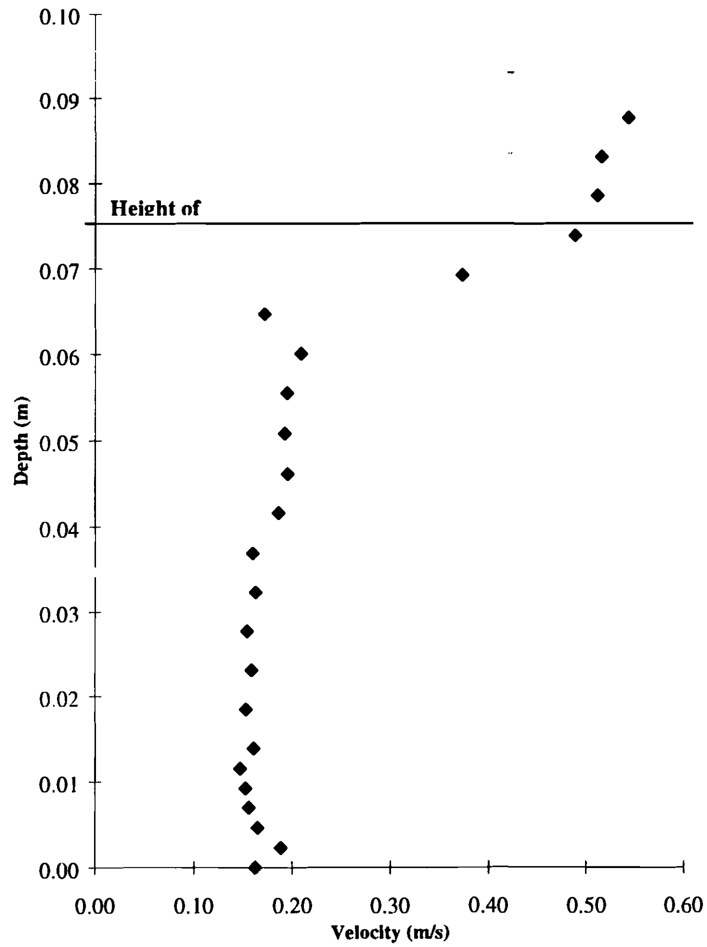

Located 12.7 mm downstream of rod

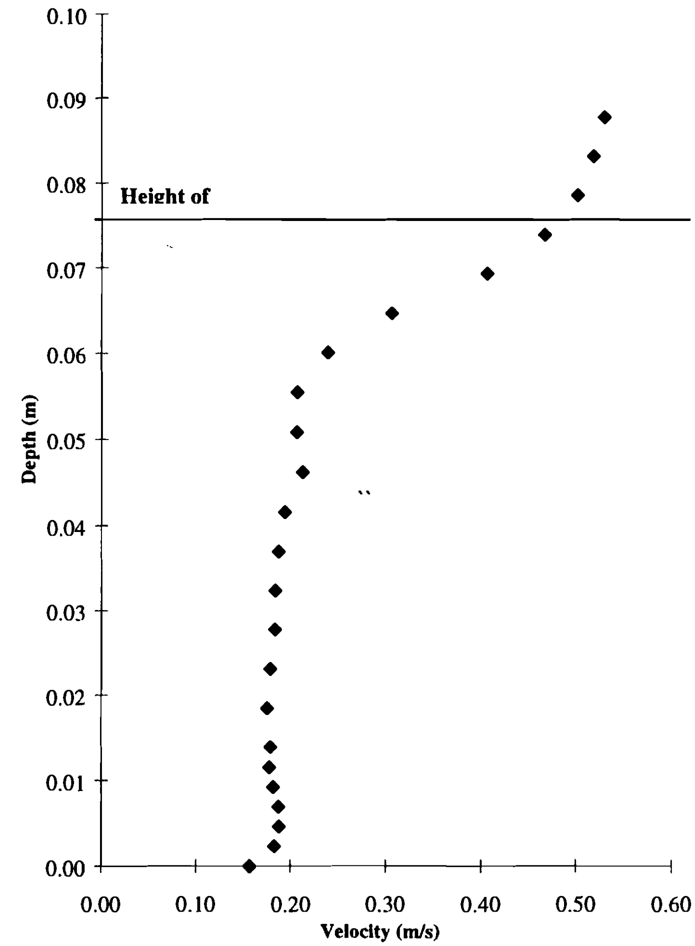

Located 25.4 mm downstream of rod

Figure A6: Velocity Profiles for Linear Formation of 76.2 mm Rods with s/d = 8 (Submerged case)

Table A15: Experiment 5C Measurement Point 1

Average Velocity (m/s)	Depth (m)	Maximum Velocity (m/s)	Minimum Velocity (m/s)	Standard Deviation (m/s)	Number of Samples	Sampling Frequency (Hz)	3rd Moment Skew	Kurtosis
0.1621	0.0000	0.3629	-0.1140	0.0775	96	0.700	-0.117	3.813
0.1884	0.0023	0.4477	-0.0537	0.0844	335	2.295	0.099	2.906
0.1649	0.0046	0.4232	-0.1140	0.0857	606	4.109	-0.041	2.960
0.1562	0.0069	0.4119	-0.1140	0.0890	975	6.528	-0.023	2.797
0.1526	0.0092	0.4609	-0.1254	0.0919	1024	6.861	-0.055	2.806
0.1468	0.0139	0.4364	-0.1499	0.0928	957	6.438	0.065	2.862
0.1606	0.0185	0.4609	-0.1140	0.0912	1084	7.203	0.057	3.003
0.1528	0.0231	0.4609	-0.0895	0.0888	1500	11.433	0.096	2.830
0.1585	0.0277	0.5061	-0.0650	0.0889	1500	10.873	0.284	3.001
0.1536	0.0323	0.5061	-0.1838	0.0882	1500	12.997	0.131	2.965
0.1625	0.0370	0.5985	-0.0650	0.0858	1500	12.128	0.260	3.409
0.1595	0.0416	0.4609	-0.1725	0.0862	1500	11.076	0.042	3.171
0.1856	0.0462	0.4948	-0.0537	0.0735	1500	13.045	0.145	3.143
0.1945	0.0508	0.4722	-0.0763	0.0774	1484	9.935	0.154	2.867
0.1919	0.0554	0.5872	-0.0895	0.0831	1500	12.970	0.300	3.611
0.1939	0.0601	0.4835	-0.1612	0.0862	1500	10.687	0.032	3.317
0.2082	0.0647	0.5420	-0.1009	0.0906	1500	10.832	0.189	2.998
0.1711	0.0693	0.6683	-0.3214	0.1753	1500	12.213	0.033	2.324
0.3721	0.0739	0.7022	-0.0763	0.1170	1500	17.824	-0.789	3.822
0.4879	0.0785	0.6909	0.2385	0.0736	1500	22.511	-0.394	3.156
0.5111	0.0832	0.7022	0.3252	0.0615	1500	23.373	-0.282	2.996
0.5149	0.0878	0.6683	0.3365	0.0567	1500	83.466	-0.143	2.553
0.5424	0.0924	0.7154	0.3874	0.0555	1500	102.293	-0.153	2.675

Table A16: Experiment 5C Measurement Point 2

Average Velocity (m/s)	Depth (m)	Maximum Velocity (m/s)	Minimum Velocity (m/s)	Standard Deviation (m/s)	Number of Samples	Sampling Frequency (Hz)	3rd Moment Skew	Kurtosis
0.1565	0.0000	0.2517	0.0914	0.0477	16	0.237	0.577	2.044
0.1831	0.0023	0.4609	-0.0047	0.0652	446	4.600	0.448	4.043
0.1879	0.0046	0.3987	-0.0292	0.0632	845	9.034	0.167	3.145
0.1871	0.0069	0.3874	-0.0160	0.0645	1052	11.691	0.027	2.745
0.1817	0.0092	0.4477	-0.0292	0.0642	1039	11.466	0.186	3.292
0.1777	0.0139	0.4364	0.0066	0.0632	1008	8.941	0.249	3.398
0.1788	0.0185	0.4835	0.0311	0.0669	1024	9.114	0.412	3.559
0.1753	0.0231	0.3987	-0.0160	0.0631	1022	10.165	0.098	3.063
0.1789	0.0277	0.3987	-0.0292	0.0669	1008	9.824	0.227	2.810
0.1830	0.0323	0.4477	-0.0047	0.0667	1500	10.544	0.201	3.089
0.1837	0.0370	0.4722	-0.0537	0.0676	1088	11.379	0.124	3.272
0.1871	0.0416	0.4119	0.0066	0.0671	1024	11.301	0.129	2.932
0.1934	0.0462	0.4609	-0.0160	0.0691	1020	10.196	0.144	3.190
0.2123	0.0508	0.4948	-0.0292	0.0740	1004	7.103	0.184	3.152
0.2061	0.0554	0.5061	-0.0292	0.0752	1500	14.645	0.231	3.154
0.2066	0.0601	0.5307	-0.0650	0.0808	1500	20.243	0.128	3.521
0.2388	0.0647	0.5533	-0.0405	0.0895	1023	8.947	0.304	3.082
0.3062	0.0693	0.5646	-0.0405	0.0987	720	6.837	-0.602	3.966
0.4059	0.0739	0.6683	0.0801	0.0898	1344	10.381	-0.516	3.140
0.4669	0.0785	0.6456	0.1649	0.0680	1038	13.576	-0.479	3.316
0.5010	0.0832	0.6909	0.2630	0.0610	1500	16.560	-0.225	3.014
0.5174	0.0878	0.6683	0.3252	0.0563	1500	14.931	-0.221	2.901
0.5291	0.0924	0.6683	0.3629	0.0522	511	8.760	-0.287	3.242

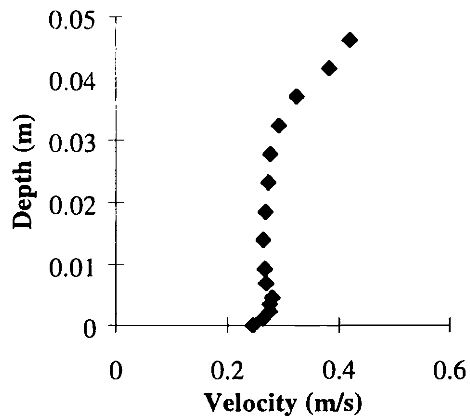

Measurement Point 1

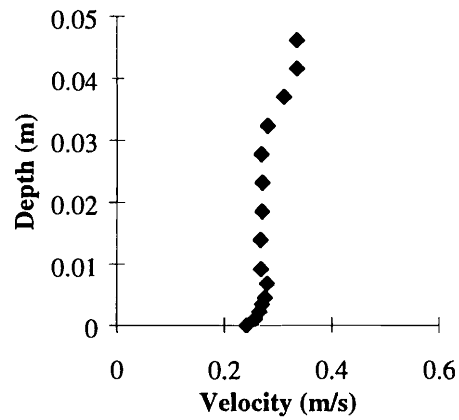

Measurement Point 2

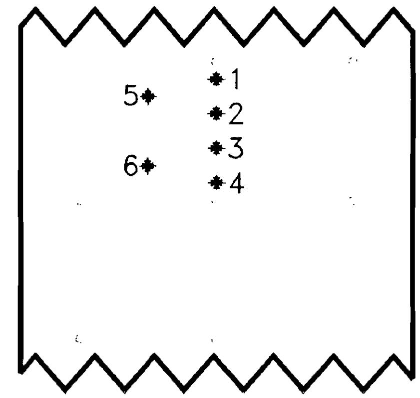

1 - 12.7 mm downstream of dowel

2 - 38.1 mm downstream of dowel

3 - 63.5 mm downstream of dowel

4 - 88.9 mm downstream of dowel

5 - 25.4 mm downstream of dowel
50.8 mm left of centerline

6 - 76.2 mm downstream of dowel
50.8 mm left of centerline

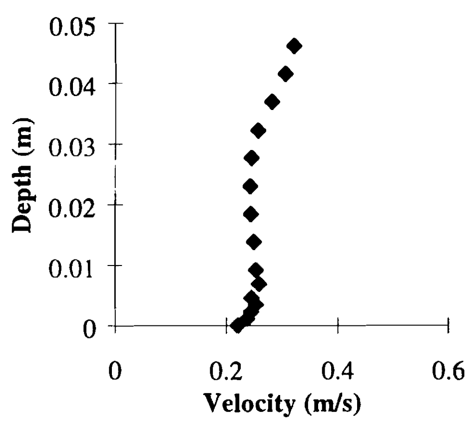

Measurement Point 3

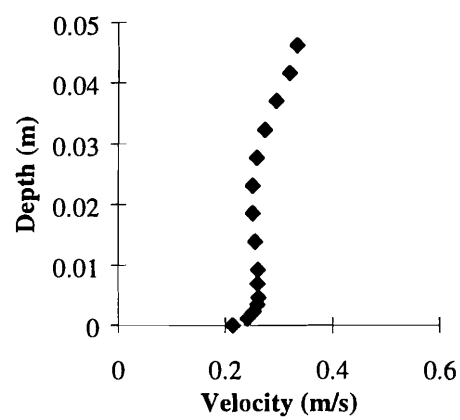

Measurement Point 4

Figure A7: Profiles for Single-layered Experiment 6A (Linear s/d =16).

(Points 5 and 6 on next page)

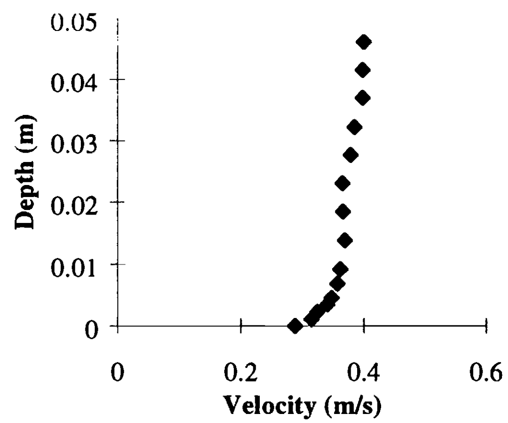

Measurement Point 5

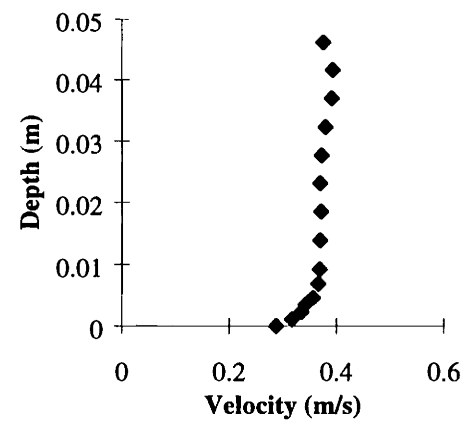

Measurement Point 6

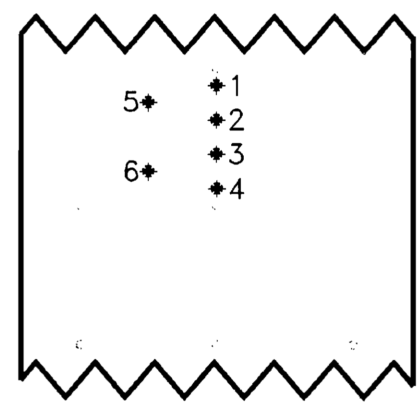

1 - 12.7 mm downstream of dowel

2 - 38.1 mm downstream of dowel

3 - 63.5 mm downstream of dowel

4 - 88.9 mm downstream of dowel

5 - 25.4 mm downstream of dowel
50.8 mm left of centerline

6 - 76.2 mm downstream of dowel
50.8 mm left of centerline

Figure A7: Profiles for Single-layered Experiment 6A (Linear s/d =16). (Points 1,2,3, and 4 on previous page)

Table A17: Experiment 6A Measurement Point 1

Average Velocity (m/s)	Depth (m)	Maximum Velocity (m/s)	Minimum Velocity (m/s)	Standard Deviation (m/s)	Number of Samples	Sampling Frequency (Hz)	3rd Moment Skew	Kurtosis
0.2452	0.0000	0.4189	-0.0214	0.0877	119	0.909	-0.907	4.162
0.2634	0.0011	0.4802	-0.0567	0.0692	1178	21.254	-0.502	4.009
0.2754	0.0023	0.5155	-0.0789	0.0741	3021	54.341	-0.686	4.719
0.2753	0.0035	0.4802	-0.1012	0.0723	2612	77.133	-0.764	4.803
0.2792	0.0046	0.5266	-0.1012	0.0760	5000	132.325	-0.849	4.744
0.2686	0.0069	0.5155	-0.1477	0.0868	5000	162.627	-0.677	4.011
0.2659	0.0092	0.5043	-0.1718	0.0903	5000	164.232	-0.632	3.783
0.2637	0.0139	0.5266	-0.2424	0.0886	5000	195.461	-0.850	4.531
0.2678	0.0185	0.5266	-0.0901	0.0801	5000	185.524	-0.651	4.219
0.2731	0.0231	0.5396	-0.1588	0.0875	5000	201.314	-0.734	3.966
0.2765	0.0277	0.5749	-0.1718	0.0940	5000	179.012	-0.890	4.267
0.2913	0.0323	0.5155	-0.1477	0.0958	5000	222.922	-0.949	4.282
0.3235	0.0370	0.5638	-0.1365	0.0826	5000	234.217	-1.365	6.230
0.3819	0.0416	0.5508	-0.0102	0.0464	5000	227.066	-0.686	6.959
0.4195	0.0462	1.2418	-0.0102	0.1217	1316	8.812	1.193	9.309

Table A18: Experiment 6A Measurement Point 2

Average Velocity (m/s)	Depth (m)	Maximum Velocity (m/s)	Minimum Velocity (m/s)	Standard Deviation (m/s)	Number of Samples	Sampling Frequency (Hz)	3rd Moment Skew	Kurtosis
0.2409	0.0000	0.4560	0.0808	0.0616	1011	15.158	0.138	2.633
0.2569	0.0011	0.4672	0.0474	0.0567	3186	37.099	0.070	2.919
0.2649	0.0023	0.4672	0.0362	0.0594	5000	62.021	-0.097	2.956
0.2696	0.0035	0.5043	0.0920	0.0586	5000	111.941	-0.094	2.931
0.2750	0.0046	0.4560	0.0474	0.0623	5000	130.150	-0.300	3.030
0.2784	0.0069	0.5043	0.0362	0.0662	5000	169.061	-0.096	2.740
0.2672	0.0092	0.4672	0.0474	0.0639	5000	183.529	-0.127	2.751
0.2659	0.0139	0.4802	0.0362	0.0697	5000	210.598	-0.018	2.703
0.2698	0.0185	0.4802	0.0474	0.0687	5000	211.161	-0.022	2.879
0.2703	0.0231	0.4913	0.0009	0.0689	5000	209.539	-0.198	2.890
0.2682	0.0277	0.4913	0.0474	0.0696	5000	204.883	-0.049	2.871
0.2803	0.0323	0.4802	0.0121	0.0696	5000	211.127	-0.280	2.877
0.3101	0.0370	0.5155	-0.0325	0.0648	5000	218.070	-0.447	3.365
0.3344	0.0416	0.5043	0.1161	0.0571	5000	212.693	-0.484	3.313
0.3337	0.0462	0.5155	0.1272	0.0497	5000	67.586	-0.154	3.615

Table A19: Experiment 6A Measurement Point 3

Average Velocity (m/s)	Depth (m)	Maximum Velocity (m/s)	Minimum Velocity (m/s)	Standard Deviation (m/s)	Number of Samples	Sampling Frequency (Hz)	3rd Moment Skew	Kurtosis
0.2199	0.0000	0.3834	0.1035	0.0580	122	2.351	0.418	3.243
0.2369	0.0011	0.3946	0.0700	0.0519	1002	19.835	0.099	3.016
0.2441	0.0023	0.4188	0.0923	0.0530	2170	47.273	0.310	2.981
0.2523	0.0035	0.4561	0.0811	0.0533	2624	71.824	0.282	3.027
0.2443	0.0046	0.4319	0.0700	0.0515	4140	115.322	0.202	2.873
0.2578	0.0069	0.4673	0.0923	0.0562	5000	129.670	0.210	2.873
0.2520	0.0092	0.4673	0.0923	0.0572	5000	160.315	0.280	2.935
0.2487	0.0139	0.4431	0.0923	0.0546	5000	170.958	0.216	2.744
0.2436	0.0185	0.4561	0.0700	0.0589	5000	194.391	0.305	2.824
0.2421	0.0231	0.4673	0.0811	0.0578	5000	183.443	0.252	2.813
0.2447	0.0277	0.4431	0.0588	0.0556	5000	191.728	0.111	2.866
0.2563	0.0323	0.4561	0.0811	0.0572	5000	198.943	0.031	2.776
0.2803	0.0370	0.4673	0.0811	0.0575	5000	205.314	-0.092	2.885
0.3045	0.0416	0.4561	0.1035	0.0487	5000	218.474	-0.181	3.107
0.3198	0.0462	0.4431	0.1390	0.0422	5000	173.475	-0.119	2.993

Table A20: Experiment 6A Measurement Point 4

Average Velocity (m/s)	Depth (m)	Maximum Velocity (m/s)	Minimum Velocity (m/s)	Standard Deviation (m/s)	Number of Samples	Sampling Frequency (Hz)	3rd Moment Skew	Kurtosis
0.2134	0.0000	0.3834	0.0588	0.0498	219	1.492	0.127	3.177
0.2408	0.0011	0.3834	0.0923	0.0479	884	14.842	0.322	2.830
0.2531	0.0023	0.4076	0.1147	0.0505	1149	30.342	0.277	2.757
0.2594	0.0035	0.4188	0.1147	0.0486	2111	51.505	0.166	2.961
0.2614	0.0046	0.4319	0.1035	0.0521	3780	80.901	0.170	2.738
0.2597	0.0069	0.4431	0.0811	0.0537	3416	99.667	0.189	2.657
0.2598	0.0092	0.4188	0.0923	0.0521	5000	138.558	0.137	2.695
0.2544	0.0139	0.4319	0.1035	0.0539	3734	109.587	0.252	2.747
0.2505	0.0185	0.4076	0.1035	0.0514	3958	130.228	0.258	2.785
0.2497	0.0231	0.4431	0.1035	0.0536	5000	121.138	0.383	2.870
0.2579	0.0277	0.4188	0.1035	0.0513	5000	146.080	0.174	2.701
0.2730	0.0323	0.4673	0.0923	0.0510	5000	141.665	0.093	2.812
0.2944	0.0370	0.4673	0.1278	0.0498	5000	163.345	-0.067	2.788
0.3191	0.0416	0.4804	0.1390	0.0445	5000	154.338	-0.094	3.130
0.3331	0.0462	0.4916	0.1875	0.0434	5000	99.700	0.061	2.926

Table A21: Experiment 6A Measurement Point 5

Average Velocity (m/s)	Depth (m)	Maximum Velocity (m/s)	Minimum Velocity (m/s)	Standard Deviation (m/s)	Number of Samples	Sampling Frequency (Hz)	3rd Moment Skew	Kurtosis
0.2875	0.0000	0.4076	0.1520	0.0508	219	2.689	0.069	2.693
0.3143	0.0011	0.4561	0.1632	0.0437	1730	44.161	-0.161	2.885
0.3237	0.0023	0.4804	0.2005	0.0433	2647	81.676	-0.015	2.756
0.3402	0.0035	0.4561	0.1763	0.0435	5000	145.915	-0.210	2.775
0.3473	0.0046	0.4916	0.1632	0.0440	5000	186.156	-0.090	2.762
0.3564	0.0069	0.4916	0.2005	0.0445	5000	202.785	-0.256	2.870
0.3612	0.0092	0.4916	0.2005	0.0482	5000	211.855	-0.286	2.733
0.3688	0.0139	0.4916	0.2005	0.0484	5000	228.842	-0.403	2.757
0.3649	0.0185	0.5158	0.1875	0.0499	5000	220.637	-0.229	2.661
0.3647	0.0231	0.5270	0.2005	0.0490	5000	211.778	-0.303	2.803
0.3779	0.0277	0.5028	0.2117	0.0504	5000	221.953	-0.261	2.513
0.3846	0.0323	0.5158	0.2248	0.0457	5000	237.474	-0.385	3.040
0.3978	0.0370	0.5028	0.2490	0.0374	5000	230.249	-0.205	3.098
0.3975	0.0416	0.5158	0.2248	0.0359	5000	226.131	-0.347	3.257
0.4004	0.0462	0.5401	0.2845	0.0346	1700	29.205	0.075	3.168

Table A22: Experiment 6A Measurement Point 6

Average Velocity (m/s)	Depth (m)	Maximum Velocity (m/s)	Minimum Velocity (m/s)	Standard Deviation (m/s)	Number of Samples	Sampling Frequency (Hz)	3rd Moment Skew	Kurtosis
0.2876	0.0000	0.3946	0.1632	0.0522	79	0.607	-0.310	2.628
0.3168	0.0011	0.4785	0.1520	0.0461	3929	26.229	-0.115	2.944
0.3347	0.0023	0.4897	0.1763	0.0452	5000	46.058	-0.065	2.955
0.3421	0.0035	0.4897	0.2005	0.0455	5000	90.421	-0.113	2.756
0.3559	0.0046	0.4897	0.1875	0.0446	3549	120.427	-0.272	3.048
0.3663	0.0069	0.5009	0.2117	0.0441	5000	132.019	-0.234	2.896
0.3684	0.0092	0.4897	0.2005	0.0435	5000	144.134	-0.275	3.001
0.3699	0.0139	0.5009	0.1875	0.0473	5000	133.575	-0.345	2.932
0.3709	0.0185	0.5009	0.1875	0.0481	5000	159.052	-0.305	2.800
0.3690	0.0231	0.5009	0.1875	0.0506	5000	186.923	-0.380	2.767
0.3721	0.0277	0.5363	0.1520	0.0473	5000	156.801	-0.367	3.067
0.3789	0.0323	0.5121	0.1875	0.0459	5000	194.456	-0.532	3.331
0.3905	0.0370	0.5251	0.2360	0.0422	5000	218.639	-0.406	3.031
0.3928	0.0416	0.5009	0.2733	0.0369	5000	195.182	-0.087	2.684
0.3750	0.0462	0.5251	0.2117	0.0392	5000	186.127	-0.148	3.359

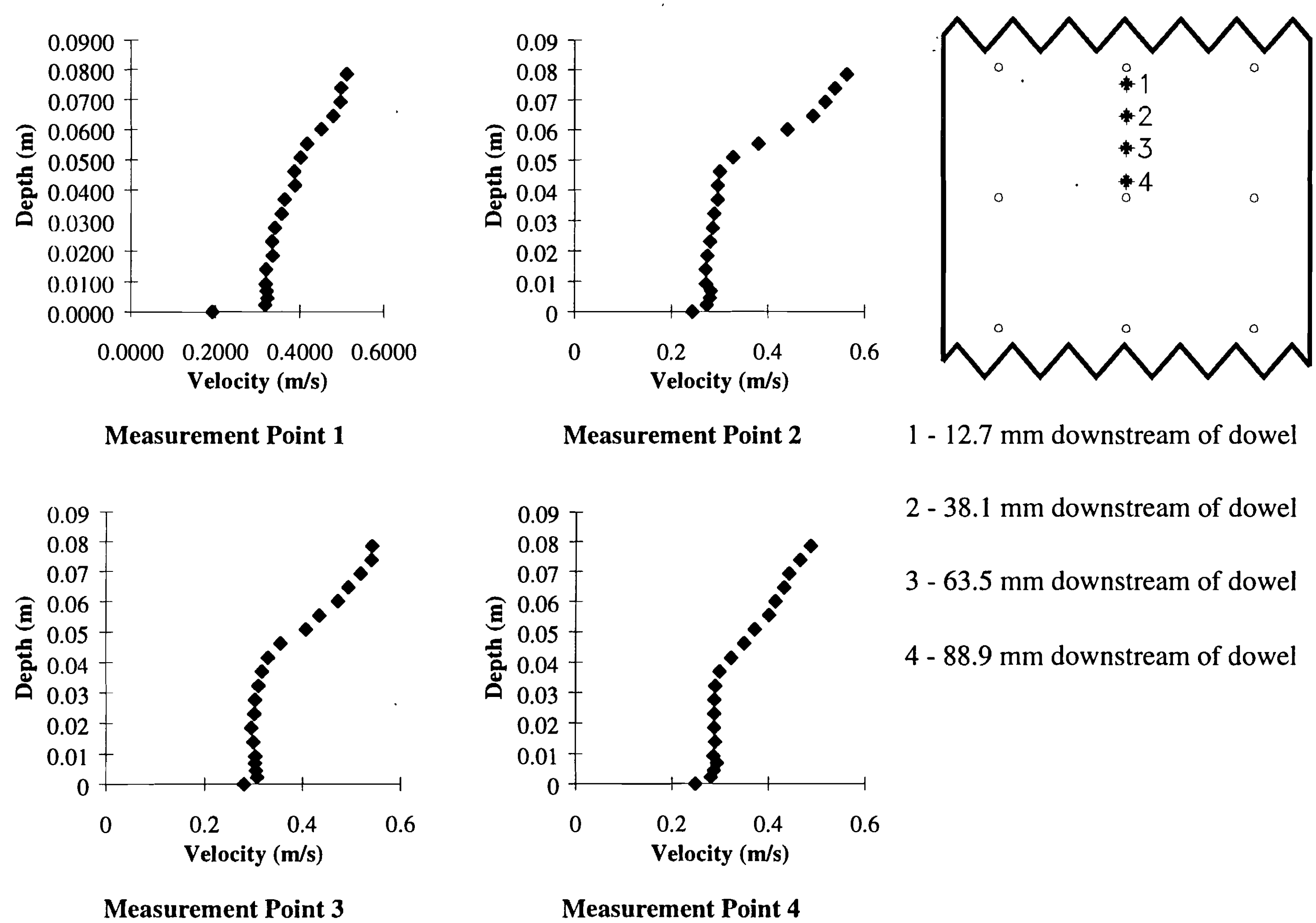

Figure A8: Profiles for Single-layered Experiment 6C (Linear s/d=16 Submerged Case).

Table A23: Experiment 6C Measurement Point 1

Average Velocity (m/s)	Depth (m)	Maximum Velocity (m/s)	Minimum Velocity (m/s)	Standard Deviation (m/s)	Number of Samples	Sampling Frequency (Hz)	3rd Moment Skew	Kurtosis
0.1927	0.0000	0.5325	-0.1612	0.0987	322	2.252	-0.050	3.455
0.3175	0.0023	0.5815	-0.1254	0.0844	767	18.233	-0.999	6.478
0.3226	0.0046	0.6287	-0.0895	0.0892	3064	42.943	-0.724	4.555
0.3204	0.0069	0.6174	-0.1857	0.0932	2402	58.831	-0.974	5.568
0.3189	0.0092	0.5929	-0.1612	0.0950	2403	77.705	-0.799	4.604
0.3191	0.0139	0.7135	-0.1857	0.0954	3315	90.115	-0.588	4.476
0.3349	0.0185	0.6061	-0.1367	0.0901	3342	90.334	-0.633	4.513
0.3334	0.0231	0.6061	-0.1140	0.0911	3310	86.311	-0.774	4.704
0.3403	0.0277	0.6287	-0.1140	0.0878	3353	111.148	-0.532	5.196
0.3565	0.0323	0.6664	-0.1857	0.0879	5000	140.426	-0.908	5.403
0.3634	0.0370	0.7267	-0.1367	0.1021	5000	136.812	-0.760	4.623
0.3883	0.0416	0.7757	-0.1367	0.1104	5000	144.238	-0.765	4.476
0.3862	0.0462	0.7964	-0.2686	0.1284	5000	132.603	-0.799	4.302
0.4008	0.0508	0.7569	-0.2912	0.1447	5000	130.811	-1.045	4.517
0.4167	0.0554	0.8059	-0.2328	0.1439	5000	152.363	-1.070	4.659
0.4502	0.0601	0.8568	-0.2686	0.1346	5000	160.356	-1.280	5.656
0.4782	0.0647	0.7757	-0.1970	0.0940	5000	149.289	-1.555	8.899
0.4949	0.0693	0.6664	0.2234	0.0546	5000	182.529	-0.295	3.597
0.4969	0.0739	0.6664	0.3176	0.0479	5000	177.399	-0.199	3.154
0.5108	0.0785	0.6777	0.3176	0.0460	5000	80.307	-0.119	3.208

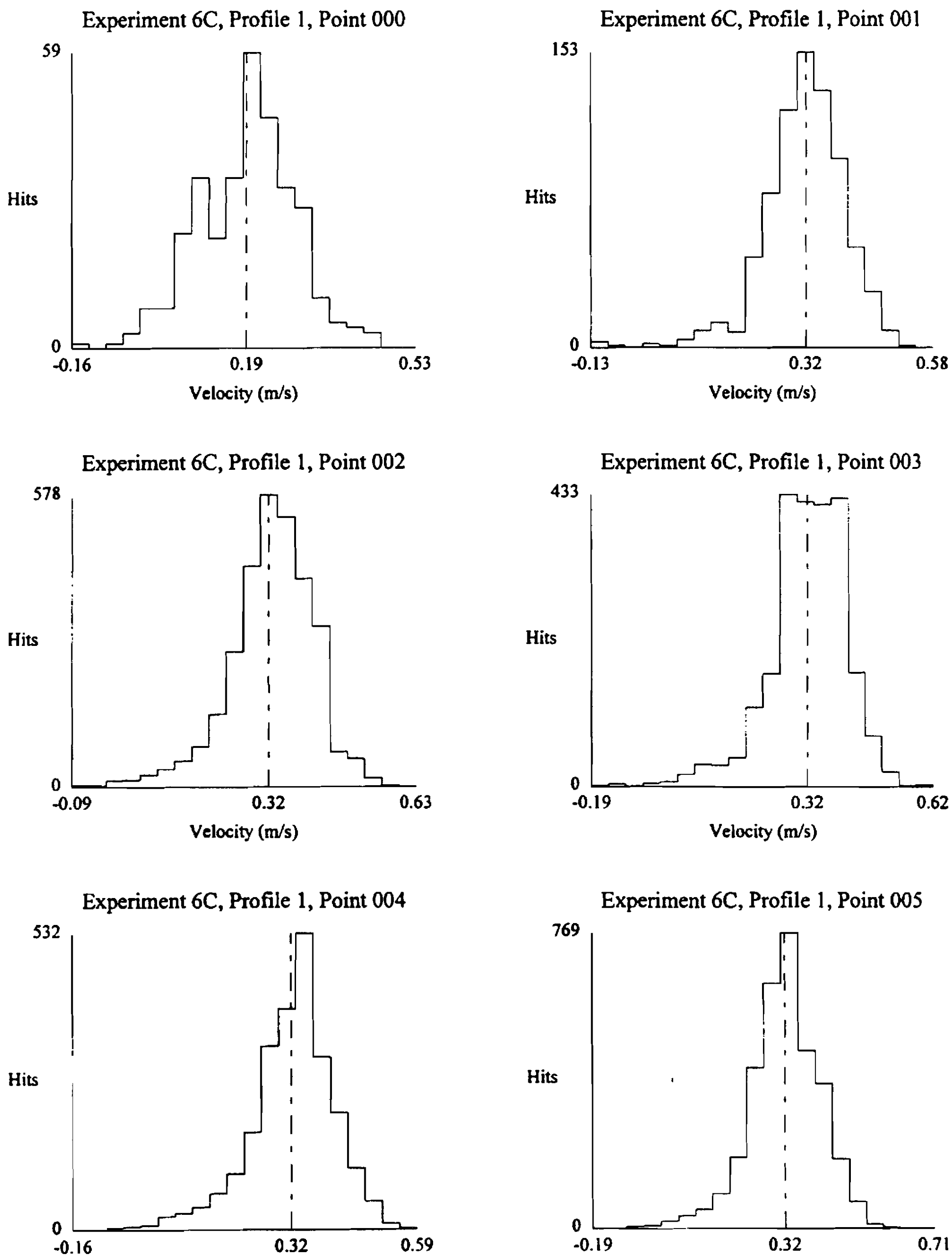

Figure A9: Histograms for Experiment 6C (Linear s/d=16), Profile 1

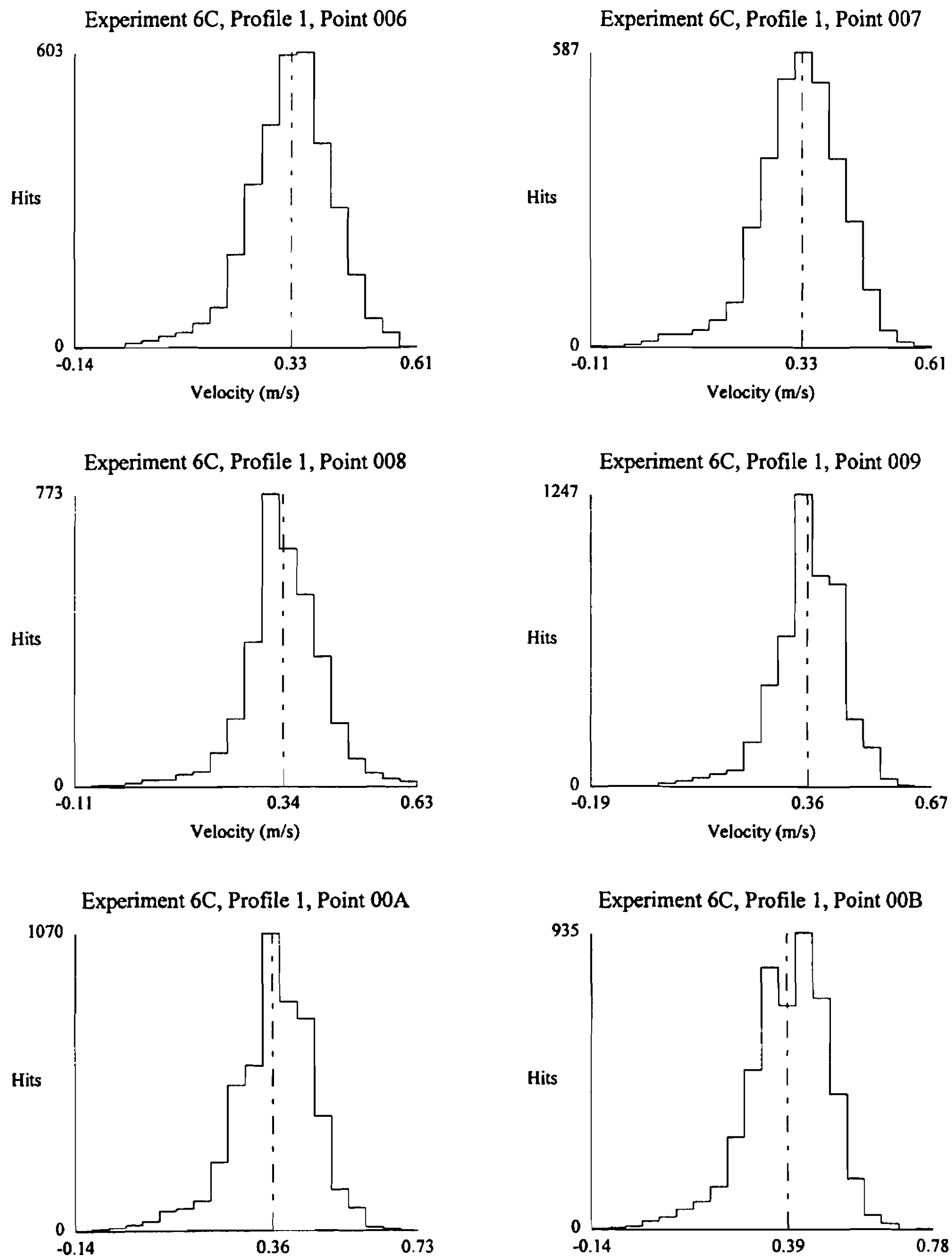

Figure A9 continued....

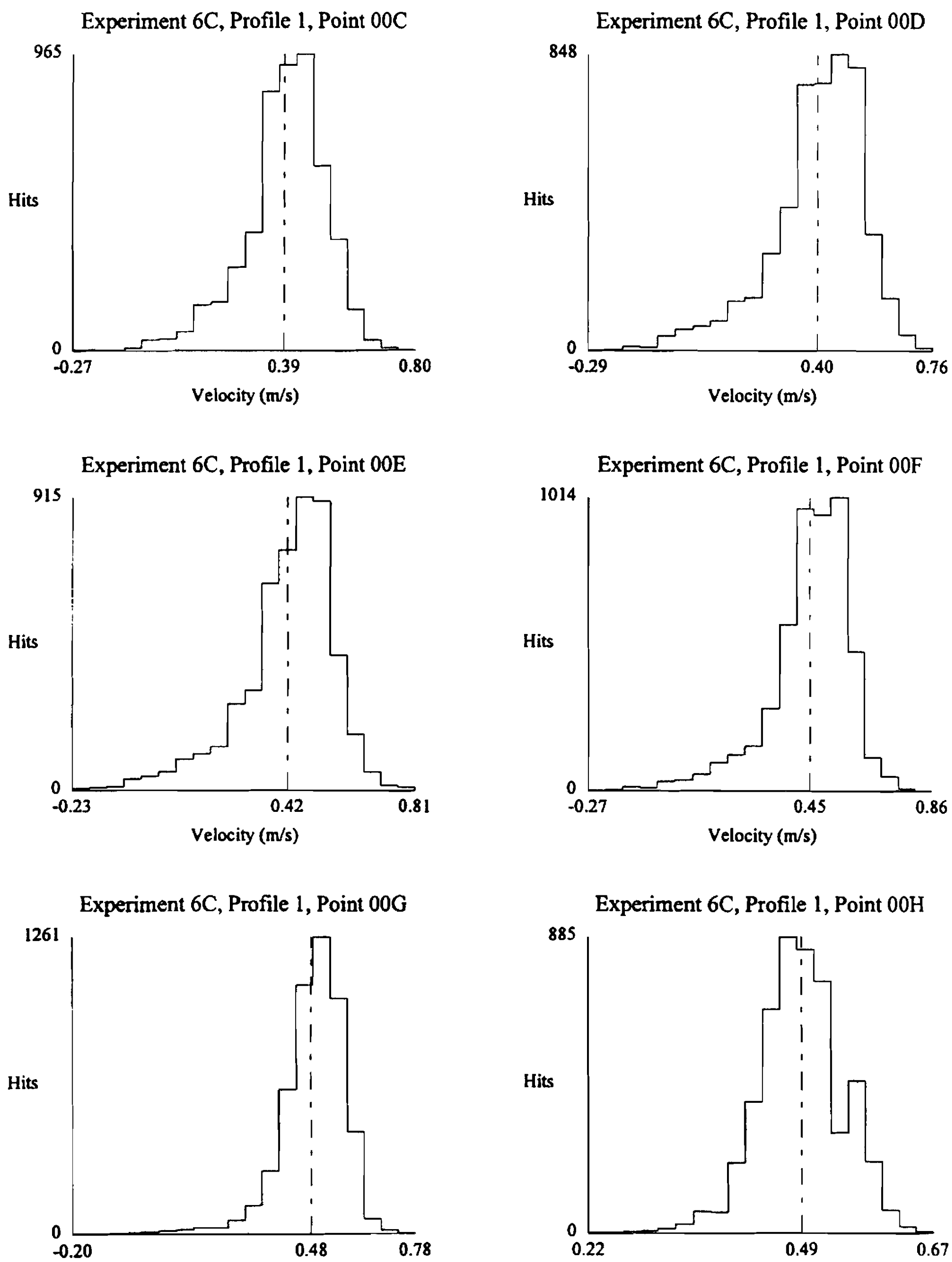

Figure A9 continued....

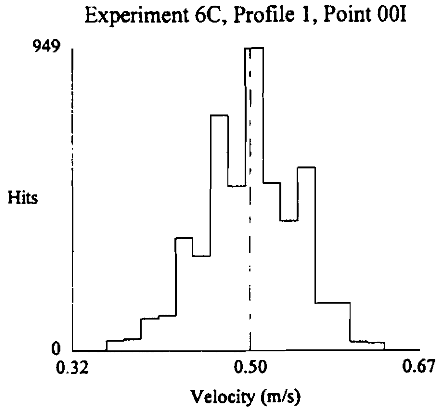

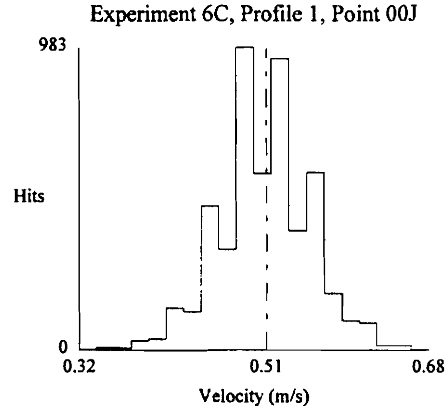

Figure A9 continued....

Table A24: Experiment 6C Measurement Point 2

Average Velocity (m/s)	Depth (m)	Maximum Velocity (m/s)	Minimum Velocity (m/s)	Standard Deviation (m/s)	Number of Samples	Sampling Frequency (Hz)	3rd Moment Skew	Kurtosis
0.2432	0.0000	0.5325	0.0933	0.0660	272	3.619	0.444	3.758
0.2732	0.0023	0.4967	0.0594	0.0736	880	21.667	0.059	2.877
0.2797	0.0046	0.5815	0.0594	0.0761	1839	57.158	-0.005	3.068
0.2813	0.0069	0.5325	0.0707	0.0687	2416	76.844	-0.025	2.916
0.2712	0.0092	0.5212	0.0349	0.0755	5000	100.079	0.114	2.803
0.2706	0.0139	0.6174	0.0349	0.0777	5000	123.557	0.156	2.905
0.2742	0.0185	0.5815	0.0481	0.0743	3790	115.848	0.005	3.016
0.2800	0.0231	0.5684	0.0349	0.0782	5000	111.298	0.062	2.817
0.2858	0.0277	0.5684	0.0481	0.0769	5000	111.654	0.068	3.062
0.2891	0.0323	0.5929	0.0481	0.0800	5000	114.291	0.029	2.949
0.2959	0.0370	0.5684	0.0236	0.0806	5000	115.367	0.021	2.876
0.2958	0.0416	0.6532	0.0481	0.0890	5000	117.039	0.152	2.869
0.2998	0.0462	0.6532	-0.0217	0.0933	5000	102.888	0.081	2.969
0.3276	0.0508	0.6532	0.0349	0.0953	5000	121.888	0.012	2.759
0.3801	0.0554	0.7022	-0.0443	0.0899	5000	112.720	-0.369	3.293
0.4393	0.0601	0.6909	0.1159	0.0781	5000	137.005	-0.586	3.635
0.4928	0.0647	0.6909	0.2140	0.0552	5000	141.251	-0.542	4.154
0.5179	0.0693	0.6664	0.2762	0.0514	5000	146.779	-0.608	3.749
0.5374	0.0739	0.7267	0.3252	0.0496	5000	120.110	-0.184	3.371
0.5622	0.0785	0.7456	0.3629	0.0497	3086	20.662	-0.052	3.559

Table A25: Experiment 6C Measurement Point 3

Average Velocity (m/s)	Depth (m)	Maximum Velocity (m/s)	Minimum Velocity (m/s)	Standard Deviation (m/s)	Number of Samples	Sampling Frequency (Hz)	3rd Moment Skew	Kurtosis
0.2804	0.0000	0.4609	0.1404	0.0633	288	5.440	0.212	2.929
0.3068	0.0023	0.5420	0.1291	0.0619	959	14.611	0.085	2.864
0.3044	0.0046	0.5175	0.1159	0.0657	1152	24.957	0.243	2.891
0.3030	0.0069	0.5061	0.0801	0.0650	1550	39.481	0.211	2.864
0.3032	0.0092	0.5307	0.1159	0.0644	3632	54.507	0.164	2.930
0.2997	0.0139	0.5646	0.0669	0.0643	4220	56.438	0.173	2.842
0.2950	0.0185	0.5420	0.0914	0.0649	2607	74.754	0.261	3.010
0.3009	0.0231	0.5533	0.1159	0.0651	2432	75.107	0.276	2.802
0.3021	0.0277	0.5061	0.1046	0.0671	2095	77.893	0.266	2.921
0.3092	0.0323	0.5175	0.1159	0.0688	3199	78.517	0.163	2.639
0.3164	0.0370	0.5646	0.0801	0.0676	2767	84.771	0.252	3.092
0.3286	0.0416	0.5646	0.1046	0.0688	5000	89.084	0.154	2.813
0.3534	0.0462	0.6570	0.0669	0.0757	4300	92.878	-0.003	2.976
0.4050	0.0508	0.6570	0.1536	0.0774	5000	115.057	-0.220	2.770
0.4332	0.0554	0.6570	0.1159	0.0793	4127	105.653	-0.499	2.911
0.4704	0.0601	0.6456	0.1895	0.0675	5000	93.959	-0.669	3.553
0.4921	0.0647	0.6570	0.1649	0.0639	3981	96.043	-0.815	4.225
0.5175	0.0693	0.6683	0.2385	0.0535	3743	90.471	-0.618	3.763
0.5398	0.0739	0.7361	0.2875	0.0525	1823	44.994	-0.148	3.512
0.5409	0.0785	0.6456	0.4609	0.0400	32	0.566	0.328	2.676

Table A25(A): Experiment 6C Measurement Point 4

Average Velocity (m/s)	Depth (m)	Maximum Velocity (m/s)	Minimum Velocity (m/s)	Standard Deviation (m/s)	Number of Samples	Sampling Frequency (Hz)	3rd Moment Skew	Kurtosis
0.2477	0.0000	0.4119	0.0801	0.0631	224	2.391	0.095	2.538
0.2801	0.0023	0.4948	0.1536	0.0578	302	5.886	0.400	2.940
0.2865	0.0046	0.4609	0.1291	0.0576	1628	18.437	0.247	2.832
0.2925	0.0069	0.4948	0.0801	0.0578	2110	31.507	0.274	3.005
0.2856	0.0092	0.5061	0.1291	0.0592	1855	33.879	0.285	2.974
0.2886	0.0139	0.5061	0.1291	0.0578	1296	32.865	0.159	2.790
0.2863	0.0185	0.4722	0.1291	0.0558	1534	39.977	0.321	2.744
0.2868	0.0231	0.4609	0.1159	0.0594	2272	55.876	0.220	2.737
0.2874	0.0277	0.4948	0.1159	0.0557	1664	47.220	0.231	3.087
0.2888	0.0323	0.4948	0.1159	0.0584	1567	40.886	0.216	3.003
0.2976	0.0370	0.5420	0.1159	0.0622	1710	53.488	0.250	2.900
0.3212	0.0416	0.5872	0.0914	0.0669	3615	31.398	0.055	2.774
0.3487	0.0462	0.5420	0.1159	0.0681	2144	52.735	-0.043	2.642
0.3710	0.0508	0.5646	0.0914	0.0727	1758	53.137	-0.234	2.812
0.4007	0.0554	0.5872	0.1046	0.0709	2080	63.523	-0.423	3.026
0.4135	0.0601	0.5759	0.1781	0.0658	1792	57.288	-0.550	3.137
0.4310	0.0647	0.5872	0.1781	0.0607	1599	48.217	-0.699	3.643
0.4415	0.0693	0.6343	0.2140	0.0530	1760	59.306	-0.346	3.345
0.4642	0.0739	0.6230	0.2385	0.0541	2112	50.612	-0.407	3.227
0.4862	0.0785	0.7267	0.3120	0.0602	112	1.545	0.291	4.722

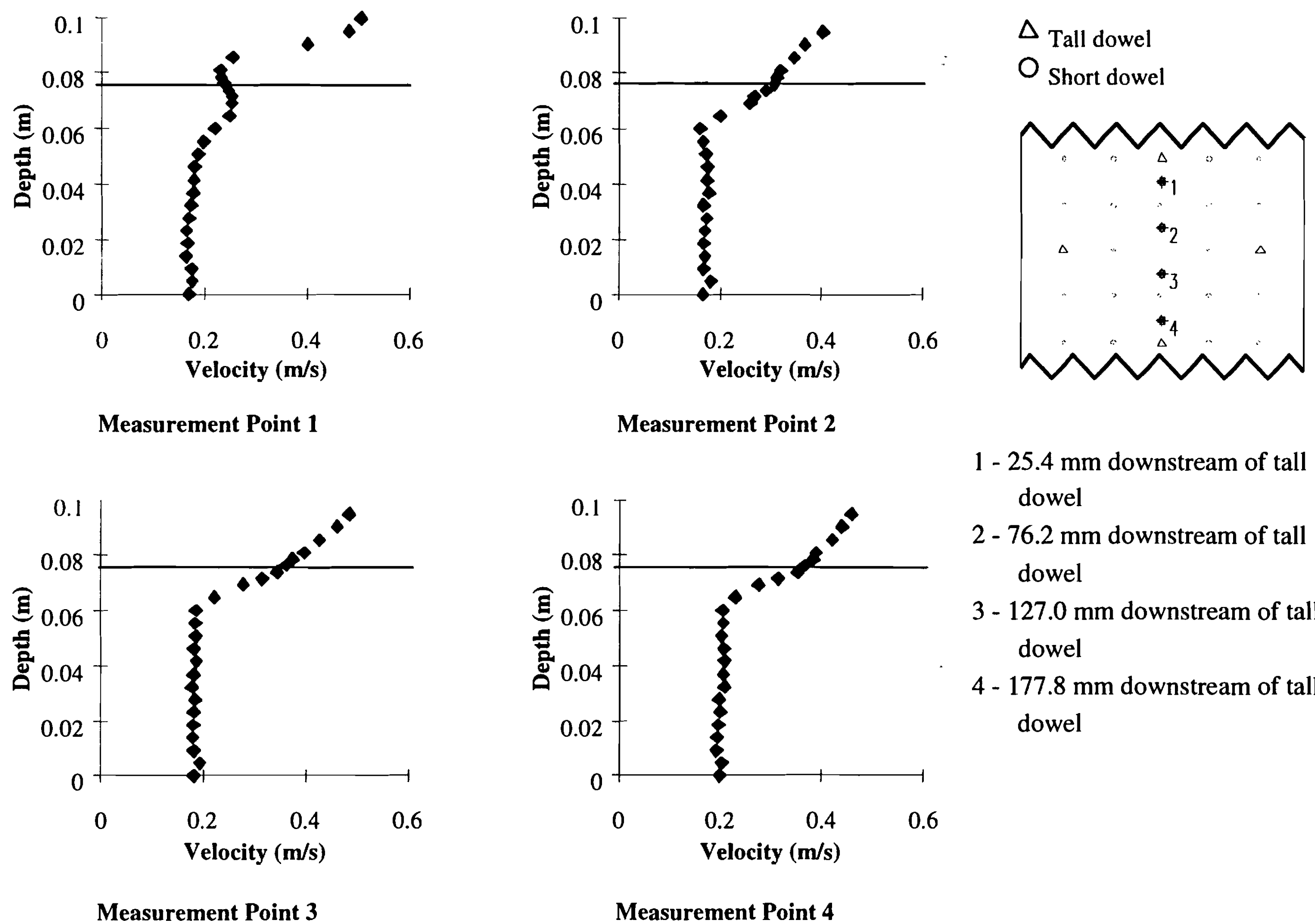

1 - 25.4 mm downstream of tall dowel
2 - 76.2 mm downstream of tall dowel
3 - 127.0 mm downstream of tall dowel
4 - 177.8 mm downstream of tall dowel

Figure A10: Profiles for Double-layered Experiment 7 (Linear s/d=8 Short, Staggered s/d = 16 Tall).

Table A26: Experiment 7 Measurement Point 1

Average Velocity (m/s)	Depth (m)	Maximum Velocity (m/s)	Minimum Velocity (m/s)	Standard Deviation (m/s)	Number of Samples	Sampling Frequency (Hz)	3rd Moment Skew	Kurtosis
0.1706	0.0000	0.3369	0.0122	0.0597	574	9.851	0.179	2.725
0.1757	0.0046	0.4120	0.0122	0.0585	2500	95.885	0.233	3.195
0.1746	0.0092	0.4852	0.0009	0.0627	2500	147.107	0.180	3.042
0.1643	0.0139	0.3989	0.0009	0.0604	2500	155.549	0.299	2.917
0.1670	0.0185	0.3745	0.0009	0.0635	2500	156.906	0.186	2.681
0.1656	0.0231	0.3857	-0.0216	0.0661	2500	159.993	0.254	2.860
0.1694	0.0277	0.3857	-0.0460	0.0637	2500	157.118	0.111	2.871
0.1737	0.0323	0.4232	-0.0217	0.0649	2500	141.903	0.121	2.816
0.1777	0.0370	0.5325	-0.0104	0.0673	2500	138.660	0.291	3.661
0.1788	0.0416	0.4364	-0.0443	0.0657	2500	127.028	0.077	2.909
0.1809	0.0462	0.3874	-0.0330	0.0638	2500	129.208	0.022	2.807
0.1877	0.0508	0.4119	-0.0217	0.0623	2500	105.823	0.109	3.034
0.1986	0.0554	0.4477	0.0009	0.0669	2500	139.145	0.126	3.027
0.2199	0.0601	0.4967	0.0123	0.0702	2500	137.767	0.133	3.020
0.2484	0.0647	0.4967	0.0123	0.0757	2500	142.311	-0.025	2.935
0.2531	0.0693	0.5684	-0.0330	0.0820	2500	154.392	0.043	2.919
0.2530	0.0716	0.5325	-0.0443	0.0877	2500	161.939	-0.118	2.868
0.2462	0.0739	0.5457	-0.0575	0.0915	2500	147.185	-0.032	2.757
0.2384	0.0762	0.6287	-0.0801	0.0984	2500	145.565	-0.025	2.721
0.2328	0.0785	0.6532	-0.0330	0.0959	2500	156.214	0.048	2.674
0.2312	0.0808	0.6061	-0.0443	0.1038	2500	157.835	0.142	2.523
0.2556	0.0854	0.5815	-0.1254	0.1061	2500	159.559	0.073	2.571
0.4005	0.0901	0.6532	-0.0217	0.0966	2500	170.960	-0.746	3.715
0.4819	0.0947	0.8473	0.1649	0.0657	2500	199.400	-0.322	4.350
0.5059	0.0993	1.2621	-0.1499	0.1201	652	6.427	1.600	12.033

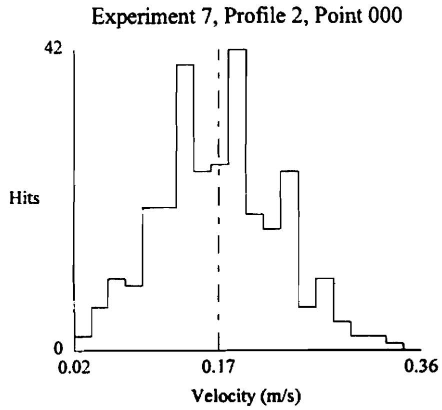

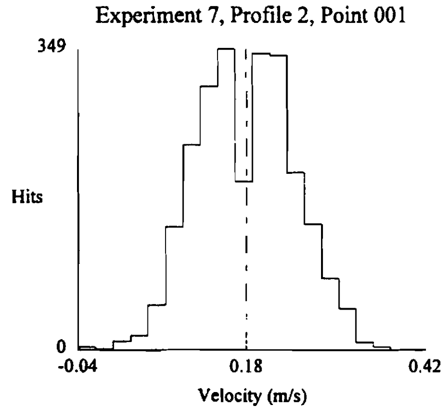

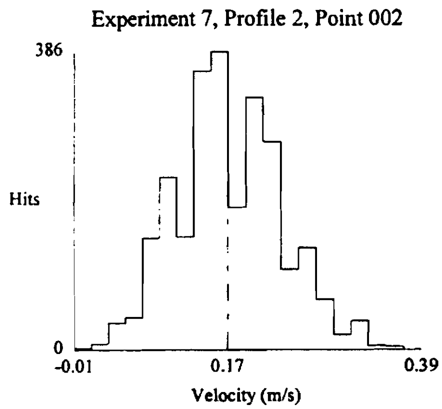

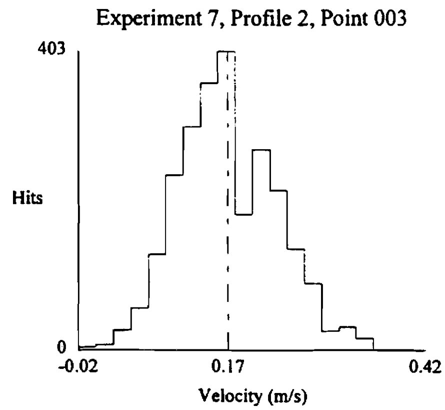

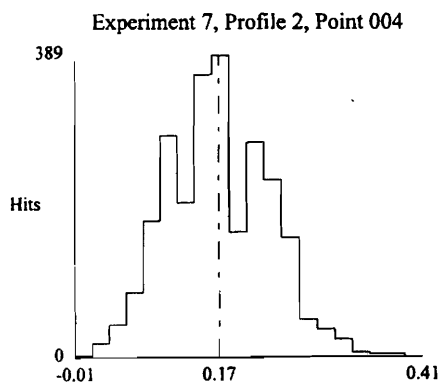

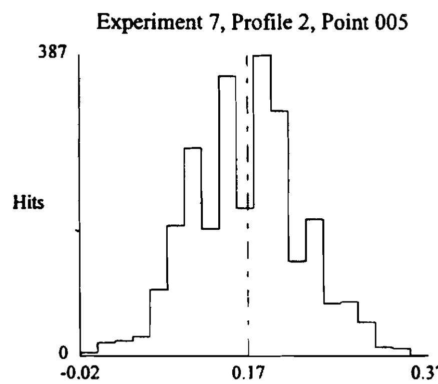

Figure A11: Histograms for Experiment 7 (Linear s/d=8 Short, Staggered s/d=16 Tall), Profile 2

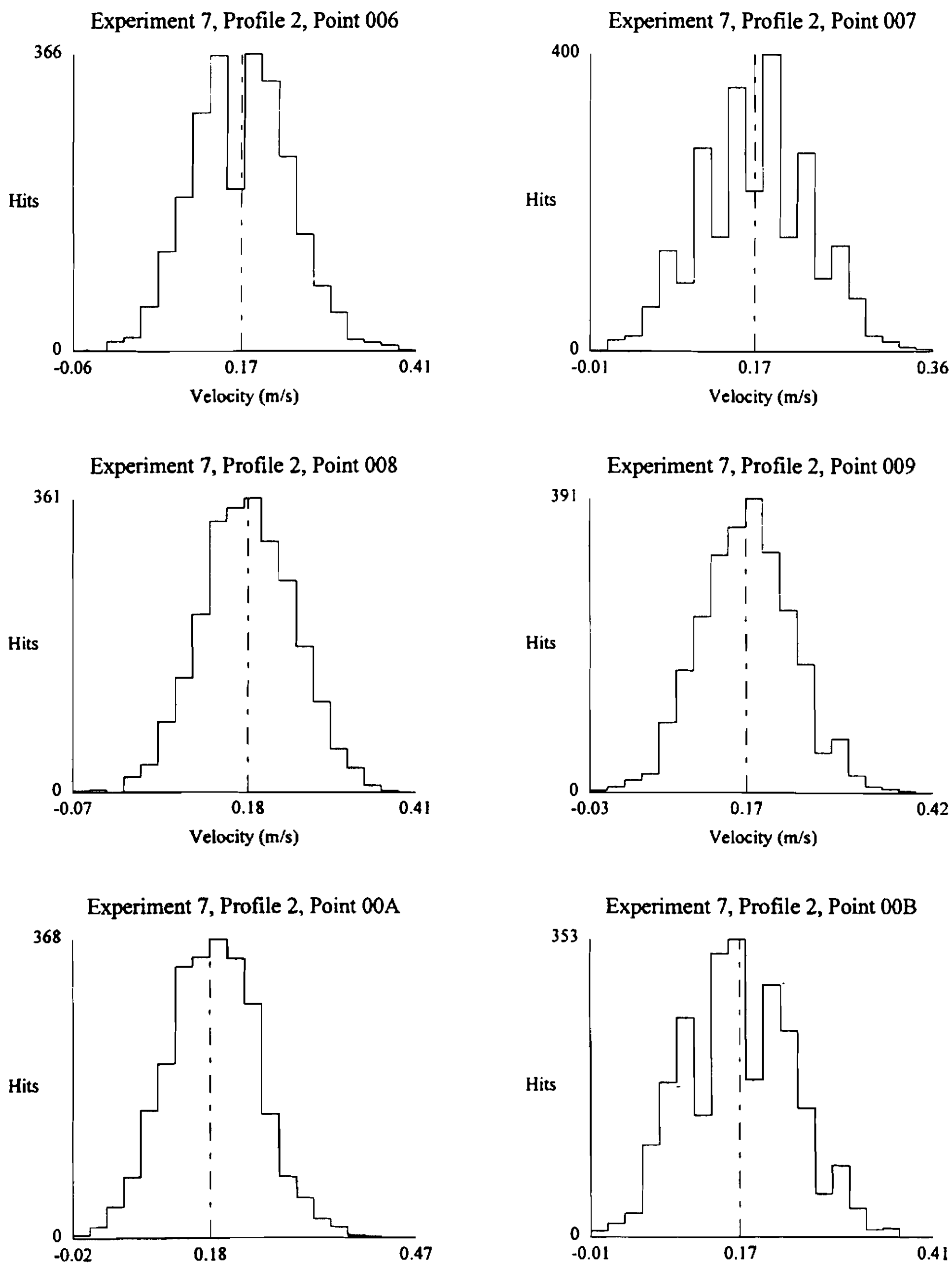

Figure A11 continued....

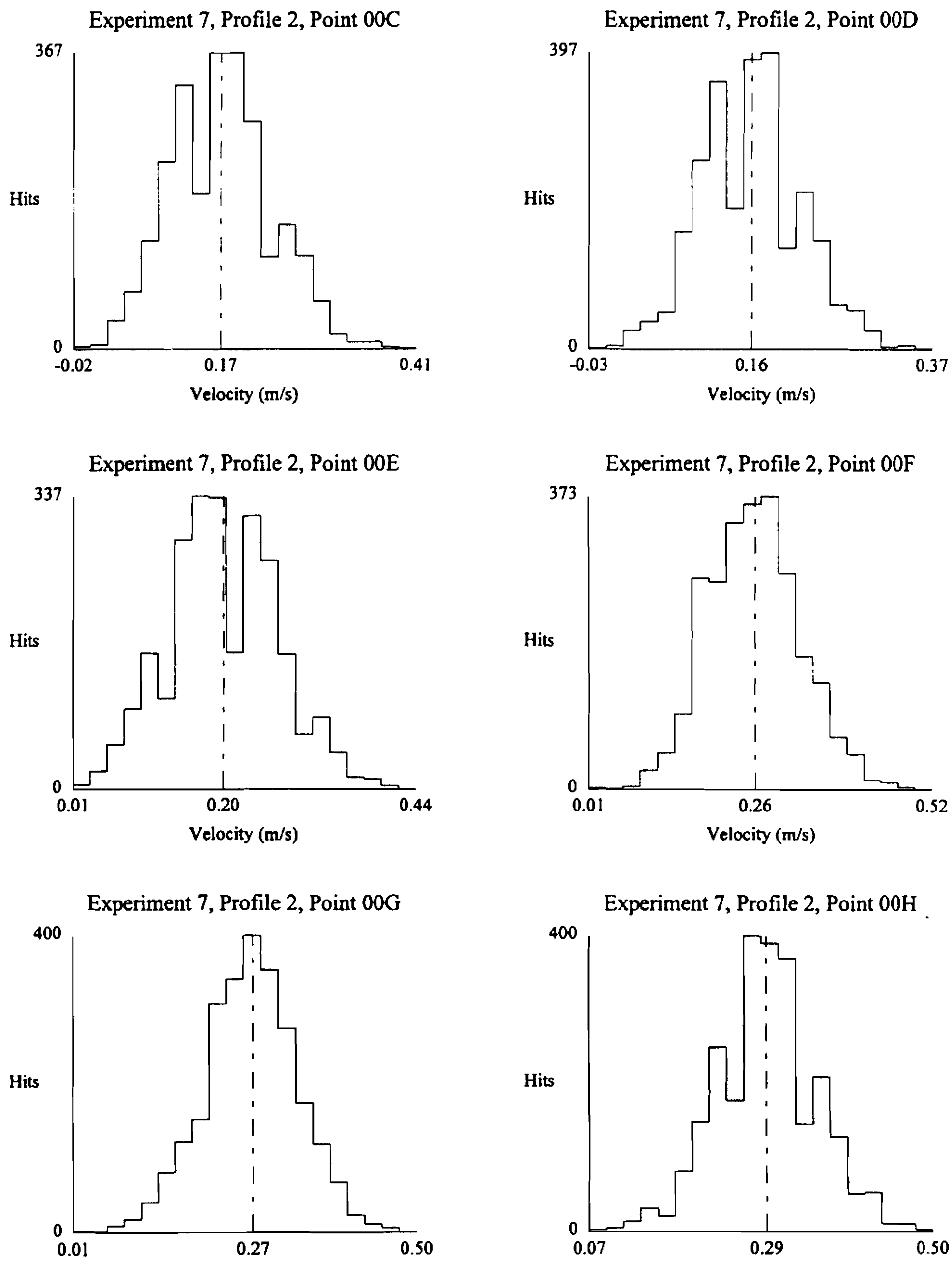

Figure A11 continued….

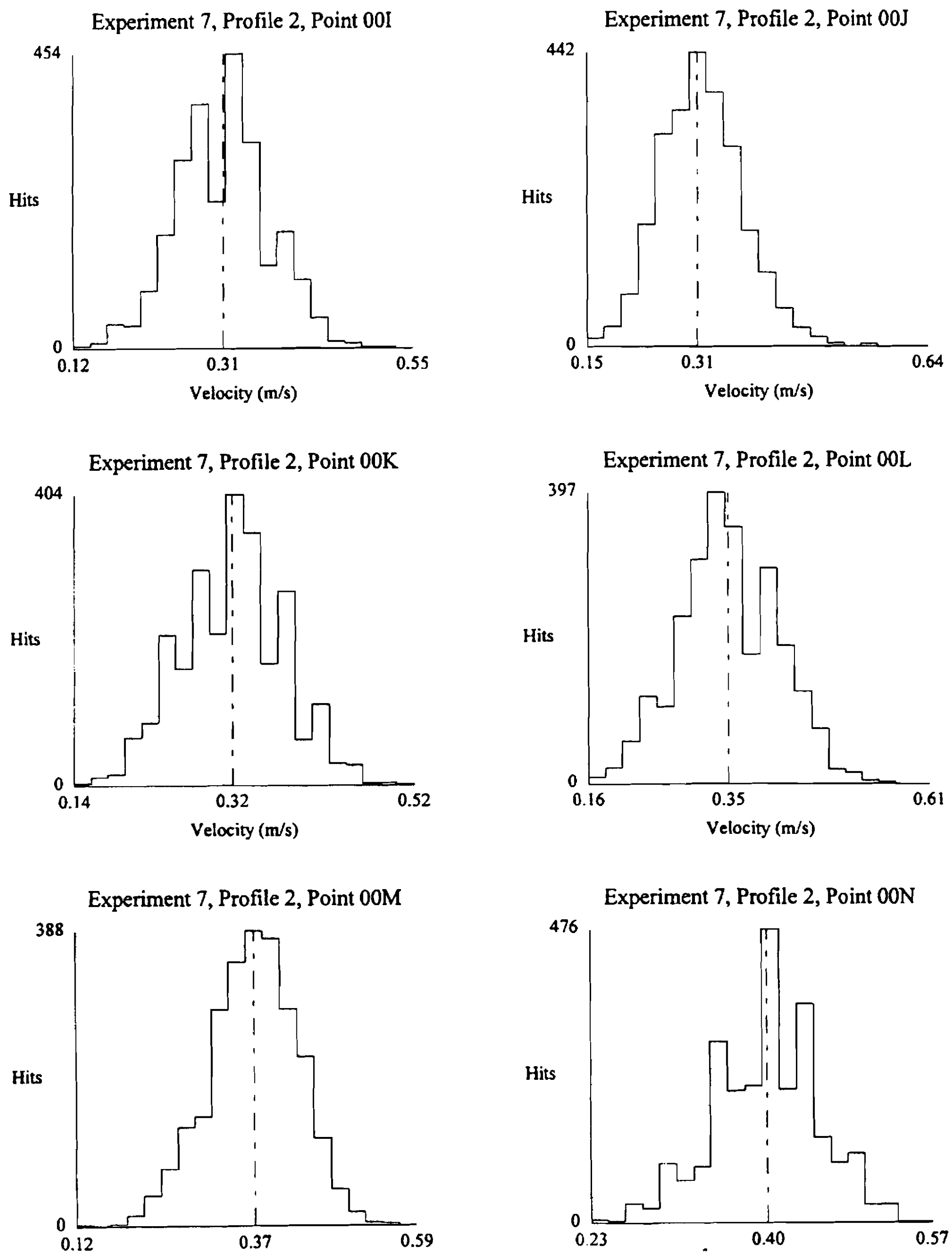

Figure A11 continued....

Table A27: Experiment 7 Measurement Point 2

Average Velocity (m/s)	Depth (m)	Maximum Velocity (m/s)	Minimum Velocity (m/s)	Standard Deviation (m/s)	Number of Samples	Sampling Frequency (Hz)	3rd Moment Skew	Kurtosis
0.1666	0.0000	0.3629	0.0236	0.0595	287	3.062	0.251	3.074
0.1813	0.0046	0.4232	-0.0443	0.0624	2500	48.610	0.127	2.914
0.1677	0.0092	0.3874	-0.0104	0.0611	2500	86.553	0.221	2.813
0.1692	0.0139	0.4232	-0.0217	0.0632	2500	97.153	0.220	2.964
0.1671	0.0185	0.4119	-0.0104	0.0613	2500	106.192	0.238	2.986
0.1692	0.0231	0.3742	-0.0217	0.0620	2500	93.837	0.102	2.978
0.1732	0.0277	0.4119	-0.0575	0.0630	2500	115.175	0.221	3.209
0.1678	0.0323	0.3629	-0.0104	0.0599	2500	116.867	0.119	2.807
0.1773	0.0370	0.4119	-0.0688	0.0652	2500	119.040	0.080	2.947
0.1737	0.0416	0.4232	-0.0330	0.0629	2500	122.044	0.107	2.891
0.1761	0.0462	0.4722	-0.0217	0.0634	2500	102.510	0.165	3.177
0.1724	0.0508	0.4119	-0.0104	0.0650	2500	104.970	0.166	2.727
0.1662	0.0554	0.4119	-0.0217	0.0630	2500	121.042	0.245	3.006
0.1596	0.0601	0.3742	-0.0330	0.0596	2500	122.100	0.181	2.910
0.1996	0.0647	0.4364	0.0123	0.0680	2500	138.942	0.147	2.831
0.2587	0.0693	0.5212	0.0123	0.0676	2500	161.884	0.113	3.136
0.2673	0.0716	0.4967	0.0123	0.0665	2500	160.666	-0.097	3.223
0.2899	0.0739	0.4967	0.0707	0.0617	2500	159.624	-0.041	3.222
0.3063	0.0762	0.5457	0.1159	0.0583	2500	156.400	0.006	3.118
0.3116	0.0785	0.6419	0.1536	0.0594	2500	156.192	0.404	3.655
0.3182	0.0808	0.5212	0.1404	0.0581	2500	168.979	0.067	2.682
0.3453	0.0854	0.6061	0.1649	0.0638	2500	183.909	0.089	2.861
0.3666	0.0901	0.5929	0.1159	0.0637	2500	181.692	-0.229	3.019
0.4028	0.0947	0.5684	0.2272	0.0526	2500	80.778	-0.153	3.006

Table A28: Experiment 7 Measurement Point 3

Average Velocity (m/s)	Depth (m)	Maximum Velocity (m/s)	Minimum Velocity (m/s)	Standard Deviation (m/s)	Number of Samples	Sampling Frequency (Hz)	3rd Moment Skew	Kurtosis
0.1818	0.0000	0.4364	0.0443	0.0617	278	3.183	0.506	3.738
0.1936	0.0046	0.3874	0.0066	0.0632	1771	33.563	-0.003	2.742
0.1820	0.0092	0.3874	-0.0160	0.0625	2500	57.251	0.014	2.947
0.1796	0.0139	0.4364	-0.0650	0.0623	2500	35.637	0.158	3.171
0.1798	0.0185	0.4477	-0.0047	0.0627	2500	69.494	0.165	3.050
0.1824	0.0231	0.4477	-0.0047	0.0631	1781	31.495	0.198	3.055
0.1845	0.0277	0.3987	-0.0047	0.0609	2500	64.717	-0.001	2.905
0.1779	0.0323	0.3742	-0.0405	0.0650	2500	79.731	0.001	2.676
0.1819	0.0370	0.3874	-0.0047	0.0611	2500	89.188	0.054	2.704
0.1865	0.0416	0.4364	-0.0405	0.0655	2500	76.326	0.003	2.995
0.1824	0.0462	0.4119	-0.0047	0.0627	2500	84.064	0.170	2.979
0.1851	0.0508	0.4232	-0.0292	0.0636	2500	92.447	0.101	2.953
0.1838	0.0554	0.4948	-0.0047	0.0663	2500	100.592	0.439	3.511
0.1850	0.0601	0.4364	-0.0160	0.0668	2500	88.067	0.196	3.117
0.2215	0.0647	0.5061	-0.0047	0.0701	2500	78.826	0.034	3.080
0.2784	0.0693	0.5646	0.0556	0.0665	2500	94.291	-0.080	3.208
0.3140	0.0716	0.5175	0.0801	0.0636	2500	93.275	-0.292	3.098
0.3433	0.0739	0.5759	0.0443	0.0569	2500	101.328	-0.206	3.622
0.3604	0.0762	0.5307	0.1536	0.0527	2500	105.167	-0.033	3.177
0.3742	0.0785	0.5420	0.1536	0.0540	2500	115.105	-0.094	3.095
0.3969	0.0808	0.5759	0.2140	0.0534	2500	116.658	-0.068	2.681
0.4263	0.0854	0.6230	0.2385	0.0557	2500	115.617	-0.161	2.835
0.4606	0.0901	0.6230	0.2875	0.0496	2500	110.410	-0.142	2.958
0.4845	0.0947	0.6230	0.3365	0.0504	506	7.043	0.027	2.987

Table A29: Experiment 7 Measurement Point 4

Average Velocity (m/s)	Depth (m)	Maximum Velocity (m/s)	Minimum Velocity (m/s)	Standard Deviation (m/s)	Number of Samples	Sampling Frequency (Hz)	3rd Moment Skew	Kurtosis
0.1999	0.0000	0.3365	0.0669	0.0564	60	0.631	0.069	2.996
0.2022	0.0046	0.3987	-0.0160	0.0654	2500	56.853	0.025	2.827
0.1922	0.0092	0.4119	-0.0160	0.0644	2500	96.364	0.169	2.819
0.1930	0.0139	0.4477	-0.0047	0.0658	2500	83.618	0.192	2.939
0.1952	0.0185	0.3987	-0.0292	0.0658	2500	87.023	-0.017	2.710
0.1986	0.0231	0.4364	-0.0292	0.0680	2500	70.647	0.053	2.675
0.1967	0.0277	0.4609	-0.0292	0.0666	2500	58.039	0.048	2.793
0.2076	0.0323	0.4835	-0.0047	0.0655	2500	79.848	0.019	2.929
0.2048	0.0370	0.4232	0.0066	0.0678	2500	75.356	0.043	2.659
0.2070	0.0416	0.4609	-0.0160	0.0692	2500	62.806	0.118	2.892
0.2066	0.0462	0.4609	-0.0047	0.0647	2500	57.995	0.077	2.762
0.2016	0.0508	0.4364	0.0198	0.0666	1602	47.575	0.057	2.792
0.2054	0.0554	0.5175	0.0066	0.0680	2500	63.488	0.175	3.067
0.2043	0.0601	0.4477	-0.0047	0.0722	2500	56.664	0.237	2.959
0.2285	0.0647	0.4835	-0.0405	0.0741	2500	75.153	0.068	2.789
0.2735	0.0693	0.5061	-0.0763	0.0725	2500	72.294	-0.214	3.016
0.3128	0.0716	0.5307	0.0311	0.0717	2500	68.933	-0.376	3.350
0.3520	0.0739	0.5307	0.1404	0.0578	2500	44.001	-0.243	3.104
0.3658	0.0762	0.5533	0.1291	0.0537	2500	46.092	-0.091	3.241
0.3817	0.0785	0.5420	0.0914	0.0537	2500	48.705	-0.117	3.041
0.3879	0.0808	0.5420	0.2140	0.0489	1927	65.132	-0.117	2.791
0.4202	0.0854	0.5533	0.2385	0.0485	2500	86.388	-0.049	2.805
0.4385	0.0901	0.5872	0.2630	0.0472	2500	97.141	-0.220	2.975
0.4578	0.0947	0.6098	0.3252	0.0502	438	2.930	-0.267	3.110

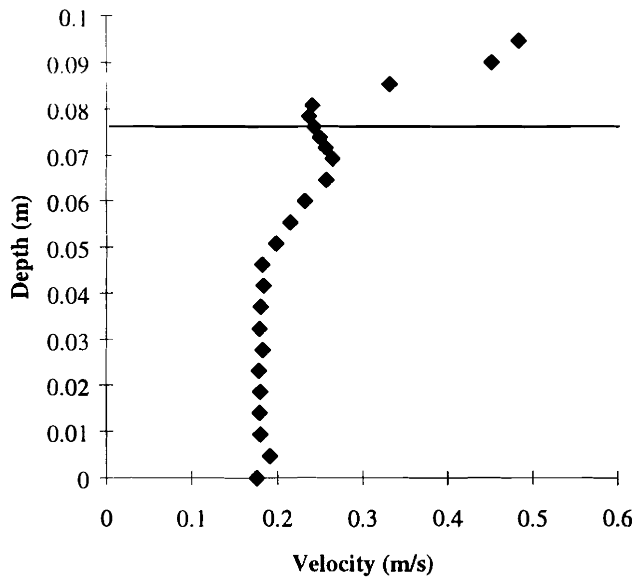

Measurement Point 1

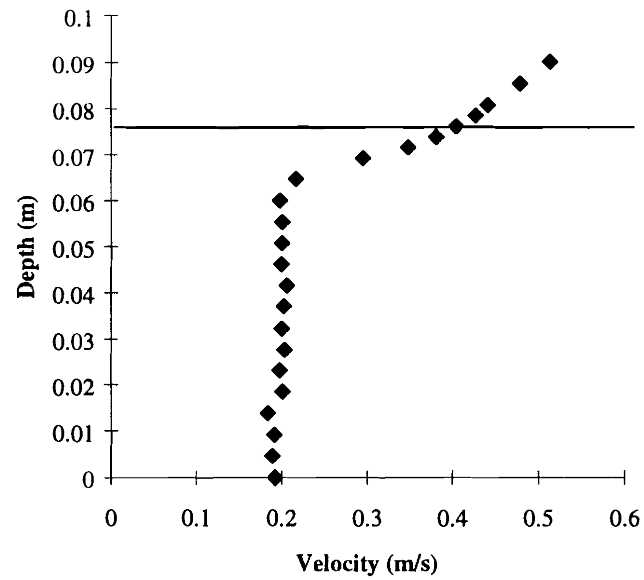

Measurement Point 2

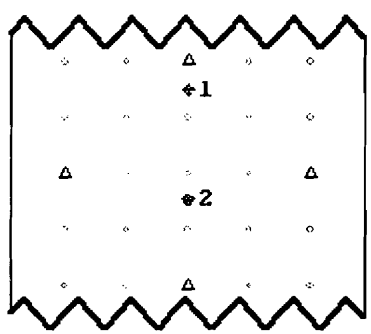

Δ Tall dowel
O Short dowel

1 - 25.4 mm downstream of tall dowel
2 - 127.0 mm downstream of tall dowel

Figure A12: Profiles for Double-layered Experiment 8 (Linear s/d=8 Short, Staggered s/d = 16 Tall)

Table A30: Experiment 8 Measurement Point 1

Average Velocity (m/s)	Depth (m)	Maximum Velocity (m/s)	Minimum Velocity (m/s)	Standard Deviation (m/s)	Number of Samples	Sampling Frequency (Hz)	3rd Moment Skew	Kurtosis
0.1758	0.0000	0.3535	0.0556	0.0542	322	2.146	0.350	3.217
0.1906	0.0046	0.3780	-0.0160	0.0570	2067	19.133	-0.030	3.002
0.1798	0.0092	0.4006	-0.0160	0.0589	2500	34.515	0.031	2.891
0.1790	0.0139	0.3893	-0.0160	0.0566	2500	34.173	0.060	2.911
0.1795	0.0185	0.3893	-0.0160	0.0582	1575	26.857	0.053	2.891
0.1777	0.0231	0.3648	-0.0047	0.0582	1575	29.990	0.220	2.936
0.1826	0.0277	0.3893	-0.0537	0.0596	1582	39.206	0.098	3.145
0.1787	0.0323	0.3893	-0.0047	0.0612	1530	37.684	0.000	2.928
0.1803	0.0370	0.3780	0.0066	0.0605	1727	39.230	0.118	2.928
0.1840	0.0416	0.3648	-0.0292	0.0598	1726	41.093	-0.042	2.788
0.1826	0.0462	0.3535	-0.0160	0.0579	1579	34.896	-0.025	2.889
0.1985	0.0508	0.3893	0.0198	0.0588	1539	29.947	0.051	2.860
0.2147	0.0554	0.4477	0.0198	0.0652	1640	42.318	0.118	2.918
0.2316	0.0601	0.4967	-0.0650	0.0717	1588	43.200	0.026	2.984
0.2568	0.0647	0.5570	0.0198	0.0737	2500	46.096	0.058	3.220
0.2640	0.0693	0.5815	0.0066	0.0811	1633	38.023	-0.098	2.894
0.2563	0.0716	0.5080	0.0066	0.0815	2500	53.198	-0.056	2.843
0.2494	0.0739	0.5080	-0.0537	0.0834	1561	48.236	-0.087	3.233
0.2427	0.0762	0.4967	-0.0405	0.0900	1636	43.825	-0.036	2.833
0.2366	0.0785	0.5325	-0.0405	0.0917	2500	50.424	0.090	2.675
0.2403	0.0808	0.5929	-0.0763	0.0928	1683	49.257	0.039	2.879
0.3313	0.0854	0.6664	-0.0650	0.0995	1704	58.396	-0.293	2.994
0.4515	0.0901	0.7569	0.1046	0.0752	1647	57.755	-0.432	4.545
0.4831	0.0947	1.2734	0.1046	0.0792	1091	15.699	1.150	12.636

Table A31: Experiment 8 Measurement Point 2

Average Velocity (m/s)	Depth (m)	Maximum Velocity (m/s)	Minimum Velocity (m/s)	Standard Deviation (m/s)	Number of Samples	Sampling Frequency (Hz)	3rd Moment Skew	Kurtosis
0.1921	0.0000	0.3497	0.0556	0.0585	128	1.085	0.069	2.651
0.1892	0.0046	0.3874	-0.0405	0.0652	879	8.308	-0.049	2.948
0.1911	0.0092	0.3987	0.0066	0.0638	1871	12.630	0.054	2.781
0.1836	0.0139	0.3497	-0.0047	0.0630	528	14.461	-0.202	2.654
0.2005	0.0185	0.4232	-0.0537	0.0681	2063	13.734	-0.031	2.940
0.1979	0.0231	0.4477	-0.0537	0.0683	1040	17.502	0.006	2.998
0.2034	0.0277	0.4232	-0.0047	0.0658	592	14.168	-0.135	3.213
0.1996	0.0323	0.3987	-0.0047	0.0728	784	18.728	-0.015	2.731
0.2024	0.0370	0.4477	-0.0047	0.0687	1471	20.390	0.087	2.771
0.2057	0.0416	0.3987	-0.0047	0.0705	1344	18.928	-0.093	2.889
0.1997	0.0462	0.4232	-0.0160	0.0713	1071	26.289	-0.012	2.853
0.2005	0.0508	0.4722	-0.0292	0.0676	1056	22.505	0.031	3.030
0.2009	0.0554	0.4119	0.0443	0.0639	704	24.901	0.115	2.918
0.1980	0.0601	0.4364	-0.0292	0.0738	1599	25.418	0.186	2.855
0.2166	0.0647	0.4722	-0.0292	0.0738	878	17.992	-0.001	3.086
0.2954	0.0693	0.5061	-0.0405	0.0801	879	19.309	-0.351	3.310
0.3479	0.0716	0.5646	0.0198	0.0731	1472	26.759	-0.347	3.601
0.3812	0.0739	0.5533	0.1291	0.0645	1612	25.698	-0.236	3.011
0.4044	0.0762	0.5759	0.1159	0.0598	1695	25.622	-0.444	3.864
0.4270	0.0785	0.5985	0.2385	0.0551	2500	24.641	-0.205	2.993
0.4410	0.0808	0.6098	0.2630	0.0522	2500	27.604	-0.157	3.090
0.4784	0.0854	0.6683	0.2630	0.0524	1216	23.428	-0.239	3.183
0.5130	0.0901	0.7154	0.3742	0.0451	528	5.327	0.229	3.827

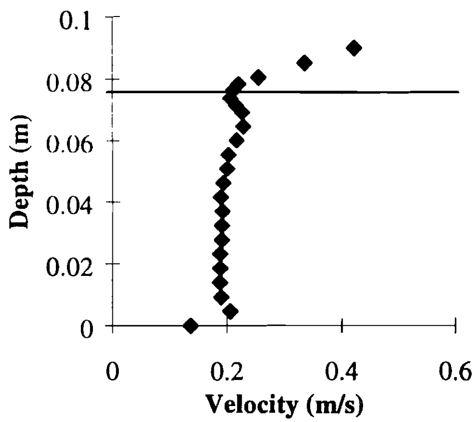

Measurement Point 1

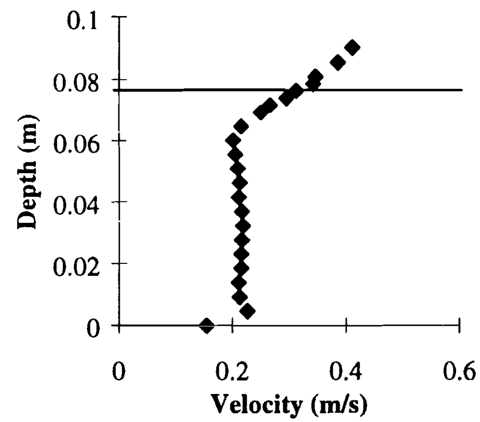

Measurement Point 2

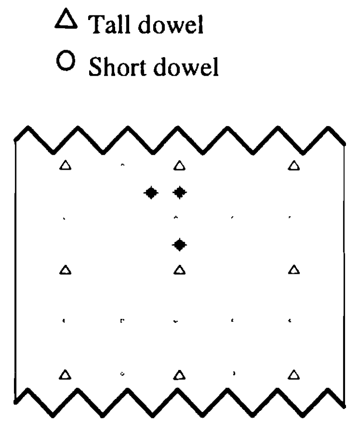

1 - 25.4 mm downstream of tall dowel
2 - 76.2 mm downstream of tall dowel
3 - 25.4 mm downstream of tall dowel, 25.4 mm left of CL

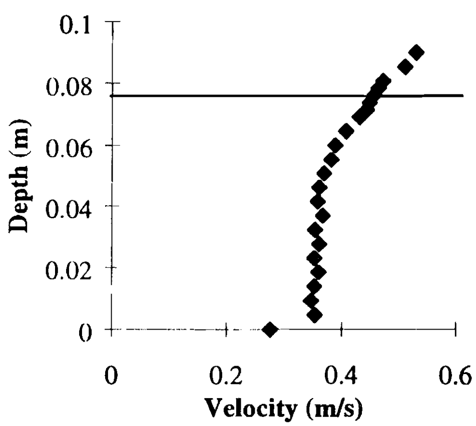

Measurement Point 3

Figure A13: Profiles for Double-layered Experiment 9 (Linear s/d=8 Short, Linear s/d = 16 Tall)

Table A32: Experiment 9 Measurement Point 1

Average Velocity (m/s)	Depth (m)	Maximum Velocity (m/s)	Minimum Velocity (m/s)	Standard Deviation (m/s)	Number of Samples	Sampling Frequency (Hz)	3rd Moment Skew	Kurtosis
0.1360	0.0000	0.4608	-0.8794	0.1267	249	3.295	-3.541	25.724
0.2054	0.0046	0.4233	-0.9357	0.0923	542	10.804	-5.359	63.944
0.1897	0.0092	0.4233	-0.9451	0.0774	1032	15.995	-3.282	48.373
0.1875	0.0139	0.7142	-0.1248	0.0766	1274	15.339	0.352	5.301
0.1877	0.0185	0.6166	-0.0047	0.0708	1047	16.622	0.351	3.992
0.1881	0.0231	0.4608	-0.0648	0.0705	1429	18.815	0.159	3.164
0.1907	0.0277	0.4364	-1.1610	0.0852	1046	17.704	-3.784	62.539
0.1909	0.0323	0.4477	-0.3895	0.0769	887	17.071	-0.210	6.514
0.1917	0.0370	0.4364	-0.0404	0.0745	961	20.306	0.007	2.888
0.1890	0.0416	0.4120	-0.0404	0.0753	853	18.828	0.142	2.777
0.1938	0.0462	0.4477	-0.0648	0.0737	1080	21.152	0.096	2.977
0.2005	0.0508	0.4233	-0.0291	0.0740	1521	26.379	0.085	2.881
0.2029	0.0554	0.4852	-0.7236	0.0766	1217	23.649	-1.449	20.024
0.2166	0.0601	0.5566	-0.0291	0.0772	1272	19.258	0.204	3.418
0.2280	0.0647	0.4965	0.0066	0.0747	763	16.440	0.150	2.835
0.2258	0.0693	0.4965	-0.0047	0.0822	1054	19.815	0.014	2.920
0.2157	0.0716	0.4477	-0.0291	0.0772	977	19.260	-0.012	2.966
0.2053	0.0739	0.5096	-0.1136	0.0813	1306	22.164	0.130	3.374
0.2095	0.0762	0.4721	-0.0047	0.0808	886	17.864	0.213	2.950
0.2194	0.0785	0.5566	-0.0648	0.0832	1132	18.270	0.145	3.159
0.2544	0.0808	0.6054	-0.0160	0.0860	1082	20.701	0.325	3.227
0.3354	0.0854	0.6298	-0.1004	0.0936	1212	21.901	-0.255	3.375
0.4214	0.0901	0.6298	0.0910	0.0835	885	14.833	-0.373	3.468

Table A33: Experiment 9 Measurement Point 2

Average Velocity (m/s)	Depth (m)	Maximum Velocity (m/s)	Minimum Velocity (m/s)	Standard Deviation (m/s)	Number of Samples	Sampling Frequency (Hz)	3rd Moment Skew	Kurtosis
0.1542	0.0000	0.5416	-0.0892	0.0746	1524	22.388	0.526	4.490
0.2256	0.0046	0.4721	0.0066	0.0717	2500	53.187	0.135	2.909
0.2122	0.0092	0.4721	-0.0047	0.0699	2500	67.403	0.107	2.909
0.2107	0.0139	0.4721	-0.1136	0.0721	2500	79.519	0.149	2.978
0.2151	0.0185	0.4946	-0.0160	0.0757	2500	79.796	0.177	2.821
0.2149	0.0231	0.5416	-0.2412	0.0718	2500	77.728	0.105	3.561
0.2162	0.0277	0.7781	-0.0648	0.0739	2500	75.127	0.245	4.262
0.2184	0.0323	0.4946	0.0066	0.0732	2500	83.727	0.101	2.903
0.2166	0.0370	0.4477	-0.0648	0.0737	2500	84.087	0.037	3.081
0.2110	0.0416	0.4477	-0.0160	0.0704	2500	82.211	0.059	2.824
0.2128	0.0462	0.4721	-0.0291	0.0742	2500	76.107	0.183	2.816
0.2092	0.0508	0.4608	-0.0404	0.0741	2500	80.286	0.021	3.056
0.2048	0.0554	0.4364	-0.0047	0.0750	2500	76.862	0.073	2.808
0.2011	0.0601	0.4608	-0.0160	0.0780	2500	81.678	0.283	2.745
0.2151	0.0647	0.4946	-0.0047	0.0785	2500	75.654	0.190	2.957
0.2501	0.0693	0.5753	0.0066	0.0743	2500	82.182	-0.050	3.024
0.2658	0.0716	0.5303	0.0197	0.0755	2500	83.249	-0.099	2.968
0.2947	0.0739	0.5190	0.0310	0.0720	2500	78.804	-0.030	2.890
0.3121	0.0762	0.5528	0.0554	0.0713	2500	76.723	-0.063	3.092
0.3418	0.0785	0.6335	0.0798	0.0713	2500	78.948	0.073	3.106
0.3462	0.0808	0.5641	0.1398	0.0677	2500	88.003	0.018	2.710
0.3855	0.0854	0.5997	0.0554	0.0658	2500	88.744	-0.125	3.177
0.4109	0.0901	0.5997	0.1905	0.0631	2500	65.367	-0.314	3.234

Table A34: Experiment 9 Measurement Point 3

Average Velocity (m/s)	Depth (m)	Maximum Velocity (m/s)	Minimum Velocity (m/s)	Standard Deviation (m/s)	Number of Samples	Sampling Frequency (Hz)	3rd Moment Skew	Kurtosis
0.2752	0.0000	0.4608	0.0798	0.0596	2500	75.389	-0.160	2.886
0.3529	0.0046	0.4834	0.2018	0.0428	2500	126.756	-0.081	3.043
0.3463	0.0092	0.5059	0.1774	0.0454	2500	139.472	-0.201	3.334
0.3520	0.0139	0.5190	0.1530	0.0459	2500	138.566	-0.294	3.412
0.3595	0.0185	0.5641	0.1905	0.0482	2500	138.843	-0.066	3.033
0.3520	0.0231	0.5303	0.1905	0.0482	2500	150.577	0.010	2.997
0.3607	0.0277	0.5303	0.1905	0.0495	2500	143.140	-0.127	3.288
0.3535	0.0323	0.5641	0.1530	0.0528	2500	156.813	0.015	3.177
0.3666	0.0370	0.5641	0.1774	0.0493	2500	164.628	-0.305	3.315
0.3579	0.0416	0.5641	0.1774	0.0544	2500	154.292	-0.081	3.161
0.3604	0.0462	0.5190	0.1905	0.0503	2500	163.243	-0.062	2.939
0.3690	0.0508	0.5753	0.1905	0.0556	2500	150.398	-0.157	3.180
0.3814	0.0554	0.5885	0.1042	0.0574	2500	158.949	-0.083	3.303
0.3888	0.0601	0.5885	0.1286	0.0618	2500	156.365	-0.102	3.355
0.4076	0.0647	0.6335	0.1774	0.0571	2500	148.795	0.116	3.351
0.4312	0.0693	0.6448	0.2149	0.0566	2500	146.353	0.146	3.131
0.4438	0.0716	0.6448	0.1905	0.0584	2500	162.368	0.012	3.100
0.4490	0.0739	0.6335	0.2750	0.0564	2500	154.176	0.191	2.643
0.4564	0.0762	0.6448	0.2393	0.0550	2500	158.673	0.179	3.108
0.4646	0.0785	0.6692	0.2881	0.0589	2500	162.714	0.099	2.901
0.4724	0.0808	0.6805	0.3125	0.0552	2500	157.677	0.155	2.931
0.5107	0.0854	0.6805	0.3369	0.0505	2500	160.063	-0.112	2.922
0.5300	0.0901	0.7462	0.3125	0.0562	2500	114.965	-0.007	3.179

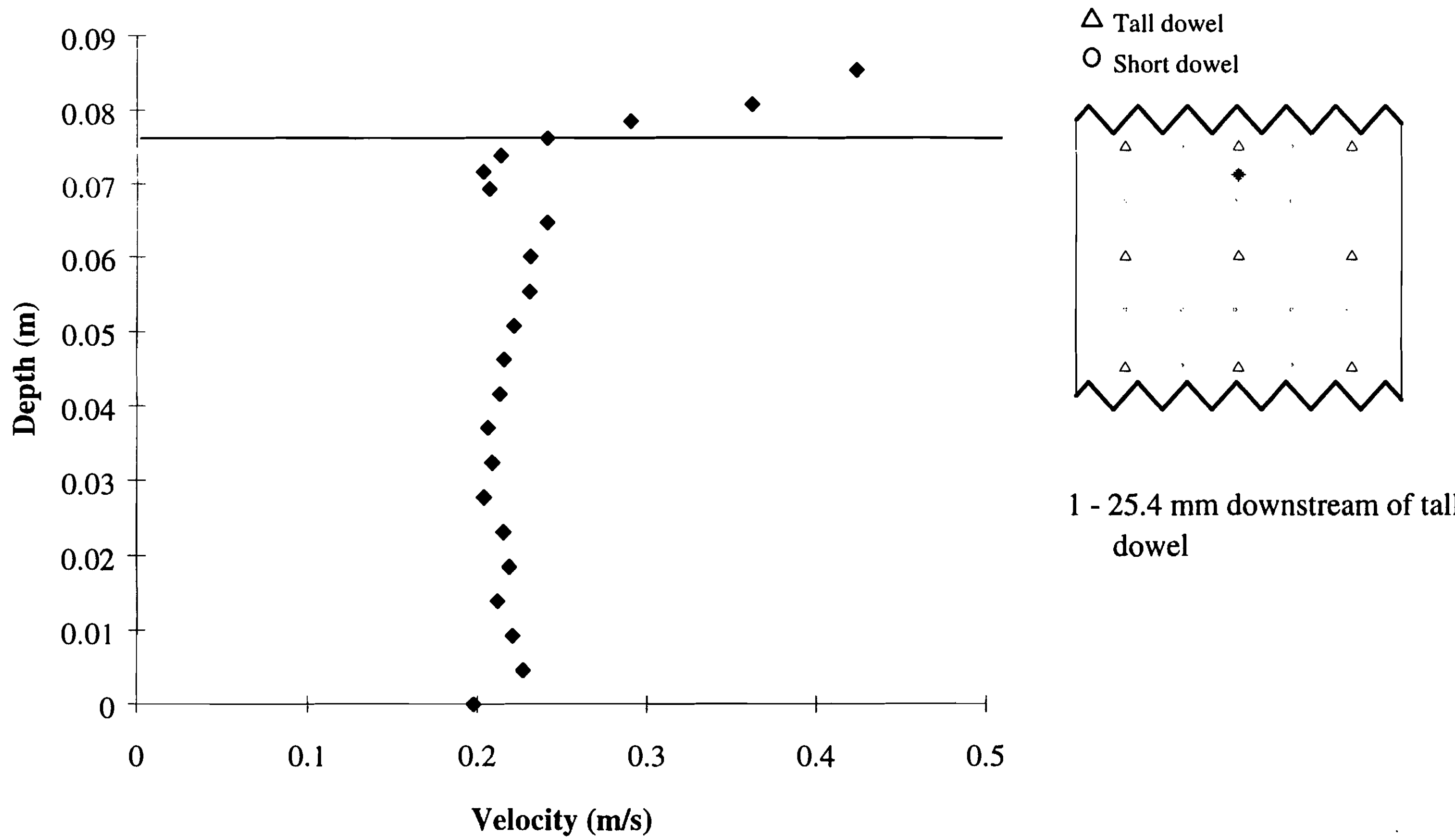

Figure A14: Profiles for Double-layered Experiment 10 (Linear s/d=8 Short, Linear s/d = 16 Tall)

Table A35: Experiment 10 Measurement Point 1

Average Velocity (m/s)	Depth (m)	Maximum Velocity (m/s)	Minimum Velocity (m/s)	Standard Deviation (m/s)	Number of Samples	Sampling Frequency (Hz)	3rd Moment Skew	Kurtosis
0.1976	0.0000	0.4364	-0.0217	0.0682	1120	14.680	0.351	3.260
0.2268	0.0046	0.5061	-0.2912	0.0758	1744	63.520	-0.117	4.364
0.2203	0.0092	0.7889	-0.0104	0.0749	2500	68.760	0.247	4.066
0.2117	0.0139	0.4722	-0.0217	0.0743	2500	73.842	0.105	2.809
0.2183	0.0185	0.4609	-0.5137	0.0764	2500	73.260	-0.324	5.946
0.2149	0.0231	0.6098	-0.0330	0.0769	2500	75.374	0.185	3.107
0.2036	0.0277	0.5175	-0.2083	0.0741	1736	74.802	0.000	3.519
0.2083	0.0323	0.4609	-0.0688	0.0764	2500	73.505	0.113	2.713
0.2058	0.0370	0.4722	-0.1367	0.0752	2500	76.683	-0.018	2.915
0.2126	0.0416	0.4477	-0.0688	0.0727	2500	69.430	0.004	2.858
0.2151	0.0462	0.5175	-0.0217	0.0702	2500	80.105	0.020	3.004
0.2211	0.0508	0.5307	-0.0801	0.0734	2500	85.905	0.090	3.420
0.2304	0.0554	0.4722	0.0236	0.0695	2500	83.056	0.022	2.962
0.2307	0.0601	0.4722	-0.0914	0.0736	2500	84.087	0.054	2.952
0.2406	0.0647	0.5759	-0.0104	0.0796	2500	82.206	0.070	2.933
0.2065	0.0693	0.5175	-0.0575	0.0772	2500	75.829	0.091	3.052
0.2029	0.0716	0.5420	-0.0575	0.0776	2500	80.406	0.202	3.018
0.2134	0.0739	0.5175	-0.0330	0.0823	2500	79.172	0.184	2.873
0.2407	0.0762	0.5307	-0.0104	0.0852	2500	79.731	0.151	2.845
0.2899	0.0785	0.5872	0.0009	0.0895	2500	82.576	-0.056	2.801
0.3618	0.0808	0.6230	-0.0217	0.0894	2500	82.577	-0.439	3.374
0.4234	0.0854	1.0472	0.0481	0.0792	2500	58.965	-0.140	5.280

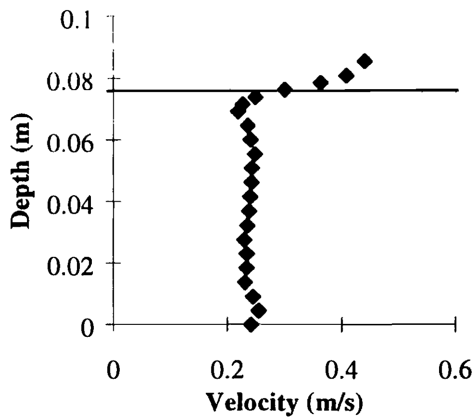

Measurement Point 1

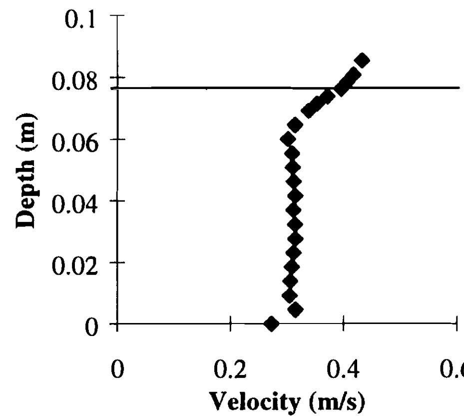

Measurement Point 2

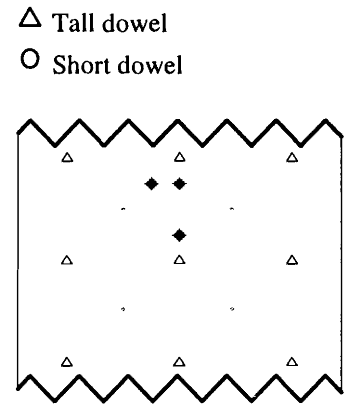

1 - 25.4 mm downstream of tall dowel
2 - 76.2 mm downstream of tall dowel
3 - 25.4 mm downstream of tall dowel, 25.4 mm left of CL

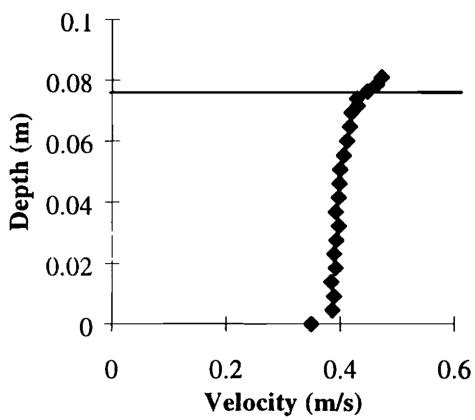

Measurement Point 3

Figure A15: Profiles for Double-layered Experiment 11 (Staggered s/d=8 Short, Linear s/d = 16 Tall)

Table A36: Experiment 11 Measurement Point 1

Average Velocity (m/s)	Depth (m)	Maximum Velocity (m/s)	Minimum Velocity (m/s)	Standard Deviation (m/s)	Number of Samples	Sampling Frequency (Hz)	3rd Moment Skew	Kurtosis
0.2409	0.0000	0.5190	0.0197	0.0765	207	3.470	0.325	3.876
0.2545	0.0046	0.5885	-0.1248	0.0772	1760	23.239	-0.058	3.503
0.2445	0.0092	0.4834	-0.0291	0.0712	1536	33.239	0.041	3.257
0.2304	0.0139	0.5190	0.0066	0.0771	1581	38.328	0.173	2.922
0.2329	0.0185	0.4834	-0.0160	0.0783	1673	50.900	0.105	3.059
0.2338	0.0231	0.5059	0.0197	0.0773	1710	65.635	0.095	2.843
0.2291	0.0277	0.5059	-0.0291	0.0791	2500	58.836	0.017	2.952
0.2347	0.0323	0.5059	-0.0291	0.0777	2500	71.297	0.032	3.000
0.2378	0.0370	0.5190	0.0066	0.0746	2500	71.972	0.005	2.986
0.2400	0.0416	0.4946	0.0066	0.0760	2500	48.768	-0.013	2.859
0.2422	0.0462	0.5059	-0.0047	0.0746	2500	68.184	-0.090	2.939
0.2427	0.0508	0.5641	-0.0047	0.0769	2500	62.509	0.079	3.267
0.2479	0.0554	0.5641	0.0197	0.0757	2500	77.612	0.027	3.204
0.2403	0.0601	0.5303	-0.1004	0.0764	2500	69.164	0.002	3.013
0.2351	0.0647	0.5753	-0.0291	0.0837	2500	51.179	-0.049	3.250
0.2182	0.0693	0.5416	-0.0779	0.0869	2500	64.690	0.045	2.936
0.2266	0.0716	0.5753	-0.0648	0.0898	2500	59.995	0.137	2.708
0.2485	0.0739	0.5303	-0.0779	0.0940	2500	66.802	-0.053	2.645
0.3000	0.0762	0.6335	-0.1136	0.0996	2500	63.286	-0.202	2.988
0.3631	0.0785	0.6805	0.0197	0.0918	2500	80.072	-0.489	3.313
0.4084	0.0808	0.6561	0.0554	0.0835	2500	59.899	-0.587	3.492
0.4411	0.0854	1.2267	0.1042	0.0830	2475	16.500	0.495	10.314

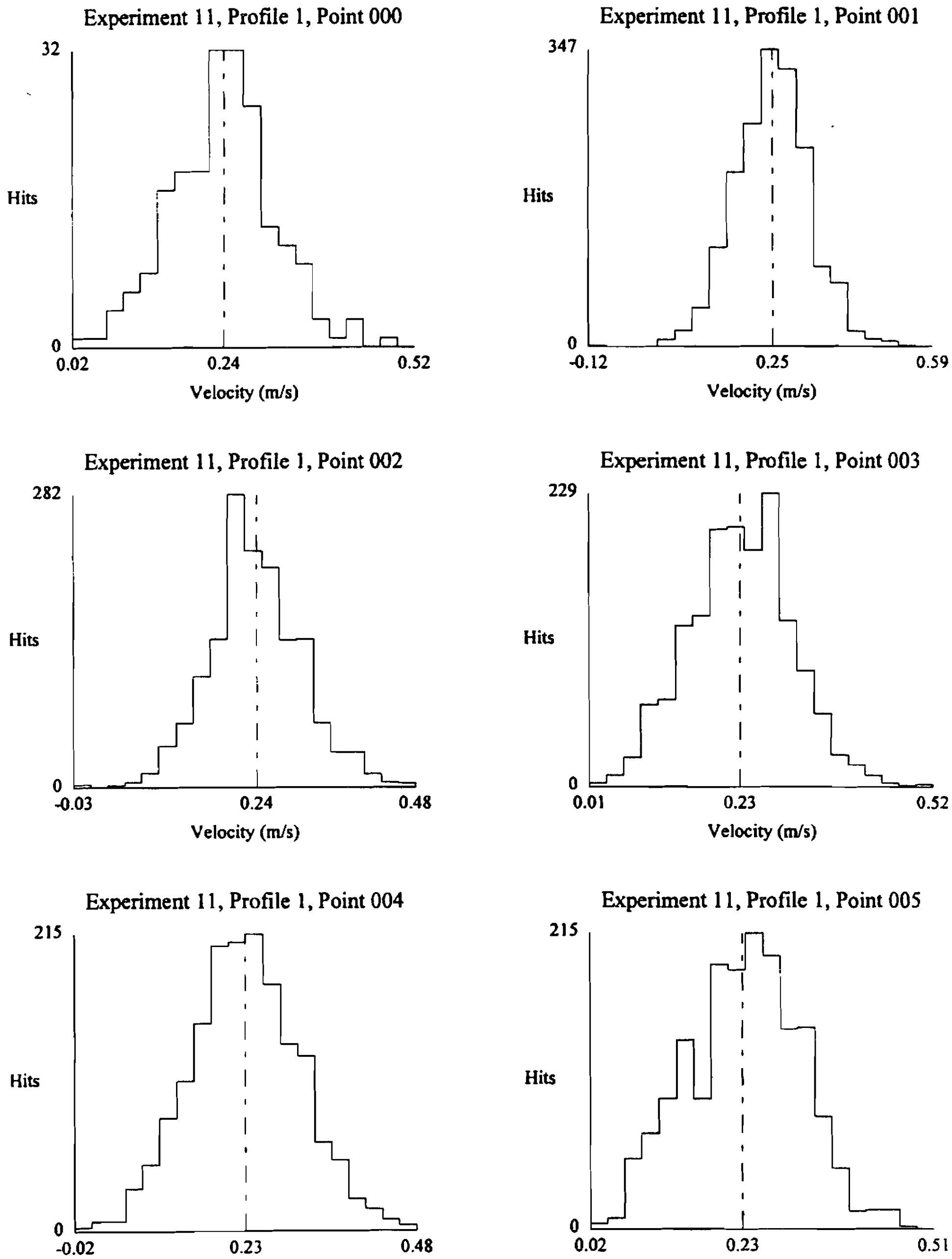

Figure A16: Histograms for Experiment 11 (Staggered s/d=8 Short, Linear s/d=16 Tall), Profile 1

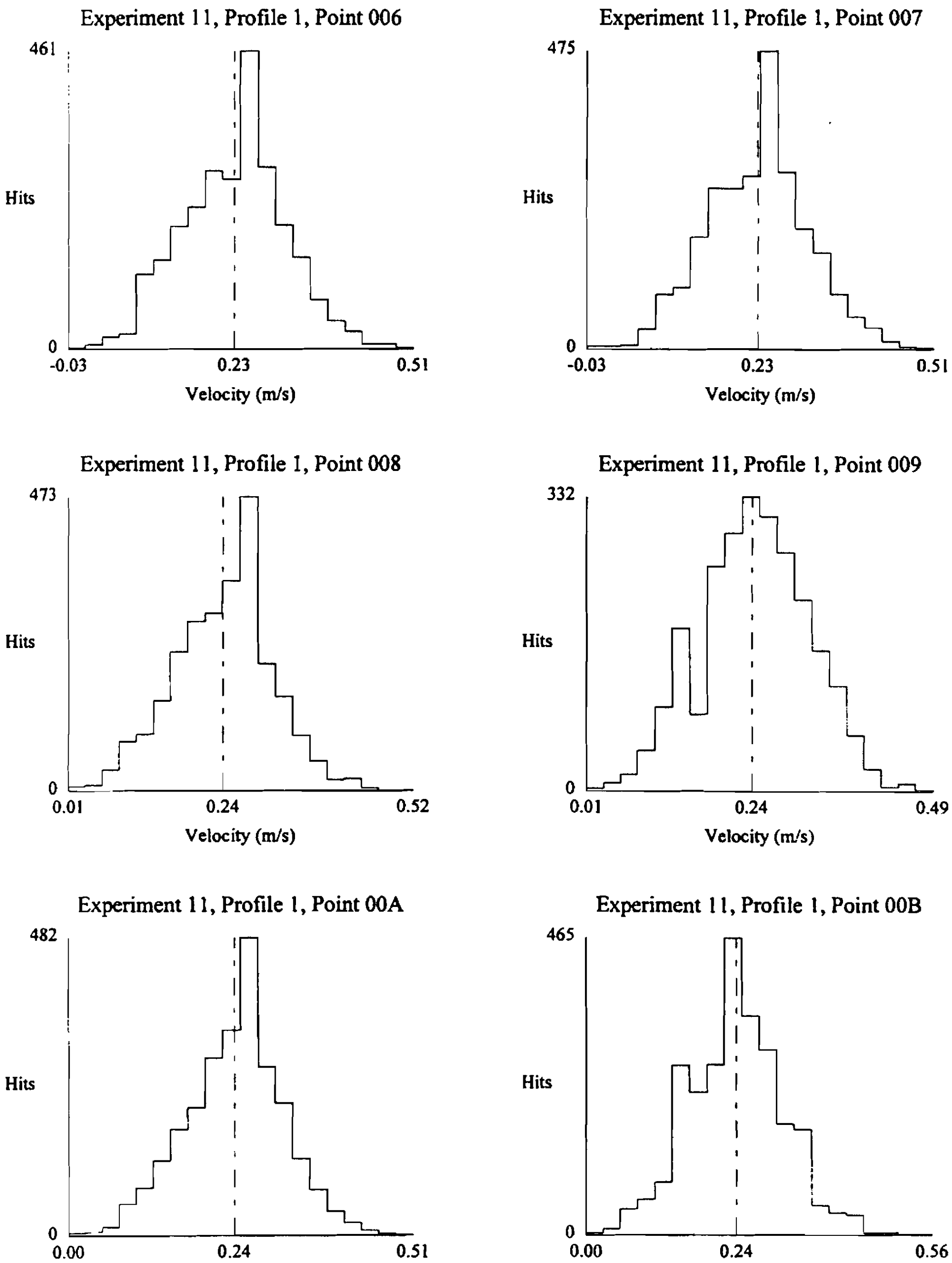

Figure A16 continued....

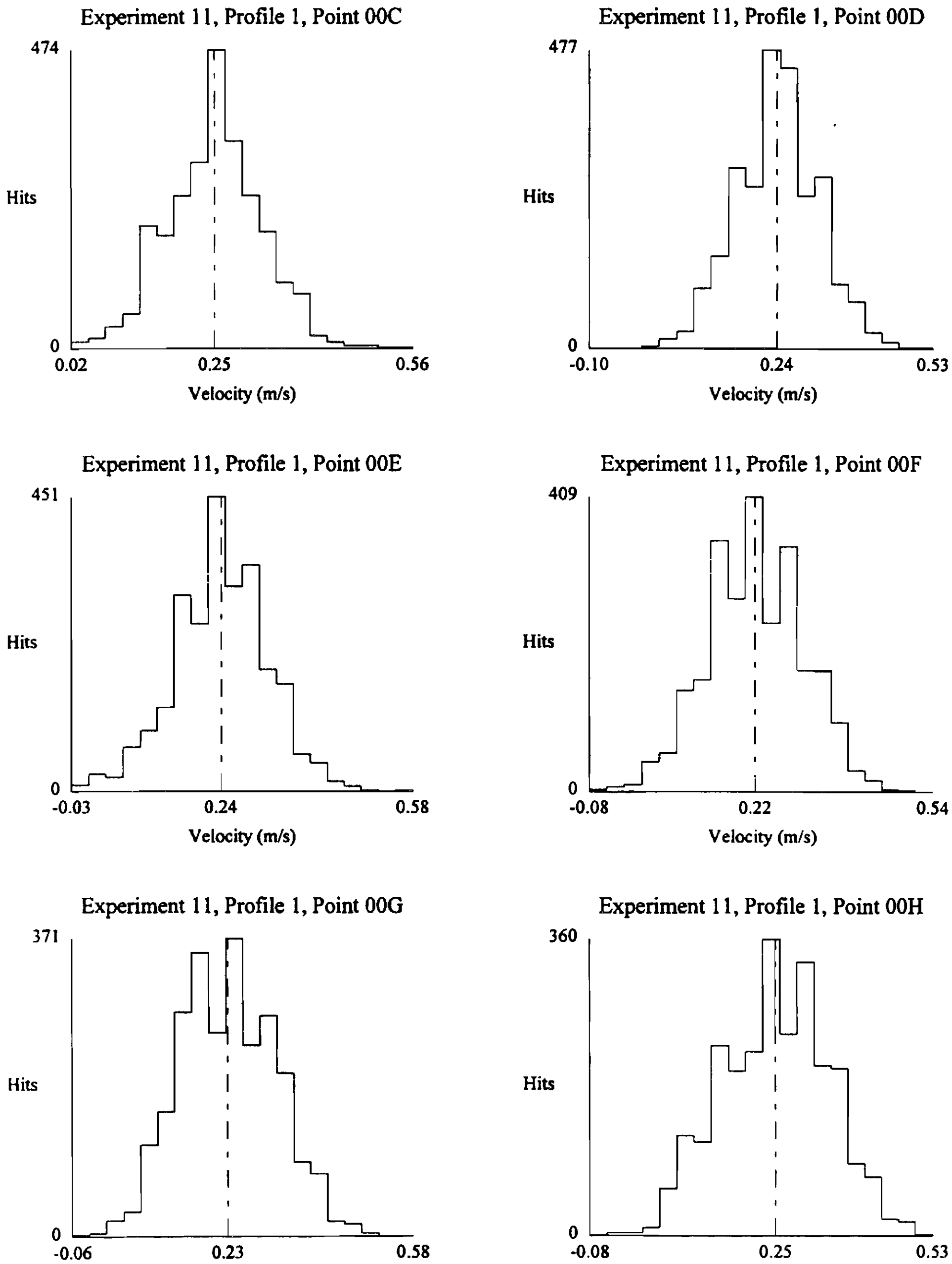

Figure A16 continued....

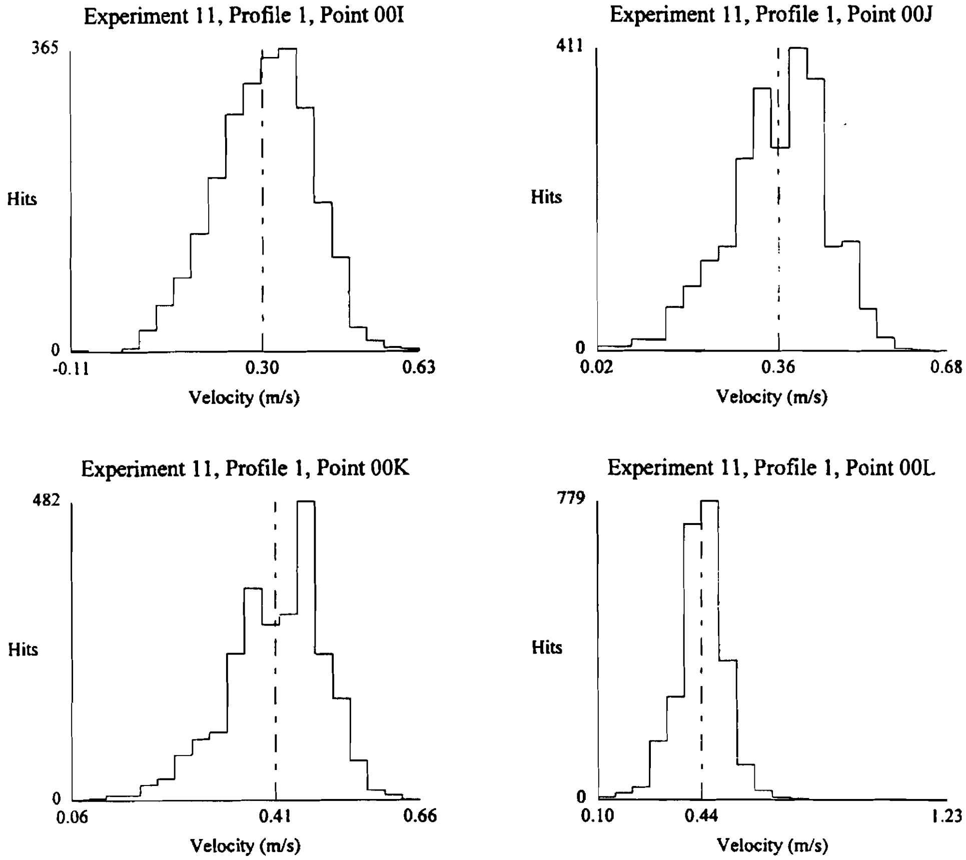

Figure A16 continued....

Table A37: Experiment 11 Measurement Point 2

Average Velocity (m/s)	Depth (m)	Maximum Velocity (m/s)	Minimum Velocity (m/s)	Standard Deviation (m/s)	Number of Samples	Sampling Frequency (Hz)	3rd Moment Skew	Kurtosis
0.2724	0.0000	0.4232	0.1404	0.0528	254	5.137	0.136	2.990
0.3152	0.0046	0.4835	0.1404	0.0557	3232	161.563	0.006	2.593
0.3049	0.0092	0.5307	0.1159	0.0576	4024	201.188	0.047	2.654
0.3060	0.0139	0.4948	0.0669	0.0576	4087	204.310	0.036	2.821
0.3089	0.0185	0.5175	0.1046	0.0550	3856	192.730	0.057	2.857
0.3113	0.0231	0.5061	0.1536	0.0579	3652	182.575	0.071	2.687
0.3149	0.0277	0.4948	0.1404	0.0574	3607	180.346	0.023	2.670
0.3142	0.0323	0.5175	0.1291	0.0571	4046	202.296	0.020	2.754
0.3114	0.0370	0.4948	0.1046	0.0587	3944	197.183	0.022	2.708
0.3150	0.0416	0.5061	0.1159	0.0576	3572	178.587	-0.010	2.949
0.3123	0.0462	0.4722	0.1291	0.0552	3630	181.484	-0.045	2.720
0.3103	0.0508	0.4835	0.1291	0.0590	3850	192.375	-0.025	2.654
0.3093	0.0554	0.5061	0.1536	0.0565	3822	191.080	0.147	2.854
0.3019	0.0601	0.5061	0.1404	0.0562	3600	179.912	0.201	2.793
0.3143	0.0647	0.4948	0.1404	0.0580	3821	191.025	0.037	2.666
0.3386	0.0693	0.5061	0.1291	0.0581	3181	159.027	-0.134	2.654
0.3536	0.0716	0.5307	0.1649	0.0593	3532	176.552	-0.265	2.769
0.3717	0.0739	0.5985	0.1781	0.0578	3925	196.215	-0.148	2.827
0.3954	0.0762	0.5759	0.1781	0.0556	3715	185.733	-0.336	3.050
0.4069	0.0785	0.5646	0.2026	0.0521	3469	173.446	-0.279	3.085
0.4179	0.0808	0.5759	0.2385	0.0507	2378	118.880	-0.379	3.058
0.4329	0.0854	0.4722	0.3629	0.0333	16	0.772	-0.527	1.963

Table A38: Experiment 11 Measurement Point 3

Average Velocity (m/s)	Depth (m)	Maximum Velocity (m/s)	Minimum Velocity (m/s)	Standard Deviation (m/s)	Number of Samples	Sampling Frequency (Hz)	3rd Moment Skew	Kurtosis
0.3483	0.0000	0.4722	0.1649	0.0485	263	13.139	-0.498	3.840
0.3857	0.0046	0.5061	0.2026	0.0410	2813	140.567	-0.492	3.447
0.3888	0.0092	0.5175	0.2026	0.0436	3478	173.847	-0.448	3.411
0.3836	0.0139	0.5307	0.2140	0.0441	3400	169.970	-0.366	3.222
0.3911	0.0185	0.5420	0.2385	0.0441	4339	216.929	-0.146	2.948
0.3885	0.0231	0.5175	0.2272	0.0410	4195	209.695	-0.313	3.300
0.3927	0.0277	0.5175	0.1781	0.0430	4125	206.231	-0.232	3.066
0.3968	0.0323	0.5175	0.2272	0.0416	4968	248.368	-0.202	3.140
0.3913	0.0370	0.5307	0.2026	0.0422	5305	265.247	-0.345	3.586
0.3963	0.0416	0.5061	0.2385	0.0421	4246	212.274	-0.319	3.070
0.3969	0.0462	0.5646	0.2026	0.0438	5321	266.038	-0.044	3.476
0.3981	0.0508	0.5646	0.2272	0.0427	5215	260.746	-0.066	3.491
0.4045	0.0554	0.5872	0.1895	0.0463	5481	274.043	0.028	3.313
0.4097	0.0601	0.5872	0.2517	0.0447	5218	260.822	0.131	3.432
0.4150	0.0647	0.5646	0.2026	0.0451	4744	237.179	0.061	3.255
0.4179	0.0693	0.5759	0.2272	0.0450	4851	242.512	-0.105	3.406
0.4284	0.0716	0.6098	0.2517	0.0476	5011	250.524	0.088	3.037
0.4276	0.0739	0.6230	0.2517	0.0506	5147	257.342	0.059	2.987
0.4462	0.0762	0.5985	0.2630	0.0477	5001	250.045	0.010	2.771
0.4623	0.0785	0.6098	0.2272	0.0488	5307	265.335	-0.138	3.168
0.4708	0.0808	0.6098	0.2875	0.0469	4293	214.627	-0.089	2.945

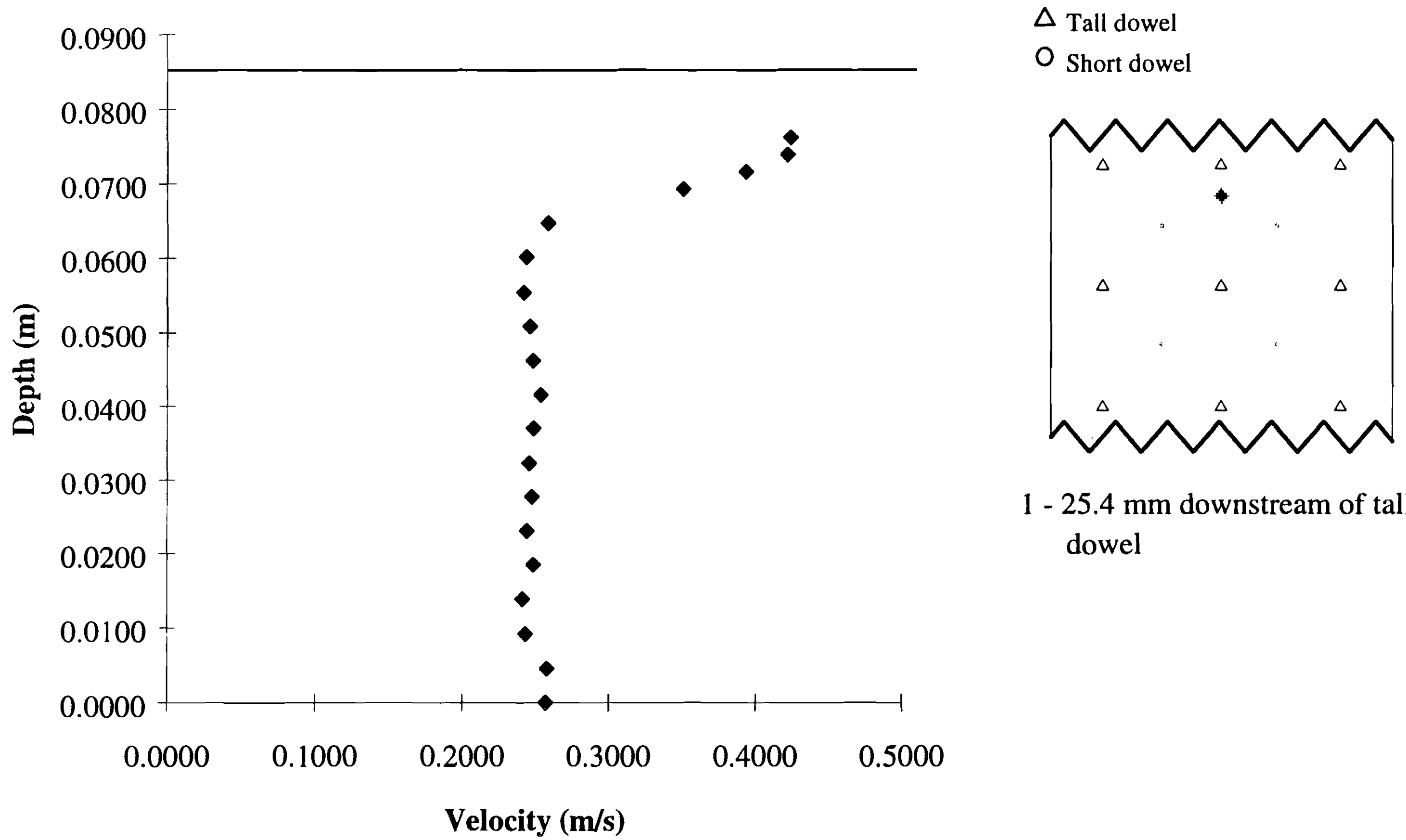

Figure A17: Profiles for Double-layered Experiment 12 (Staggered s/d=8 Short, Linear s/d = 16 Tall)

Table A39: Experiment 12 Measurement Point 1

Average Velocity (m/s)	Depth (m)	Maximum Velocity (m/s)	Minimum Velocity (m/s)	Standard Deviation (m/s)	Number of Samples	Sampling Frequency (Hz)	3rd Moment Skew	Kurtosis
0.2570	0.0000	0.5061	0.0311	0.0807	264	13.191	0.598	3.862
0.2578	0.0046	0.5307	0.0066	0.0800	1412	70.546	-0.164	2.928
0.2430	0.0092	0.5307	-0.0160	0.0812	2193	109.635	0.148	3.107
0.2410	0.0139	0.5307	0.0066	0.0823	2078	103.887	0.114	2.859
0.2484	0.0185	0.5872	0.0066	0.0816	2672	133.548	0.069	2.929
0.2441	0.0231	0.5533	-0.0537	0.0813	2582	129.075	0.003	3.058
0.2472	0.0277	0.5307	-0.0537	0.0811	3066	153.297	-0.055	3.006
0.2458	0.0323	0.5420	-0.0537	0.0821	3456	172.778	0.090	3.027
0.2486	0.0370	0.5646	-0.0650	0.0778	3570	178.423	-0.039	2.941
0.2532	0.0416	0.5872	0.0066	0.0758	3535	176.699	-0.142	3.178
0.2482	0.0462	0.4948	-0.0047	0.0801	3482	174.098	-0.170	2.768
0.2461	0.0508	0.5061	-0.0763	0.0781	3534	176.698	-0.117	3.005
0.2417	0.0554	0.5175	-0.0405	0.0817	3634	181.662	-0.124	2.774
0.2433	0.0601	0.5307	-0.0650	0.0905	3388	169.397	-0.183	2.668
0.2584	0.0647	0.5061	-0.0292	0.0905	3069	153.388	-0.222	2.531
0.3504	0.0693	0.5759	0.0066	0.0806	3383	169.138	-0.792	3.675
0.3934	0.0716	0.6230	0.0198	0.0620	3311	165.528	-0.900	5.078
0.4218	0.0739	0.6098	0.1291	0.0543	2450	122.388	-0.791	5.166
0.4240	0.0762	0.7682	0.2026	0.0582	659	32.943	0.312	6.495

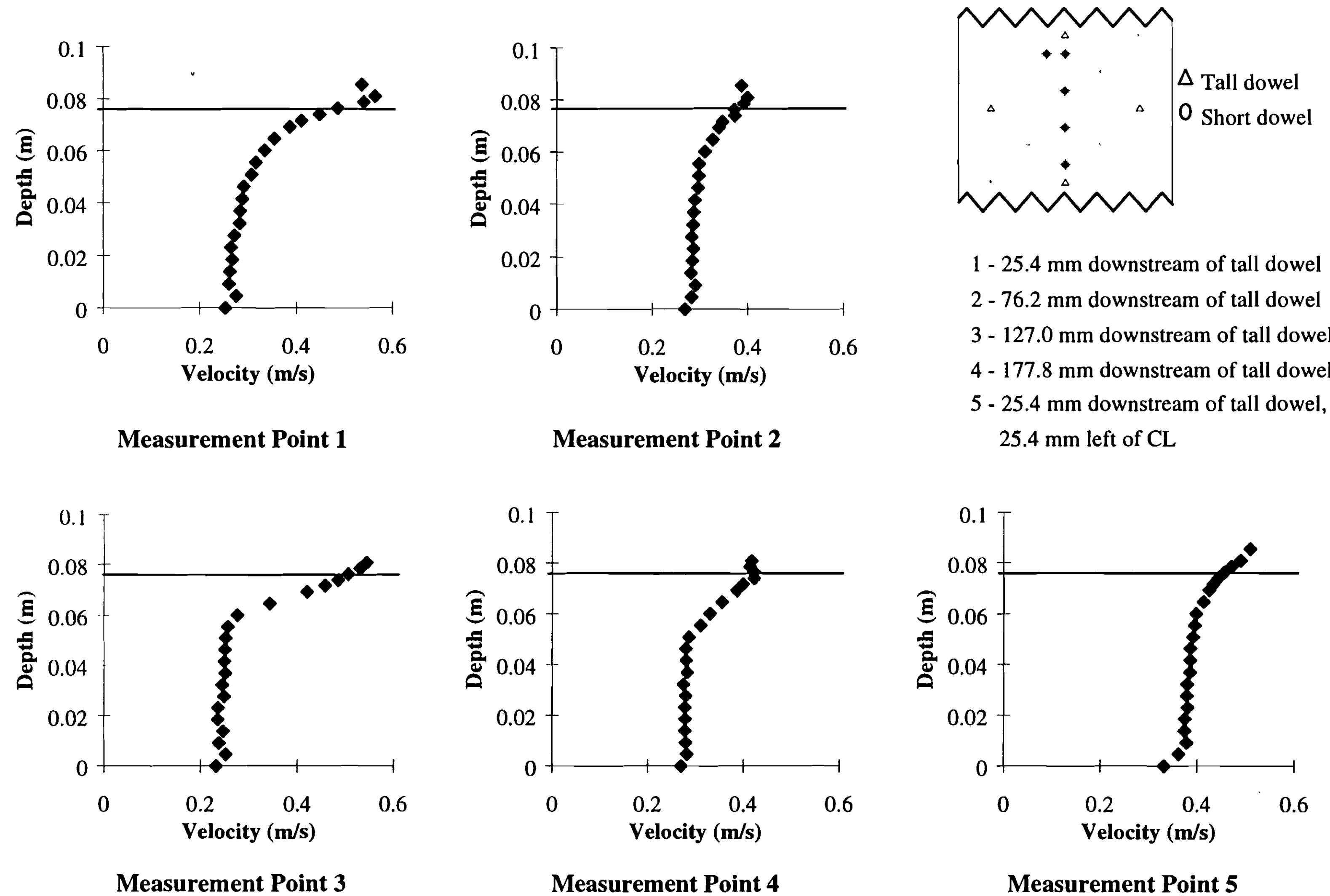

Figure A18: Profiles for Double-layered Experiment 13 (Staggered s/d=8 Short, Staggered s/d = 16 Tall)

Table A40: Experiment 13 Measurement Point 1

Average Velocity (m/s)	Depth (m)	Maximum Velocity (m/s)	Minimum Velocity (m/s)	Standard Deviation (m/s)	Number of Samples	Sampling Frequency (Hz)	3rd Moment Skew	Kurtosis
0.2524	0.0000	0.4835	0.0198	0.0735	549	27.431	-0.078	3.027
0.2750	0.0046	0.5872	0.0066	0.0769	4596	229.777	-0.164	3.169
0.2600	0.0092	0.5420	-0.0160	0.0775	5042	252.063	-0.166	2.865
0.2616	0.0139	0.5420	-0.0405	0.0799	5261	263.031	-0.110	3.024
0.2668	0.0185	0.5175	-0.0160	0.0779	5337	266.820	-0.248	3.086
0.2638	0.0231	0.5061	-0.0160	0.0780	5235	261.725	-0.205	2.964
0.2710	0.0277	0.5061	0.0066	0.0744	5523	276.128	-0.295	3.027
0.2818	0.0323	0.5533	0.0066	0.0744	5596	279.780	-0.321	3.162
0.2832	0.0370	0.5175	-0.0047	0.0754	5542	277.070	-0.319	3.141
0.2877	0.0416	0.5420	-0.0537	0.0759	5442	272.075	-0.290	3.156
0.2902	0.0462	0.5175	0.0198	0.0720	5374	268.691	-0.379	2.997
0.3064	0.0508	0.5872	-0.1009	0.0737	4760	237.983	-0.379	3.475
0.3160	0.0554	0.6098	-0.0650	0.0776	5400	269.997	-0.324	3.530
0.3343	0.0601	0.6343	-0.0047	0.0846	5495	274.748	-0.448	3.394
0.3535	0.0647	0.6230	0.0198	0.0919	5631	281.498	-0.642	3.227
0.3861	0.0693	0.6796	-0.0650	0.1018	5266	263.277	-0.722	3.358
0.4102	0.0716	0.7154	-0.0292	0.0969	5712	285.567	-0.928	3.989
0.4478	0.0739	0.6796	0.0556	0.0834	5728	286.380	-1.199	5.212
0.4859	0.0762	0.7474	0.0198	0.0759	5689	284.411	-1.658	7.671
0.5408	0.0785	0.7361	0.1649	0.0519	6017	300.831	-1.228	8.005
0.5641	0.0808	1.2847	0.1291	0.0552	5209	260.420	0.357	13.978
0.5356	0.0854	1.1282	-0.1254	0.1260	145	6.886	-0.598	10.696

Table A41: Experiment 13 Measurement Point 2

Average Velocity (m/s)	Depth (m)	Maximum Velocity (m/s)	Minimum Velocity (m/s)	Standard Deviation (m/s)	Number of Samples	Sampling Frequency (Hz)	3rd Moment Skew	Kurtosis
0.2683	0.0000	0.3987	0.1536	0.0560	47	2.332	-0.008	2.744
0.2820	0.0046	0.4477	0.0914	0.0521	3460	172.963	0.085	2.774
0.2896	0.0092	0.4722	0.0801	0.0526	4490	224.413	0.015	2.924
0.2806	0.0139	0.4477	0.1291	0.0507	4902	245.041	0.186	2.816
0.2834	0.0185	0.4477	0.0198	0.0500	4953	247.625	0.061	2.950
0.2857	0.0231	0.4722	0.1046	0.0531	5191	259.539	0.260	2.886
0.2826	0.0277	0.4722	0.1046	0.0534	5332	266.598	0.005	2.810
0.2852	0.0323	0.4948	0.1046	0.0519	5326	266.295	0.091	2.902
0.2867	0.0370	0.4948	0.0669	0.0554	5477	273.820	0.085	2.936
0.2889	0.0416	0.4722	0.1291	0.0552	5492	274.570	0.019	2.562
0.2954	0.0462	0.5061	0.1159	0.0558	5410	270.488	0.173	2.881
0.2980	0.0508	0.5533	0.0801	0.0561	5310	264.977	0.153	3.235
0.2985	0.0554	0.5420	0.1159	0.0586	5542	277.095	0.197	2.999
0.3100	0.0601	0.5061	0.1159	0.0586	5644	282.196	0.054	2.763
0.3268	0.0647	0.5759	0.1291	0.0649	5622	281.079	0.188	2.778
0.3398	0.0693	0.5533	0.1159	0.0679	5602	280.057	0.046	2.672
0.3471	0.0716	0.6683	0.1536	0.0680	5513	275.622	-0.037	2.688
0.3723	0.0739	0.5985	0.1291	0.0705	5654	282.687	-0.217	2.821
0.3719	0.0762	0.6098	0.1291	0.0705	5449	272.423	-0.165	2.685
0.3919	0.0785	0.5872	0.1404	0.0671	5820	290.986	-0.341	2.843
0.3992	0.0808	0.6098	0.1159	0.0636	5096	254.774	-0.389	3.156
0.3871	0.0854	0.5175	0.2385	0.0588	138	6.616	-0.453	2.868

Table A42: Experiment 13 Measurement Point 3

Average Velocity (m/s)	Depth (m)	Maximum Velocity (m/s)	Minimum Velocity (m/s)	Standard Deviation (m/s)	Number of Samples	Sampling Frequency (Hz)	3rd Moment Skew	Kurtosis
0.2318	0.0000	0.4477	0.0669	0.0754	84	4.031	0.254	2.676
0.2517	0.0046	0.5759	-0.0047	0.0768	2638	131.852	-0.181	3.239
0.2373	0.0092	0.5533	-0.0160	0.0779	3644	182.085	0.019	2.994
0.2461	0.0139	0.5175	-0.0650	0.0812	2670	133.458	-0.051	3.028
0.2354	0.0185	0.5759	-0.0537	0.0837	4178	208.874	-0.025	2.942
0.2360	0.0231	0.4948	-0.0292	0.0768	4633	231.604	-0.030	2.841
0.2481	0.0277	0.5175	-0.0650	0.0784	4363	218.062	-0.025	3.094
0.2444	0.0323	0.5307	0.0066	0.0768	4949	247.408	-0.019	3.000
0.2507	0.0370	0.4948	-0.0292	0.0758	5312	265.580	-0.117	3.107
0.2487	0.0416	0.6230	-0.0160	0.0770	5183	259.119	-0.003	3.353
0.2498	0.0462	0.5646	-0.0160	0.0771	5484	274.169	-0.039	3.077
0.2513	0.0508	0.5533	-0.0405	0.0831	5260	262.969	0.009	2.936
0.2555	0.0554	0.5307	-0.0292	0.0819	5388	269.381	-0.080	2.735
0.2759	0.0601	0.5307	-0.1009	0.0859	5059	252.948	-0.262	2.984
0.3418	0.0647	0.5872	-0.1009	0.0795	5151	257.522	-0.669	3.768
0.4202	0.0693	0.6230	0.1159	0.0636	5379	268.932	-0.854	4.495
0.4576	0.0716	0.6098	0.1536	0.0524	5546	277.258	-0.721	4.702
0.4850	0.0739	0.6456	0.2140	0.0450	5566	278.204	-0.298	3.427
0.5058	0.0762	0.6909	0.3252	0.0455	5720	285.988	-0.260	3.287
0.5304	0.0785	0.7022	0.3252	0.0397	5536	276.783	-0.119	3.415
0.5442	0.0808	0.7361	0.3742	0.0434	3404	168.903	0.025	3.220

Table A43: Experiment 13 Measurement Point 4

Average Velocity (m/s)	Depth (m)	Maximum Velocity (m/s)	Minimum Velocity (m/s)	Standard Deviation (m/s)	Number of Samples	Sampling Frequency (Hz)	3rd Moment Skew	Kurtosis
0.2691	0.0000	0.4477	0.1291	0.0503	690	34.438	0.223	3.017
0.2817	0.0046	0.4835	0.0914	0.0500	4810	240.419	0.054	2.994
0.2795	0.0092	0.4722	0.1046	0.0525	5758	287.888	0.070	2.913
0.2778	0.0139	0.4722	0.1046	0.0533	5658	282.869	0.140	2.926
0.2779	0.0185	0.4835	0.1046	0.0518	5553	277.649	0.147	2.891
0.2773	0.0231	0.4948	0.0914	0.0536	5527	276.325	0.154	3.097
0.2787	0.0277	0.4722	0.1159	0.0538	5498	274.836	0.159	2.621
0.2745	0.0323	0.4722	0.1046	0.0529	5604	280.200	0.065	2.765
0.2820	0.0370	0.4948	0.1159	0.0530	4380	218.976	0.161	2.817
0.2798	0.0416	0.4722	0.1046	0.0541	5131	256.524	0.121	2.849
0.2794	0.0462	0.4722	0.0556	0.0536	5411	270.527	0.206	2.869
0.2863	0.0508	0.5175	0.1046	0.0576	5434	271.670	0.238	3.031
0.3098	0.0554	0.5420	0.0914	0.0665	5302	265.047	0.204	2.804
0.3289	0.0601	0.5533	0.0914	0.0719	5547	277.331	0.168	2.647
0.3552	0.0647	0.5985	0.1291	0.0687	5899	294.903	-0.093	2.977
0.3862	0.0693	0.5533	0.1536	0.0621	5887	294.269	-0.300	2.844
0.3993	0.0716	0.5646	0.2026	0.0561	5897	294.842	-0.208	2.804
0.4215	0.0739	0.6098	0.2026	0.0563	5940	296.984	-0.234	3.318
0.4222	0.0762	0.5872	0.1536	0.0533	5748	287.369	-0.417	3.538
0.4133	0.0785	0.5872	0.2026	0.0506	5431	271.527	-0.207	3.268
0.4163	0.0808	0.5759	0.2385	0.0513	3160	157.976	0.025	3.015

Table A44: Experiment 13 Measurement Point 5

Average Velocity (m/s)	Depth (m)	Maximum Velocity (m/s)	Minimum Velocity (m/s)	Standard Deviation (m/s)	Number of Samples	Sampling Frequency (Hz)	3rd Moment Skew	Kurtosis
0.3319	0.0000	0.4609	0.2140	0.0520	33	1.609	0.048	2.829
0.3616	0.0046	0.4835	0.2026	0.0406	5607	280.338	-0.242	2.991
0.3778	0.0092	0.5061	0.2026	0.0405	6178	308.888	-0.303	3.073
0.3741	0.0139	0.5175	0.2140	0.0401	6585	329.206	-0.087	3.136
0.3740	0.0185	0.5061	0.2272	0.0392	6390	319.476	-0.308	3.171
0.3805	0.0231	0.5307	0.2385	0.0399	6550	327.475	-0.071	3.225
0.3790	0.0277	0.4948	0.2272	0.0399	6517	325.769	-0.096	2.886
0.3799	0.0323	0.4948	0.2026	0.0402	6817	340.792	-0.340	3.295
0.3854	0.0370	0.5420	0.1781	0.0405	6964	348.146	-0.234	3.071
0.3861	0.0416	0.5175	0.2272	0.0411	6840	341.990	-0.074	3.038
0.3861	0.0462	0.5533	0.2026	0.0441	6452	322.565	0.050	3.143
0.3917	0.0508	0.5646	0.2385	0.0411	6600	329.948	-0.094	3.428
0.3947	0.0554	0.5759	0.2385	0.0438	6734	336.638	-0.107	3.270
0.3978	0.0601	0.5985	0.2385	0.0449	6938	346.876	0.103	3.320
0.4132	0.0647	0.5872	0.2630	0.0448	6908	345.396	0.185	3.346
0.4251	0.0693	0.6456	0.2762	0.0481	6764	338.155	0.381	3.496
0.4336	0.0716	0.5985	0.2630	0.0492	6756	337.752	0.118	2.964
0.4429	0.0739	0.6098	0.2762	0.0498	6735	336.714	0.072	2.792
0.4561	0.0762	0.6230	0.2875	0.0503	6819	340.880	0.022	2.836
0.4705	0.0785	0.6456	0.2762	0.0558	6979	348.935	0.087	2.682
0.4894	0.0808	0.6909	0.3120	0.0597	6840	341.954	0.245	2.590
0.5084	0.0854	1.0371	0.3613	0.0541	485	24.150	1.964	20.377

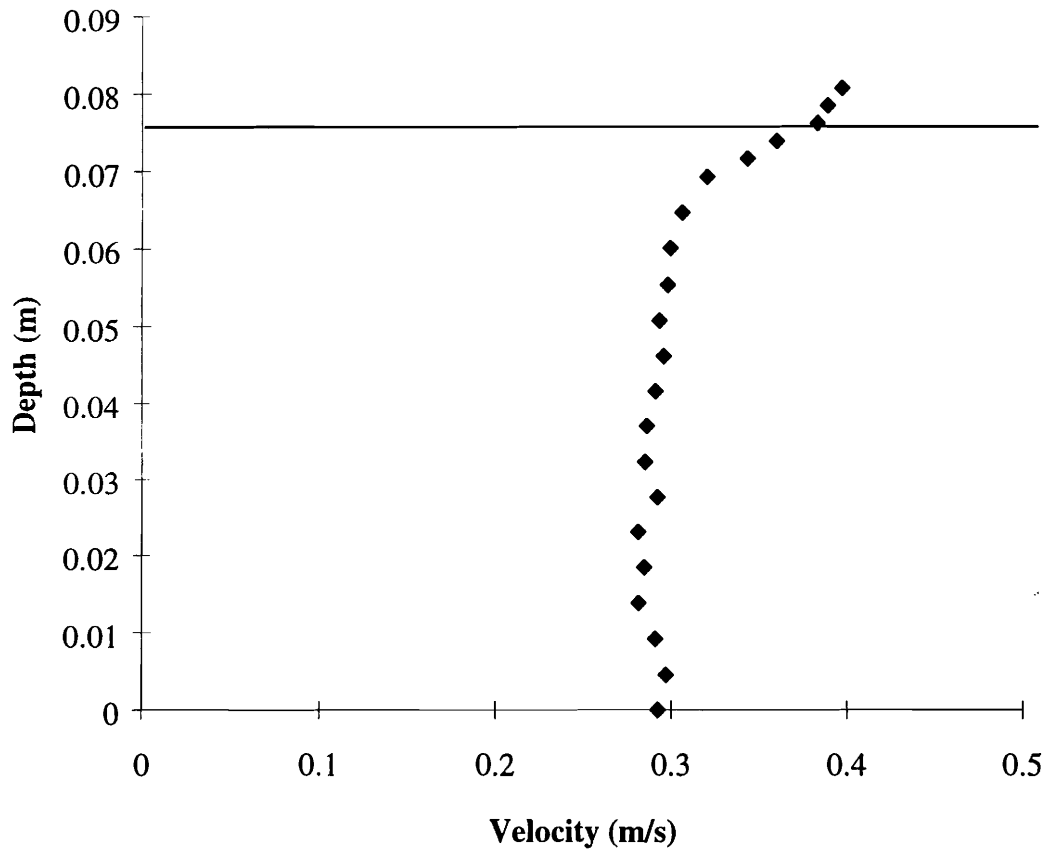

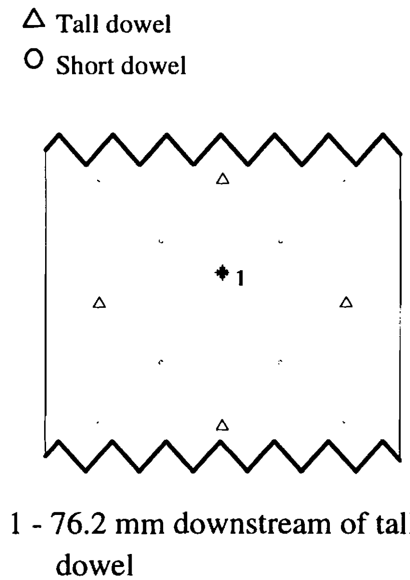

Figure A19: Profiles for Double-layered Experiment 14 (Staggered s/d=8 Short, Staggered s/d = 16 Tall)

Table A45: Experiment 14 Measurement Point 1

Average Velocity (m/s)	Depth (m)	Maximum Velocity (m/s)	Minimum Velocity (m/s)	Standard Deviation (m/s)	Number of Samples	Sampling Frequency (Hz)	3rd Moment Skew	Kurtosis
0.2921	0.0000	0.3857	0.2393	0.0491	10	0.487	0.396	1.804
0.2969	0.0046	0.4946	0.1042	0.0550	3901	195.018	0.230	3.024
0.2907	0.0092	0.4721	0.1154	0.0543	4763	238.138	-0.014	2.841
0.2812	0.0139	0.4608	0.1042	0.0553	5279	263.899	-0.010	2.754
0.2843	0.0185	0.4834	0.0910	0.0536	5620	280.925	0.154	2.870
0.2810	0.0231	0.4608	0.1042	0.0539	5385	269.235	0.087	2.775
0.2918	0.0277	0.4946	0.1286	0.0552	5360	267.973	0.133	2.825
0.2849	0.0323	0.4608	0.0910	0.0538	5715	285.744	-0.010	2.672
0.2859	0.0370	0.4946	0.1286	0.0526	5781	289.007	0.140	2.872
0.2905	0.0416	0.5059	0.1042	0.0539	5763	288.140	0.050	2.706
0.2953	0.0462	0.4946	0.1286	0.0549	5481	274.023	0.063	2.929
0.2929	0.0508	0.4721	0.1154	0.0558	5311	265.525	0.019	2.699
0.2975	0.0554	0.5190	0.0910	0.0579	5490	274.500	-0.049	2.772
0.2987	0.0601	0.4834	0.0685	0.0561	5817	290.829	0.023	2.769
0.3059	0.0647	0.5641	0.1042	0.0575	5775	288.714	0.005	2.890
0.3198	0.0693	0.4946	0.0910	0.0625	5453	272.622	-0.167	2.768
0.3427	0.0716	0.5753	0.1154	0.0643	5939	296.922	-0.240	2.694
0.3597	0.0739	0.5753	0.1154	0.0620	5888	294.373	-0.266	2.831
0.3827	0.0762	0.5753	0.1398	0.0581	5612	280.592	-0.317	3.106
0.3883	0.0785	0.5753	0.1530	0.0547	4356	217.684	-0.324	3.258
0.3966	0.0808	0.5303	0.2262	0.0511	921	46.044	-0.301	2.723

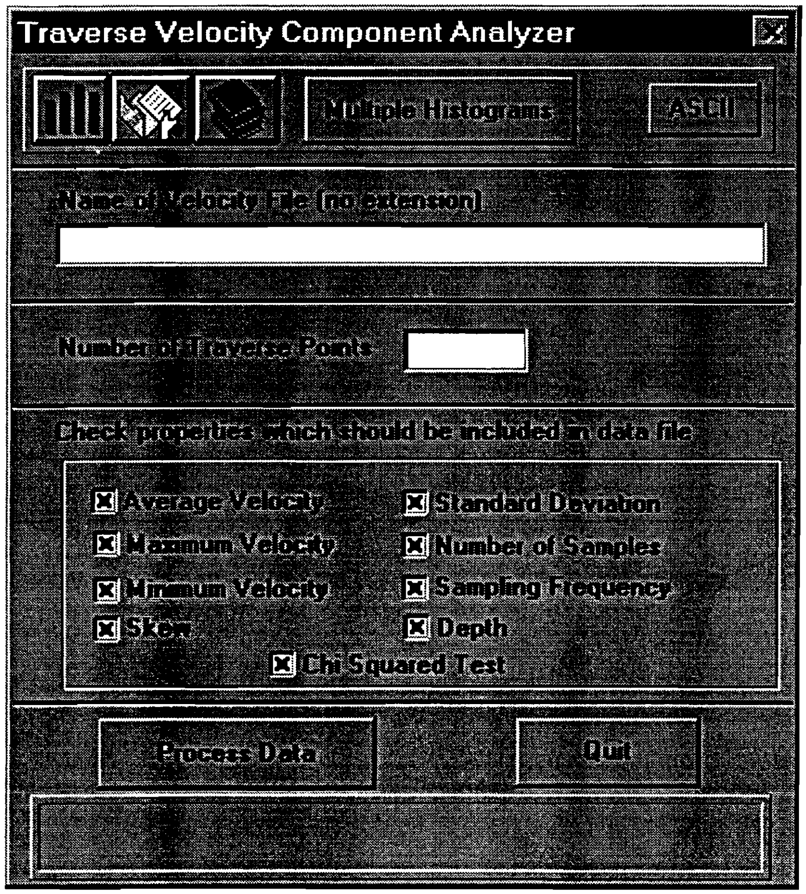

Figure A20: User Dialog Box for Data Processing Software

The dialog box pictured above is the interactive mechanism for the user to process data for experiments. All program code related to the calculations checked in the dialog box above is shown on the following pages.

```
Sub Command3D3_Click ()
Static STAT As Single
Static AT As Single
Static TT As Single
Static UVEL As Single
Static Prefix As Single
Static DataRate As Single
Static Elapsed As Single
Static X As Single
Static Y As Single
Static Z As Single
Static TDay  As Integer
Static Validated As Integer
Static TMonth As Integer
Static Attempted As Integer
Static TYear As Integer
Static THour As Integer
Static TMinute As Integer
Static TSecond As Integer
Static St, Skew2, Kurtosis As Double
Static AvgVelocity As Double
Static TotalVelocity As Double
Static StandardDeviation As Double

    OpenHist.Filter = "List Files (*.lst)|*.lst|"
    OpenHist.FilterIndex = 2
    OpenHist.Action = 1

Open OpenHist.Filename For Input As #5


Do While Not EOF(5)
Input #5, TheFile, TheNumber, TheDescription
    Text1.Text = TheFile
    Text2.Text = TheNumber
```

```
Open Text1.Text + ".OUT" For Output As #2

For P = 0 To (CInt(Text2.Text) - 1)
    Counter = 0
    TotalVelocity = 0
    MaximumVelocity = 0
    MinimumVelocity = 100000000
    I = P

    If P < 10 Then
        Ext2 = ".00" + CStr(P)
    ElseIf P >= 10 And P < 36 Then
        Ext2 = ".00" + Chr$(55 + P)
    End If


    Open (Text1.Text + Ext2) For Binary As #1
    Label4.Caption = "Processing File: " + Text1.Text + Ext2
    Label4.Refresh

    Get #1, 1, TMonth
    Get #1, 3, TDay
    Get #1, 5, TYear
    Get #1, 7, THour
    Get #1, 9, TMinute
    Get #1, 11, TSecond
    Get #1, 21, Attempted
    Get #1, 25, Validated
    Get #1, 33, DataRate
    Get #1, 37, Elapsed
    Get #1, 41, X
    Get #1, 45, Y
    Get #1, 49, Z

    Points = Validated
    Counter = 0
```

```
Get #1, 235, STAT
Do While Not EOF(1)
    If Counter = Points Then
        Exit Do
    End If
    Get #1, , STAT
    Get #1, , AT
    Get #1, , TT
    Get #1, , UVEL

    Holder(Counter) = CDbl(UVEL)
    TotalVelocity = TotalVelocity + CDbl(UVEL)

    If UVEL > MaximumVelocity Then
        MaximumVelocity = CDbl(UVEL)
    End If
    If UVEL < MinimumVelocity Then
        MinimumVelocity = CDbl(UVEL)
    End If

    Counter = Counter + 1
Loop
Close #1

If TotalVelocity > 0 Then
    AvgVelocity = TotalVelocity / Counter
Else
    AvgVelocity = 0
End If
St = 0
For M = 0 To Counter - 1
    St = St + Abs((Holder(M) - AvgVelocity) ^ 2)
Next M
Skew2 = 0
Kurtosis = 0
StandardDeviation = Sqr(St / (Counter - 1))
For M = 0 To Counter - 1
    Skew2 = Skew2 + (Holder(M) - AvgVelocity) ^ 3
    Kurtosis = Kurtosis + Abs((Holder(M) - AvgVelocity) ^ 4)
```

```
Next M
Skew2 = Skew2 / ((StandardDeviation ^ 3) * Counter)
Kurtosis = Kurtosis / ((StandardDeviation ^ 4) * Counter)

If Check3D7.Value = True Then
    NumOfEntries% = Counter
    Increm% = NumOfEntries% \ 2
    Do Until Increm% < 1
        For V% = Increm% + 1 To NumOfEntries%
            Temp = Holder(V%)
            For J% = V% - Increm% To 1 Step -Increm%
                If Temp >= Holder(J%) Then Exit For
                Holder(J% + Increm%) = Holder(J%)
            Next J%
        Holder(J% + Increm%) = Temp
        Next V%
        Increm% = Increm% \ 2
    Loop
    If Counter / 2# = Int(Counter / 2#) Then
        Median = (Holder(Counter / 2 - 1) + Holder(Counter / 2)) / 2#
    Else
        Median = Holder(Int(Counter / 2))
    End If

End If

If Check3D9.Value = True Then
    Call CHISQUARED(AvgVelocity, StandardDeviation ^ 2, Ext2, P)
End If


If I = 0 Then
    If Check3D1.Value = True Then
        Print #2, "Average",
    End If
    If Check3D8.Value = True Then
        Print #2, "Depth",
    End If
    If Check3D2.Value = True Then
```

```
    Print #2, "Maximum",
End If
If Check3D3.Value = True Then
    Print #2, "Minimum",
End If
If Check3D4.Value = True Then
    Print #2, "Standard",
End If
If Check3D5.Value = True Then
    Print #2, "Number",
End If
If Check3D6.Value = True Then
    Print #2, "Sampling",
End If
If Check3D7.Value = True Then
    Print #2, "3rd",
End If
Print #2, "Kurtosis",

Print #2,

If Check3D1.Value = True Then
    Print #2, "Velocity",
End If
If Check3D8.Value = True Then
    Print #2, "",
End If
If Check3D2.Value = True Then
    Print #2, "Velocity",
End If
If Check3D3.Value = True Then
    Print #2, "Velocity",
End If
If Check3D4.Value = True Then
    Print #2, "Deviation",
End If
If Check3D5.Value = True Then
    Print #2, "of",
End If
```

```
    If Check3D6.Value = True Then
        Print #2, "Frequency",
    End If
    If Check3D7.Value = True Then
        Print #2, "Moment",
    End If
    Print #2, " ",
    Print #2,

    If Check3D1.Value = True Then
        Print #2, "(m/s)",
    End If
    If Check3D8.Value = True Then
        Print #2, "(m)",
    End If
    If Check3D2.Value = True Then
        Print #2, "(m/s)",
    End If
    If Check3D3.Value = True Then
        Print #2, "(m/s)",
    End If
    If Check3D4.Value = True Then
        Print #2, "(m/s)",
    End If
    If Check3D5.Value = True Then
        Print #2, "Samples",
    End If
    If Check3D6.Value = True Then
        Print #2, "(Hz)",
    End If
    If Check3D7.Value = True Then
        Print #2, "Skew",
    End If
    Print #2, "",
    Print #2,

End If
```

```
    If Check3D1.Value = True Then
        Print #2, Format(AvgVelocity, "0.0000"),
    End If
    If Check3D8.Value = True Then
        Print #2, Format(Y / 1000#, "0.0000"),
    End If
    If Check3D2.Value = True Then
        Print #2, Format(MaximumVelocity, "0.0000"),
    End If
    If Check3D3.Value = True Then
        Print #2, Format(MinimumVelocity, "0.0000"),
    End If
    If Check3D4.Value = True Then
        Print #2, Format(StandardDeviation, "0.0000"),
    End If
    If Check3D5.Value = True Then
        Print #2, Counter,
    End If
    If AT > 0 Then
        If Check3D6.Value = True Then
            Print #2, Format(Counter / CDbl(AT), "0.0000"),
        End If
    Else
        If Check3D6.Value = True Then
            Print #2, "0.0000",
        End If
    End If
    If Check3D7.Value = True Then
        Print #2, Format(Skew2, "0.0000"),
    End If
    Print #2, Format(Kurtosis, "0.0000"),
    If Check3D9.Value = True Then
        Print #2, TheAnswer,
        Print #2, CHISQ,
    End If
    Print #2,

Next P
```

```
Close #2
Loop
Close #5

NextStep2:
Label4.Caption = ""
MsgBox "Finished Processing", 64


End Sub

Sub CHISQUARED (Average As Double, STDEVI As Double, Ext2 As Variant, THECOUNT As Variant)
Static Holder(10000) As Single
Static BIN(70) As Integer
Static STAT As Single
Static AT As Single
Static TT As Single
Static UVEL As Single
Static Prefix As Single
Static DataRate As Single
Static Elapsed As Single
Static X As Single
Static Y As Single
Static Z As Single
Static TDay  As Integer
Static Validated As Integer
Static TMonth As Integer
Static Attempted As Integer
Static TYear As Integer
Static THour As Integer
Static TMinute As Integer
Static TSecond As Integer
Static St As Double
Static AvgVelocity As Double
Static TotalVelocity As Double
Static StandardDeviation, XTERM, Sum As Double
Static TheoFreq(63), dATerm(63), ATerm(63), tTerm(63) As Double
Static OMINUSE(63), OMINUSESQ(63) As Double
```

```
On Error GoTo ErrorHandler4
Erase Holder, BIN
Open Text1.Text + Ext2 For Binary As #1
Open Text1.Text + ".h" + CStr(THECOUNT) For Output As #6


Counter = 0
TotalVelocity = 0
MaximumVelocity = 0
MinimumVelocity = 100000000

Get #1, 1, TMonth
Get #1, 3, TDay
Get #1, 5, TYear
Get #1, 7, THour
Get #1, 9, TMinute
Get #1, 11, TSecond
Get #1, 21, Attempted
Get #1, 25, Validated
Get #1, 33, DataRate
Get #1, 37, Elapsed
Get #1, 41, X
Get #1, 45, Y
Get #1, 49, Z


Points = Validated
Counter = 0

Get #1, 235, STAT
Do While Not EOF(1)
    If Counter = Points Then
        Exit Do
    End If
    Get #1, , STAT
    Get #1, , AT
    Get #1, , TT
```

```
    Get #1, , UVEL

    Holder(Counter) = CDbl(UVEL)
    TotalVelocity = TotalVelocity + CDbl(UVEL)

    If UVEL > MaximumVelocity Then
        MaximumVelocity = CDbl(UVEL)
    End If
    If UVEL < MinimumVelocity Then
        MinimumVelocity = CDbl(UVEL)
    End If

    Counter = Counter + 1
Loop
Close #1

AvgVelocity = TotalVelocity / Counter
St = 0
Total95 = 0

For M = 0 To Counter - 1
    St = St + Abs((Holder(M) - AvgVelocity) ^ 2)
Next M
StandardDeviation = Sqr(St / (Counter - 1))


For M = 0 To Counter - 1
    If Holder(M) >= (AvgVelocity - 2# * StandardDeviation) And Holder(M) <= (AvgVelocity + 2# * StandardDeviation) Then
        Total95 = Total95 + 1
    End If

    For J = 1 To 33

        If Holder(M) >= MinimumVelocity + CDbl(J - 1) * (MaximumVelocity - MinimumVelocity) / 33# And Holder(M) <
MinimumVelocity + CDbl(J) * (MaximumVelocity - MinimumVelocity) / 33# Then
            BIN(J) = BIN(J) + 1
        End If

    Next J
```

```
Next M

XTERM = MinimumVelocity
CHISQ = 0

For M = 0 To 32
    XTERM = XTERM + (MaximumVelocity - MinimumVelocity) / 33#
    tTerm(M) = (XTERM - AvgVelocity) / StandardDeviation
    Sum = 0
    For M2 = -22# To tTerm(M) Step .001
        Sum = Sum + .001 * 2.718281828 ^ ((-(M2 ^ 2#)) / 2#)
    Next M2
    Sum = Sum * 1# / ((2 * 3.14159) ^ .5)
    ATerm(M) = Sum
    If M = 0 Then
        dATerm(M) = ATerm(M)
    Else
    dATerm(M) = Abs(ATerm(M) - ATerm(M - 1))
End If

TheoFreq(M) = Counter * dATerm(M)
If TheoFreq(M) = 0 Then
    CHISQ = 1000
Else
    OMINUSE(M) = (CDbl(BIN(M + 1)) - TheoFreq(M))
    OMINUSESQ(M) = Abs((OMINUSE(M)) ^ 2) / TheoFreq(M)
    CHISQ = CHISQ + OMINUSESQ(M)
End If

If M = 0 Then
    Print #6, "Upper",
    Print #6, "Average",
    Print #6, "Standard",
    Print #6, "t",
    Print #6, "A",
    Print #6, "dA",
    Print #6, "Theoretical",
    Print #6, "Observed",
    Print #6, "o - e",
```

```
    Print #6, "CHI SQ.",
    Print #6,
    Print #6, "Limit",
    Print #6, "Velocity",
    Print #6, "Deviation",
    Print #6,
End If

    Print #6, Format(XTERM, "0.000"),
    Print #6, Format(AvgVelocity, "0.0000"),
    Print #6, Format(StandardDeviation, "0.0000"),
    Print #6, Format(tTerm(M), "0.00000"),
    Print #6, Format(ATerm(M), "0.00000"),
    Print #6, Format(dATerm(M), "0.00000"),
    Print #6, Format(TheoFreq(M), "0.00000"),
    Print #6, Format(BIN(M + 1), "0.00000"),
    Print #6, Format(OMINUSE(M), "0.00000"),
    Print #6, Format(OMINUSESQ(M), "0.00000"),
    Print #6,

Next M

If CHISQ <= 43.8 Then
    TheAnswer = "Yes"
Else
    TheAnswer = "No"
End If

Close #6
Exit Sub
ErrorHandler4:
MsgBox "File has invalid format", 48
Close #1
Exit Sub

End Sub
```